HYPERSONIC TURBULENT SEPARATION
INDUCED BY FLARES

J.R.A. Lowder, B. Eng.

June 1983

A thesis submitted for the degree of
Doctor of Philosophy
of the
University of London
and for the
Diploma of Imperial College

Department of Aeronautics
Imperial College of Science and Technology
Prince Consort Road
London, S.W.7 2AZ

Abstract

A series of separated flow experiments has been conducted in the Imperial College No. 2 Gun Tunnel at Mach 9 and test core unit Reynolds number of 1.29 x 10^5/cm and 5.17 x 10^5 cm. A turbulent cold wall boundary layer was generated over a 65 cm long cone-cylinder forebody fitted with a range of axisymmetric and asymmetric flares having included half angles below, and well above, the incipient separation threshold. The resulting two classes of flow were compared to determine the extent to which three dimensional influences, such as transverse pressure gradient and mass flux, effect the behaviour of an otherwise quasi-two dimensional separation region. Pitot measurements were taken around the cylinder circumference, and at several different axial locations, to establish the position of transition and development state of the boundary layer at separation. Surface pressure and heat transfer measurements were taken throughout the cylinder/flare interaction regions. Data from the axisymmetric flows were compared with flat-plate-wedge results obtained by other researchers in the same facility, and a large sample of data available in the literature. Specific relationships for established plateau pressure, shear layer deflection angle, cavity scale and pressure overshoot value, are subsequently introduced. Results from the asymmetric separated flow experiments were then compared with a set of two dimensional reference flows derived from the flat-plate-wedge and axisymmetric data base. Overall dimensions of the perturbed separation bubbles were found to be enhanced or suppressed in comparison with the reference flows, depending on circumferential position and local flare deflection angle. A consistent means of identifying these trends is developed and the influence of transverse pressure gradient and mass flux quantatively examined. A relationship between cavity length scales and flare pressure overshoot coefficient, identified for the reference flows, was found to correlate the perturbed flows quite well. Heat transfer distributions were found to spatially correspond well with their surface pressure counterparts. The experimental results were compared with a two dimensional attached flow prediction utilising a free interaction pressure

rise. The theoretical position for separation was subsequently found to coincide with the measured plateau peak heating value.

LIST OF CONTENTS

List of Contents (Continued)   Page

(v)

List of Contents (Continued)

NOMENCLATURE

a   Sonic velocity

C_f Friction coefficient, $\dfrac{\tau}{\frac{1}{2}\rho U^2}$

$C_p(\ )$ Pressure Coefficient, $\dfrac{P - P(\ )}{\frac{1}{2}\gamma P(\ ) M(\ )^2}$

where subscripts are region (e) or (∞).

C_{p_I} Incipient separation pressure coefficient

$\dfrac{P_I - P(\ )}{\frac{1}{2}\gamma P(\ ) M(\ )^2}$ where subscripts are region (e) or (∞).

C_{p_r} Reattachment pressure coefficient, $\dfrac{P_r - P_p}{\frac{1}{2}\gamma P_p M_p^2}$

$\hat{C}_p$ Reattachment pressure overshoot coefficient

$\dfrac{\hat{P} - P(\ )}{\frac{1}{2}\gamma P(\ ) M(\ )^2}$ where subscripts are region (e) or (∞).

E   Energy defect thickness

F(X)   Erdos & Pallone separation pressure rise function defined in Figure 40

H   Total enthalpy

K   Empirical function identified for Elfstrom's plateau pressure correlation defined in Figure 46

L' Position ($X = L'$) of wall surface temperature discontinuity

L_{sep} Distance from separation point to wedge/flare intersection line

ℓ Shortest distance between separation and reattachment points

M or   Mach number where subscripts are region (e), (∞) or (p)
M( )

N   Velocity profile exponent defined as $Y/\delta = (U/U_e)^{\frac{1}{N}}$.

n   Normal from (ℓ) to wedge/flare intersection line

P   Surface pressure

NOMENCLATURE (continued)

$\hat{P}$ Reattachment pressure overshoot value

Pd   Tunnel driver pressure

P_I Wedge/Flare recovery pressure measured at incipient separation

Pinv   Wedge/Flare recovery pressure, predicted for an inviscid uniform flow

Po   Measured reservoir pressure (Tunnel barrel)

Po( )   Total pressure where subscript is region (e) or (∞)

Pt   Measured Pitot pressure

Q   Ratio $\dot{q}/\dot{q}_L$

$\dot{q}$ Heat transfer rate.

$\dot{q}_L$ Heat transfer rate at wedge/flare intersection line for attached uniform stream

$\dot{q}o$ Heat transfer rate at given point (X) for flow over a wall of uniform temperature

$\dot{q}s$ Heat transfer rate at given point X (where $X > L'$) for flow over a wall with surface temperature discontinuity located at $X = L'$

$\hat{\dot{q}}$ Post reattachment peak heat transfer value

R   Radial distance from cylinder axis of symmetry

Re( )   Reynolds number based on length scale and region prescribed in parenthesis, i.e.

$$\text{Re}\delta o = \frac{\rho(e) \ U(e) \delta o}{\mu(e)} \quad \text{for cone-cylinder geometry}$$

Rc   Cylinder radius

R   Reynolds number based on wall friction velocity and boundary layer height just ahead of separation i.e.

$$\frac{\rho w \ U\tau \ \delta o}{\mu w}$$

Re∞/cm   Unit Reynolds number of undisturbed tunnel free stream

$\left. \begin{array}{l} \text{Rex}_{tr} \\ \text{Re}\Delta x_{tr} \end{array} \right\}$ Transition Reynolds numbers defined in Figure 16a

r   Recovery factor

St   Stanton number, $\dfrac{\dot{q}}{\rho(\ ) \ U(\ ) \ (Hr - Hw)}$

NOMENCLATURE (continued)

T()   Static temperature in region prescribed in parenthesis

Tr   Recovery temperature

$$T(\ \ ) \cdot \left[1 + r \cdot \frac{(\gamma - 1)}{2} \cdot M(\ \ )^2 \right]$$

To( ) Total temperature in region prescribed in parenthesis

U( )   Velocity in X-direction in region prescribed in parenthesis

U_τ Friction velocity, $(\tau w / \rho w)^{\frac{1}{2}}$

x   Horizontal length scale (abscissa), see also Figure 30 for clarification of data presentation. Also horizontal distance from nozzle exit plane, Figure 3.

xo   Position at which surface pressure departs from undisturbed value, i.e. start of separation pressure rise.

xr   Distance from wedge/flare intersection line to reattachment point.

X_S Position at which Erdos & Pallone separation pressure rise function, F(X), attains a value of 4.22 in turbulent boundary layer flows.

Y   Ordinate from model cylinder surface

Z   Length scale normal to X, Y - axes

NOMENCLATURE (continued)

Greek Symbols

α Wedge/flare local angle of incidence

αi Incipient separation angle

β Flare semi-angle

Γ Energy thickness

γ Ratio of specific heats

ΔX Upstream influence length, see Figure 57

$\Delta x\hat{p}$ Distance from wedge/flare intersection line to position of maximum pressure overshoot value, $\hat{P}$, see also Figure 57

$\Delta x(\dot{q})$ Heat transfer equivalent of ΔX

$\Delta x(\hat{\dot{q}})$ Heat transfer equivalent of $\Delta x\hat{p}$

$\Delta\dot{q}s$ Difference in the experimental separated flow and theoretical attached flow ratio of $\dot{q}/\dot{q}_L$ at the separation point prescribed by $F(X) = 4.22$

δ Boundary layer height, see also Figure 23

δL Boundary layer height at flare intersection line (flare removed)

δo Undisturbed boundary layer height at beginning of separation pressure rise

δ^* Displacement thickness

θ Momentum thickness

θs Angle between surface prescribed by line (ℓ) and model surface

$\mu(\ )$ Absolute viscosity in region ( )

$\nu(\ )$ Kinematic viscosity, $\mu(\ )/\rho(\ )$ in region ( ).

$\overline{\Pi}$ Wake component

$\rho(\ )$ Density in region ( ).

τ Shear Stress

$\emptyset$ Polar co-ordinate, see Figure 5

NOMENCLATURE (continued)

Subscripts

e   Region behind cone-cylinder bow shock and shoulder expansion, at the boundary layer edge, and either:

        (i)   At the flare intersection line in the undisturbed flow or,

        (ii) Just ahead of separation

j   Region inside separation bubble at the detached shear layer boundary with the cavity reverse flow field, (jet boundary).

p   Plateau free stream

r   Unless otherwise specified – point of reattachment

w   Undisturbed condition at the model surface at the wedge/flare intersection line.

∞ Tunnel free stream region and/or region behind weak bow shock system of hollow cylinder or flat plate, outside the boundary layer.

LIST OF FIGURES

List of Figures (continued)

List of Figures (continued)

List of Figures (continued)

LIST OF TABLES

ACKNOWLEDGEMENTS

1. GENERAL INTRODUCTION

Hypersonic turbulent boundary layer separation has been the subject of many studies in the literature. Most of these relate to nominally two-dimensional flows and some to their axisymmetric equivalents, although these are rarely found in any practical situation. The ultimate purpose of the present research programme was to investigate the effect of weak three-dimensionality on a separated flow.

It is obviously important at the outset to investigate a two-dimensional flow field such that its perturbed case can be closely compared with a reference condition. It was decided to employ the axisymmetric configuration of a cone-cylinder-flare as this reference. This had the advantages of eliminating end effects, which are an inadvertent, but often important, consequence of tests on 'two-dimensional' models; it also proved particularly convenient from the viewpoint of instrumentation and from the fact that it leads on directly from Coleman's (1973) studies. On the debit side it introduced some extra flow field complexity, producing a bow shock and accompanying expansion process, compared with the relatively weak leading edge disturbance of, say the flat plate.

The perturbed separation conditions were obtained by offsetting the symmetry of the flare such that local regions of mild transverse pressure gradient would be set up in the vicinity of the interaction. This method was chosen in preference to setting the whole geometry at incidence and the fundamental structure of the approaching boundary layer was therefore preserved for both sets of experiments. The interaction regions generated by these geometries, in consequence, would embody most of the mechanisms common to previous studies although some differences in detail would be expected to arise in say, levels of pressure and heat transfer. It is useful to consider these mechanisms here.

Shock induced separation is a highly non-linear process. The reasons for this are various but we can identify several

which are directly relevant to the present study with the help of Figure 1: Firstly, the turning of a hypersonic stream through a large angle by a shock is a non-linear process, notwithstanding the fact that the stream itself will be non-uniform; next, for the range of flow deflections of interest, the scale of the bubble varies from an order of magnitude less than the thickness of the approaching boundary layer to, perhaps, an order of magnitude greater; thirdly, even for the longest separation bubbles the mixing region is unlikely to reach an equilibrium state before reattachment occurs (i.e. independent of the conditions at separation), so that a fairly detailed knowledge of mixing layer dynamics is required; finally, the flow field immediately downstream of reattachment is dominated by the non-linear interaction between the separation and reattachment shocks. These effects combine to produce a sequence of events which are more clearly described by considering how the flow field develops as the wedge/flare angle is increased for fixed conditions in the approach stream.

At low enough angle the influence upstream of the compression corner is extremely small, limited to one boundary layer thickness or less generally. Apart from the region in the immediate vicinity of the corner, the flow field is dominated very much by the momentum of the outer part of the boundary layer which tends to behave as an inviscid rotational stream with little contribution from the viscous or Reynolds stresses. The resulting flow exhibits a single, but rather diffuse, shock in the corner region and the only indication of the possible onset of separation lies in the growth of pressure and heat transfer rates just ahead of the corner. The precise point at which flow recirculation commences has been the subject of much debate in the literature and there are almost as many criteria for 'incipient separation' conditions as there have been authors. Gross separation only becomes visible in the Schlieren system for fairly large flow deflections, typically 30 degrees or more for the present tests. Further increases in corner angle cause the cavity region to grow rapidly with a clearly visible separation and reattachment shock structure. During this stage of development certain features of the pressure and heat transfer

distributions remain relatively constant and to a certain extent characterise the nature of high speed boundary layer separation. These features form the basis of comparison between different experiments. Consequently, over this range of bubble size and corresponding corner angle it is traditional to partition the description of the interaction in terms of the static pressure response rather than physical features evident in the Schlieren system, which are generally few. Firstly there is the region of pressure rise up to separation. Here the boundary layer is considered to be growing under a self induced pressure gradient, independent of downstream conditions, and governed only by similarity principles and local free stream conditions. The term 'Free Interaction' is used to describe this process and free interaction prediction methods have been quite successful in the past although it will be shown later in the text that the pressure rise beyond separation cannot be treated independently of the downstream conditions. The initial pressure rise subsequently blends with the so called 'plateau' region, evident for well established bubble sizes, and which dominates the flow field to within one boundary layer thickness of reattachment. At reattachment the free shear layer divides and the subsequent pressure recovery also exhibits free interaction behaviour in so much as the shape of the distribution remains more or less constant and independent of the bubble size or the position of reattachment. The recirculating fluid undergoes vigorous mixing with the advancing shear layer, the remaining fluid is turned downstream largely by the action of a reattachment shock which, in turn, may interact with the separation shock to generate a pressure overshoot and subsequent relaxation downstream of the reattachment point. As with the plateau region, the details of reattachment are not properly understood, mainly because it is difficult to probe the separation bubble structure without grossly disturbing the natural flow field. Most correlations concerned with these regions are therefore limited to unobtrusively measured, or inferred properties, namely surface pressure, heat transfer rates and local plateau free stream Mach number. It is not surprising that this uncertainty has rendered analysis of the post reattachment region almost intractable with the exception of the final pressure recovery value which usually corresponds with

the inviscid flow solution for the geometry in question.

The complete flow field is evidently highly unpredictable with our present knowledge limited to isolated features of the interaction region. This thesis sets out to improve our physical understanding of the simple two-dimensional case and attempts to extend these, and earlier, conclusions to the more practical three-dimensional problem.

This particular study lies within the broader field of interest to scientists and engineers principally engaged in the design of orbital re-entry vehicles where shock wave-boundary layer interactions cannot wholly be avoided.

2. BACKGROUND AND LITERATURE SURVEY

As stated in the general introduction, it is important to establish a rigorous set of two dimensional criteria with which to compare the effects of mild three dimensionality. Preliminary tests on the asymmetric models indicated that these effects were in fact quite subtle. Comparison of the results with the basic Reynolds number response of the two-dimensional cavity suggested that a detailed knowledge of the boundary layer input conditions would also be required if the results were to be meaningfully compared with other work in this field. Consequently, the following discussion not only concentrates on two-dimensional studies, it also includes several important contributions made outside the specific field of turbulent separation. These additional references are concerned with the development of the undisturbed boundary layer. They have been found extremely useful in providing some explanation for the diverse behaviour of the numerous cavity flows studied over the last three decades.

2.1 THE COMPRESSIBLE TURBULENT BOUNDARY LAYER

Much of the impetus of high speed research has been devoted to establishing the principal difference between the compressible and incompressible stream. A useful starting point to a historical review of the study of compressible turbulent boundary layers would, therefore, be to note development of transformation theories since World War II. The ability to predict the performance of high speed vehicles has been paramount during this period and for the simple case of undisturbed flow the parameter of most importance has obviously been the skin friction and its close association with heat transfer. By invoking 'plausible' physical assumptions about the compressible turbulent stream many authors have sought to reduce the governing equations to the more tractable incompressible form. Early prior art in this field has been reviewed by Coles (1962), who cites the work of Dorodnitsyn (1942), Van Le (1953) and Mager (1958). In discussing his own theory of 1962, Coles pointed to some of the inherent difficulties

in attempting to reduce the compressible case to an 'observable' incompressible flow. The point being that for a transformation to be rigorous a genuine kinematic and dynamic correspondence between the incompressible and compressible flow should exist such that the shear stress distributions should also correspond. Unfortunately, in recent years these difficulties have grown more complex rather than having succumbed to analytical treatment. It is now generally accepted that the turbulence structure of the compressible stream can be vastly different from the low speed case and a rigorous basis for transforming structural difference is unlikely to be found. Nevertheless, the results of transformation theories still remain interesting for their empirical value and several of the more successful formulae have been subsequently reviewed by Hopkins et al (1971). These authors concluded that the theory due to Van Driest (1956) and Coles (1962) gave fair agreement with experiment in the range M = 5.9 to 7.8 whereas those due to Sommer and Short (1955) and Spalding and Chi (1964) were found to underpredict values of skin friction. The Van Driest theory was also found to give the most satisfactory transformation of velocity profile data into the incompressible law of the wall and velocity defect curves. This aspect of the transformation process has proved particularly valuable in the comparative study of compressible layers since it provides a basis for determining the analogous state of profile development in terms of equivalent incompressible flow. The wake parameter formulated by Coles (1956) has played a central role in such comparisons and several authors, e.g. Elfstrom (1971), Coleman (1973), Edwards (1976) have noted a tendency for this parameter to be suppressed at a given Re_θ as the Mach number is increased.

The variation of the velocity power law exponent (N) with Re_θ has also proved a useful characterisation of mean flow development. Johnson and Bushnell (1970) surveyed a considerable range of experimental data using these parameters and found that in the range $Re_\theta < 8000$, for increasing Re_θ, the exponent rises sharply before relaxing onto a steadily increasing almost linear trend. This overshoot in (N) was closely associated with evidence of transition and the subsequent gentle

rise following the overshoot seemed to correspond to the developing wake. The trends appeared more clearly in the data for flat plates, cones and hollow cylinders, presented as one class of flow. Tunnel wall data, on the other hand, were found to be less consistent with no evidence of overshoot in (N). It is now believed that this lack of overshoot reflects the favourable pressure gradient often experienced by tunnel wall boundary layers. Differences in profile development history such as this are thought to significantly affect the outcome of separation studies conducted in the two classes of flow.

Boundary layer development trends can often be obscured by the unexpected behaviour of transition in compressible streams. Many authors have studied this problem, including Potter and Whitfield (1962), Pate and Schueler (1969), Page and Sernas (1970), Wagner et al (1969) and Narasimha and Viswanath (1975). Several of these authors concluded that great care must be taken to ensure that the flow field is free from acoustic disturbances if reliable transition trends are to be determined. Effects due to compression, transverse curvature, streamline curvature and expansion are discussed by Bradshaw (1973) under the broad heading of extra strain rates. These effects are also known to significantly influence the transition and development history of both the compressible and incompressible streams.

The tendency for transition to move to higher Reynolds number, particularly under cold wall hypersonic conditions, has been noted by Bushnell and Morris (1971). In a survey of hypersonic data these authors concluded that the effect of low density and high viscosity (high recovery temperature) in the vicinity of the wall can significantly delay post transitional development. This leads to so-called 'low Reynolds number' behaviour which is characterised by non-equilibrium features in the velocity profiles at relatively high Re_θ (i.e. underdeveloped wake). Bradshaw (1973) in commenting on the structural differences of the hypersonic stream has suggested that the enhanced growth of the viscous sublayer is the single most important difference between the compressible and

incompressible case since this can be an order of magnitude larger for a given Re_θ . Above Mach 5 these effects are thought to contribute significantly towards the breakdown of the inner layer analysis successfully developed for low speed flows. Axisymmetric geometries are also thought to have a considerable influence on boundary layer development. Evidence for the effect of concave transverse curvature (i.e. nozzle walls) has tended to be obscured in the literature by the presence of mean flow pressure gradients. Geometries with convex transverse curvature (i.e. hollow or solid cylinders) on the other hand are normally free from these external influences and a clearer indication of the effects of axisymmetry should in principle be possible. However, from a historical point of view the unit Reynolds number in many hypersonic facilities has been too low to permit the development of turbulent layers on such geometries. Hence, a wealth of nozzle wall data prevail in the literature. However, an indication of the influence of convex transverse curvature is given by the work of Probstein and Elliott (1956). These authors demonstrated that the Crocco integral for unity Prandtl number and zero pressure gradient in laminar layers was also valid for all δ/R in axisymmetric flows. As with the two-dimensional case, substitution of the temporal mean values of the turbulent flow derivatives extends the usefulness of this integral to the turbulent case with an appropriate choice of recovery factor. Their analysis suggested that the terms embodying the effect of transverse curvature in the momentum equation behave like a favourable pressure gradient. Thus, transition and boundary layer development should be delayed by 'positive' axisymmetry. Limited experimental evidence for these effects can be found in the work of Robinson (1974) at Mach 2.8 ($\delta/R \sim 1$) and in the hollow cylinder heat transfer experiments of Coleman (1973) at Mach 9 ($\delta/R \sim 0.3$). However, precise details of the range of δ/R where significant influences should arise are sadly lacking in the literature for compressible streams and the subject is clearly worthy of further research.

The most recent and relevant experiments to the current work have been conducted by Bartlett et al (1979) in the

Imperial College No. 2 gun tunnel. These experiments were conducted at one of the two Reynolds number conditions and the same Mach number as the present study. The work was a repeat of the earlier flat plate experiments performed by Elfstrom (1971) and later by Coleman (1973) but in this case more highly developed instrumentation was employed including the application of the electron beam fluorescence technique for measuring the mean and fluctuating density components. Results from the time averaged quantities have confirmed the slow development of the hypersonic boundary layer. This work is also notable for the total temperature measurement performed by Edwards and later the local probe Reynolds number calibration performed by Bartlett. This careful, and difficult, set of experiments has enabled one of the few reliable comparisons with the Van Driest (1951) modification of the Crocco relationship. The results were found to be in fair agreement with this traditional quadratic solution to the energy equation, (Pr close to unity, $\partial P / \partial x = 0$ and Tw = const.) for a recovery factor of 0.89.

In the last decade there have been some interesting developments in the use of hot wire anemometry to measure turbulence quantities in compressible layers, e.g. Owen and Horstman (1972), Rose (1973), Mikulla and Horstman (1975/6) and Laderman and Demetriades (1979). One of the principal challenges to turbulence high speed research today is to establish the limits of applicability of Morkovin's hypothesis (Favre 1964) which contends that the direct effect of density fluctuations on turbulence is small if the root-mean-square density fluctuation is small compared to the absolute density. In practice, this implies that the structural properties of the boundary layer (e.g. correlation coefficients, spectrum shapes, etc.) below Mach 5 should not vary significantly from the imcompressible case. Above Mach 5 this situation becomes less certain as it is believed that acoustic (or pressure) disturbances become much stronger and can interact with vorticity producing mechanisms and thus alter the basic structure of the layer. Owen and Horstman (1972) concluded that these effects were still minimal at Mach 7 in an axisymmetric

layer, $\delta/R \sim 0.15$. However, Bradshaw (1975), in a fairly extensive discussion of this and other work in the context of Morkovin's hypothesis, points out that the effect of mean density gradients is not covered by Morkovin's simplifying assumption. The strong normal density gradient in a compressible stream may, therefore, have a significant effect on the entrainment properties of the outer layer. Bradshaw has suggested that this may be the cause of the two or threefold decrease in standard deviation of the intermittent interface position from its low-speed value (e.g. Klebanoff (1955), M = 0.05 σ/δ = 0.14; Owen and Horstman (1972) M = 6.7, σ/δ = 0.08; Laderman and Demetriades (1974), M = 9.4 σ/δ = 0.07). The full implications of this mechanism remain unclear but it has further been suggested by Bradshaw that such structural changes would almost certainly control low Reynolds number effects; i.e. the tendency for wake development to become suppressed at high Mach numbers.

A substantial amount of the experimental data available in the literature has recently been recompiled by Fernholz and Finley (1977). The sixty sets of data selected and reviewed by the authors do not include the specific case of the cone-cylinder configuration at high Mach number. The current experiments should, therefore, redress this imbalance.

2.2 INCIPIENT SEPARATION

Practically all compressible flow research conducted on separated flows has addressed the specific problem of determining incipient separation conditions. For the case of the turbulent stream, a precise definition for the conditions under which reverse flow begins is problematical in view of the unsteadiness of the inner layer. Moreover, the scale upon which this initially takes place will be small and of the order of the sublayer thickness ($\sim 0.1\delta$). At high Mach number, with the limitations of tunnel experimental conditions, boundary layers have rarely exceeded a height of 3 cm. Measurement of the incipient state has therefore been difficult and the results very much open to interpretation. It can now be said with some confidence that this measurement problem has been compounded

in the past by compressibility effects and the development state of the approach stream chosen for investigation. Hence with an understandable proliferation of incipient separation criteria coupled with physical effects due to Mach number and Reynolds number, which have yet to be fully specified, even the broadest indication of incipient separation behaviour has been slow in emerging. For the range of Reynolds numbers and Mach numbers of practical interest a crude pattern of behaviour has, however, begun to emerge in the last few years. This pattern suggests that for an increase in free stream Mach number, for a fixed state of development and similar wall conditions in the · approach stream, the boundary layer resistance to an adverse pressure gradient will increase. For constant Mach number the resistance appears to decrease following transition but then increases as the interaction region is moved further downstream where the boundary layer approaches the low speed equivalent of an equilibrium state, (i.e. developed wake). The latter range of response spans three decades in $Re_{\delta L}$ which, as yet, no single experiment has encompassed. It is important, therefore, to consider the contributions made and techniques employed by many authors to gain a complete picture of the phenomenon. All data from the experiments discussed here can be found in Figure 35.

The earliest (and frequently quoted) experiments specifically undertaken to determine incipient separation conditions were the flat plate compression wedge studies performed by Kuehn (1959), $2 < M_\infty < 4$, $10^4 < Re_{\delta L} < 10^5$. Kuehn used the first appearance of an inflection point in the upstream influence surface pressure response as the criterion for the beginning of reverse flow, (method (a)). The incipient separation wedge angle (α_i) was found to increase with Mach number but reduced for increasing $Re_{\delta L}$ (M_∞ = const). Curiously, the rate of decay of α_i with $Re_{\delta L}$ was also found to be a strong function of Mach number; being far more abrupt at the highest value (M_∞ = 4). It has frequently been suggested in the literature that Kuehn's boundary layers must have been in a post transitional state and the reducing trend of α_i with $Re_{\delta L}$ therefore reflected the relaxation of the input profile. However,

the fact that boundary layer trips were used does lead to some uncertainty over Kuehn's input conditions. An interesting aspect of this work which seems to have been neglected of late was the strong hysteresis effect of the incipient separation condition noted on curved surfaces when the effective deflection is varied dynamically. In this situation it was found that, under constant approach conditions, the collapse of the cavity occurred at a lower value of (αi) than when (α) was being increased. Kuehn (1961) later extended his work to axisymmetric models and demonstrated the same basic Reynolds number trends for (αi) although higher absolute values were obtained.

Sterrett and Emery (1962) extended the Mach number range to the hypersonic regime employing a flat plate wedge, (4.8 < M < 5.8, $Re_{\delta L} \sim 10^5$). Using the same criteria as Kuehn, they observed the same Mach number and Reynolds number trends. To achieve higher values of $Re_{\delta}L$ they utilized surface roughness to trigger transition. In so doing, they acknowledged that some uncertainty over the true state of their input conditions must remain. Similar hysteresis effects to those discovered by Kuehn were also found. However, this work is probably best known for the extremely high effective turning angles achieved without separation when curved surfaces are used. In one case, with an interaction close to the end of transition, they achieved an effective flow deflection in excess of 46 deg. which was above the theoretical angle for a detached shock.

Early controversy over the behaviour of (αi) began with the high Reynolds number tunnel wall experiments of Roshko and Thomke (1969), (2 < M < 5, 10^5 < $Re_{\delta}L$ < 10^6). Using three additional criteria they observed quite the opposite trends for αi than the previous two authors. Briefly, there were:
Method
b) Plotting corner angle vs. α and noting the deflection angle for which the corner pressure ceased to rise.
c) Using an orifice-dam situated close to the corner on the wedge and detecting the onset

of reverse flow.

d) Extrapolating to zero the separation length (determined from upstream and downstream orifice dams).

For values of wedge angle just below αi they found no appreciable upstream influence. This contrasted with Kuehn's results which gave significant upstream influence for (α) much less than (αi). They concluded that the different Reynolds number trend observed by previous workers could be due to an increased relative thickness of the sublayer at lower Reynolds number or the fact that tripped boundary layers are intrinsically underdeveloped. (This latter suggestion had also been made earlier by Zukoski (1967) who was studying interactions ahead of forward facing steps). Surprisingly, all four of the above methods chosen to pinpoint the incipient reverse flow condition gave consistent values for (αi). Clearly, the observed abrupt change from attached to separated flow will have reduced the scope for experimental scatter in these comparisons. However, this tendency may be a further indication of the structural differences between the highly developed nozzle wall layer and the post transitional stream.

Elfstrom (1971) in his flat plate compression wedge studies, $(M\infty \sim 9,\ 10^5 <\ Re\ \delta L\ < 10^6)$, found that Kuehn's criterion was difficult to apply where high wedge pressure gradients exist. Instead he used methods (a) and (b) above with separation and reattachment determined by Schlieren photography. He also proposed an additional criterion specifically for high Mach number wedge interactions. He noticed that for his fully separated flows the peak pressure on the wedge exceeded the attached flow condition by up to 30%. He subsequently suggested that the disappearance of the overshoot should mark the incipient wedge angle. The criterion was found to work quite well and further lead to the idea that the high Mach number boundary layer could be treated as an inviscid rotational stream with a slip condition at the wall. He argued that the wedge angle at which the slip Mach number produces a detached corner shock should prescribe (αi). The slip condition was specified by extrapolating the Mach number profile to the wall.

Elfstrom's work will be more extensively discussed later in this thesis. It is sufficient to add here that, while perhaps physically incomplete, this criterion enabled Elfstrom to develop a correlation based on a family of profiles suggested by Green (1970/2). The slip Mach number was subsequently formulated as a unique function of the friction velocity Reynolds number, $\bar{R} = (\bar{P}wU\tau\delta L)/\mu w$ (M∞ = const., Tw/T∞ = const).

The resulting correlation for (αi) showed a steep decline in the vicinity of $\bar{R}_{v}$ 10^3 but a steady increase above this value. This latter trend was found to be strongly influenced by the effect of the wake component on the slip Mach number. A link between the developing wake and the incipient separation trend reversal noted by Roshko and Thomke was thus established.

Spaid and Fishett (1972) (tunnel wall/compression wedge, $M\infty_v$ 2.9, $10^4 < Re\delta L < 10^5$) introduced a further two criteria in a study which also included some of the earlier techniques. These were:

Method

e) Extrapolation of the separation length (determined by a liquid line technique) to zero.

f) First appearance of the separation shock in Schlieren photographs.

Methods (a) and (b) were also used and confirmed the trends found by Kuehn giving similar absolute values for (αi) although some difference in the sensitivity of each method to changes in ReδL were observed. Method (e) gave much lower values of αi ($\sim$13° compared with $\sim$18°) and method (f) gave values as low as 6°. Neither of the latter two sets of data showed any sensitivity to ReδL.

These comparisons were performed under constant adiabatic wall conditions. In a second series of cold wall tests higher values for (αi) were observed, in keeping with Elfstrom's earlier results. The authors concluded that the liquid line technique was the most sensitive way of observing a region of zero wall shear stress, provided this was to be the criterion for the onset of separation. Other methods, which depended on the

measurement of pressure, would be less sensitive to this condition and would only respond when the interaction had developed sufficiently to cause significant changes in the flow structure. They pointed out that this conflicted with the results of Roshko and Thomke who found good agreement between various methods, but for higher Reynolds numbers.

Batham (1972) (flat-plate-wedge   i.e. FPW, Mach 7, in the range $10^5 < Re_{\delta L} < 10^6$) appears to have used Kuehn's criterion for determining α_i. He demonstrated the same Reynolds number trend as Elfstrom although the dependence of α_i on $Re_{\delta L}$ was greater, as were the absolute values of α_i. Batham concluded that both the steeper Reynolds number trend and the higher absolute values of α_i were due to the fact that his interaction had been set up closer to the end of transition.

Coleman (1973) supplemented Elfstrom's work by investigating heat transfer rates for wedge and flare interactions at identical tunnel conditions. With the exception of certain model configurations (see Section 5) pressure and heat transfer distributions corresponded well. However, the behaviour of peak heating rates at incipient separation was less clear than the pressure response. Whereas the attached wedge flow pressure distributions could be predicted with some accuracy, and thus provide a reference from which to perceive an overshoot, this was not the case for heat transfer. Moreover, for axisymmetric experiments, under attached flow conditions, an inherent overshoot in pressure and heat transfer was observed at the flare intersection line, indicating a tendency for the flow to behave two-dimensionally before relaxing to the conical flow condition. Consequently, Coleman was unable to use his heat transfer results in an analagous form of Elfstrom's overshoot criterion for determining (α_i). Instead he found good agreement between method (d) using Schlieren photography, and method (g) which involved plotting the heat transfer rate at a point on the wedge, just behind the intersection line, against (α), and detecting a sudden reversal in slope. He was thus able to demonstrate the same trends and absolute values as Elfstrom for the FPW configuration although the axisymmetric results were slightly higher

($\simeq 2°$). Kuehn had also observed this difference between 'equivalent' two dimensional and axisymmetric flows but to a slightly larger extent ($\simeq 5°$). Bradshaw (1973) has suggested that this may be due to the influence of extra strain rates in axisymmetric flows (see Section 4). However, the author is of the opinion that differences in the location of transition must also be considered carefully as this effect certainly appears to dominate a great deal of the experimental evidence to date in both axisymmetric and nominally two-dimensional flows.

Appels (1974) re-examined all the criteria mentioned so far and conducted experiments on a tunnel wall wedge at Mach 3, 5 and 5.4 with $9 \times 10^4 < Re_{\delta L} < 6 \times 10^5$. He confirmed Kuehn's inference that very small regions of separation exist for wedge angles much lower than indicated by some methods. He used oil flow visualization and took great care to introduce only discrete quantities of oil into the flow, thus ensuring the minimum interference with the interaction. He demonstrated that the method of extrapolating separation lengths to zero (by whichever measurement technique) could be misleading if the rate of reduction in cavity length becomes highly non linear in the limit $\alpha \rightarrow 0$. Using his own data, typical differences in (αi) for large and small cavity extrapolations were 20 deg. and 10 deg. respectively.

Appels' results clearly imply that published trends for (αi) cannot be relied upon for engineering purposes until sensitive and consistent measurement techniques have been employed across the complete range of Reynolds number of interest. His own data produced an increasing trend with $Re_{\delta L}$ and therefore directly conflicted with the trends observed by Elfstrom and Coleman in the same decade of $Re_{\delta L}$ (cold wall), but at higher Mach number. His explanation for this was based on Elfstrom's observation that incipient separation is closely linked with the developing wake in a turbulent layer. He argued that, since his experiments had been conducted in a tunnel wall in the region of a favourable pressure gradient, the boundary layer would be in a relatively advanced state of development for a given value of $Re_{\delta L}$, as similarly demonstrated by Johnson and Bushnell (1970).

Boundary layer studies confirmed the existence of a developed wake and placed the predicted response of (αi), according to Elfstrom's theory, in the region where (αi) should be increasing with wall friction Reynolds number. The conflict with Elfstrom's experimental results was thus convincingly removed. However, on the strength of these studies, past and future claims for the successful measurement of absolute values for (αi) clearly require close scrutiny. Moreover, the choice of $Re\delta L$ as the correlating parameter for broad comparisons could be misleading in the light of Elfstrom's theory.

Law (1974) performed adiabatic flat plate wedge experiments at Mach 2.9 in the range $10^5 < Re\delta L < 10^6$. Methods (a), (b), (e) and (f) were employed to determine (αi). Law gives no indication of his boundary layer input condition other than length Reynolds number in the range 10^7 to 10^8. His data were the first to indicate an increasing trend in the decade 10^5 $Re\delta L < 10^6$ and this provided further 'indirect' support for Elfstrom's theory. Law's data will be discussed more fully later in this thesis (see Section 5).

Settles et al (1976) compared the results from two different experiments:
    (i) Tunnel-wall-wedge
        $M = 2.9,\ 5 \times 10^5 < Re\delta L < 7.6 \times 10^6$
    (ii) Ogive-cylinder-flare
        $M = 2.9,\ 1.5 \times 10^5 < Re\delta L < 6 \times 10^5$

Studies of the undisturbed boundary layer in each case indicated very little change in the wake component as Reynolds number was increased and the test stream was subsequently judged to have reached so-called 'equilibrium' conditions. A review of all the available criteria was made with a distinction drawn between the methods which were considered to be capable of detecting 'significant' reverse flows only, and those considered suitable for ascertaining the presence of a 'small' recirculation region. The notion of incipient separation heralded by a sudden disappearance in wall shear stress was rejected on the grounds that this particular condition had so far eluded all experimenters particularly in the case of compression wedge flows. In their

own experiments, Settles and his co-workers found evidence of a small recirculation zone ($\sim$1mm) at angles as low as 10 deg. Using a kerosene-graphite evaporation technique for surface flow visualization they demonstrated a similar asymptotic behaviour for the growth of separation length against wedge/flare angle as found by Appels (method (e)). Methods (a), (b), and (f) were also employed and it was concluded that the complete spread of data gave no indication of a Reynolds number trend for (αi). However, if the results for method (e), the most sensitive method, are viewed independently, similar trends as found by Roshko and Thomke, at roughly the same conditions, can be identified. Moreover, these specific results were found by the author (not shown) to lie remarkably close to the prediction given by Elfstrom's theory for Settles' tunnel conditions. Surprisingly, by asserting that no Reynolds number trend could be detected these researchers seem to have apportioned equal credibility to each of the techniques employed which, of course, conflicts with the development of their earlier arguments. Although Elfstrom's theoretical result lay within the general spread of (αi) detected in this decade of ReδL, these workers considered the theory inconclusive on the grounds that wall shear had been neglected. However, in fairness, Elfstrom in his own work has suggested that the theory may not be accurate below Mach 4 due to the inviscid assumption. The agreement between Elfstrom's theory and the oil flow visualization results of Settles et al may, therefore, be fortuitous.

Holden (1974/5) conducted a host of experiments on compression wedge configurations for the conditions $6.5 < M < 13$ and $10^5 < Re_{\delta L} < 10^7$. Separation was judged to have been obtained when the time average of surface shear at one point on the surface was zero. Skin friction gauges were used to determine this condition but it is unclear in both the above references to what extent the surface skin friction gauge was able to resolve the interaction. Nevertheless, the trends for (αi) with ReδL published by Holden are in agreement with those of Elfstrom and Coleman at similar Mach numbers.

2.3 'FULLY ESTABLISHED' SEPARATION

The term 'fully established' is taken here to refer to an interaction exhibiting the characteristic features of a compressible turbulent separation region; i.e. a region exhibiting a clearly defined separation pressure rise blending with a pressure 'plateau' and finishing with either a full recovery to the ramp condition or a pressure overshoot with recovery further downstream for hypersonic flows (M $\geqslant$ 5). However, the appearance of these features in fact marks the end of the first stage of development of the cavity. This initial development begins with the incipient separation condition but is extremely difficult to characterize because pressures, heat transfer rates and cavity scale (upstream influence), grow relatively quickly as the ramp angle is increased. Consequently, with the exception of cavity scale, there are few tangible means with which to compare 'developing' cavities, and it is perhaps not surprising that most authors have concentrated their efforts on the 'established' rather than the 'developing' flow.

For the case of fully established separation no theory has yet been developed which can reliably predict both the extent of the interaction as well as the complete pressure distribution. The prospects for predicting heat transfer rates throughout the region are, therefore, even less promising at the moment. However, a number of empirical and semi-empirical correlations have been identified which relate to specific features of the cavity and several authors, e. g. McDonald (1965), Appels (1974/5), have brought these together to give a 'piece-meal' analytical description of the interaction (see Section 2.4). Unfortunately, the success of these methods appears limited to specific sets of experimental data taken from restricted Reynolds number regimes. The critical problem facing researchers, therefore, remains that of determining the position of separation and reattachment for the complete Reynolds number range, given a variety of boundary layer input conditions. Once this can be achieved, construction of the cavity pressure field can be attempted with perhaps greater success, using existing correlations.

Examination of the experimental data available to date indicates that growth and decay of the established turbulent cavity is consistent with the incipient separation trends discussed earlier. Generally it has been observed that when (αi) decreases with increasing $Re\delta L$, for a fixed Mach number and ramp angle, the scale of the cavity, measured in boundary layer thicknesses, is found to increase with an accompanying increase in plateau pressure and overshoot pressure, for hypersonic flows. The converse is found for an increase in αi with increasing $Re\delta L$.

With this strong similarity in behaviour between the incipient condition and the established cavity it is tempting to suggest that the two processes may both be influenced by a common agency residing in the approach stream. However, unlike the incipient separation process, where relatively well defined input conditions usually exist, cavity scale must also be strongly influenced by the rapidly developing turbulent wake within the cavity and the subsequent re-entrainment of the reverse flow. Unfortunately, conditions prevailing in the recirculation region are difficult to extract experimentally. Consequently, whereas some progress in correlating the incipient separation condition has been made by examining the input velocity and Mach number profile (Elfstrom 1971), the equivalent task of establishing the conditions ahead of reattachment has been considerably more difficult. It is important, therefore, to consider previous work which has studied how the flow develops from the separation point and to ascertain, if possible, to what extent any preconditioning of the detached shear layer influences the overall behaviour of the separation region.

Early work by Bogdonoff and his co-workers (1955) indicated that the initial pressure rise in a turbulent boundary layer interaction was independent of the agency provoking separation. Holder et al (1955) later attempted a physical explanation for this and suggested that, since the flow in the vicinity of separation must be in equilibrium, a local thickening of the boundary layer ahead of separation must balance the induced pressure rise. Thus the separation process must be

'self-induced' and independent of downstream conditions. Chapman et al (1958) used similar arguments and introduced the well-known phrase describing the process; "free interaction." Erdos and Pallone (1962) working from these earlier attempts to rationalize the phenomenon developed a semi-empirical correlation which has subsequently stood the test of time and supports some of their earlier claims for its 'universal' applicability. This has the form:

$$F(X) = Cp(Me^2 - 1)^{\frac{1}{4}}/ (2Cfe)^{\frac{1}{2}} \qquad \text{--- (2.1)}$$

Where F(X) is a dimensionless function of the distance from the origin of the interaction and takes the value of 4.22 at separation and 6 in the plateau. Unfortunately, the applicability of the correlation beyond separation has become less clear as more data have become available. Several authors have found that the region downstream of separation is still mildly dependent on the strength of the pressure discontinuity provoking the interaction, (10, 34, 56). This directly conflicts with the 'free interaction' principle, and it is probable that the analysis produced by Erdos and Pallone is invalid beyond the separation point insomuch as the effects of the reverse flow field, stagnating just behind the separation point, are not considered.

Surprisingly, the simple empirical correlation for plateau pressure (Pp) produced by Elfstrom (1972) of the form:

$$Pp/Pinv \sim fn(Me) \qquad \text{--- (2.2)}$$

produces a good collapse of data for a wide range of angles and Mach number. The use of the inviscid uniform flow solution for the ramp recovery pressure (Pinv) implicitly caters for variation in ramp angle. The success of the correlation would suggest that gross plateau conditions are prescribed by local free stream turning rather than the details of the input shear layer.

The plateau free stream Mach number (Mp) also appears to play an important role in determining reattachment pressure. Batham (1969) developed a theory to cover this region based on the earlier free interaction analysis of Erdos and Pallone. He argued that flow turning beneath the reattachment shock system must also be self-induced and primarily governed by local approach conditions, namely, Mp and the Reynolds shear stress

residing near the stagnation streamline. Batham's correlation takes the form,

$$Cpr = K \; (Cf_j / \sqrt{Mp^2 - 1})^{\frac{1}{2}}$$

where K is to be determined from a number of experiments and Cf_j is taken from the range of values suggested by Chow and Korst (1963) for assymptotic mixing layers. In fact, a straightforward plot of Cpr against Mp gives a good collapse of data, and this is further confirmed in the current work.

The success of Batham's theory certainly suggests that free interaction exists at reattachment in well developed flows where the separation pressure rise and the reattachment pressure rise are quite distinct and separated by the plateau. As perhaps expected the shape of the pressure distribution at reattachment is also usually found to be similar to that at separation, adding further weight to the free interaction proposition.

For hypersonic flows, the region beyond reattachment has so far eluded analytical treatment save for the final recovery pressure which usually corresponds closely to the inviscid uniform flow solution for flare or ramp turning. In particular, attempts to predict the magnitude of the pressure overshoot value in hypersonic flows have not been too successful. Many authors have suggested that the overshoot arises from a double compression produced by the separation and reattachment shocks. However, calculations on this basis at Mach 9 by Elfstrom (1971), taking the plateau pressure as indicative of the conditions behind the first shock, generally overpredict the peak pressure, except at high ramp angles. It is possible that the location of the intersection of these two shocks and subsequent expansion and/or compression process immediately downstream, coupled with the effective thickness of the reattaching shear layer (i.e. displacement thickness) are important parameters in this region. If the Mach number and ramp angle are sufficiently high then the full effect of a double compression may reach the ramp surface before an expansion fan can attenuate the compression field. At low Mach numbers (M < 5), and moderate ramp angles, the separation pressure rise has generally been found to blend smoothly with the ramp recovery condition

without an overshoot, indicating perhaps that a consolidated reattachment shock has not yet formed or that the compression and expansion fields have become fully attenuated at the ramp surface.

2.4 CALCULATION METHODS

An early attempt to provide a closed solution to the variety of equations and empirical relationships describing specific parts of the established interaction was undertaken by McDonald (1965). This work followed from various contributions by Chapman, et al (1958), Korst, et al (1959) and later Sanders and Crabtree (1963), and Cooke (1963). McDonald's theory is based on the hypothesis that the reattached velocity profile after recompression is close to an 'equivalent' flat plate profile. Limited experimental evidence from Chapman's results was used to support this hypothesis for a relatively low Mach number flow (M $\sim$ 2.7). Unfortunately, this hypothesis is unlikely to be valid for hypersonic flows having a pressure overshoot. Nevertheless, McDonald's correlation procedure is worthy of note since it provides an indication of the intricacy of this type of calculation.

The object of the calculation procedure is to achieve the appropriate flat plate shape parameter in the post reattachment region by adjusting the position of separation. Values of cavity development length, plateau pressure and reattachment pressure then implicitly emerge from the analysis. Briefly the details of the method are as follows; given the wedge angle, initial Mach number, momentum thickness, and an assumed location for separation.

(i) The pressure rise to separation is predicted using the theoretical relation given by Ray (1962).

(ii) The flow deflection in (i) is then used as the first approximation for the free shear layer deflection and plateau conditions given by Mager's (1956) relationship.

(iii) The plateau free shear layer momentum thickness is then assumed to be close to the value at separation given by the method of Reshotko and Tucker (1955).

(iv) The velocity profile downstream of separation is then predicted using Kirk's (1959) method which assumes the shear layer to be asymptotic and emanating from a false origin with no initial boundary layer. The profile is located spatially using the analysis suggested by Korst et al (1959).

(v) There then follows an elaborate iterative operation which seeks to match the reverse mass flow with the length of stagnation streamline necessary for this reverse mass flow to originate. The locus of the stagnation streamline below which the reverse flow is generated within the mixing layer is initially specified and, following the iteration, this defines a velocity profile at reattachment consistent with the assumption for the location of separation.

(vi) The post-reattachment boundary layer development, in terms of the momentum thickness and shape parameter, is then calculated using the analysis of McDonald (1964). The results are compared with the flat plate prediction for shape parameter given by Maskell's (1951) curve fit to the data of Ludwieg and Tillman (1950), transformed to compressible flow using Mager (1959).

(vii) If the shape parameter is larger than the flat plate prediction the separation point is moved downstream, and vice versus if the shape parameter is smaller.

The method is clearly very complicated. Comparisons with experimental data for cavity scale were found by McDonald to be

very sensitive to the final pressure recovery ratio. With the benefit of hindsight, McDonald's analysis is arguably an attempt to overcome the need for an accurate reattachment criterion insomuch as his 'flat plate' recovery profile hypothesis prescribes the position of separation and implicitly locates reattachment whereupon a crude reattachment model is utilized. The difficulty of establishing a reliable reattachment criterion had previously been dealt with by Nash (1962) who according to McDonald had indicated in unpublished work that his own criterion was not reliable and that reattachment pressure was sensitive to both Mach number and Reynolds number.

$$N = (P_r - P_2)/(P_3 - P_2)$$ where P_r = reattachment pressure
P_2 = plateau pressure
P_3 = recovery pressure

where, according to White (1963), N takes the value of 0.4 for flows in the region Me = 2. Both the results of Nash and White were, however, confirmed by McDonald's analysis and on this basis Appels (1975) chose to retain the value N = 0.4 in a more recent attempt to simplify the problem at much higher Mach number.

Appels' procedure was as follows:

(i)   Assuming the separation position, and knowing the free stream conditions, the separation angle and plateau conditions were calculated using the 'free interaction' theory of Erdos and Pallone.

(ii)   With the knowledge of wedge angle and the conditions in (i) the reattachment angle is calculated. Nash's criterion is then used to determine the reattachment pressure and with the assumption of isentropic turning this prescribes the Mach number and velocity on the dividing streamline ahead of the stagnation point.

(iii) The data in (ii) now specify the boundary conditions for the Chapman and Korst (1955) free shear layer model (also used by Cooke (1963) in a similar analysis). The length of

jet boundary required to achieve the reattachment stagnation condition is then calculated and compared with the initial estimate for the position of separation.

(iv) The analysis proceeds iteratively with the new value for the position of separation. This iteration is only required if the known input conditions are a strong function of the separation position.

Although the details of the post reattachment region are not covered in the analysis it is clear that the calculation of cavity scale can be considerably simplified if accurate information regarding reattachment is available. However, it is doubtful that Nash's criterion is adequate for this task and in the light of Batham's analysis some further consideration of the Reynolds shear stress residing in the vicinity of reattachment is probably needed. This also points to an important deficiency in the Chapman and Korst model which utilizes a classical eddy viscosity relationship in transforming the diffusion equation set up to model the free shear layer. This point is dealt with later in this thesis.

In concluding this survey, it is perhaps sufficient to note that while Appels' and McDonald's analysis may have limited applicability, insomuch as their predicted results only gave moderate agreement for a limited sample of data, they do constitute the first attempts to assemble prior knowledge of the separation process into one coherent analytical tool. Further extensions of this theoretical approach, using the additional data and correlations now available in the literature, have yet to be attempted.

3. EXPERIMENTAL FACILITY AND PROCEDURE

3.1 THE IMPERIAL COLLEGE NO. 2 GUN TUNNEL

A full description of this facility is given by Needham et al (1970). The performance envelope is shown in Figure 2 with the two test conditions indicated. The extent of the uniform flow regime generated by the Mach 9 nozzle is shown in Figure 3. Typical total pressure data measured adjacent to the nozzle throat are shown in Figure 4. The steady running periods are indicated in the figures and these correspond to 3 ms and 5 ms of flow duration for the high and low Reynolds number conditions respectively. Traces were obtained for each run using a Kistler piezoelectric transducer. A real gas correction factor for the measured total pressure values was estimated using the computer program developed by Culotta and Richards (1970). Thermodynamic equilibrium was assumed to have been achieved at the nozzle exit plane and the free stream total temperature for the two operating points was inferred from the reservoir conditions. A complete table of tunnel conditions is given below. Tunnel recalibration tests conducted by Edwards (1976), which included total temperature measurement, have verified the operating conditions given below:

TABLE 1: Tunnel Operating Conditions

Po_∞ N/m^2	P_∞ N/m^2	To deg.K	T_∞ deg.K	M_∞	Re_∞/cm
1.47×10^7 (2125 psia)	7.30×10^2 (0.1059 psia)	1070	63.13	8.93	1.29×10^5
6.56×10^7 (9515 psia)	2.49×10^3 (0.3605 psia)	1070	58.36	9.31	5.17×10^5

TABLE 2: Local Flow Conditions (Cone-Cylinder Forebody, X= 65 cm)

Poe N/m^2	Pe N/m^2	Toe deg.K	Te deg.K	Tw/Te	Me	Re_e/cm
9.24×10^6 (1340 psia)	6.89×10^2 (0.100 psia)	1070	70.8	4.166	8.4	1.12×10^5
4.03×10^7 (5850 psia)	2.48×10^3 (0.360 psia)	1070	67.0	4.403	8.65	4.35×10^5

All experiments required at least two operators in the tunnel control room; one monitoring instrumentation and the other controlling the tunnel pumping sequence. A rigid procedure is required for safe and successful operation of this facility and this is given in reference (70). Typical 'turn-around' times for a single run were 60 minutes and 45 minutes for the high and low Reynolds number conditions respectively. Approximately 500 tunnel runs were required for the present experiments which comprised of ten model builds spread over a period of three years. Each build required about six weeks of tunnel occupancy time of which three were actually available for tunnel operation since parts of the facility are shared by the department low density Nitrogen tunnel.

3.2 SIGNAL CONDITIONING AND DATA ACQUISITION

Analogue signals from the test section were fed to sixteen Fylde operational amplifiers installed in the laboratory signal conditioning unit. The output signals were then processed on different occasions by two separate systems. The surface pressure and heat transfer surveys were predominantly achieved using Tektronix 502A dual-beam oscilloscopes fitted with Polaroid Land cameras and simultaneously triggered. The steady running period on the total pressure record was then matched with each channel response and a line faired through the relevant point on the photograph. A hand calculation then yielded the desired data point. The boundary layer surveys were achieved using a recently installed high speed digital sampling system. Analogue outputs from the operational amplifiers were sampled at 4 MHz (approximately 1000 samples per channel are available for actual data storage) and the signals stored in a 4 x 16K bite core. The system is linked to the department Nova computer and a software package developed by Bartlett (1974) was used to export and import data to the laboratory control room. The response from each channel was systematically checked after each run on a visual display unit (VDU). Essentially the VDU output is identical to the photograph in the former case and Bartlett's program renders the operator free to make an individual decision over which part of the run averaging of the signal should be

made. Results obtained using both systems simultaneously were found to be consistent within ±2% of each other.

3.3 MODEL DESIGN AND SCOPE OF OPERATION

The mechanical design of the three dimensional model evolved from several basic requirements of the experimental programme. Firstly, there was a requirement to generate a separated flow at similar conditions to the work of Coleman and Elfstrom. However, in this case the flow was to be perturbed such that the effects of a transverse pressure gradient and induced cross flow on the separation bubble behaviour could be studied. The two effects as far as possible being isolated by a careful choice of geometry.

As indicated in the introduction, a two dimensional reference model would also be required at the outset and it was important that, as far as possible, this model should generate an identical flow field upstream of both the two and three dimensional interaction regimes.

3.3.1 Design Considerations for Creating a Transverse Pressure Gradient in the Vicinity of Separation

Examination of the data provided by Coleman (1973) suggested that separation is fully established by the cone-cylinder geometry for a flare deflection angle of 35 degrees. Incipient separation was estimated to occur at approximately 30 degrees and a substantial separation zone was produced at 40 degrees. The flare reattachment pressure fields varied considerably over this range and it was considered important to reproduce these conditions locally with the proposed three dimensional models. The solution finally chosen involved tilting a 37.5 degree and a 32.5 degree half-angle flare by 2.5 degrees relative to the cylinder axis. This would provide the required range of local deflection angles in addition to generating a circumferential pressure gradient at reattachment associated with the asymmetry of each flare, see Figure 5. From a series of geometric constructions it was found that the

circumferential cylinder/flare intersection line could be kept almost normal to the free stream flow by carefully controlling the Y-displacement of the flare virtual apex from the cylinder axis. In fact, less than 0.025 cm variation in the X-dimensional location of the intersection line was ultimately achieved around the cylinder circumference during manufacture. Since the plane of the intersection line between the cylinder and flare was virtually normal to the undisturbed flow it could be assumed that the resulting interaction would be predominantly influenced by a circumferential variation in reattachment surface geometry with an accompanying local transverse gradient in the pressure recovery region of the flare. The starting processes within the developing cavity around the circumference would be similar to the axisymmetric case insomuch as adjacent streamlines should approach the interaction at the same instance. The influence of cross flow, if any, would in principal be delayed until the shear layer had entered the transverse pressure gradient developing well into the flare pressure recovery region. The constructions resulted in geometries A and B, Figure 5.

3.3.2 Design Considerations for Inducing Cross Flow in the Vicinity of Separation

A large number of model permutations were available for this task once the two principal geometries in section 3.3.1 had been chosen. It was decided to restrict this case to a geometry having a circumferentially uniform local deflection angle of 35 degrees since this angle was common to the two previous cases. By marginally displacing the axis of a 35 degree half-angle flare parallel to the cylinder axis a tilted intersection plane between the flare and cylinder can be achieved (geometry C, Figure 5). Since the axes of the cylinder and flare remain parallel a constant local deflection angle of 35 degrees is maintained around the cylinder circumference. In principle, the circumferential pressure gradient induced by the geometry should be zero but adjacent streamlines should reach the flare intersection line at different instances causing a cross flow velocity component to develop locally. By virtue of the three dimensional nature of the intersection line this effect would be strongest at the

$\emptyset$ = ± 90 deg. locations where a maximum slope of 8 degrees would result. At $\emptyset$ = 0 and 180 degrees the intersection line is normal to the free stream and this slope is zero. However, for an attached flow passing over the geometry, surface streamlines on the flare would be expected to diverge at $\emptyset$ = 0 and converge at $\emptyset$ = 180 deg. Some of these features can be deduced from the side elevation of the model shown in Figure 5 where it can also be seen that the meridianal intersection points at $\emptyset$ = 0 and 180 degrees are displaced with respect to the X-axis.

Unfortunately, with this model arrangement, adjacent streamlines arriving at the intersection line would undergo differing levels of cross-flow inducement, depending on their circumferential position. This was unavoidable. However, since the local deflection angle was constant around the circumference, it was concluded that the resulting cavity flow should be predominantly influenced by large transverse mass fluxes within the separation bubble, accompanied by a relatively small transverse pressure gradient. This flow should therefore exhibit features governed more strongly by the internal mixing dynamics of the separation bubble in contrast with the flows developed by geometries A and B where a strong circumferential pressure gradient could be expected to dominate interaction with the local free stream in the vicinity of the cavity.

3.3.3 Model Geometric Anomalies

It is necessary to point out that in all three geometries (A, B and C) the surface deflection angle at the flare inter-section line prescribed by the flare half-angle, and/or axis tilt, effectively decays downstream of this position on the model relative to an equivalent axisymmetric conical flow experiencing the same initial deflection. This is purely a consequence of model asymmetry and can, perhaps, be visualized more easily for the extreme case of geometries A and B where the flare axis is notionally put at 90 degrees to the cylinder axis, or alternatively, the flare is displaced by as much as one cylinder diameter below the cylinder axis, in the case of geometry C. The effect will be small for the present geometries, i.e. less than 1/2 degree over the entire length of the flares, and will

occur at all values of $\emptyset$ except 0 and 180 degrees. At these locations the free stream flow vector lies in the same plane of symmetry as the flare axis and surface streamlines will experience a constant deflection angle as they pass over the model. In practice, due to the relatively small cavity flows developed in the current study (i.e. less than 25% of the flare slant height), the reattachment angles experienced by the local free stream between the two meridians will not vary significantly from those prescribed by the geometry at the intersection line.

3.3.4 Instrumentation Constraints

Having arrived at the three basic configurations, it became clear that a hollow cylinder forebody could not be employed. Although this would have provided an expansion free shear layer ahead of the interaction, this would have required each cylinder and flare assembly to be heavily instrumented.

The problem arises because the intrinsic coordinate systems of the cylinder and flare are not aligned. This leads to a rather complicated situation. For instance, if it is desired to study the cavity flow at a fixed value of $\emptyset$ and local deflection angle, the full instrumentation density must be achieved along the x-coordinate at that specific physical location on the model. Lines of instrumentation set at different values of $\emptyset$ will, of course, be sensing conditions prescribed at a different local deflection angle. Hence the method of rotating adjacent lines of flare instrumentation about the cylinder axis to achieve a dense instrumentation pitching at one particular value of $\emptyset$, as for axisymmetric geometries, would not be possible in this case.

The problem was overcome by splitting the experimental programme into two main sections. The first was to be comprised of flare measurements; achieved by rotating each flare about its own axis, thus bringing adjacent lines of instrumentation into play at a fixed value of $\emptyset$ and local deflection angle. The second was to be comprised of a corresponding series of cylinder measurements; achieved by rotating a set of 'dummy' flares about the cylinder axis. The

entire circumference of the geometries could now be fully investigated with just a few lines of instrumentation fitted to each of three flares and one cylinder. Unfortunately the instrumented flare assemblies would require a strong and closely toleranced coupling at the cylinder/flare interface. Consequently the engineering solution precluded flow within the cylinder forebody and the solid cone-cylinder geometry used by Coleman was subsequently chosen as the most suitable configuration.

For the heat transfer experiments a single instrumentation module was designed which could be mounted in any of the three instrumented flares. The module was constrained to slide parallel to the flare slant height and a vernier screw arrangement permitted small increments of the surface to be traversed in stages. Although the flare half-angles were different in each case a single 'compromise' profile for the module surface was eventually found which gave less than 0.0025 cm surface imperfection over the maximum travel of the unit (0.75 cm).

A removable module was also designed for the cylinder heat transfer instrumentation. After some early experimental difficulties a similar instrumentation module was developed for the cylinder pressure transducers. This had the advantage of allowing the transducers to be mounted with very short pipe runs within the cylinder body.

The following sets of models were therefore required to fully investigate the three basic geometries:

     (i)   One nose cone (10 degrees half angle, after Coleman)

    (ii)   Two cylinder forebodies, one allowing flare rotation about the cylinder axis and instrumented, the other allowing flares to rotate about their own axes and uninstrumented. (This latter configuration required three cylinder subassemblies to provide a profiled and gas-tight rotating seal for the three instrumented flares.)

(iii)   6 flares, 3 rotating about the cylin-
der axis and uninstrumented, 3
rotating about their own axes and
instrumented, each 3 corresponding
to geometries A, B and C.

Details of the flare mountings and instrumentation layouts
are shown in Figures 6 and 7 which have been sketched from
two out of several engineering drawings produced by the author
for the department workshops. The models were stressed to
give over a factor of two in safety under the worst possible
tunnel starting conditions. These were deemed to be the result
of a full pressure recovery behind a normal shock propagating
on one side of the model partitioned by the $\emptyset = 0 - 180°$ plane of
symmetry. This is the plane of least stiffness for the complete
model and tunnel test section mounting frame.

3.3.4   Axisymmetric Reference Model

The axisymmetric reference experiments were performed
using models previously employed by Coleman. Some modifica-
tions to the flare mounting fixtures were required but it is
important to state that the forebody geometry was identical for
both the two dimensional and three dimensional experiments.
Overall dimensions of the No. 2 Tunnel and typical model layout
are given in Figure 8. Views of some of the finished machined
asymmetric and axisymmetric model subassemblies are shown in
the photograph, Figure 9.

3.4   INSTRUMENTATION

3.4.1   Static Pressure

It can be seen from the data (Section 5 and 6) and
Figures 6 and 7 that the surface pressure investigation covered
the region bounded by the beginning of the interaction and the
relaxation to an otherwise undisturbed pressure recovery on the
flare. For the three dimensional experiments, tappings on the
cylinder were arranged such that a composite pitch of 4 holes/cm

could be achieved by displacing the flare intersection line in the x-direction by up to 0.5 cm (i.e. less than 0.8% of the undisturbed boundary layer run). For the axisymmetric experiments a similar pitching could be achieved with Coleman's model by rotating the cylinder to adjacent rows. Three rows were fitted to the instrumented flares to give the same pitch. Copper tube (0.24 cm, I.D.) was used and connected via Esco silicon rubber tubes (0.15 cm I.D.) to 0 - 75 psia and 0 - 5 psia Solatron and Statham bonded strain gauge transducers. After some early experimental difficulties modification of the cylinder pipe runs was found necessary owing to the extremely low pressures encountered during the low Reynolds number investigations, (i.e. as low as 0.09 psia). Ultimately, reliable readings were achieved in the cavity region by installing the transducers close to the measuring station inside the cylinder (Figure 6), although even here the accuracy of data taken ahead of the interaction in the undisturbed boundary layer was difficult to gauge.

3.4.2 Pitot Pressure

The pitot specification for these tests arose from the work conducted by Bartlett (1975). Figure 10 gives details of one of the two probe assemblies used. Each rake contained 20 probes and was designed to investigate the entire circumference of the cylinder. The support flare half angle (α = 20 deg.) was set well below the incipient separation angle (α = 30 deg.) established by Coleman for the 65 cm station. As a further measure to avoid the effects of upstream influence the probes were set well forward of the flare intersection line. Stiffening of the extended tubes was therefore considered necessary. A complete assembly is shown in operation in Figure 10 which is a synchronous Schlieren/flash exposure. Further Schlieren pictures, taken at four of the six possible combinations of tunnel condition and station, confirmed that the pitot heads were well in front of the disturbance propagated by the rake support. (The most forward station was upstream of the nozzle exit plane and could not be photographed). Probe heights were fixed during manufacture but were systematically checked using an especially adapted micrometer incorporating an electronic contact indicator

mounted on a machined V-block which could be accurately held down on the cylinder surface.

3.4.3 Heat Transfer

Throughout the entire duration of this experimental programme heat transfer instrumentation for high speed applications was undergoing development. Thin film Platinum resistance thermometers mounted on formed Pyrex, used previously by Coleman amongst others, were considered unsuitable in view of the strong tendency for the Pyrex slab to lift proud of the model surface. For the three dimensional experiments, where local gradients in heat transfer were likely to be functions of both the (X) and ($\emptyset$) co-ordinates, this simple arrangement was felt inadequate. The method finally chosen by the author involved the manufacture of a mild-steel jig into which 35 quartz beads could be individually mounted. These beads were ground and polished as shown in Figure 7 from 0.3 cm quartz rod. The jig assembly was then mounted in a vacuum sputtering chamber and a 3 micron film of Platinum deposited over a region measuring 0.3 cm x 0.03 cm on the top face. This process was carried out by the Department of Electrical Engineering at Imperial College. Wire leads were then soldered to the sputtered beads under a microscope and the final element was subsequently potted in the instrumentation module using an epoxy-resin for insulation. Resistance tests were performed at each stage of manufacture and the failure rate was disappointingly high ($\sim$50%). Nevertheless, once mounted, the complete unit was found to give good service under highly abrasive conditions. A typical increase in film resistance before and after completing a series of tunnel experiments was less than 1% of the starting value. The theory and operation of thin film heat transfer gauges is given by Schultz and Jones (1973). The signal output from these gauges was processed using a series of electrical analogue circuits available in the tunnel data conditioning unit.

3.4.4 Flow Visualisation

The test facility incorporates a single pass Schlieren

system with an optical path of approximately 50 metres (due to unusually cramped conditions). Consequently, this system tends to produce photographs with a grainy texture in regions of undisturbed flow due to convection currents outside the chamber. The argon spark light source is triggered from a transducer placed close to the piston starting position in the barrel. A record of the trigger pulse was collected on the same Polaroid photograph as the total pressure signal thus ensuring that the Schlieren photo and data corresponded exactly. The exposure time (or spark discharge time) was measured using a photo-electric diode circuit in a single test made early in the series and was found to have an effective duration of 1 microsecond. Assuming an average tunnel free stream velocity of 1400 m/s, this system was therefore able to resolve the passage of large density fluctuations to within 1.5 mm. This was found adequate to resolve some of the finer details of the interaction shock system as can be seen in the photographs, Figures 11 to 12 and 60 to 77.

4. RESULTS AND DISCUSSION OF THE AXISYMMETRIC TURBULENT BOUNDARY LAYER STUDY

4.1 PREDICTED FLOW FIELD AND EXPERIMENTAL COMPARISONS

A computer program based on the method of rotational characteristics, (Pullin 1974), was employed to obtain a prediction of the forebody flow field at $M\infty = 9.31$. The results are shown in Figures 13, 14 and 15. The first disturbance from the cone shoulder expansion fan interacts with the bow shock wave after an axial run of 28 cms. The interaction generates a region of rotational flow some distance outboard of the cylinder surface. The boundary of the rotational layer relaxes slightly toward the cylinder surface as the flare intersection line (X = 65 cm) is approached. The region is characterised by radial gradients of total pressure, Poe and entropy. This is distinct from the boundary layer in the real flow, and it is important to assess its likely effect upon the experimental flare pressure field. Figure 15 shows the predicted variation of Poe with radial position at X = 65 cm. The result indicates that the slip-stream effect from the bow shock may be of significance for the highest flare angle, ($\alpha = 40$) where the reattachment pressure field may not have relaxed fully before streamlines from this region intersect the flare. The flare surface' and position of ($\hat{P}$) for the extreme case in the present experiments is included in the Figure to clarify this point.

The forebody static pressure distribution, which was measured by Coleman, is compared with the theoretical result in Figure 14. The agreement is good with little change in pressure for the final 30 cm of boundary layer development up to the location of the flare intersection line. In the vicinity of the cone shoulder Figure 13 indicates that a strong radial static pressure gradient should exist outboard of the cylinder. Moderate surface pressure gradients are evident in Coleman's experimental results for the same location. The experimental results are obviously connected with a viscous interaction between the boundary layer and free stream as the flow adjusts from conical to axisymmetric flow downstream of the shoulder.

Both the theoretical and experimental results for this region suggest that it is important to consider the cumulative effect of forebody geometry on the boundary layer developed in these experiments, particularly with respect to transition behaviour. This is discussed further in the next section.

4.2   TRANSITION

Natural transition was chosen in order to maintain some degree of compatibility with the experiments of Coleman and Elfstrom and to avoid the possibility of anomalous effects which can sometimes arise with tripped hypersonic flows where development lengths are inadequate. The location of transition was investigated using the surface pitot method outlined by Richards and Stollery (1966). The results are shown in Figure 16 (a). The corresponding heat transfer distribution obtained by Coleman for the high unit Reynolds number tunnel condition is shown in Figure 16 (b).

For $Re_\infty/cm = 5.17 \times 10^5$ the heat transfer distribution is fairly constant and the surface pitot pressure is relaxing over the entire length of the cylinder, indicating that transition has occurred before the cone shoulder. The results for $Re_\infty/cm = 1.29 \times 10^5$ are quite different and exhibit a steep rise in pitot pressure characteristic of a transitional boundary layer. The transition Reynolds numbers are given in Table 3 which is a summary of data obtained from the Imperial College No. 2 tunnel, to date. The parameters are defined in Figure 16 (a).

TABLE 3: Transition Data from the No. 2 Gun Tunnel				
Author	Model Type	M_∞	Re_∞/cm $\times 10^{-5}$	$Re\Delta x_{tr}$ $\times 10^{-6}$	Rex_{tr} $\times 10^{-6}$
Elfstrom	Flat Plate	8.93	1.29	1.8	4.1
"	"	9.31	5.17	6.3	13.8
Coleman	"	8.93	1.29	2.2	5.0
"	"	9.31	5.17	7.1	14.1
"	Hollow	8.93	1.29	3.6	6.2
"	Cylinder	9.31	5.17	9.4	19.3
Experiment*	Cone	8.93	1.29	3.9	6.7
"	Cylinder	9.31	5.17	$\leqslant 7.4$	$\ll 7.4$

*Note: These data are based on conditions downstream of the cone shoulder.

The shrouded model tests of Pate and Schuler (1969) have confirmed that the location of transition can be strongly influenced by nozzle wall acoustic radiation resulting in a spurious unit Reynolds number trend. It is believed that the radiation field becomes focused on the model geometry and boundary layer, triggering premature instabilities. The position of transition is then dependent on the intersection of the Mach cone originating from the nozzle transition plane. For constant Mach number in the free stream, but varying nozzle transition location, (i.e. varying unit Reynolds number), a false Reynolds number trend can be imposed on the model transition regime. It is probable that the results in Table 3 have all come from flows enveloped in radiation field and accurate quantitative comparisons between the three different geometries are difficult to make. It should be mentioned that during the present experiments the model support was placed within 0.5 cm of Coleman's original position. The heat transfer and surface pitot distributions for the high unit Reynolds number are therefore considered mutually compatible.

With the above comments in mind, and considering say, the high unit Reynolds number condition, the hollow cylinder transition Reynolds number (Rex_{tr}) obtained by Coleman is perceptibly higher than the flat plate value. Coleman suggested that this increase was in agreement with the analysis of Probestein and Elliot (1956) who concluded that the shear stress derivative in the transformed momentum equation, which embodies the effects of transverse curvature, behaves like an external favourable pressure gradient. The inference being that transition will be delayed on axisymmetric bodies. Eckert (1952) concluded that transverse curvature effects only became appreciable when δ/R approaches unity. The present results, and those of Coleman, were obtained for δ/R in the region of 0.3. The effects of axisymmetry on the cylinder should therefore be weak although a 37% increase in Rex_{tr} is evident in the above comparison. The possibility of anomalous effects due to nozzle acoustic radiation cannot therefore be ruled out as a contributing factor in this difference.

It is interesting to note that the data for the flat plate and hollow cylinder geometries in Table 3 exhibit strong unit Reynolds number trends for the parameter Rex_{tr} whereas for the cone cylinder geometry they do not. In this case, at $Re\infty/cm$ = 1.29×10^5 the value of Rex_{tr} is similar to the hollow cylinder result but it is clear from Figure 16 that transition is barely completed at the flare intersection line and the boundary layer has physically taken longer to develop. Increasing $Re\infty/cm$ to 5.17×10^5 failed to produce an increase in Rex_{tr}. Instead, rapid development has occurred over the nose cone giving rise to an even lower value of Rex_{tr} compared with the flat plate. The subsequent run of post transitional flow is increased by over 200%. The state of the boundary layer reaching the flare intersection line in the current experiments therefore covers a wider range of development than was experienced by Coleman and Elfstrom using the same tunnel conditions.

Evidently, changes in unit Reynolds number can have an uncharacteristic influence on cone-cylinder transition behaviour. The reason for this is probably connected with the location of transition relative to the cone shoulder. Transition before the shoulder will be influenced by: -

    i)   Concave streamline curvature

   ii)   Lateral divergence

 iii)   Compression

Whereas transition after the shoulder will be influenced by:

   iv)   Convex streamline curvature

    v)   Lateral convergence

   vi)   Expansion

Bradshaw (1972) has classified these effects as "extra rates of strain" and from empirical studies concluded that the effects of mean compression on the Reynolds stresses, in particular, are unexpectedly large under such conditions and must therefore be taken into consideration along with the effects of streamline curvature and lateral divergence. He concludes that the conditions i) to iii) increase turbulence intensity and iv) to vi) reduce or "freeze" the turbulent field. The results obtained by

Rose (1973) for a shock wave boundary layer interaction certainly suggest that the maximum Reynolds shear stress is significantly increased under the influence of mean compression. Conversely, Page and Sernas (1970) have observed the apparent suppression of turbulence in a Prandtl-Meyer expansion. Evidence for the additional effects of streamline curvature and divergence is confused, at present, and the quantitative influence of "extra strain" in turbulent fields continues to be the subject of current research in low speed flows.

These observations indicate that the cone-cylinder transition behaviour is far more complicated than the equivalent flat plate and hollow cylinder case. The possibility of anomalous effects on transition due to changes in unit Reynolds number is, in these experiments, compounded by even greater influences arising from model geometry. However, it is clear from the experimental results that the boundary layer entering the flare pressure field at the low unit Reynolds number is just post transitional and the turbulence structure is therefore likely to be underdeveloped; whereas at the high unit Reynolds number, a considerable run of post transitional flow is achieved. These conclusions are further supported by the results of several boundary layer surveys performed on the cone-cylinder geometry.

4.3 BOUNDARY LAYER SURVEYS

Six pitot pressure profiles, three at each tunnel condition, were obtained using the probe assembly described in Section 3.4.2 The measuring stations were set at regular axial intervals of 25 cm with the final position set at the flare intersection line (flare removed). The Rayleigh pitot formula was used, along with the usual assumption of constant static pressure across the boundary layer, to calculate Mach number profiles. Velocity profiles were obtained using the linear Crocco relation for the temperature distribution given below.

$$\frac{T}{Te} = 1 + r.\frac{(\gamma-1)Me^2}{2} \cdot \left[1 - \left(\frac{u}{ue}\right)^2\right] + \frac{Tw - Tr}{Te}\left[1 - \frac{u}{ue}\right] \text{---(4.1)}$$

where $\frac{Tr}{Te} = 1 + r.\frac{(\gamma-1)}{2} Me^2$ and $r = 0.89$

also $\frac{u}{ue} = \frac{M}{Me} \cdot \frac{a}{a_e} = \frac{M}{Me}\left[\frac{T}{Te}\right]^{1/2}$ $\qquad$ ---(4.2)

By substituting (4.2) in equation (4.1) a quadratic in $(T/Te)^{\frac{1}{2}}$ is obtained the solution of which can then be used in equation (4.2) to yield u/ue. The method therefore follows the standard two dimensional approach, in the absence of measured total temperature profiles. Probestein and Elliott (1956) demonstrated that the Crocco Integral, for unity Prandtl number and zero pressure gradient in laminar boundary layers, is also valid for all δ/R in axisymmetric flows. As with the two dimensional case, substitution of the temporal mean values of the turbulent flow derivatives extends the validity of this integral to turbulent boundary layers, with an appropriate choice of recovery factor. Without specific knowledge of the turbulent Prandtl number distribution for these experiments the commonly accepted recovery factor for two dimensional flow has been used. Calculation errors in the velocity profiles due to axisymmetric effects may therefore exist due to an incomplete knowledge of the Reynolds stress behaviour under transverse curvature. It is also acknowledged that the boundary layers developed in these experiments may suffer from a history of pressure gradient effects developed over the nose cone. The use of the linear Crocco relationship may therefore be inappropriate for those profiles taken close to the nozzle shoulder, at x = 25 cm.

The results are shown in Figure 17 through to Figure 22. The method used to calculate (δL) is shown in Figure 23 which also includes a comparison of data obtained by Coleman and Elfstrom. It can be seen that the estimated error for δL is quite high, typically two probe heights or 0.1δ at x = 65 cm. The quality of the data is disappointing, particularly in view of the additional probe development work which was undertaken to improve on the results obtained by Elfstrom.

Initially, it was thought that the experimental scatter may have been due to a 'repeatable' flow asymmetry compounded by the use of a circumferential array of pitot tubes. However, an extensive re-examination of each station, by monitoring five equispaced probes simultaneously, gave no indicating of 'repeatable' (or persistent) asymmetry in the flow. The additional data points tended, if anything, to enlarge on an

already perplexing state of affairs leading to a distinctly random spread of data towards the outer reaches of the boundary layers. In this region, in particular, pitot pressures varied considerably on a run to run basis, regardless of any given probe or position. Curiously, the experimental scatter in the outer regions also appears to get worse towards the rear of the model. It should be added that the quality of the unprocessed analogue signals obtained in the outer region was consistent with that obtained closer to the cylinder wall. Consequently, it was not possible to discriminate on the basis of uncharacteristic pressure fluctuations during the prescribed steady running period. Moreover, the data are normalized with the measured reservoir pressure (Po) and run to run variations should therefore be largely accounted for.

Unfortunately no satisfactory explanation for the experimental scatter has yet been found. However, it may be relevant to note that the data obtained by Bartlett et al (1979) in the same facility, but using a flat plate model, exhibit the same tendencies although to a lesser extent. The probe specification for Bartlett's experiments was similar to that used here but there is no evidence, to date, to suggest a fault in the design. In view of the good quality of the unprocessed signals, and the tendency for steady state readings taken from individual probes to vary on a run to run basis, it is conceivable that random asymmetry may be present in the test flow core. Such a situation could be visualized if transition did not always occur symmetrically around the nozzle wall from one run to the next. For the reason stated in Section 4.1.2 this would also lead to variations in the location of transition on the model in both the axial and circumferential sense. The integrated effect of test core asymmetry on the bow shock system, coupled with the use of a circumferential array of measurement probes, would certainly be expected to cause large differences in pitot pressure around the model. For instance, at a nominal free stream condition of $M\infty = 9.3$ and $Po = 9500$ psia, a one degree positive variation in mean flow direction would be sufficient to cause over a 20% reduction in total pressure behind the bow shock. This, in turn, would result in a similar reduction in the pitot

measurement downstream. Put crudely, this could amount to a 40% difference in reading between two diametrically opposed probes during a given run. In fact, less than half of this flow deflection (i.e. ½ degree) would be sufficient to account for the experimental scatter in the current results. This suggestion is also compatible with Bartlett's observations since, for the flat plate configuration, the leading edge shock is considerably weaker and the integrated effects of asymmetry on the total pressure behind this disturbance would also be significantly smaller. Moreover, Bartlett's pitot rake would have been inherently insensitive to the cumulative error to be expected with a circumferential rake, since his instrumentation lay at the center of the plate and virtually in one plane of symmetry. It is important to state that pitot probes are, themselves, relatively insensitive to flow asymmetry. The effect discussed here results from the non-linear behaviour of total pressure behind varying strengths of oblique shock.

The main difficulty with the above suggestion is the fact that the unprocessed signals gave no hint of unsteadiness in the test core. This would suggest that any minor deflections in the flow remained relatively stable during a given run. This is rather difficult to imagine if one considers that nearly twenty nozzle exit diameters of test-core flow past the model during the five milliseconds steady running period. Hence, apart from these rather speculative suggestions the problem really remains a mystery and clearly needs further experimentation and analysis.

In spite of the experimental error, the effect of the radial pressure gradient predicted earlier for the shoulder region (Figure 13) is clearly evident in the pitot results for $x = 25$ cm and $y > 0.5$ cm in Figures 17 and 20. Here, the rise in static pressure through the expansion fan produces an increase in pitot pressure even though there is no predicted gradient in total pressure for these values of (R). The results for $x = 45$ and 65 cm are predicted to be in a region of weak normal pressure gradient, i.e.

$(Pe - Pw)/Pw < 2\%$ (Section 4.1.1)

and the usual boundary layer assumptions are considered fully justified at these stations. For the velocity profiles shown in Figure 19 and 22 the effects of the radial pressure gradient at x = 25 cm are masked by the square rooting of the Mach number and temperature terms in the Crocco relation. This process also tends to obscure the experimental scatter as can be seen by comparing the remaining profiles with their pitot pressure counterparts.

Velocity profile development trends are shown in Figure 24 where differences in profile shape can be identified. The low Reynolds number results are developing in a non-similar fashion toward the flare intersection line, consistent with the evidence of transition, whereas the high Reynolds number profiles exhibit similarity, indicative of post transitional behaviour. A direct comparison made at the intersection line (Figure 25) indicates that the transitional profile is marginally fuller.

Hopkins et al (1970) found that the Van Driest (1951) function yielded the best transformation of nonadiabatic wall velocity profiles to the equivalent incompressible values. The function is shown below along with the equation for the Law of the Wall and Wake (Coles 1956).

VAN DRIEST II

$$\frac{\bar{u}}{u_\tau} = \frac{1}{D\left(\frac{Cfe}{2} \cdot \frac{Tw}{Te}\right)^{\frac{1}{2}}} \quad Sin^{-1}\left[\frac{2D^2 U/Ue - E}{(E^2 + 4D^2)^{\frac{1}{2}}}\right] + Sin^{-1}\left[\frac{E}{(E^2 + 4D^2)^{\frac{1}{2}}}\right]$$

$$\text{where } D = \left[(0.2)Me^2 \cdot \frac{Te}{Tw}\right]^{\frac{1}{2}}$$

$$E = \frac{Te}{Tw} + D^2 - 1$$

---(4.3)

COLES

$$\frac{\bar{u}}{u_\tau} = \frac{1}{Ki} \ln \bar{R} (Y/\delta) + Bi + \frac{\pi}{Ki} w(Y/\delta)$$

---(4.4)

where Ki = 0.41, Bi = 5.0

The wake function (w) has been approximated following the method of Alber and Coats (1969):

$$W(Y/\delta) = 1 - Cos\pi (Y/\delta)$$

The experimental and theoretical results are compared in Figure 26. Smoothed data have been used in order to clarify the development of the wake region. The theoretical values of π were taken from the tabulation given by Coles (1956). The flat plate result, recently obtained by Bartlett (1979), is also shown for comparison.

Differences between the flat plate and axisymmetric profiles at Reθ = 11300 and 13000 respectively, are apparent with the latter distribution exhibiting a slightly more advanced state of development in the wake region. However, apart from this the two profiles are quite similar. The low Reynolds number distribution is clearly in a much earlier state of development and does not exhibit a wake region of any significance.

Perhaps the most striking aspect of these profiles is the fact that they are all extremely underdeveloped compared with low speed results at similar length Reynolds numbers. This has been a frequent observation in high speed experiments and is generally believed to be the result of the trend toward high transition Reynolds numbers at hypersonic conditions. As discussed in Section 2, the delay in hypersonic transition is thought to be connected with high wall recovery temperatures and an increased turbulence damping effect close to the wall, (i.e. high μ, low ρ), in comparison with the free stream conditions.

4.4 BOUNDARY LAYER PARAMETERS

Numerical integration of the raw data proved difficult due to the experimental scatter. Instead, the trapezoidal rule was applied to a locus manually faired through the experimental results. The integral parameters for the six profiles were then obtained using the simplified formula for axisymmetric flows where $0.01 < \delta / Rc < 1.0$, namely:

$$\delta^* + \delta^{*2} / 2Rc = \int_0^\delta (1 - \rho U / \rho e Ue)(1 + Y/Rc)\, dy \qquad \text{---(4.5)}$$

$$\theta + \theta^2 / 2Rc = \int_0^\delta \frac{\rho U}{\rho e Ue} (1 - U/Ue)(1 + Y/Rc)\, dy. \qquad \text{---(4.6)}$$

$$E + E^2 / 2Rc = \int_0^\delta (\rho U / \rho e Ue)\left[(1 - U^2/Ue^2)(1 + Y/Rc)\right] dy \qquad \text{---(4.7)}$$

where Rc is the cylinder radius, δ^* the displacement thickness, θ the momentum defect thickness, E the kinetic energy defect thickness and δ the local boundary layer height.

The results are shown in Table 4 and are mapped in Figure 27 where it can be seen that the lower Reynolds number parameters are developing more rapidly between x = 45 cm and 65 cm.

TABLE 4:   Boundary Layer Integral Parameters

Re_∞ /cm x 10^{-5}	X(cm)	δ^*(cm)	θ (cm)	E (cm)	δ^*/θ
1.29	25	0.228	9.5×10^{-3}	0.016	24 (result suspect)
	45	0.302	0.016	0.029	18.9
	63.6	0.528	0.029	0.054	18.2
5.17	25	0.279	0.015	0.027	18.6
	45	0.387	0.020	0.036	19.35
	65	0.518	0.030	0.055	17.27

Surprisingly the thicknesses at the intersection line (x = 63.6, and 65 cm, flare removed) are virtually identical within the experimental accuracy. This somewhat unexpected result suggested that further examination of the profiles entering the interaction was needed to bring out any important differences in detail.

Evidence of structural differences between the two sets of profiles was ultimately obtained by plotting power law exponent trends against momentum thickness Reynolds number. The exponent (N) in the relation:

$$y/\delta = (u/ue)^{1/N}$$

was obtained by fitting a straight line to a logarithmic plot of the smoothed data and measuring the slope. The results are shown in Figure 28. The characteristic overshoot in (N), noted by Johnson and Bushnell (1970), amongst others, as a feature of transitional flows, is clearly evident for low values of $Re\theta$. The value for x = 25 cm and $Re\infty$ /cm = 1.29 x 10^5 is, however,

inconsistent with the general trend and probe wall interference may be the cause of this discrepancy. This may also explain the high value of shape parameter calculated for this profile in Table 4. It is interesting to note the wide range in $Re\theta$ generated by the cone-cylinder geometry. As noted in Section 4.1.2 this is probably a consequence of the relatively accelerated and delayed transition trends noted for this geometry at the two tunnel conditions, when compared with the flat plate and hollow cylinder results of Elfstrom and Coleman.

4.5 SKIN FRICTION

The skin friction values in equation 4.3 were calculated from measured Stanton numbers where

$$St = \dot{q}/(\rho eUe (Hr - Hw)) \text{ and } 2St/Cfe = 1.16$$

The choice of Reynolds analogy factor above is consistent with the recommendations of Chi and Spalding (1966) and was made in the absence of any conclusive evidence for a more suitable value under high Mach number, cold wall conditions. Table 5 lists the skin friction results from the cone-cylinder experiments and also includes recalculated estimates of Cfe from Coleman's flat plate and hollow cylinder heat transfer experiments, using the same Reynolds analogy factor.

TABLE 5: Skin Friction Coefficients At Wedge/Flare Intersection Line					
Model	Conditions			Station cm	Cfe
	$Me(\infty)$	$Re_e(\infty)/cm$ $\times 10^{-5}$	$Re\theta$ $\times 10^{-3}$		$\times 10^4$
Flat Plate (Coleman)	9.31	5.17	4.65	42.7	7.40
Hollow Cyl (Coleman)	9.31	5.17	3.86	45.7	6.78
Hollow Cyl (Coleman) (forced transition)	8.93	1.29	2.68	45.7	7.85
Cone Cyl. (exp.)	8.65	4.35	13.05	65.0	5.41
Cone Cyl. (exp.)	8.40	1.12	3.25	63.6	6.60

The momentum thickness Reynolds numbers for Coleman's data

above were computed from the relation:

$$\Gamma = \theta \left(\frac{2St}{Cf}\right) \cdot \frac{(Hr - Hw)}{(He - Hw)}$$

$$\qquad\qquad ---(4.8)$$

(assuming $\frac{2St}{Cf} = 1.16$)

where values for Γ were computed by Coleman from the energy integral relationship:

$$\Gamma = \int_{o}^{x} \frac{\dot{q}w(x) \; R^{\varepsilon}(x) \; dx}{\rho e Ue (Hw-He) R_{x}^{\varepsilon}} \qquad\qquad ---(4.9)$$

Where R = body radius.

Note:

$\varepsilon = 0$ for flat plate flows.

$\varepsilon = 1$ for axisymmetric and conical flows.

Hopkins and Inouye (1971) undertook a fairly extensive evaluation of theories for predicting turbulent skin friction and heat transfer in compressible flows. They concluded that the Van Driest II (1956) theory provided the best agreement of cold wall flat plate data with established incompressible theory. They based their comparisons on the transformed momentum thickness Reynolds number ($Re\theta$) in order to avoid discrepancies arising from an incorrect (or judicious) choice of turbulent boundary layer origin. The same procedure has been adopted here for the data given in Table 5 and the results are shown in Figure 29.

In this analysis values of $\overline{Re}\theta$ were computed from

$$\overline{Re}\,\theta = F\theta \; Re\theta$$

and $\qquad \overline{Cf}e = Fc \; Cfe$

where $F\theta$ and Fc are the Van Driest transformation functions given by:

$$F\theta = \mu e/\mu w = (Te/Tw)^{.76} \qquad\qquad ---(4.10)$$

$$Fc = 0.2r \; Me^{2}/(Sin^{-1}\alpha + Sin^{-1}\beta) \qquad ---(4.11)$$

where $\alpha = (2A^2 - B)/(4A^2 + B^2)^{\frac{1}{2}}$

$\beta = B/(4A^2 + B^2)^{\frac{1}{2}}$

$A = (0.2r\ Me^2/F)^{\frac{1}{2}}$

$B = (1 + 0.2r\ Me^2 - F)/F$

$F = Tw/Te$

The data in Figure 29 are compared with the Kárman-Schoenherr incompressible skin friction prediction given below:

$$1/\overline{Cfe} = 17.08\ (\log_{10}\ \overline{Re}\theta\ )^2 + 25.11\ (\log_{10}\ \overline{Re}\theta\ ) + 6.012$$

$$\text{---}(4.12)$$

This equation has been verified by several authors (including Locke (1952) using direct skin friction measurements) and is believed to be accurate within $\pm$ 5% in the range $4 \times 10^5 < \overline{Re}x < 5 \times 10^8$.

It is important to note that these comparisons are highly sensitive to the choice of Reynolds analogy factor. Nevertheless, it can be seen that the flat plate result falls very close to the prediction whereas the hollow-cylinder and cone cylinder values fall progressively below the prediction. The trend with $Re\ \theta$ is, however, consistent in each case. The relatively suppressed axisymmetric results contradict early theoretical work by Eckert (1952) who proposed a first order correction of the form:

$$Cf(cyl)/Cf(fp) = (1 + \overline{B}\ \delta/R)^{1/5}$$

which predicts a 2% increase in Cfe for these experiments. The range or 'band width' of the experimental points plotted in Figure 29 is similar to that found by Hopkins and Inouye in their own comparisons. Hence, it is not possible with this limited set of data to discriminate between what may be a genuine reduction in friction coefficient for axisymmetric bodies or inherent experimental error.

The use of heat transfer data to infer skin friction by invoking the Reynolds analogy hypothesis leaves much to be desired. Experimental verification of the theoretical result is invariably obscured by the assumptions concerning the turbulent processes within the boundary layer. At high Mach number knowledge of the turbulent field in the present class of flows remains inadequate at the moment and, without specific examination, parameters such as recovery factor and turbulent Prandtl number must be broadly inferred from the literature. These uncertainties are compounded by axisymmetry and varying upstream history in the present comparisons.

Alternative experimental methods which use velocity profile data in the log law region, e.g. Sivasegaram (1971), or Preston tube measurements using an appropriate calibration formula, e.g. Hopkins et al (1970) while perhaps giving consistent results for a given experiment, still suffer from the fundamental defect that Cfe is inferred. Coleman (1973), in a review of the experimental problem, concluded that the floating element balance technique was probably the only reliable way of measuring Cfe at extreme conditions. Unfortunately even this method remains questionable when used in short duration facilities where instrumentation response is pushed to the limits and buoyancy effects, due to surface imperfections, are difficult to account for. The floating element also has a poor resolution capability particularly when investigating small changes in skin friction close to a separation region. Here the size of the element required for reasonable results can be greater than the cavity region under investigation. Clearly, more work with axisymmetric configurations is required in this field and the present data stand as a basis for future comparisons.

5. RESULTS AND DISCUSSION OF THE AXISYMMETRIC SEPARATED FLOW EXPERIMENTS

5.1 HOLLOW-CYLINDER FLARE (HCF) - AFTER COLEMAN (GENERAL OBSERVATIONS)

Coleman's data for this configuration are given in Figures 30 and 31. Coleman noted a close similarity between his data and the flat plate results obtained by Elfstrom at the same tunnel conditions. All of the characteristic two dimensional features are evident, e.g. plateau pressure region, reattachment pressure overshoot, but some differences in detail were found to exist. In particular the incipient separation angle at each tunnel condition was found to be approximately two degrees higher. Coleman also noted that the attached flow pressure distribution rose to the predicted wedge value before relaxing to the conical flow solution. Consequently for attached flows the interaction in the corner region was apparently two dimensional. This inherent overshoot in surface pressure for axisymmetric flows precluded the use of Elfstrom's two dimensional criterion for establishing incipient separation. Elfstrom's criterion depended on the first appearance of a pressure peak on the wedge. Clearly in the case of these experiments this assumption was unsafe and the incipient separation angles quoted by Coleman were therefore determined by extrapolating the separation length (L_s) vs. corner angle (α) to zero. The experimental problem of measuring or inferring incipient separation conditions is discussed more fully in Section 5.3.1. It is pertinent to mention here that the detail of the separation regions produced by Coleman and Elfstrom constitute the main basis of comparison for the present experimental results. A fuller discussion of these earlier experiments is therefore included in the general text to follow.

5.2 CONE-CYLINDER-FLARE (CCF) - GENERAL OBSERVATIONS

Coleman (1973) conducted a number of experiments using different nose configurations for the same basic cylinder-flare geometry. These included the CCF configuration for $\alpha = 30$ and 35 degrees at $Re\infty/cm = 5.17 \times 10^5$. This work has been

extended here to include the case for $\alpha = 40$ degrees at $Re\infty/cm =$ 5.17 x 10^5 and $\alpha= 30$, 35 and 40 degrees at $Re\infty/cm = 1.29$ x 10^5. The results are shown in Figures 32 and 33.

For the extreme case of $\alpha= 40$ degrees and higher Reynolds number condition (Figure 32) the cavity developed during the experiment was unexpectedly large and extended upstream of the first surface pressure tapping. In order to obtain details of the separation pressure rise, the flare was incrementally repositioned downstream and additional data obtained from the leading pressure tappings. Schlieren evidence had indicated that a downstream shift of 1 cm for the flare intersection line (i.e. 1.5% of boundary layer development run) would be sufficient to embrace the beginnings of the interaction. In the event, a shift of 4 cm was required, indicating that the cavity dimensions had increased substantially as a result of the change in reference conditions. The reasons for this are unclear but the results do appear to confirm the computer prediction described in Section 4.1.1 which indicated that, for this extreme case, the reattachment flow field may be influenced by the bow shock slip stream. As described earlier, this layer approaches the cylinder surface towards the rear of the model (Figure 13) and will intersect the flare at a slightly lower position if the flare is repositioned downstream. Other effects such as the growth of the input boundary layer thickness over an additional run of 4 cm would not account for the substantial increase in cavity size. Unfortunately the full significance of this anomaly was not appreciated until after the experimental programme had been completed and correlations of cavity scale were being investigated. However, it should be added that in view of the evidence for free interaction at separation in these experiments (to be described shortly) the data obtained under the displaced reference conditions are still useful. Moreover, the data obtained in the plateau and on the flare (i.e. $-7.8<(X-L) <8$ cm) were, of course, obtained prior to the change in flare position and therefore remain as a valid basis for comparison. The cavity dimensions and position of separation for this case were subsequently deduced from the Schlieren photograph which was also taken prior to the change in the flare position.

Given the difficulties experienced for the case of $\alpha = 40$ degrees and high Reynolds number it can nevertheless be seen that there exists an established region of separation with a well defined separation and reattachment shock structure (Figure 11). The plateau pressure distribution rises slightly toward the intersection line but attains the same value at the corner as Coleman's result for $\alpha = 35$ degrees. The pressure rise at reattachment does not begin for some way along the flare as a consequence of the large cavity region. Evidently under certain conditions the influence of the reattachment pressure field on the cavity region is limited. This behaviour is characteristic of 'Freely Interacting' shear layers and the evidence here gives further support to the idea that both separation and reattachment are essentially 'Free Interaction' processes for large cavity regions. It has been suggested by Batham (1971) that a freely interacting reattachment pressure field is largely governed by local approach conditions. The current results support this view, and it can be seen that as (α) is increased, and the reattachment zone climbs to a higher flare position, the general shape of the pressure distribution remains unaltered but its location is carried with the reattachment process, leaving the plateau pressure field free to extend its influence well beyond the intersection line.

Departure from two dimensional behaviour at the intersection line would appear to occur between $\alpha = 30$ and 35 degrees, and there are clear pressure overshoots for $\alpha = 35$ and 40 degrees. For $\alpha = 30$ degrees the pressure relaxes to the inviscid prediction; however at x = 35 and 40 degrees the flow is manifestly separated and the pressure recovery following $\hat{P}/P\infty$ is incomplete within the range of the instrumentation. Both the (HCF) and (CCF) data exhibit increased experimental scatter in this region and this may well be associated with the problems described in Section 4.1.3 where the possibility of random asymmetry in the tunnel flow has already been discussed.

Figure 33 shows that a reduction in unit Reynolds number reduces the extent of separation. This is compatible with the trend found by Coleman and Elfstrom although the undisturbed

thickness parameters in the current experiments varied only slightly. Two dimensional behaviour in the corner region is extended to $\alpha = 35$ degrees but there is limited photographic evidence to suggest that a small cavity region does exist at this angle, Figure 12. In general the maximum pressure ratios $(\hat{P}/P\infty)$ generated at the low Reynolds number condition are considerably reduced in comparison with the previous set of data.

5.3   CORRELATIONS OF SEPARATED FLOWS

5.3.1   Incipient Separation

Many methods have been suggested in the literature for the detection of incipient separation conditions. Practically all of these techniques give different answers according to their sensitivity to reverse flow. For instance, in the tests conducted by Appels (1974) differences of up to 10 degrees for (αi) in the same experiment were observed between simple interpretation of Schlieren photographs and the more sensitive oil flow visualization method. These and other techniques have been evaluated at length by Sterrett and Emery (1962), Roshko and Thomke (1969), Spaid and Frishett (1972) and Settles et al (1975), to mention a few. None of these authors reached a firm conclusion as to which method was the most reliable. In view of the evidence of separation obtained by Appels at very low angles it is conceivable that some intermittent recirculating flow is always present ahead of a surface discontinuity and, in the limit ($\alpha \rightarrow o$), such a flow would probably require a statistical criterion to define incipient separation.

Since an absolute definition is problematical it is necessary to choose some intermediate condition of practical significance. For the present tests (αi) was determined by extrapolating the measured separation length to zero (Figure 34). The results are shown in Table 2 along with the results obtained by Elfstrom and Coleman when specifically using this method. The separation length (Lsep) is defined as the distance between separation and the corner. The location of separation for the (CCF) flows was determined using the Erdos and Pallone reference point specified in Figures 40 and 41.

TABLE 6 : Incipient Separation Angles				
Model	$M\infty$ (e)	$Re\infty$/cm x 10^{-5}	αi (deg.)	Comments
2D-Wedge	8.93	1.29	31	
2D-Wedge	9.31	5.17	30	
HCF	8.93	1.29	33	
HCF	9.31	5.17	32	
CCF	8.4	1.29	~ 35	Insufficient Data
CCF	8.65	5.17	30	

It can be seen that some doubt exists for the cone-cylinder flare at the lower unit Reynolds number. This arose because the pressure distribution for α= 35 deg. did not attain the Erdos and Pallone reference value $(F(X) = 4.22)$ ahead of the flare although there is Schlieren evidence of separation. However, no separation shock structure is apparent and the two dimensional wedge pressure is not exceeded on the flare. This suggests that the incipient separation angle must be very close to 35 deg., a value significantly higher than observed for the equivalent hollow cylinder flow. Consequently the CCF results exhibit the same trends as the flat plate and hollow cylinder studies but, as indicated here and earlier, the lower unit Reynolds number CCF flow exhibits the greatest resistance to separation of all three experiments. The current values have been added to the traditional composite presentation shown in Figure 35.

Since a universally acceptable definition of incipient separation has yet to be established the accuracy of existing correlation methods must also remain difficult to gauge. Nevertheless, these methods do provide some basis for understanding the physical problem and several theories are compared here.

Todisco and Reeves (1969) used a momentum integral method to predict (αi) and their result is shown in Figure 36. Their theory is based on the equilibrium boundary layer solutions of Mellor and Gibson (1966) and shows a monotonic increase in (αi) with (Me). As such, the prediction is implicitly independent of

Reynolds number. Elfstrom has suggested that the method could probably be modified to account for these effects by adjusting the input conditions and using, instead, Cole's law of the wall and wake for the transformed profiles. The underdeveloped nature of the boundary layers produced in the current experiments (Figure 26) certainly suggests that the use of equilibrium profiles at high Mach number might cause significant errors for say $Re\delta_L < 10^6$. However, the present experimental results for (αi) agree quite well with the correlation in spite of both this difference, and the inherent differences in the approach stream for the two tunnel conditions.

The adiabatic wall correlation due to Kessler et al (1970), as presented by Elfstrom (1971), is shown in Figure 37. Surprisingly the higher Reynolds number (CCF) cold wall value is in good agreement but the theory generally appears to break down in the region $Re\delta o /Me^2 \sim 10^2$. Here, the effect of wall temperature ratio and the proximity of transition may well be significant for high Mach number flows as indicated by Elfstrom's results and the present CCF data point for $Re\infty /cm = 1.29$ x 10^5. The trend reversals apparent in Figure 35 are also implied by the correlation for a constant Mach number. However, the correlating parameters give little indication of why these should occur.

The semi-empirical correlation originally due to Needham (1965) and Roshko and Thomke (1966), as subsequently modified and presented by Elfstrom et al (1971), is shown in Figure 38. The correlation is based on the Chapman (1958) order of magnitude analysis for shock interactions. In principle, separation can be expected whenever the pressure rise across an interaction exceeds the plateau pressure for free interaction. Chapman's analysis indicates that the free interaction pressure rise should be proportional to the product $Me^{3/2}$. $Cfe^{1/2}$, to the first order (although Elfstrom chose the product $Me^{5/2}$ $Cfe^{1/2}$ to improve agreement with his data and those of other workers). In practice, streamline curvature in the corner region of wedge type flows will serve to reduce the severity of the initial interaction pressure gradient. Consequently, this class

of flow can probably sustain a much higher overall pressure rise before the appearance of separation than might otherwise be expected from simple shock interaction theory. This point can be seen clearly in Figure 38, particularly for the present experimental results. Here, the wedge recovery pressure for incipient separation far exceeds the plateau pressure ultimately achieved at higher flare incidences. Evidently the correlating parameters still appear useful in spite of this apparent theoretical defect, and it can be seen that the present CCF results fall close to the general trend observed by other workers for strictly two dimensional flows.

Elfstrom (1971) suggested that the hypersonic turbulent boundary layer could be treated as an inviscid rotational layer having a wall slip condition (or wall Mach number). He proposed that the wedge angle at which this theoretical wall layer first produced a detached shock should, in effect, correspond to the first appearance of a small separation region in the viscous sublayer of the real flow. To determine the wall Mach number he used a set of analytical profiles suggested by Green (1970/72) and extrapolated the linear portion to the wall. This method is sensitive to Cole's wake component, incorporated in Green's profiles, and Elfstrom subsequently found that changes in the theoretical incipient separation angle at constant local Mach number were strongly dependent on the value of this component. Using the further observation by Coles (1962) that the development of the wake appears to be a function of $\bar{R}$, Elfstrom proposed the correlation shown in Figure 39 which predicts αi at various Mach numbers over a common range of $\bar{R}$, under adiabatic wall conditions. A reversal in αi is predicted at high Reynolds numbers and this appears to conform with the adiabatic wall results of Kuehn, and Roshko and Thomke. Elfstrom's cold wall prediction for $Me = 9$ is also plotted in Figure 39 and this, again, appears to be in good agreement with his data at this condition. However, the cold wall axisymmetric results of Coleman and the present work are not in good general agreement. This may be due to the influence of axisymmetry as well as the proximity of transition, i.e. low Reynolds number effects in underdeveloped hypersonic boundary layers. Note,

for instance, that the higher Reynolds number CCF result obtained from a relatively well developed boundary layer does in fact fall close to the two dimensional prediction.

Interpretation of axisymmetric data correlated with $\bar{R}$ in this fashion is difficult. Coles (1962) in his original work lists many cases where boundary layers having a pressure gradient history do not conform to the simple wake development rule. Hence, Elfstrom's theory may only be appropriate for either; (i) ideal flows where development from transition through to an invariant wake profile has occurred without perturbation in the local free stream, or, (ii) sufficient development under zero pressure gradient has been achieved for the influence of the initial perturbation to be negligible. This may explain the good agreement obtained for the higher Reynolds number CCF result. It will be recalled from Section (4) that the boundary layer at this condition sustained a considerable run of post transitional development downstream of the cone shoulder pressure field.

Perhaps the most significant contribution of Elfstrom's theory is the suggestion of a strong connection between wake development and tendency for experimental values of αi to exhibit a trend reversal. It will be shown later, in Section 5.3.6., that this behaviour also appears to be linked to the trend in cavity size for values of α greater than αi.

5.3.2 Separation Pressure Rise

Using experimentally determined values of Stanton number and a Reynold's analogy factor of 1.16, data from Coleman (1973) and the current experiments have been fitted to the two dimensional 'free interaction' correlation of Erdos and Pallone, Figure 40. Elfstrom's 2D-wedge results have also been computed, (Figure 41). The axisymmetric data correlate as well as the 2D data, except for two test conditions namely:

i) $\text{HCF}, \alpha = 40$, $\text{Re}_\infty / \text{cm} = 5.17 \times 10^5$

ii) $\text{CCF}, \alpha = 40$, $\text{Re}_\infty / \text{cm} = 1.29 \times 10^5$

The cavity size produced for these flows was less than $2\delta_L$ and separation does not appear to have been fully established. Hence the pressure field ahead of the flare in each case still appears to be under considerable influence from the reattachment zone. Nevertheless, the rise to the separation reference point $(F(x) = 4.22)$ follows the theoretical curve quite closely and even for these two exceptions the initial response of the shear layer is of a 'free interaction' type.

The figures demonstrate the continued usefulness of the free interaction principle at high Mach number for determining the general shape of the pressure distribution at separation. Disagreement in absolute values of pressure does however exist and this has probably occurred for a number of reasons. Firstly, the instrumentation pitch chosen for all the configurations is rather coarse and when this is combined with the experimental scatter it is difficult to fit the data through the reference point on the theoretical curve. Secondly, a weak dependency on downstream conditions is evident for both sets of data and this is not allowed for in the theory. However, an important point to be gained from the figures is the observation that large differences in detail due to axisymmetric effects are not apparent within the experimental scatter. Hence, for the purpose of later comparisons, it is useful to note that the conditions at separation in the current series of experiments conform. broadly to the two dimensional theory, provided the cavity region is larger than, say, $2\delta_L$.

5.3.3 Plateau Pressure

Two predictions based on integral methods are shown in Figure 42. The Todisco and Reeves theory grossly overpredicts plateau pressure at high Mach number. This may be due to the assumption of a simple Prandtl – Meyer flow in the local free stream. The theory of Reshotko and Tucker (1955) gives better agreement with the more recent high Mach number data shown in the figure. Both theories neglect any influence due to Reynolds number.

The free interaction correlations of Erdos and Pallone (1962) and Popinsky and Ehrlich (1966) go some way to account for Reynolds number effects. The current results and those of Law (1975), Roshko and Thomke, and Batham have been calculated and added to the curves provided by Watson et al (1969) in Figure 43. Reynolds number appears in these correlations indirectly via the friction coefficient which was chosen as a basis for the analysis. It follows from the behaviour of hypersonic boundary layers discussed in Chapters 2 and 4 that the assumptions made for the dependency of Cfe on Re_x (in this case Cfe $= (1/Re_x^{1/10})$) may well influence the success of these correlations at high Mach number. However, the extent to which Reynolds number plays a significant role in determining the plateau pressure of these flows is obscured by several factors. For example, an abundance of evidence in the literature indicates that downstream conditions also have an important influence. All of the plateau pressure data reviewed thus far continue to exhibit a mild dependency on wedge angle long after the separation region has been established. This can be seen clearly in a comparison of Elfstrom's 2D-wedge data and the cone-cylinder-flare data in Figure 44. Data from both tunnel conditions are shown in the figure but the low Reynolds number results, where a plateau in the pressure distribution is difficult to find, have been computed from the mean pressure measured between separation and the first reading on the wedge/flare.

A fortuitous, but useful, method for clarifying plateau pressure response to Reynolds number, whilst accounting for its dependence on wedge angle, can be demonstrated by defining a pressure coefficient:

$$Cp_p = (P_p - Pe) \; / \; (\tfrac{1}{2}\gamma Pe \, Me^2) \qquad\qquad ---(5.1)$$

and plotting Cp_p against corner angle as shown in Figure 45. Two distinct data bands emerge and it is interesting to note that the upper band is formed by data taken from flows shown earlier to exhibit free interaction behaviour, whereas the points on the lower band come from flows not having a well established plateau pressure except at high incidence.

Some important observations can be made from this result:

(i)   The two data bands are now clearly associated with the two Reynolds number regimes of the experiments.

(ii)   The data in each band correlate well, irrespective of the local geometry, i.e. wedge or flare.

(iii)   The trends are converging with increasing (α) indicating that the influence of Reynolds number, if any, is declining with (α) and increased cavity dimensions.

In both instances the increase in Cp_p suggests that the angle at which the shear layer leaves the surface is increasing with (α) but the rate of increase is reduced for those established flows exhibiting free interaction behaviour. The established plateau pressure results fall close to the region prescribed by the Erdos and Pallone correlation given below for both Reynolds number conditions, namely:

$$Cp_p = F(X) \ (2 \ Cfe)^{\frac{1}{2}} \ / \ (Me^2 - 1)^{\frac{1}{4}} \qquad\qquad \text{---(5.2)}$$

where $F(X) = 6$ for turbulent flows (reference 36) and Cfe was evaluated from heat transfer data.

From the limited sample of data the results in Figure 45 indicate that, at low incidence, Reynolds number can have a dramatic influence on the mean cavity pressure whereas at high incidence, when a free interaction can be clearly identified at separation, any influence due to Reynolds number has practically vanished within the experimental scatter. This latter set of conditions may in part explain the success of Elfstrom's (1972) correlation shown in Figure 46 where all the data presented have come from well established cavity flows. In this correlation the effect of Reynolds number is once more omitted and the influence of the corner angle is introduced through the use of the predicted pressure recovery for an inviscid uniform flow field.

No physical explanation of the success of this correlation is

apparent in the literature, and this is perhaps not surprising since most experiments show that the final pressure recovery (Pinv) occurs well downstream of the reattachment 'throat'. Hence, it is extremely difficult to conceive of a mechanism emanating from the recovery region that could influence even the reattachment zone, quite apart from the plateau region. In view of this, it would seem reasonable to suggest that the use of (Pinv) in fact characterises the influence of the local free stream which behaves as though it were negotiating a double-wedge geometry formed by the cavity region and the solid boundary of the model.

The close collapse of data onto the single curve in Figure 46 also indicates that cavity geometry is prescribed a priori over the range of Mach numbers examined. For instance, at fixed Mach number Elfstrom's correlating parameters suggest that there is a unique relationship for (P_p) such that:

$$P_p = fn(Pinv), \text{ alone.}$$

Hence, for given free stream conditions and corner angle, the geometry of the cavity region apparently gives rise to a specific value of (P_p).

In order to extract this relationship from Elfstrom's plot, an empirical function has been identified which fits the original data presented by Elfstrom remarkably well. This function is shown below and constitutes the solid line in Figure 46.

$P_p/Pinv = EXP(K)$ (Valid for $2 \leqslant Me \leqslant 14$)
where $K = (0.48 - 1.23 L_n (Me)$
and Pinv is the final pressure on the wedge
or flare, taken from shock tables.
(Note: EXP(K) will further reduce to the form
$1 \cdot 616/Me^{1 \cdot 23}$)

The plateau pressure coefficient defined earlier now becomes:

$$Cp_p = \frac{(Pinv/Pe)e^k - 1}{\frac{1}{2}\gamma Me^2} \qquad \text{---(5.4)}$$

The specific prediction for Me = 9 has also been plotted in Figure 45. The agreement is excellent for the established separated flows with the correct trend predicted for CPp. The low incidence/low Reynolds number data fall well below the prediction as expected.

If it is tacitly accepted that the cavity local free stream does behave as though it were negotiating a double wedge geometry, then it is possible to take this analysis one further useful step. The plateau pressure, by this argument, would correspond to the surface pressure experienced by the first wedge formed by the separated shear layer. The angle of this wedge is analogous to the mean angle of the dividing streamline within the cavity or, alternatively, a notional separation angle θ_s. Thus, given the empirical fit to Elfstrom's correlation, a range of θ_s values can be determined for well established cavities with simply a knowledge of Me and α and the use of the shock relations. A brief analysis is given in Appendix 1 and the results are shown in Figure 47. Data from the literature and the current experiments have been added to show the possible range of usefulness of such a plot. The boundaries presented by Elfstrom's incipient separation prediction method and the strong shock solution are also introduced to clarify the region where separation can be expected. Although not an explicit prediction of separation, the figure could prove useful in aiding crude predictions of separation cavity dimensions once reliable methods for determining the length of the dividing streamline have been accomplished. Unfortunately, the rather vague distinction between "underdeveloped" and "fully developed" cavities indicated in Figure 45 would need to be more rigorously defined first. This requirement may well prove to be the basis upon which the influence of Reynolds number on plateau pressure gains much greater significance in future.

5.3.4 Reattachment Pressure

The resolution of the Schlieren photographs was found inadequate to determine the reattachment points accurately. Instead, the dividing streamline concept was assumed and a line was drawn from the previously calculated separation point at an angle corresponding to the 2D wedge oblique shock solution for the plateau pressure rise. Reattachment pressures were then taken from the experimental data for the intersection point on the flare. This method was first tested using the two dimensional pressure distributions measured by Elfstrom and was further compared with his schlieren photographs. The results were consistent with Elfstrom's original values and both the 2D-wedge and CCF results are compared with Batham's prediction in Figure 48. The axisymmetric results lie close to the 2D data and an extrapolation of the theoretical prediction. This figure provides further evidence of flow similarity between the two basic geometries.

Batham's method closely follows the free interaction arguments developed by Erdos and Pallone, for separation, with the exception that the friction coefficient is now evaluated on the free jet boundary. The analysis of Chow and Korst (1963), employed in Batham's theory for an asymptotic error function profile, had shown that this friction coefficient could be expressed as a simple function of local free stream Mach number. Both free interaction theories therefore employ the traditional hypothesis that the entering layer is self similar and independent of downstream conditions. However, as with the measured plateau pressure values, the present results for reattachment and those of Elfstrom, appear to show a mild but consistent dependency on corner angle. Since an accurate visual check on the position of reattachment was possible with Elfstrom's data, this tendency cannot be dismissed as a consequence of the simplifying dividing streamline assumption. Hence, the data suggests that the position of reattachment in these flows climbs slightly higher into the pressure recovery region as the corner angle increases. Although a relatively small effect in Figure 48, the trend may be connected with differing starting conditions at

separation and the state of development achieved by the mixing layer just before reattachment. In particular the magnitude of the turbulent shear stress on the stagnation streamline could certainly be expected to influence the shape and position of the reattachment pressure field. Strictly speaking, any major departure from the fully developed state assumed by Chow and Korst in their analysis should invalidate the use of their results in Batham's method. Hence, it is encouraging to note from the present results that a simple extension of Batham's theoretical curve still appears reasonably useful even at these high Mach numbers.

5.3.5 Reattachment Pressure Overshoot

Figure 49 shows the reattachment overshoot coefficient $(\hat{C}p)$ plotted against local deflection angle for the geometries studied by Coleman and Elfstrom including the present work. It is interesting to note that no data points sit on the theoretical curve for attached conical flow. This further reflects the two dimensional tendency of the flows discussed earlier. Surprisingly the 2D-wedge and CCF high Reynolds number data lie on one locus. This similarity must be due, in part, to both flows having an incipient separation angle close to 30 degrees. However, the close correspondence of the slopes would suggest that the local free stream and shock system for each geometry have similar development histories. The low unit Reynolds number data do not have quite the same clarity of behaviour but the results are compatible with the incipient separation trends. The theoretical value for $\hat{C}p$ using the method suggested by Elfstrom is also shown for the high unit Reynolds number data. In this method, $\hat{C}p$ is calculated by turning a two dimensional free stream through the theoretical separation and reattachment shocks prescribed by the plateau pressure rise and final recovery value Pinv. Practically all of the experimental points fall well below the theoretical curve. This apparent suppression of pressure overshoot is thought to be due to an expansion field propagating from the intersection point of the separation and reattachment shocks, close to the edge of the reattached boundary layer.

Elfstrom suggested that the appearance of the pressure overshoot was a good guide to the onset of hypersonic separation. Using this criterion to determine incipient separation angles he found good agreement with other methods. Coleman noted that this technique was unsuitable for axisymmetric flow since, owing to the local two dimensional behaviour at the intersection line, there was an inherent tendency for the pressure to overshoot the attached flow conical shock solution. However, some indication of the approach to gross separation for both 2D and axisymmetric bodies can be achieved by examining the behaviour of the pressure gradient ahead of $\hat{P}$ and the subsequent position of $\hat{P}$ relative to the wedge/flare intersection line. In all the high Mach number data recorded in the literature (i.e. $Me > 5$) the following pattern of events can be identified as (α) is increased through the incipient condition for gross separation.*

i) $\alpha < \alpha i$ - Pressure gradient ahead of $\hat{P}$ is low and the pressure distribution approaches $\hat{P}$ asymptotically.

ii) $\alpha \approx \alpha i$ - Pressure gradient ahead of $\hat{P}$ increases and $\hat{P}$ moves closer to the intersection line.

iii) $\alpha > \alpha i$ - Pressure gradient ahead of $\hat{P}$ remains constant (indicative of free interaction at reattachment) and $\hat{P}$ begins to move away from the intersection line as the cavity becomes larger.

These observations lead to an interesting relationship between the upstream influence parameter (Δx) and the position and magnitude of $(\hat{P})$. The correlation is shown in Figure 56 and discussed in Section 5.3.6.

*See, for instance, Figures 30 through 33 and also the asymmetric CCF data, Figures 60 to 77.

5.3.6 <u>Interaction Scale</u>

Evidently Reynolds number plays a crucial role in determining the scale of the interaction for these experiments. In particular the low Reynolds number flows exhibit a far greater resistance to separation and from the evidence of transition (Section 4.1.2) it is possible that this increased resistance is connected with the closer proximity of the end of transition to the separation point. In this respect the (CCF) cavity behaviour and transition trend are similar to the (HCF) and flat plate results of Coleman and Elfstrom. Batham (1971) also noted this effect in his flat plate study at Mach 7 in the same decade of $Re\delta_o$. As with the present results, the variation in thickness parameters in his survey was also insufficient to explain the reduction in separation bubble size. Batham suggested that the higher skin friction generally associated with the end of transition reflected a high shear stress gradient close to the wall. This would then result in a reduced reverse flow at reattachment since the free interaction equilibrium condition, which implicitly locates the dividing streamline, would then be reached lower in the detached shear layer.

Batham's suggestion implies that, as the wall shear stress profile is convected through the cavity toward reattachment, the magnitude of the shear stress gradient remains related in some way to the starting value. Unfortunately, this mechanism does not consistently describe the behaviour of cavities developed in the higher decade of $Re\delta$ (i.e. $\sim 10^7$). Here several workers (see Figure 35 for authors) have found that an increase in Reynolds number also reduces the scale of the interaction. In these latter cases the wall shear stress gradient, and general state of the approaching boundary layer will have been closer to so called "equilibrium" conditions and the mechanism suggested by Batham should have produced larger rather than smaller cavity regions. Clearly, additional mechanisms must be at work within the cavity and it would be reasonable to assume that the magnitude of the turbulent Reynolds stress in the mixing layer, and its relationship with the mechanism of scavenging reversed fluid from the reattached zone, must also play a major part in

determining the complete size of the recirculating region.

In hypersonic flows, where experimental conditions rarely achieve cavity dimensions greater than $10\,\delta_o$ it is, however, conceivable that the mixing layer may not have relaxed to a state prescribed by the local cavity flow field but may still be strongly influenced by the conditions prior to separation. The current experiments, and those conducted by Elfstrom and Coleman, fall into this latter category of flows. Direct measurement of the cavity velocity and turbulent fields in the experiment was not attempted; consequently it has not been possible to develop Batham's earlier suggestions. However, a useful examination of Reynolds number influences on cavity scale can still be attempted by referring to dimensions prescribed by the surface pressure distribution.

To examine cavity scale more closely an upstream influence parameter (Δx), after Settles et al (1975), has been employed. This is defined in Figure 50 which also shows the effect of (α) on (Δx) for the axisymmetric geometries. Estimation of (Δx) below the incipient separation angle is difficult and limited very much by the choice of instrumentation pitch. The accuracy in this region is, therefore, poor ($\pm$ 25%), however, it can be seen that in general (Δx) varies smoothly with (α) and this conforms with the view that separation originates as a small region of recirculation at very low deflection angles, Appels (1975), Winterwerp (1975).

Reynolds number effects on a normalized version of Settle's parameter are shown in Figures 51 and 52. The choice of (δ_o) for scaling with (Δx) is somewhat arbitrary but of little consequence in the case of the (CCF) results where the thickness parameters were found to vary insignificantly. Both sets of data show different trends above and below the incipient separation angles, (αi 32 degrees), which corresponds to the region $\Delta x/\delta_o \approx 1.5$.

This behaviour is preserved within the experimental scatter and is fundamentally different to the trend observed by Settles,

albeit at M_∞ = 2.9, where $\Delta x/\delta_0$ consistently reduced with increasing $Re\delta_0$ even for well separated flows. Settle's results, therefore, correspond more with the lower incidence tests of Figures 51 and 52. An alternative method of presentation is shown in Figures 53 and 54. Here, the influence of Reynolds number is further clarified, and it is quite evident that the higher Reynolds number cavities are developing much more rapidly with increasing wedge/flare angle.

Due to a fortuitous similarity in $Re\delta_0$ for the flat plate and axisymmetric geometries, at the low unit Reynolds number condition, it has been possible to make a direct comparison of $\Delta x/\delta_0$ over the complete test range in (α). This is shown in Figure 55. The data closely correspond at low incidence but diverge considerable once separation has become established, ($\alpha \approx 32$ deg.) The significance of this comparison is perhaps less clear than former cases of fixed geometry and varying $Re\delta_0$, in view of vastly differing upstream histories and possible geometric effects. An indication of these differences is given in the figure by the parameter X_t/δ_0 where X_t is the distance from the maximum surface pitot pressure (or maximum surface heat transfer value) to the intersection line. The parameter characterises the proximity of the cavity to the transition regime in the approaching boundary layer. The CCF data are clearly derived from a post transitional cavity whereas the FP-wedge and HCF results have been obtained from a region well downstream from the transition process. The fact that the high incidence HCF and FP-wedge cavities are growing more rapidly with (α) adds some weight to the suggestion that the development state of the approach stream may be an important factor in determining cavity scale in these experiments.

To summarize the observations made in this section so far the following general points can be made.

    i)   Obviously for fixed geometry and local free stream conditions, increasing (α) causes an increase in upstream influence.

ii) For fixed geometry and incidence, increasing $Re_{\delta o}$ at constant Mach number causes an increase in upstream influence for $\alpha > \alpha i$ and this trend is apparently reversed for $\alpha < \alpha i$. (NB αi is also a mild function of $Re_{\delta o}$ in these experiments. It is used here as a convenient reference angle and no direct connection with the trends is implied.)

iii) For fixed local free stream conditions, and incidence, the flat plate results of Elfstrom give the highest upstream influence values, and the (CCF) geometry, the lowest.

iv) The trends for well separated flows in ii) and iii) may be connected with the location of transition and the subsequent state of approaching boundary layer.

It is apparent that an upstream influence parameter has some value when making qualitative comparisons between different flow systems. Quantitative use of the parameter has proved much more difficult. Law (1975), employing this parameter, has compared empirical predictions by Roshko and Thomke (1975) and Settles and Bogdonoff (1973) with limited agreement at Mach 2.96, (Figure 56). These correlations were found by the author to fail completely at high Mach number and corner angles more typical of the current tests. These difficulties are obviously linked with the highly non-linear response of $(\Delta x / \delta o)$ with, say, (α) and $(Re_{\delta o})$, and a more satisfactory method for correlating interaction scale is clearly required.

The onset of hypersonic turbulent separation was found in the work by Settles et al (1975) and Appels (1975), in particular, to be a gradual process starting from extremely small regions of recirculating flow which then grow with corner angle

to affect the whole shear layer. This suggests that a broader appreciation of the process over the entire range of (α) investigated can be achieved by referring to length scales associated with the interaction which do not approach zero when gross separation ceases.

The upstream influence parameter used by Settles et al, (Δx), has already been discussed. A similar parameter for the flare or wedge pressure distribution is also readily identified. ($\Delta \hat{x p}$ - defined in Figure 57). By plotting $\Delta \hat{x p}/\Delta x$ versus $\hat{Cp}$ an indication of the growth of the complete cavity region, from perceived attached conditions to well separated flow, can be observed.

From the data available two main categories of flow appear evident at the present time: -

    i)   Flows above Me or M∞ = 5.8 (Figure 57)

    ii)   Flows in the region Me or M∞ = 3 (Figure 58)

It is particularly interesting to note the correspondence of points in Figure 57 over a wide range of $\hat{Cp}$ and $\Delta \hat{x p}/\Delta x$ especially the results of Elfstrom which almost entirely span the available data in the literature. The nominal threshold for gross separation is also shown in this figure but this relates specifically to flows for Me ⩾ 5.8. Plotted in this manner it would appear that hypersonic turbulent shear flows all have the same basic response to increasing corner angle (or strong adverse pressure gradient), irrespective of geometry or differing approach conditions.

The effects of large changes in Mach number and Reynolds number are apparent in Figure 58. These flows behave similarly although, from the original data, it was found that gross separation was occurring well before any steep rise in $\hat{Cp}$. The transitional data of Johnson (1968) are also shown for high Mach number in this second graph. Again, the behaviour is similar but the low incipient separation angle observed in the original

data, a feature of very low Reynolds number flows, results in suppressed values of $\hat{C_p}$ at low values of $\Delta xp/\Delta x$. Note, however, that the steep increase in $\hat{C_p}$ still occurs over the same range of $\Delta xp/\Delta x$ as for the higher Reynolds number turbulent boundary layer flows. The choice of correlating parameters in Figures 57 and 58 was somewhat fortuitous and arose from the desire to link the principal dimensions of the cavity with an easily identified, and measured, pressure value characterising the whole interaction region.

Further clarification of the relationship can be obtained by following the cavity development trend derived from Elfstrom's results, (Figure 57). Starting with the point at $\Delta xp/\Delta x = 15$, which corresponds to a wedge angle of 28 degrees, and proceeding to the left of this point, it can be seen that increasing (α) by only two degrees has produced a large drop in $\Delta xp/\Delta x$ to approximately 5. The original data shows that the flow is still attached at this point and $\hat{C_p}$ has increased only slightly with (α). Progressive 2 degree increments in (α) produce a more rapid increase in $\hat{C_p}$ with a corresponding reduction in $\Delta\hat{x p}/\Delta x$, and for well separated flows the correlation suggests that the ratio $\Delta xp/\Delta x$ is very nearly constant. Consequently, established cavity regions appear to grow almost equally ahead and downstream of the intersection line. This is shown more clearly in Figure 59. Here, the length of a notional dividing streamline (ℓ) has been computed from the position of separation and the angle prescribed by the oblique shock solution for the plateau pressure rise. The ratio (ℓ/n), where (n) is the normal to the compression corner, is seen to be almost constant for those experiments conducted in the Imperial College No. 2 Tunnel. The choice of δ_o for scaling with (ℓ) and (n) in the figure is arbitrary.

For hypersonic turbulent flows (say $Me \geqslant 5.8$) the method of presentation in Figure 57 does not appear to be too sensitive to Reynolds number. However, there remains an obvious difficulty with the choice of correlating parameters in so much as neither $\hat{C_p}$ nor $\Delta\hat{x p}/\Delta x$ can be derived a priori at the present time. Moreover, for low values of $\Delta\hat{x p}/\Delta x$ the parameter $\hat{C_p}$ is increasing

asymptotically rendering a foreknowledge of $\hat{C}_p$ by other means desirable for good accuracy. The parameters $\hat{C}_p$ and Δx have previously been shown to be sensitive to Reynolds number (Figures 49, 51 and 52). Consequently, although both here and in the literature there has been some success in predicting incipient separation (Elfstrom, 1973), reattachment pressure (Batham) and elements of established cavity geometry (Figure 47), there remains the fundamental problem of determining the extent of cavity growth ahead and downstream of reattachment, given details of the incoming boundary layer. Once this can be achieved the usefulness of correlations such as that shown in Figure 57, when applied as simple "first order" design tools, will obviously be significantly enhanced.

6. RESULTS AND DISCUSSION OF THE THREE DIMENSIONAL SEPARATED FLOW STUDY

6.1 PRESSURES AND SCALE

In view of the complex nature of the geometries tested in this latter series of experiments it is convenient to introduce an abbreviated notation to classify the principal flow paths (or meridians) under investigation. The key to this notation is: Geometry/ α- local/ $\emptyset$ - Tunnel Condition i.e. A/40/0 - HP corresponds to the surface line lying in the xy-plane of symmetry of geometry (A) where α - local = 40 deg. and $\emptyset$ therefore equals zero degrees, taken for the High Pressure tunnel condition (Re∞/cm = 5.17 x 10^5). Similarly B/32.5/90-LP corresponds to the surface line in the xy-plane of geometry (B) where α- local = 32.5 deg. (nominally) and $\emptyset$ = ± 90 deg., taken for the Low Pressure condition (Re∞/cm = 1.29 x 10^5). Consequently, the nine flow paths covered in these three dimensional studies are characterised by the following notation and symbols for the two tunnel conditions employed (see Table 7, note the raw data shown in Figures 60 to 77 are computerised plots employing a single symbol. Note also that for clarity the location of pressure tappings is also indicated in these figures).

Table 7			
Asymmetric CCF - Notation & Symbols (Figures 79 onwards)[*]			
Me = 8.65, Re∞ = 5.17 x 10^5		Me = 8.4, Re∞ = 1.29 x 10^5	
A/40/0 - HP	◕	A/40/0 - LP	◠
A/37.5/90 - HP	◑	A/37.5/90 - LP	D
A/35/180 - HP	◒	A/35/180 - LP	▽
B/35/0 - HP	▤	B/35/0 - LP	⬒
B/32.5/90 - HP	▥	B/32.5/90 - LP	⬓
B/30/180 - HP	▬	B/30/180 - LP	⬓
C/35/0 - HP	△	C/35/0 - LP	△
C/35/90 - HP	◭	C/35/90 - LP	▷
C/35/180 - HP	▲	C/35/180 - LP	▽

* unless otherwise stated

A complete set of data giving the measured and calculated parameters derived from all the asymmetric cavity flows can be found in Appendix 3. Data for the reference axisymmetric flows is also included in this presentation.

6.1.1 General Observations (Pressures and Scale)

Figures 60 through to 77 show that all the basic features of hypersonic separated flow are retained in the surface pressure distributions for the cone-cylinder asymmetric-flare geometries, e.g. a separation pressure rise, followed by a plateau and overshoot, with subsequent relaxation downstream. Moreover, the same basic response to Reynolds number is evident, as for the axisymmetric (or reference) flows; i.e. well developed cavity regions can be seen for $Re\infty/cm = 5.17 \times 10^5$ but at $Re\infty/cm = 1.29 \times 10^5$ cavity geometries are considerably reduced in scale. A clearer overall picture of the range of flows developed can be gained by referring to Figure 78 which maps the approximate geometry (side elevations) of all the separation regions generated during this second group of experiments.

Referring specifically to the higher Reynolds number data in the left column of Figure 78, two distinct boundary layer responses emerge for the three geometries and it is encouraging to note that these broadly correspond to the two basic model design strategies for flow field development outlined in Sections 3.3.1 and 3.3.2. Here it was intended that geometries (A) and (B) should induce effects due to a transverse pressure gradient in the vicinity of reattachment, and geometry (C) should induce effects due to a sloping flare intersection line. It can be seen that, in the case of geometries (A) and (B), local cavity dimensions do appear to be influenced by the local deflection angle insomuch as the separation line running from $\emptyset = 0$ to 180 deg. is pitched in the same 'sense' as the 2.5 deg. tilt on the two flares. However, in the case of geometry (C), where the local deflection angle does not vary circumferentially, the slope of the separation line is, surprisingly, opposite to that of the pitched flare intersection line. Evidently, although there is broad conformity with the original experimental objectives, there

is a significant difference in the shape of the cavities developed by the two basic classes of geometry which suggests that additional three-dimensional effects may be influencing these flows.

A further general impression of the flow behaviour can be gained by referring to Table 8 below. This table compares local features of the asymmetric separation fields with their axisymmetric equivalent flows for the higher Reynolds number tunnel condition, i.e. the region in the xy-plane for, say, geometry A, where α- local = 40 deg. (A/40/0), should be compared with the axisymmetric CCF result for α = 40 deg.

To aid interpretation of Table 8 the following additional descriptive terms have been introduced.

(i) 'Leading' angle refers to the local flare deflection angle at ∅ = 0 deg. in all cases.

(ii) 'Trailing' angle refers to the local flare deflection angle at ∅ = 180 deg. in all cases.

(iii) 'Outwash' or 'source like' flow behaviour is intended to signify a condition whereby the stream lines in the detached shear layer above the recirculating region are visualised as diverging from the meridian at ∅ = 0 deg., (see sketch A next page).

(iv) 'In-wash' or 'sink-like' flow behaviour signifies the converse of (iii) where stream lines are visualised as converging towards the ∅ = 180 deg. meridian, (see sketch B next page).

A simple hypothesis for "leading" and "trailing" angle separated flows.
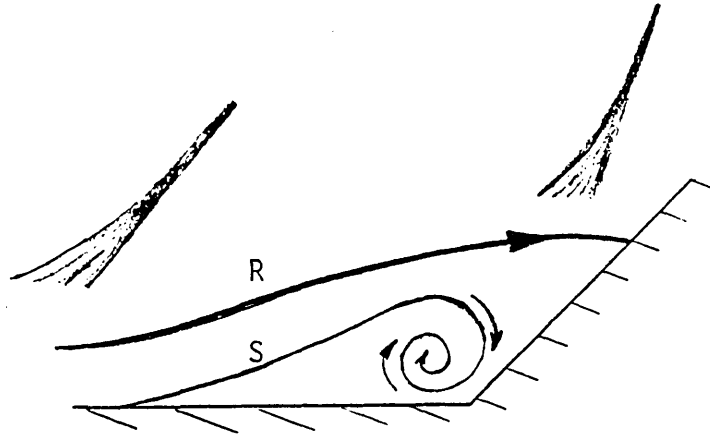
(A) "Outwash": Time average "leading" angle flow does not give closed bubble. Reattachment streamline R comes from finite height in approach boundary layer and therefore transports mass into bubble region. Separation streamline fluid rolls up and apparently disappears into a "sink" which is in fact the "source" for transverse flow.
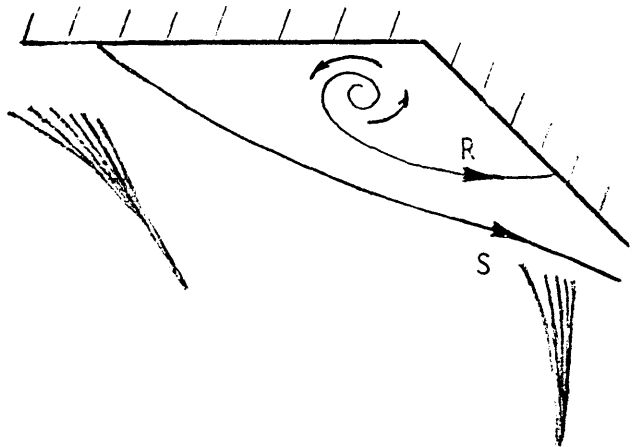
(B) "In-Wash": Transverse flow enters the "trailing" angle region and appears as the source of the reattachment streamline R. The separation streamline S does not reattach thereby providing a "sink" for the transverse flow.

TABLE 8

COMPARISON OF AXISYMMETRIC CCF AND ASYMMETRIC CCF

SEPARATION FIELDS (PRESSURES AND SCALE)

$Re_\infty/cm = 5.17 \times 10^5$ $M_\infty = 9.31$ $M_e = 8.65$	AXISYMMETRIC CCF α-deg.			ASYMMETRIC CCF GEOMETRY/α-local/$\emptyset$					
	30	35	40	A/40/0	A/35/180	B/35/0	B/30/180	C/35/0	C/35/180
P_p/P_∞	1.2*	4.37	5.39	4.90	4.79	4.48	4.26	4.07	5.26
Δx cm	0.80	3.75	7.31	6.40	5.50	2.80	1.70	2.10	4.00
$\hat{P}/P_\infty$	34.10	64.50	104.46	92.57	67.93	56.27	37.82	53.53	56.92

*No plateau - Flow unseparated - Average value of P/P_∞ taken ahead of flare.

Consider first the A/40/0 result and its axisymmetric equivalent, (α= 40 deg.). Here it can be seen that local plateau pressure, upstream influence, and maximum pressure ratio for Model (A) have been slightly suppressed by the effect of asymmetry in the vicinity of the $\emptyset$ = 0 deg. meridian. Since the 'trailing' local deflection angle at $\emptyset$ = 180 deg. for this geometry is 35 degrees this general response can be visualised as the effect of 'outwash' from the fluid interaction region lying above the $\emptyset$ = 0 deg. meridian. As perhaps expected, the A/35/180 result exhibits enhanced values for the above parameters, compared with the axisymmetric result for α= 35 deg., and this can be visualised as the effect of 'inwash' into the fluid interaction region lying above the $\emptyset$ = 180 deg. meridian. Geometry (B) falls into the same class as Geometry (A), insomuch as both configurations incorporate flares with a 2.5 deg. tilt relative to the approach stream, and roughly the same basic response for the B/35/0 and B/30/180 results is evident. However, it is interesting to note the presence of an established cavity region for the B/30/180 flow. This contrasts completely with the α= 30 deg. axisymmetric case, judged earlier (Section 5) to be unseparated.

The internal dynamics of the cavities developed in these flows are clearly very complicated and terms such as 'outwash' and 'inwash' probably convey an oversimplified picture of the separated free shear layer and recirculating flow fields. Nevertheless, it is useful for the moment to extend the use of these concepts to regions above the $\emptyset$ = 0 and 180 deg. meridians of geometry (C). This model appears to produce a similar response to that of geometries (A) and (B). Here, again, local conditions at $\emptyset$ = 0 deg. are suppressed, and at $\emptyset$ = 180 deg. on the whole enhanced compared with the axisymmetric result for α = 35 deg. Hence, although the 'sense' of the projected slope of the separation line between $\emptyset$ and 180 deg. opposes both the previous results, and the intrinsic pitch of the flare/cylinder intersection line for this geometry, we see that the basic response of the separated shear layer, in terms of local values of P_p/P_∞, Δx and $\hat{P}/P_\infty$, is consistant with the response for geometries (A) and (B).

It would appear from these preliminary observations that all three geometries influence the development of the flow in a similar fashion. The basis of this similarity lies in the tendency of all three geometries to exhibit suppressed local interaction pressures and dimensions in the vicinity of their leading angles and enhanced local values in the vicinity of their trailing angles, when compared with their axisymmetric equivalent flows. These processes could be crudely visualised at this stage as being the result of 'outwash' from the leading angles at $\emptyset$ = 0 degrees giving rise to 'inwash' toward the trailing angles at $\emptyset$ = 180 deg. Details of these flows are examined in the following text to establish the important parameters behind this surprisingly consistent response to three quite different geometries.

6.1.2 Pressure Rise in the Vicinity of Separation

A convenient method for examining the influence of three dimensional effects on this region of the flow is to plot pressure distributions under constant approach conditions having the origin defined as the beginning of each interaction. Data presented in this manner are shown in Figure 79. The results appear to diverge above a pressure ratio of 2.5 whereas below this value most of the experimental points share a common locus. This suggests that the initial pressure rise in each case may conform to a similarity rule; but beyond separation, which is thought to exist in the region of $P/P\infty$ = 3 for these flows, the separating shear layer is perhaps beginning to experience the effects of differing reattachment conditions. Consistent trends for the post separation region , which might be associated with flare asymmetry, are difficult to identify within the experimental scatter. However, some evidence exists in the figure to suggest that the pressure gradient beyond separation for the leading angle of geometry (A), i.e. A/40/0, is discernibly greater than that for the trailing angle, A/35/180. These data have been used to indicate the extremities of the distributions in the figure and it can be seen that the loci do appear to converge in the vicinity of $P/P\infty$ = 2.5.

The similarity between the initial pressure rises suggests that simple two dimensional 'free interaction' theories, such as that proposed by Erdos and Pallone, may still apply in this region, Figure 80. Furthermore, by choosing to fit the data through the nominal separation reference point, given by these authors, some of the arbitrariness in determining an origin for each interaction can be avoided. As with the axisymmetric comparisons in Figure 40, efforts to confirm the reference conditions by precisely pinpointing separation on the Schlieren photographs proved inconclusive. Consequently the absolute disposition of the data relative to the correlation remains in some doubt. Nevertheless, taken as a comparative study this choice of presentation does permit further comment. Firstly, the general trends for all the results fit the correlation quite well, although agreement below the separation reference point (F(X) = 4.22) is slightly better than above this point. Secondly, the tendency for the pressure distributions to diverge above the reference point is reduced by this presentation in comparison with the absolute distributions given in Figure 79. Hence, as far as can be judged, the results for the extreme cases, A/40/0 and A/35/180, still apparently conform to the 'free interaction' hypothesis although slight differences in plateau pressure do exist.

These observations carry the physical implication that under constant approach conditions streamline divergence relative to the free stream flow vector in the vicinity of separation is minimal. Consequently the shape of the initial pressure rise in each case does not vary markedly with circumferential position, as might be expected, and any subsequent flow divergence arising from perturbed reattachment conditions, and possibly feeding back into the separation flow field, must in some way be dissipated within the cavity volume. Hence, although the re-attachment zones for these three geometries have widely differing histories the initial interaction region would appear to be independent of these influences and the general principles of the two dimensional free interaction hypothesis still seem to apply.

6.1.3 Plateau Pressure (Pp)

Plateau pressure ratios taken for the higher Reynolds number established cavity flows are shown in Figure 81, (see Table 7 for key to symbols). Surprisingly the trends for geometries (A) and (B) exhibit little variation with respect to (∅) even though in each case α - local is varying appreciably with (∅). The trend for geometry (C) is quite different. Here it is evident that plateau pressure is strongly dependent on (∅) and yet α-local is not varying circumferentially. This remarkable difference in behaviour clearly needs considering more fully and warrants further comparison with the reference flows.

It was shown earlier (Table 8) that consistent differences in plateau pressure exist for all the asymmetric high Reynolds number data when compared locally with their axisymmetric equivalent flows. These differences can also be compared using an extension of Equation 5.4 which was derived in Section 5.3.3 and which emerges as a consequence of Elfstrom's two dimensional correlation for plateau pressure.

It will be recalled from Section 5.3.3 that Elfstrom's correlation implies a unique relationship between established plateau pressure and inviscid wedge recovery pressure ($Pinv$) when the free stream Mach number is constant. This function is repeated below: -

$$C_{P_p} = (\frac{Pinv}{Pe} \cdot e^{K} - 1) / (\frac{1}{2} \gamma Me^2) \quad ---(5.4)$$

Good agreement was found previously (Figure 45) by using the conical solution for $Pinv$, rather than the two dimensional result, when correlating axisymmetric data along side those of strictly two dimensional flows. The question therefore arises as to whether this method could be further extended to cover asymmetric flows by incorporating values of $Pinv$ given in AGARD-137 for conical flow at incidence. For such flows $Pinv$ varies according to (∅) for a given cone included angle. Hence

it is possible to test the degree to which (Pp/Pinv) for the asymmetric geometries might agree with a local three dimensional prediction based on the empirical function derived from Elfstrom's correlation.

The specific result for geometry (A) at Me = 8.65 is shown in Figure 82 (a) and the more general two dimensional form of the correlation is compared with all the high Reynolds number data in Figure 82 (b). It is apparent from the first of these figures that the variation in measured plateau pressure coefficient with (∅) is far less than might have been expected. Although large differences (i.e. > 5%) are not evident at ∅ = 0, disagreement with the theoretical 3D result is significant (∿25%) at ∅ = 180 and it can be seen that, whereas the prediction calls for a steady decline in Cp_p with (∅), the experimental values have hardly varied at all; as witness earlier.

This comparison supports the view that cavities generated by (A & B)-type geometries(i.e. inclined flare axis), in particular, embody a mechanism which acts in the circumferential sense and which enables the principal features of the interaction thus far examined to settle close to, or between, those conditions expected from local two dimensional or axisymmetric behaviour and those expected from fully asymmetric conical flow. With the further evidence given in Figure 82 (b), where the spread of data relative to the two dimensional prediction can be seen, it is clear that although the plateau pressures of geometry (A & B) exhibit little intrinsic asymmetry with respect to (∅) they cannot safely be treated as locally two dimensional. This implies that any attempt to treat these regions using a simple "strip" theory approach will fail unless, perhaps, an intermediate path can be identified, a priori, as being representative of the whole geometry. An example of this approach is given by the broken line in Figure 82 (a) which corresponds to the axisymmetric prediction for α = 37.5 deg. Evidently, even this primitive method fails in the case of geometry (C), as indicated in Figure 83, where the local deflection angle is invariant with (∅) and yet experimental values of Cp_p actually increase with (∅). This contradictory behaviour would appear to place the response to

geometry (C) in a category apart from types (A) and (B). Consequently although all three cases broadly exhibit 'outwash' and 'inwash' effects in comparison with their axisymmetric equivalent flows, differences in detail clearly still exist.

In view of the 'freely interacting nature of the asymmetric separation pressure rises, and the choice of constant approach conditions for these comparisons, the effects described above are most likely to be connected with differing reattachment conditions rather than influences emanating from the separation process. In this respect it is important to note that the two categories of plateau pressure response correspond to the two basic geometric features chosen for study, namely

(a) Zero pitch on the flare intersection line but varying α-local (geometries A and B)

(b) Pitched intersection line but constant α-local (geometry C).

Evidently the reattachment region of these flows requires close examination before a fuller understanding of the effects observed here can be given. For the moment, preliminary conclusions are drawn from the preceding discussion and summarised below.

i) For geometries (A) and (B) plateau pressure decreases only slightly w.r.t. ($\emptyset$) even though α-local varies considerably.

ii) For geometry (C) plateau pressure increases w.r.t. ($\emptyset$) although α-local is constant w.r.t. ($\emptyset$). This behaviour places this cavity flow in a different category to those of types (A) and (B).

iii) As a direct result of (i), Cp_p cannot be reliably predicted using an extension of Elfstrom's correlation incorporating values of Pinv corresponding to the inviscid solution for asymmetric conical flow.

iv)   In the case of geometries (A) and (B),
Cp$_p$ can be approximated by chosing, a
priori, an intermediate geodesic path and
using the axisymmetric conical solution for
Pinv in the functional form of Elfstrom's
correlation derived in Section 5.

v)   The method in (iv) fails for geometry (C)
except at $\emptyset$ = 0 deg. where the plateau
pressure is close to the axisymmetric
result.

6.1.4   Reattachment Pressure (Pr)

Reattachment pressures were determined using the method
outlined in Section 5.3.4 and the results for the higher Reynolds
number condition are shown in Figure 81.

For geometries (A & B) stronger circumferential trends
for Pr/Pe are apparent in contrast with the behaviour of
pleateau pressure described in the previous section. It can be
seen that a reduction of approximately 30% occurs between $\emptyset$ = 0
and 180 deg. compared with only 2% for the accompanying
reduction in plateau pressure ratio. For geometry (C) the trend
is quite the reverse; moreover the data appear to be quite well
matched with local plateau pressure response. In this case a
rise of 54% in (Pr/Pe) accompanies a rise of 30% in (Pp/Pe)
between the $\emptyset$ = 0 and 180 meridians. Again, the behaviour of
the latter flow is surprising in view of the invariance of α-local
with ($\emptyset$).

Reattachment pressure coefficients (Cp$_r$) are compared
with Batham's correlation in Figure 84 along with the reference
flow values for α = 40 and 35 degrees. It was pointed out earlier
in Section 5.3.4 that reattachment pressures calculated by the
'dividing streamline intercept' method could yield spurious trends
with (α), due to the weak dependency of plateau pressure on
flare or wedge angle, if alternative methods for checking the
result were not available. The implication being that Cp$_r$ could

appear to rise with (α) even though the true reattachment pressure may be independent of (α) in accordance with the free interaction hypothesis. The evidence for a weak dependency of Cp_r on (α) for the reference flows was, however, conclusive and it is important to note the extent of this variation in Figure 84 since this provides a basis for comparing the asymmetric data. It can be seen that the variation is greater than any interpolation error (estimated to be about $\pm 15\%$) and the high incidence result agrees quite well with Batham's prediction. With these points in mind, and making allowances for any interpolation error, the data for geometry (A) would appear to correspond closely to Batham's prediction. However, the remaining data for geometries (B) and (C) clearly differ from the theory. Perhaps more significant is the fact that they disagree considerably with the axisymmetric values which have, of course, been calculated using the same technique. The trends of Cp_r with ($\emptyset$) for all the data are stronger than might have been expected from plateau pressure variations alone, although in each case reattachment pressure follows plateau pressure in the same sense (Figure 81).

The fact that data for flow (A) agree well with Batham's prediction may be associated with the longer development lengths achieved in the mixing layer by the higher incidence cavities. In considering this suggestion it is perhaps significant to note that Mp varies only slightly for all three sets of data. Consequently, under the premise that two dimensional equilibrium turning must still be upheld in the xy - plane at any meridian, the only remaining variable in this first order theory is Cf_j, the Reynolds shear stress coefficient residing on the jet boundary ahead of reattachment. In Batham's analysis Cf_j was taken as a representative measure of a shear stress coefficient residing on the stagnation streamline. The values used in the correlation were taken from those given by Chow & Korst (1963) for a two dimensional asymptotic mixing layer. The spread of data in Figure 84, therefore, raises the possibility that either three dimensional influences are affecting a parameter characterised by Cf_j or the mixing layers for flows (B) and (C) have not reached an asymptotic state in the two dimensional sense. Obviously

both effects would be expected but it can be seen from Figure 85 that there is a strong correlation between Cp_r and ℓ/δ_L for all the data which certainly suggests that these cavities, including the reference cases, have probably not achieved asymptotic conditions.

In view of this, direct effects due to asymmetry are particularly difficult to gauge. For instance, the trend of Cp_r and ℓ/δ_L between A/40/0 and A/35/180 is similar to that between the reference results for $\alpha = 40$ and 35 degrees, i.e. Cp_r decreases. The reduction of Cp_r with ℓ/δ_L for flow (A) is, therefore, consistent with the notion of outwash and inwash (i.e. reattachment emanating from a higher point in the approach stream at $\emptyset = 0$). However, this suggestion is overshadowed by the possible influence of development length on the Reynolds shear stress ahead of reattachment. The implication being that the magnitude of (τj) is still a strong function of (ℓ) and thus forces Cp_r to decrease with (ℓ/δ_L) under the conditions for a free interaction pressure rise at reattachment. Consequently the evidence suggests that reattachment in these three dimensional flows may, in fact, be dominated by the indirect influence of asymmetry insomuch as Cp_r appears to be a strong function of local development length which, in turn, is clearly dependent on flare asymmetry, (Figure 78). This would also explain the contradictory behaviour of flow (C). Here the local deflection angle does not vary with $\emptyset$ but the effect of inwash towards $\emptyset = 180$ deg. has given rise to an increased development length which results in a higher reattachment pressure as the trailing angle is approached (Figure 81).

Clearly several additional mechanisms need to be considered when examining the reattachment region of a three dimensional hypersonic cavity. Not the least of which must be the Reynolds shear stress on the reattachment streamline since, according to the free interaction hypothesis, this will determine the shape of the reattachment pressure rise and locate the reattachment position. In the flows examined here the inferred role of (Cf_j), defined in the simple two dimensional context of Batham's theory, would certainly appear to be an important

factor when separation lengths of less than say, $10\,\delta_L$, are preceding reattachment. It is possible that the influence of Cfj under these conditions may completely overshadow any effects due to a transverse shear component, say $(\tau\emptyset)$, arising from a transverse velocity component in the reverse flow field.

6.1.5 Reattachment Pressure Overshoot $(\hat{P})$

The range of $(\hat{P}/Pe)$ values observed for the reference and asymmetric flows is shown in Figure 86 which also includes the two dimensional, axisymmetric and asymmetric conical predictions for attached flow. The latter two predictions lie extremely close to one another and are indicated by a single thick line. All these data correspond to the higher Reynolds number tunnel condition.

Unlike the highly perturbed conditions prevailing at reattachment, overshoot pressure ratios for these geometries do not appear to vary significantly from the reference flow values. (The trend of $(\hat{P}/P_e)$ with (α) for the reference flows is indicated as a broken line in the figure). Notably, the results for $\emptyset = 90$ deg. (geometries A & B) correspond very closely to those expected for axisymmetric flow. This behaviour supports the view that $(\hat{P})$ is predominantly influenced by conditions developing in the local free stream as this proceeds through the separation and reattachment shock systems. Effects of the viscous interaction are transmitted to this region via strong reflections from the deflected shear layer and these will subsequently determine local shock curvature and maximum pressure recovery downstream of the double compression process. It was noted earlier that plateau Mach numbers inferred from separation pressure rise at each meridian were relatively weak functions of $(\emptyset)$. Consequently, the input conditions for the reattachment shocks generated by all these flows are fairly similar. If we further consider the close similarity of the axisymmetric and asymmetric attached flow predictions for Pinv /Pe, shown in Figure 86, it is perhaps not surprising that large deviations in $\hat{P}/Pe$ from the reference case do not occur. In this respect it is encouraging to note that

even the small differences observed here are still consistent with the notion of 'outwash' and 'inwash' in the vicinity of the reattachment shock, particularly for geometries (A & B). For instance the point A/40/0 is slightly below the reference value indicating a reduced reattachment shock angle. Conversely the point A/35/180 is slightly higher, indicating an increased reattachment shock angle relative to the reference case. This behaviour would certainly be expected if the viscous layer were diverging from the $\emptyset = 0$ surface line and converging towards the $\emptyset = 180$ deg. surface line in the post reattachment region. The results for flow (C) lie very close to each other but below the reference value for $\alpha = 35$. A satisfactory explanation for this cannot be found at the moment but the fact that $(\hat{P}/Pe)$ hardly varies at all with $(\emptyset)$ would suggest that divergence and convergence of the viscous layer in the post reattachment region was negligible in this case.

The relationship between $\hat{Cp}$ and the parameter $(\Delta\hat{xp}/\Delta x)$ found in Section 5.3.6 is compared with the three dimensional results in Figure 87. Surprisingly, the agreement is excellent and the two-dimensional relationship between $(\Delta\hat{xp})$ and (Δx) continues to be upheld under perturbed conditions even though values of (Δx) and $(\Delta\hat{xp})$, taken independently, differ appreciably from the equivalent axisymmetric reference values. This result could have significant value when calculation techniques have been developed sufficiently to cover the post reattachment region of turbulent hypersonic separated flows. For the moment, however (and as stated previously) it is difficult to foresee the immediate benefits of this presentation without reliable prediction methods for at least one of the correlating parameters.

6.1.6   Effect of Reynolds Number

As pointed out in the introduction to this chapter the effect of Reynolds number on the asymmetric flows appears to correspond with that generally observed for the reference case. From Figure 78 and Figures 60 to 77 it can be seen that dimensions and pressures are suppressed by a reduction in Reynolds number and this can be directly linked with the

changes in development of the approaching boundary layer described in Section 4.2. It will be recalled that the input boundary layer conditions for both the axisymmetric and asymmetric studies were identical. In addition, it is important to note that the dominant effect of reducing Reynolds number throughout the entire range of experiments previously conducted by Elfstrom and Coleman has also been the reduction of separation length for a given surface geometry. In concluding the discussion on pressures and scale for these present asymmetric flows, it is necessary to determine the extent to which perturbed reattachment conditions have influenced the otherwise consistent Reynolds number response observed in these earlier experiments. This can be accomplished by using the upstream influence parameter (Δx) as a guide.

The data are presented in Figure 88 (see Table 7 for symbols). The reference flow trends of ($\Delta x / \delta_L$) with $Re\delta_L$ are shown as solid lines and the shaded areas mark the extremities for the asymmetric responses between $\emptyset = 0$ and 180 degrees. Evidently the trend of upstream influence for flow (A) is, on the whole, suppressed in comparison with the reference response for $\alpha=40$ deg. but nevertheless enhanced in comparison with that for $\alpha=35$ deg. This follows from the trends indicated in Table 8. Similarly the broad response of flow (C) covers a region either side of the reference trend for $\alpha = 35$ deg.

The effect of Reynolds number variation is thus seen to be entirely consistent with the trends for axisymmetric flow and it is interesting to observe that the broad response for geometry (A) corresponds to a region where a reference set of data for $\alpha = 37.5$ deg. might have been expected.

It is also worth re-emphasising that the lower Reynolds number data for the correlation of $\Delta\hat{xp}/\Delta x$ with $\hat{Cp}$ shown in Figure 87 still agree with the basic trend found for the reference flows. Hence the Reynolds number effect on the parameter $\Delta\hat{xp}/\Delta x$ is negligible for this range of test conditions and the two dimensional relationship between these parameters, in particular, is evidently maintained under varying approach

conditions as well as perturbed cavity geometry.

6.1.7 Concluding Remarks on the Behaviour of Pressures and Scale in Perturbed Separated Flows

In Section 6.1 a simple hypothesis was advanced to describe how the transverse velocity field might develop within each of the experimental cavities. It has also been shown that experimentally measured plateau and reattachment pressures vary with respect to ($\emptyset$) for all three geometries. Clearly the manner in which transverse velocity and pressure gradients truly interact to form a given cavity geometry must be extremely complex. Nevertheless, the flow responses to each geometry appear to have been relatively consistent when compared to their axisymmetric equivalent cases. For instance, even though the local deflection angle of geometry (C) does not vary with respect to ($\emptyset$) the cavity developed in this experiment exhibited similar suppressed and enhanced dimensions at the leading and trailing angles to those cavities developed by geometries (A) and (B). An additional consistency in the behavior of the three resulting flows, which sheds further light on how the transverse flow field might be developing within the cavity, can be identified by examining the transverse pressure gradient in the vicinity of reattachment.

Figure 89 maps the initial flare pressure recovery field for geometry (C) at the high Reynolds number tunnel condition. The experimentally determined reattachment position at each of the three meridians is also shown. The reattachment pressure is seen to be increasing slowly between the $\emptyset=0$ and 180 deg. positions and yet adjacent points on the flare surface at any fixed axial position are experiencing a decline in surface pressure with respect to ($\emptyset$). The effect is shown for all three geometries in Figure 90 where the surface pressure measured at the $\emptyset = 0$, 90 & 180 deg. meridians, at a fixed axial position is normalised by the reattachment pressure at $\emptyset = 90$ deg. and plotted against ($\emptyset$). The choice of axial location and reference pressure for this presentation is arbitrary and merely chosen for numerical convenience. As indicated in the figure the

transverse pressure gradient relative to the undisturbed free stream flow vector is negative in all three cases. Hence although the local deflection angle of geometry (C) does not vary circumferentially w.r.t. ($\emptyset$) the influence of the pitched flare intersection line has given rise to a similar physical response to that produced by geometries (A) and (B) which do incorporate inherent asymmetry in the pressure recovery region through the use of tilted flares.

These data show that between any two adjacent points inside the cavity on each of the flare surfaces the transverse pressure is reducing as $\emptyset$ increases. Consequently if the transverse pressure is reducing it would be reasonable to conclude that low velocity recirculating fluid approaching the flare in each case would be directed away from the leading angle towards the trailing angle. The details of any subsequent transverse velocity field remain open to speculation but the results are consistent with the notion of "outwash" and "inwash" as described in section 6.1.

6.2   HEAT TRANSFER DISTRIBUTIONS

6.2.1   General Observations

The reference conditions obtained by Coleman (1973) are shown in Figure 91. Corresponding data for the asymmetric flows are shown in Figures 92 to 94. In order to match the general shape of these heat transfer distributions with their surface pressure counterparts two length parameters have been employed (Δx ($\dot{q}$)) and ($\Delta x(\hat{q})$). These are defined in an identical manner to (Δx) and ($\Delta x\hat{p}$) in Figure 57.

The comparisons are given in Table 9 below.

TABLE 9	COMPARISON OF UPSTREAM INFLUENCE AND POST REATTACHMENT LENGTH SCALES FOR HEAT TRANSFER AND PRESSURE DISTRIBUTIONS			
MODEL	Δx (cm)	$\Delta x(\dot{q})$ (cm)	$\Delta x \hat{p}$ (cm)	$\Delta x(\hat{q})$ (cm)
CCF-35-HP	3.8	4.8	3.1	3.8
CCF-30-HP	0.80	0.5	2.6	2.2
A/40/0	6.0	6.0	3.6	3.5
A/35/180	5.5	5.5	4.2	4.0
B/35/0	2.8	2.8	2.7	2.5
B/30/180	1.7	2.0	2.7	2.6
C/35/0	2.1	2.2	2.6	2.5
C/35/180	4.0	4.5	3.4	3.5

Evidently the cavity size generated during Coleman's heat transfer experiments for CCF-35-HP was slightly larger than that produced during his pressure measurements. With the minor exception of the present result for C/35/180 the asymmetric pressure and heat transfer distributions do appear to be mutually compatible and it is encouraging to note that the basic flow field response of enhanced and suppressed length scales between the $\emptyset$ = 0 and 180 deg. geodesics is consistent with the results discussed in Section 6.1. For instance, the value of $(\Delta x\dot{q})$ for A/35/180 is enhanced in comparison with the reference result for α = 35 deg. and similarly the result for B/35/0 is suppressed. These differences outweigh the slight discrepancy in Coleman's data and provide further evidence of the fact that the spatial disposition of heat transfer in turbulent hypersonic cavities generally corresponds to the surface pressure response.

Plateau and peak heat transfer rates are compared in Table 10.

MODEL	Pp/Pe	$\bar{q}_p$ (Wcm^2)	$\hat{P}$/Pe	$\hat{q}$ (W/cm^2)	COMMENTS
CCF-35-HP	4.85	8.19	72	151	Coleman (23)
CCF-30-HP	/	/	34	84	Unseparated
A/40/0-HP	5.44	7.93	103	90	Experiment
A/35/180-HP	5.32	6.81	75	76	"
B/35/0-HP	4.98	8.29	63	75	"
B/30/180-HP	4.73	6.81	42	60	"
C/35/0-HP	4.52	8.15	59	67	"
C/35/180-HP	5.84	7.36	64	77	"

TABLE 10 COMPARISON OF PLATEAU AND PEAK HEAT TRANSFER RATES WITH THEIR SURFACE PRESSURE COUNTERPARTS

It can be seen that the trend of plateau heating rates w.r.t. ($\emptyset$) for geometries (A) and (B) is consistent with the surface pressure trend although percentage differences are higher. However, the data for flow (C) do not exhibit this feature. Although plateau pressure rises with ($\emptyset$) the heating rate is seen to decay. An indication as to why this should occur is given by the analysis in the following section which suggests that increased cavity dimensions may reduce average heating rates due to an 'insulation' effect. This point is, therefore, covered later.

While the plateau results correspond reasonably well with the reference case it can be seen from Table 10 that the peak heating values are quite incompatible with the data for CCF-35-HP. Coleman's data for the cone-cylinder flare do not include a distribution for α = 40 deg. Consequently, a direct comparison with the result for A/40/0 is not possible. The peak heating value obtained for A/35/180,which if it were to be consistent with Coleman's data should be slightly in excess of 151 watts/cm^2, is in fact 50% below this value. The same level of disagreement exists throughout all the data corresponding to α- local = 35 deg.

This leaves a rather unsatisfactory situation since it is extremely difficult to visualise how minor perturbations in flare

geometry can give rise to highly suppressed peak heating rates. This apparent discrepancy becomes all the more surprising in view of the relatively close agreement obtained ahead of the flare intersection line, in the plateau region.

Evidently a serious incompatibility exists in the post reattachment region which prevents a direct comparison with the reference flows. Following a re-examination of the theoretical basis of thin film heat transfer gauges a possible reason for this discrepancy has emerged which suggests that individually mounted quartz beads should not be used as substrates in regions where heat transfer rates in excess of 100 watts/cm^2 can be expected. This point is discussed more fully in Section 6.2.4. It will be shown that, under cold wall conditions and high ambient heat flux, a considerable reduction in local flux to an isolated, but relatively 'heated', substrate can occur due to the thermal history of the approach stream. For the moment, however, this discussion is most effectively accomplished by considering the asymmetric results for the flare region in isolation since they are still thought to be consistent with each other.

On this basis, the data exhibit similar trends to their corresponding pressure overshoot values. In particular flows (A) and (B) clearly exhibit higher and lower values of $\hat{q}$ at the $\emptyset = 0$ and 180 deg.meridians. Hence, although the absolute values are obviously in some doubt the results certainly suggest that throughout the perturbed cavity flow field heat transfer rates broadly follow the trends prescribed by the surface pressure response. Although differences in detail do exist their general behaviour is in agreement with the results obtained by Coleman (1973) and further suggests that useful information can be extracted from the data by more detailed comparisons with the reference flows as well as the theory developed by Coleman and Stollery (1972). The following discussion therefore proceeds on a similar basis to that in Section 6.1.

6.2.2 Heat Transfer Rates in the Vicinity of Separation

An interesting feature of turbulent separation heating rates, which appears to have attracted little attention in the literature, is the tendency of $(\dot{q})$ to initially drop to a minimum before sharply rising and overshooting the mean plateau value. This behaviour is particularly noticeable in Coleman's flat plate data (Figure 45, ref. (21)) and in the current results for C/35/0 and C/35/180. Evidently the heat flux in this region behaves quite unlike the pressure response which rises steadily towards the plateau. To bring out these differences in detail it has been found useful to compare the experimental results with the heat transfer distribution expected for an attached flow undergoing a free interaction pressure rise.

Coleman and Stollery (1972) developed a heat transfer prediction method for attached flows based on earlier work by Ambrok (1957), Walker (1960) and later by Back and Cuffel (1970). This method was found to give good agreement with Coleman's experimental data. The complete analysis, with a slight modification introduced to treat the separation pressure rise, is shown in Appendix 2. Briefly, the method yields the expression:

$$Q = \frac{\dot{q}}{q_L} = \frac{\rho_e u_e}{\rho_e U_e} \frac{\left[1 + \dfrac{Tw}{Toe}\right] + \dfrac{Me^2}{5}\left[0.4 + \dfrac{Tw}{Toe}\right]}{\left[1 + \dfrac{Tw}{Toe}\right] + \dfrac{Ml^2}{5}\left[0.4 + \dfrac{Tw}{Toe}\right]} \qquad \text{---(6.1)}$$

where $\dot{q}$ is the local heat transfer rate, and $\dot{q}_L$ is the undisturbed value.

For the present comparisons Equation 6.1 reduces to

$$Q = \left(\frac{P}{Pe}\right)^{.9}\left[\frac{1 - \left(\frac{P}{Pe}\right)^{\frac{\gamma-1}{\gamma}} + .2Me^2}{.2Me^2}\right]^{\frac{1}{2}}\left[\frac{1.276 + .135\,Me^2}{.6\left(\frac{P}{Pe}\right)^{\frac{\gamma-1}{\gamma}} + .675 + .135\,Me^2}\right]^{.65}$$

$$\text{---(6.2)}$$

In Section 5.3.2 it was shown that the separation pressure rise for all the well established cavity flows was closely predicted by the 'free interaction' corralation of Erdos and Pallone. For high initial Mach number the correlation has the approximate form:

$$\frac{P}{Pe} = 1 + \frac{1}{2} F(X) \, \mathscr{Y} \, Me^{\frac{3}{2}} \, (2 \, Cfe)^{\frac{1}{2}} \qquad \qquad ---(6.3)$$

where values of F(X) are taken from the corralation curve for the dimensionless abcissa X = (x-xo)/(xs-xo). Hence with the aid of equations 6.2 and 6.3 it is possible to compute the distribution of Q for an attached two dimensional flow undergoing a 'free interaction' pressure rise.

The prediction for Me = 8.65 and Cfe = 5.41 x 10^{-4}, which corresponds to the cone-cylinder input conditions, is compared with the results for C/35/0 in Figure 95 (a). Similarly the prediction for Me = 9.31 and Cfe = 7.4 x 10^{-4}, which corresponds to the flat plate starting conditions, is compared with Coleman's wedge result for α= 38 deg. in Figure 95 (b)

It can be seen that the experimental trends differ considerably from those expected for attached flow. While this is perhaps hardly surprising the differences in themselves are quite revealing. For instance, in the case of the data for C/35/0, where Δx and $\Delta x(\dot{q})$ were shown earlier to match quite well, it is interesting to note that the maximum plateau heating rate appears to coincide with the position of separation predicted by the two dimensional theory. Furthermore, the slight decay of Q ahead of this point would appear to correspond to the initial pressure rise. One could speculate from this that viscous layer growth ahead of separation was tending to reduce the surface heat flux whereas immediately downstream of the separation point, where the reverse flow is brought to a halt and reversed once again, a 'stagnation' like process was giving rise to enhanced heating rates. However, the resolution afforded by the choice of instrumentation pitch in this region is quite low and further detailed studies possibly including turbulence measurements in the post separation region close to the wall, are clearly needed to substantiate these suggestions.

Perhaps the most interesting aspect of the comparison is the simple fact that the average plateau heating rate lies considerably below the result expected for an attached flow passing over a wedge producing the same pressure recovery as the plateau pressure. In some respects this is similar to the behaviour of laminar separation regions where it is well known that heating rates actually fall well below the starting value, e.g. Hanke and Holden (1975). Consequently, although these data confirm the enhanced plateau heat fluxes observed by Coleman and several other workers, the turbulent cavity is seen to behave like an 'insulator' giving rise to suppressed heat transfer rates in comparison to those expected for an equivalent attached wedge flow of low incidence.

The comparison of Coleman's data in Figure 95 (b) was achieved with some difficulty since the cavity dimensions prescribed by the heat transfer distribution did not match with Elfstrom's experimental pressure distribution. Differences in transition length and model positioning relative to the nozzle accoustic field may have been the cause of this discrepancy. In view of this it was not possible to determine values of xs and xo from the experimental pressure distribution which would be compatible with the measured heat transfer distribution. However, using the knowledge tentatively gained in Figure 95 (a) where $\dot{q}$ (max) was found to coincide with X = 1, a match between the theoretical and experimental distributions can be forced. On this basis the general disposition of Coleman's data is similar to the earlier comparison although the parameter $\Delta\dot{q}(s)$, indicated in the figure, is slightly larger. However, as far as can be judged within the measurement error for (a), and the resolution afforded by the instrumentation pitch, little difference actually exists between the reference and asymmetric experimental results. Consequently additional evidence is found here to suggest that the initial separation process in the perturbed cavity flows has not been influenced by asymmetry at reattachment.

6.2.3. Heat Transfer Rates in the Plateau

It was noted in the preceding section that heating rates in the plateau tend to decay from an initial maximum as the intersection line is approached. In view of this the use of the term 'plateau' heating rate would appear to be a misnomer and care must be taken to ensure that comparisons of Qp are made using a consistent criterion for calculating the average heating rate ahead of the flare. In the present work this measure is defined as the mean heat transfer rate, inclusive of the plateau overshoot value. Flows which do not exhibit this feature generally correspond to the low incidence cases where the cavities are not fully established. These data have been omitted from further comparisons. Values of Qp vs. Pp/Pe recalculated from the studies performed by Elfstrom and Coleman are compared with the present results in Figure 96 which includes the correlation suggested by Holden (1972). It can be seen that the data are very similar with a mild tendency for the θ = 180 deg. results to lie below the rest of the field. As pointed out by Coleman, Holden's correlation does not appear to match the reference data very well, however, an exponent of 0.38 for (Pp/Pe) produces extremely good agreement for the recalculated and nominally two dimensional flows, including the results for B/35/0 and C/35/0. This is indicated as a broken line in the figure.

Correlations of the form $Q = (P/Pe)^N$ obviously simplify the true physical picture and they would not be expected to give consistent agreement across a wide range of experimental conditions. Examination of equation 6.1 in Section 6.2.2 would suggest that increased heat transfer rates in attached compressible flows are predominantly the result of increased density and reduced local Mach number. The success of this simple expression would suggest that it principally reflects the influence of the density rise $(\rho p/\rho e)$ which is of the order of five for these flows. The exponent (N) is thus seen to be loosely connected with the thermodynamic parameter (1/k) which is a function of the compression process as the free stream is deflected, i.e. $(Pp/Pe) = (\rho p/\rho e)^k$.

It was noted earlier that the turbulent cavity appears to insulate the wall against the higher heat fluxes expected from an attached flow. The decay of heat flux in the plateau as the intersection line is approached is thus analogous to a reducing recovery factor induced by fluid returning from the reattachment region. A layer of low energy fluid returning from the flare or wedge would certainly be expected to reduce thermal transmittance and influence temperature recovery from the plateau free stream. It may, therefore, be significant that the results for $\emptyset$ = 180 deg. lie slightly below the results for $\emptyset$ = 0 deg. as well as below the reference trends. This would indicate that the enhanced cavity dimensions experienced by all three asymmetric flows in the vicinity of $\emptyset$ = 180 deg. have served to increase the so-called 'insulation' effect for cavities having essentially similar levels of recompression. However, these differences are quite small and evidently the perturbed geometry at reattachment has only marginally influenced the average level of plateau heating.

6.2.4 Peak Heat Transfer Rates in the Post Reattachment Region

In Section 6.2.1 it was noted that the peak heating rates measured for the asymmetric flows were inconsistent with the results obtained by Coleman for the axisymmetric cone-cylinder-flare. Although the current data appear to be self-consistent, the general levels are up to 50% below those expected using Coleman's reference flow as a guide. In view of the close agreement obtained by Coleman (1973) when comparing his data with the attached flow predictions of Coleman and Stollery, and the general level of agreement between his data and other works in the field, the source of this discrepancy sadly points to the current experiments.

Following an extensive re-examination of the experimental and theoretical technique employed by Coleman, and in the present work, a full explanation for this discrepancy has yet to be found. However, it may be relevant to note that Coleman employed Hanovia X05 platinum painted Pyrex laminae formed and mounted into the flare surface, whereas the current results were obtained using RF platinum sputtered quartz beads mounted individually. This technique was chosen to enable high resolution in the transverse plane since gradients with respect to the $\emptyset$-geodesic were expected and these would not be fully resolved by thin film elements (1.3 cm x 0.2 cm) aligned perpendicularly to the axial direction. The aspect ratio of the sputtered film on the individually mounted elements was similar to that chosen by Coleman but the absolute dimensions were considerably smaller (0.3 x 0.03 cm). In the event, it is now known that formed laminae would probably have sufficed since these gradients are quite small and the investigation has subsequently concentrated on the principal meridians which could have been covered quite well using the former technique.

With the advantage of hindsight it is now apparent that in a short duration facility the thermal history of the approach stream to an isolated substrate can have a considerable influence on the local heat flux, particularly if the ambient heat flux to the surrounding metal is high. The error arises due to a surface discontinuity in temperature. Several authors have considered this problem for an incompressible constant property boundary layer, including Rubesin (1951) and Kays (1966). Schulz and Jones (1973) have suggested that the analysis given by Kays should also give a reasonable estimate of the error experienced in compressible flows provided the wall recovery temperature is chosen instead of the free stream static temperature. An attempt to quantify the error expected from this effect is therefore given here.

The notation used in the analysis is given in Figure 97 which shows a flat plate arrangement as a first approximation of the flows studied in the current work. The figure shows an isolated substrate positioned a distance (L') from the leading

edge of an unheated section of the plate. For $x < L'$ the wall temperature is Tw_1 and for $x > L'$ this becomes TW_2 which will be the surface temperature of a semi-infinite medium beneath a thin film, also assumed to have the temperature TW_2. The heat transfer rate downstream of the surface discontinuity ($\dot{q}s$) may be evaluated following Kays as:

$$\frac{\dot{q}s}{\dot{q}o} = 1 + \frac{TW_1 - TW_2}{Tr - TW_1} \cdot \left[1 - (\frac{L'}{x})^{\frac{9}{10}} \right]^{- \frac{1}{9}} \qquad \text{---(6.4)}$$

for a turbulent boundary layer where $\dot{q}_0$ is the heat transfer rate that would exist at a position x, ($x > L'$), if the wall were at a uniform temperature TW_1. A representative value for (L') in the current experiments would be 65 cm, the distance to the flare intersection line. The 'effective' position of the thin film relative to the start of the discontinuity is difficult to judge accurately since the substrate surface is circular in these experiments. However, a representative length for (x) would certainly be of the order of 65.2 cm since the beads are only 0.3 cm in diameter. The wall recovery temperature (Tr) is nominally 1000°K and it is assumed that this condition is maintained for at least 0.01 secs. of the tunnel starting process before the measurements are taken.

Two situations are now examined. From the data obtained by Coleman and in Section 6.2.3, plateau heating rates of the order of 10 watts/cm^2 were observed. Peak heating rates on the flare measured by Coleman exceeded 150 watts/cm^2. From the thermal response expected for a semi-infinite quartz substrate given by Figure 98 it can be seen that the plateau environment should bring about a 7°C rise in substrate temperature at 10 watts/cm^2, whereas in the post reattachment region a 100°C rise can be reasonably expected after 10 milliseconds flow duration and 150 watts/cm^2 heating rate. The temperature rise of the metal surface under these condtiions is estimated to be less than 1°C and 10°C respectively. Thus a nominal value of 300°K has

been chosen for TW_1. For these conditions equation 6.4 yields:

Individual Quartz $\dfrac{\dot{q}s}{\dot{q}o} = 0.98$ (plateau)   ---(a)

Substrates $\dfrac{\dot{q}s}{\dot{q}o} = 0.73$ (post re-
                                    attachment)   ---(b)

Obviously this simplified analogy stretches Kay's analysis to the limit; however, the results in (a) and (b) go a long way towards explaining why the plateau data obtained in the current experiments agree fairly well with Coleman's results whereas in the post reattachment region large differences exist. The equivalent error for a thin film placed at infinity on a continuous substrate by this method is still 15% i.e.

$\dfrac{\dot{q}s}{\dot{q}o} \sim 0.85$ (for post reattachment conditions)

suggesting that even Coleman's measured peak heating rates may be low. Clearly further work is necessary to improve Kay's analysis and more fundamental experiments are required in regions of high heat flux to test the comparative merits of individual or continuous substrates. In view of these uncertainties a full discussion of the asymmetric results downstream of reattachment is clearly impractical. The corrected data have, however, been added to the correlation chosen by Coleman and these are shown in Figure 99.

7. CONCLUSIONS

This experimental study was conceived with the aim of reproducing a hypersonic turbulent separation region which would more closely reflect the behaviour of a high speed flow occuring in a practical aerodynamic environment. In such cases three-dimensional influences can be expected to prevail throughout the entire flow field rendering theoretical treatment extremely difficult. The study has therefore attempted to approach the problem of three dimensional separation through a logical series of progressively more complex flow situations leading to the moderately perturbed case of an asymmetric flare pressure recovery field. The experimental conditions were first determined by an examination of the approach stream and associated boundary layer. Here the use of a computer prediction for the cone-cylinder forebody flow field was found extremely useful in confirming the principal features of the experimental flow; particularly with regard to the radial pressure gradient and entropy layer emanating from the interaction between the bow shock system and cone shoulder expansion process. A marked difference in the behaviour and location of transition was noted in comparison with previous experiments conducted in the same facility and employing hollow-cylinder or flate-plate geometries. Flow distortion, 'extra rates of strain,' resulting from free stream adaptation to conical and then axisymmetric flow, was noted as having probably played a major role in producing these differences, in addition to the influence of tunnel accoustic disturbances. Confirmation of the model transition regime and its response to changes in tunnel unit Reynolds number was achieved with boundary layer surveys which also revealed the characteristic retardation in shear layer wake development frequently observed at hypersonic conditions. Calculated skin friction values, based on heat transfer measurements taken at the flare station, fell below the Kármán-Schoenherr prediction as well as values recalculated from the flate plate and hollow cylinder experiments of Elfstrom and Coleman, undertaken at the same tunnel conditions. Evidence for a genuine reduction in skin friction for the cone cylinder geometry was, however, considered inconclusive due to an

imperfect knowledge of the turbulent processes within the experimental boundary layer.

Having established the physical context and details of the approach stream, separated flow studies were undertaken utilising a series of axisymmetric flares. These experiments were an extension of earlier work undertaken by Coleman (1973) using the same geometries. The results were further compared with the flat-plate-wedge and hollow-cylinder flare studies of Elfstrom (1971) and Coleman (1973).

A high incipient separation angle was observed for the additional data taken at the lower unit Reynolds number tunnel condition, 1.29×10^5/cm. The closer proximity of transition to the separation region in comparison with the reference studies was noted as a possible contributing factor to this tendency. The incipient separation angle computed for the high unit Reynolds number tunnel condition, 5.17×10^5/cm, was found to agree with the two dimensional prediction formulated by Elfstrom but the lower Reynolds number CCF value, and HCF reference values obtained by Coleman, did not.

Separation pressure rises for the present CCF study as well as the HCF and FPW reference studies, were found to be generally well predicted by the Erdos and Pallone free interaction model. Similarly, plateau pressures recorded for all three experiments agreed well with the collapse of data and choice of correlating parameters previously employed by Elfstrom (1972) for the plateau region. A good collapse of pressure data was also achieved by defining a plateau pressure coefficient and mapping this with local flare/wedge incidence.

An empirical function was derived from the plateau pressure measurements and used to extend the usefulness of Elfstrom's correlating parameters by noting that the function prescribed the cavity geometry for a given set of free stream conditions. With the aid of the shock relations a series of curves was subsequently generated which reproduce the experimentally implied relationship between the initial shear layer deflection

angle and flare/wedge angle for a prescribed Mach number.

Reattachment pressures determined from the axisymmetric flare experiments corresponded reasonably well with the two dimensional theory developed by Batham (1969). However, reattachment pressure overshoot levels were not well predicted by assuming a classical double-wedge perturbation of the cavity local free stream, indicating the need for a better understanding of the post reattachment viscous interaction process. Despite this deficiency the location of the pressure overshoot region, relative to the flare intersection line, was found to correlate well with an overshoot pressure coefficient, when normalised by the length of the cavity upstream influence region. This somewhat unexpected result contributes a little further towards the ultimate goal of correlating overall cavity scale which, unfortunately, still eludes empirical and theoretical treatment.

Results from the axisymmetric studies, having been firmly placed in context with earlier separated flow studies, could now be used as a reliable reference base from which to draw detailed comparisons of the perturbed flows. These were found to exhibit all the common features of a hypersonic turbulent cavity region with the exception that local dimensions, pressures and heat transfer rates, were found to differ according to their circumferential location. In regions of high local flare incidence these parameters were suppressed in comparison with the equivalent axisymmetric geometry and, conversely, enhanced in regions of low flare pressure recovery. The flows therefore behaved as though recirculating fluid within the cavity was migrating, circumferentially, into regions of lower local flare incidence or pressure recovery at reattachment. No evidence of cavity unsteadiness could be detected indicating that the separation regions had adapted to a new equilibrium state prescribed by the internal dynamics of the mixing layer.

Details of the perturbed cavity flows were subsequently examined using the same techniques as had been employed for the reference flows. It was found that the shape of the pressure rise at separation was almost indistinguishable, in each

case, from the equivalent axisymmetric flow. These pressure distributions also therefore conformed to the two dimensional free interaction model of Erdos and Pallone. Plateau pressure distributions were found to differ significantly from the reference case and were poorly correlated by existing relationships. Similarly, reattachment pressures did not conform to the reference case or to Batham's criterion, except at the highest incidence conditions where comparitively large cavities were developed around the entire flare/cylinder intersection line. Reattachment pressures were subsequently found to have an observable dependance on the projected length of the free shear layer lying in a given radial plane within the cavity. After some consideration of the theoretical basis for Batham's two dimensional criterion it was also concluded that most of the cavities developed in these experiments, as well as those of Coleman and Elfstrom, had probably not achieved an asymptotic state in the mixing layer and were thus still somewhat dependent on the state of the initial boundary layer at separation.

Pressure overshoot values in the post reattachment region consistently followed the general trends observed for pressures and scale. The influence of transverse pressure gradient and mass flux had evidently been carried through the reattachment shock system into the flare pressure recovery field. Surprisingly, however, the position and magnitude of local pressure overshoot values was found to have the same relationship with the local upstream influence length as had been noted for the axisymmetric flows.

Attempts to gain a deeper understanding of the principal driving mechanisms within the perturbed flows centered on the reattachment region since it was here that the most dramatic departure from the reference flows had been noted. The transverse (or circumferential) pressure gradients in this region were subsequently found to be strongly connected with the level of cavity distortion. The 'sense' or 'sign' of the gradient in all three asymmetric flows was compatible with the notion of a transverse migration of fluid within the cavity from regions where the local pressure was high and declining in a

circumferential sense. It was subsequently concluded that both the turbulent development state within the mixing layer, as well as the local transverse pressure gradient, were important factors governing the quantity of reverse mass flow, its migration towards regions of lower local pressure and its subsequent re-entrainment into the free shear layer. These processes, in turn, would strongly influence both the longitudinal and transveres equilibrium of the cavity volume.

Heat transfer distributions for both the axisymmetric and asymmetric flows spatially corresponded well with surface pressure. However, the magnitude of heat flux in the vicinity of separation was found to differ from the monotonic pressure rise predicted and observed for free interaction regions. Comparison of the experimental results with the heat flux predicted for an attached flow undergoing a free interaction pressure rise highlighted suppressed heating ahead of separation followed by an overshoot in the plateau. It was concluded that this behaviour may be connected with viscous layer growth during the separation pressure rise followed by stagnation of the reverse flow immediately downstream. The position of plateau maximum heating was found to coincide with the theoretical position for separation predicted by the Erdos and Pallone theory, adding further weight to this suggestion.

A deficiency in the theoretical basis for using platinum resistance thermometers mounted on discrete substrates was identified for those regions of flow experiencing high local heat fluxes. A method for correcting this deficiency was examined and was found to account for much of the discrepancy observed in the present study, when comparing flare overheat values with the reference data obtained by Coleman.

8. RECOMMENDATIONS FOR FURTHER STUDY

8.1 THE NO. 2 GUN TUNNEL

The possibility of random assymmetry in the tunnel test flow core was discussed in Section 4. It was felt that such a situation might occur if the nozzle transition plane did not always remain perpendicular to the free stream. The subsequent influence of acoustic disturbances on model transition behaviour was also discussed. It is recommended that tests should be performed on the nozzle wall boundary layer to determine whether transition occurs uniformly around the circumference. Alternatively, and perhaps less expensively, a fine wire nozzle wall boundary layer trip could be employed to fix the location of the nozzle transition plane such that model transition and boundary layer response can be monitored with and without the trip. The cone-cylinder flare geometry and pitot rake assemblies used in the present study would be suitable for this task.

8.2 PREDICTION OF HYPERSONIC TURBULENT CAVITIES

The work of McDonald (1965) and Appels (1975) was discussed in Section 2 as an example of the various calculation techniques which have been attempted in the past to predict the scale of an established two-dimensional compressible turbulent separation region. Evidence is presented in the present study (Section 6) which suggests that at very high speeds, say Mach 7, some of the assumptions embodied within these theories, and that of Batham's (1971) reattachment criterion, may be incorrect. For instance, all of the above theories assume that the free shear layer is self similar and developing independently of the starting conditions (or boundary layer shear stress profile at separation). In Section 6 it was shown that, for both the reference flows and the asymmetric flows, the projected separation lengths bore a close relation to the measured reattachment pressure. This is contrary to the notion of an asymptotic turbulent free shear layer developing under equilibrium conditions, in the context of Batham's theory.

It is suggested that a representative turbulent high Mach number cavity flow should be developed and 'unobtrusively' examined for its internal mean and fluctuating flow structure under varying levels of adverse pressure gradient, (i.e., cavity scale). Fluorescent electron beam or laser anemometer techniques may be suitable for this task. For the Imperial College No. 2 Gun Tunnel facility an extended version of Coleman's hollow-cylinder-flare geometry might prove a useful starting point to a more comprehensive study.

A reliable knowledge of free shear layer development and its relationship to the state of the incoming boundary layer at separation would, in principle, lead to a better correlation of reattachment pressure and cavity scale in the case of the present study as well as possibly catering for a much broader class of high speed flows.

9. References

1. AGARD -ograph 137. Tables of Inviscid Supersonic Flow about Circular Cones at Incidence, δ = 1.4. D. J. Jones, Parts 1 and 2.

2. Alber, E. I., Coats, D.E. (1969). "Analytical Investigations of equilibrium and Non-Equilibrium Compressible Turbulent Boundary Layers," AIAA Paper 69-689.

3. Ames Research Staff (1953). "Equations, Tables, and Charts for Compressible Flow," NACA 1135.

4. Ambrok, G. S. (1957). "Approximate Solution of Equations for the Thermal Boundary Layer with Variations in Boundary Layer Structure," Soviet Physics 2 (II) pp. 1979-1986.

5. Appels, C., Backx, E. (1971). "Hypersonic Turbulent Separated Flow," V.K.I. Student Report, Belgium.

6. Appels, C. (1974 - 1975). "Compressible Turbulent Boundary Layer Separation," von Karman Institute for Fluid Dynamics, Ph.D. Thesis.

7. Back, L. H., Cuffel, R. F. (1970). "Changes in Heat Transfer from Turbulent Boundary Layers Interacting with Shock Waves and Expansion Waves," AIAA J. 8 p. 1871.

8. Bartlett, R. P., (1974 - 1977). Private Communications (see Bartlett, R. P., 1981 Ph.D. thesis, University of London, "A Study of the Mean and Fluctuating Properties of a Turbulent Hypersonic Boundary Layer")

9. Bartlett, R. P., Edwards, A. J., Harvey, J. K. and Hillier, R. (Feb., 1979). "Pitot Pressure and Total Temperature Profile Measurements in a Hypersonic Turbulent Boundary Layer at Mach 9," I.C. Aero rep. 79-01.

10. Batham, J. P. (1969). "A Reattachment Criterion for Turbulent Supersonic Separated Flow," AAIA J, vol. 7, no. 7, pp. 154 - 155.

11. Batham, J. P. (1972). "An Experimental Study of Turbulent Separating and Re-attaching Flows at High Mach Numbers," J. Fluid Mech. 52 pp. 425 - 435.

12. Bogdonoff, S. M. and Kepler, C. E. (1955). "Separation of a Supersonic Turbulent Boundary Layer," JAS, vol. 22, no. 6, pp. 414-424.

13. Bradshaw, P., (1972). "Anomalus Effects of Pressure Gradient on Supersonic Turbulent Boundary Layers," IC Aero Rept. 72-21, Also VKI Lecture Series 56, (1973).

14. Bushnell, D. M., Morris, D. J. (1971). "Shear-Stress, Eddy-Viscosity, and Mixing-Length Distributions in Hypersonic Turbulent Boundary Layers," NASA TM X-2310.

15. Chapman, D. R. and Korst, H. H., (1955). "Free Jet Boundary with Consideration of Initial Boundary Layer," Proc. 2nd Nat. Congr. for Appl. Mech., University of Michigan, Ann Arbor.

16. Chapman, D. R., Kuehn, D. M. and Larsen, H. K. (1958). "Investigation of Separated Flows in Supersonic Streams with Emphasis on the Effect of Transition," NACA Report 1356.

17. Chi, S. W., Spalding, D. B. (1966). "Influence of Temperature Ratio on Heat Transfer to a Flat Plate Through a Turbulent Boundary Layer in Air," Proceedings of the Third International Heat Transfer Conference, vol. II, Chicago, IL, pp. 41 - 49.

18. Chow, W. L., Korst, H. H. (1963). "On the Flow Structure within a Constant Pressure Compressible Turbulent Jet Mixing Region," NASA TN-D-1894.

19. Coleman, G. T., Stollery, J. L. (1972). "Heat Transfer in Hypersonic Turbulent Separated Flow," I.C. Aero rep. 72 - 05.

20. Coleman, G. T. (1972). "Tabulated Heat Transfer Rate Data for a Hypersonic Turbulent Boundary Layer over a Flat Plate," I.C. Aero rep. 72 - 06.

21. Coleman, G. T., Stollery, J. L. (1972). Heat Transfer from Hypersonic Turbulent Flow at a Wedge Compression Corner," J. Fluid Mech. 56, pp. 741 - 752.

22. Coleman, G. T. (1973). "Hypersonic Turbulent Boundary Layer Studies," Ph.D. Thesis, Univ. of London.

23. Coleman, G. T. (September, 1973). "A Study of Hypersonic Boundary Layers over a Family of Axisymmetric Bodies at Zero Incidence; Preliminary Report and Data Tabulation," I. C. Aero Report 73 - 06.

24. Coles, D. E. (1956). "The Law of the Wake in the Turbulent Boundary Layer." J.F.M. vol. 1, part 2, pp. 191 - 226.

25. Coles, D. E. (1962). "The Turbulent Boundary Layer in a Compressible Fluid," Report R-403-PR, Rand Corp., Also ARC 24,497 and Physics of Fluids" 7, pp. 1403 - 1423, (1964).

26. Cooke, J. C. (1963). "Separated Supersonic Flow." R.A.E. Note Aero No. 2879; ARC CP 706.

27. Culotta, S. and Richards, B. E. (1970). "Methods for
    Determining Conditions in Real Nitrogen Expanding
    Flows." VKI TN 58, Belgium.

28. Van Driest, E. R. (1951). "Turbulent Boundary Layers in
    Compressible Fluids," JAS, vol. 18, no. 3, pp. 145 - 150.

29. Van Driest, E. R. (1956). "Problem of Aerodynamic
    Heating." Aeronautical Engineering Review 15, p. 26.

30. Dorodnitsyn, A. (1942). "Laminar Boundary Layer in
    Compressible Fluid," Comptes Rendus (Doklady) de
    l'Academie des Sciences de l'U.R.S.S., vol. 34, pp.
    213 - 219.

31. Eckert, H. U. (1952). "Simplified Treatment of the
    Turbulent Boundary Layer Along a Cylinder in
    Compressible Flow." J. Aero. Sc. 19 pp. 23 - 28.

32. Eckert, E.R.G. (1955). "Engineering Relations for Skin
    Friction and Heat Transfer to Surfaces in High Velocity
    Flow." J. Aero. Sc 22, p. 585.

33. Edwards, A., (1976). Private Communication.

34. Elfstrom, G. M. Coleman, G. T. and Stollery, J. L. (1971).
    "Turbulent Boundary Layer Studies in a Hypersonic
    Gun Tunnel," Paper No. 11, 8th International Shock
    Tube Symposium, London, July, 1971; Also available as
    I. E. Aero Report 71 - 11, Imperial College, 1971.

35. Elfstrom, G. M. (1971). "Turbulent Separation in Hypersonic
    Flow." Ph.D. Thesis, Univ. of London; Also I.C. Aero
    rep. 71 - 16.

36. Elfstrom, G. M. (1972). "Turbulent Hypersonic Flow at a
    Wedge Compression Corner." J. Fluid Mech. 53,
    pp. 113 - 127.

37. Erdos, J. and Pallone, A. (1962). "Shock-Boundary Layer
    Interaction and Flow Separation." Heat Transfer and
    Fluid Mechanics Institute Proceedings, Stanford,
    pp. 239 - 254.

38. Favre, A. (ed) (1964). The Mechanics of Turbulence,
    Gordon and Breach, New York.

39. Fernholz, H. H., Finley, P. J. (1977). "A Critical
    Compilation of Compressible Turbulent Boundary Layer
    Data." AGARD-AG-223.

40. Green, J. E. Circa 1970/72 Private Communication to
    Elfstrom, (RAE report to be published) "A Note on the
    Turbulent Boundary Layer at Low Reynolds Number in
    Compressible Flow at Constant Pressure."

41. Hankey, L. W., Holden, M.S. (1975). "Two-Dimensional Shock Wave Boundary Layer Interactions in High Speed Flows." AGARD-AG-203.

42. Holden, M. S. (1972). "Shock Wave - Turbulent Boundary Layer Interaction in Hypersonic Flow," AIAA Paper 72 - 74 presented at AIAA 10th Aerospace Sciences Meeting.

43. Holden, M. S. (Feb., 1974). V.K.I. Lecture Series 66, AGARD Short Course. See also Part II AGARD - AG - 203 (1975).

44. Holder (1955). See Gadd, G.E., Holder, D.W., and Regan, J.D. "An Experimental Investigation of the Interaction Between Shock Waves and Boundary Layers." Proc. Roy. Soc. of London, ser. A, Vol. 226 1954, pp. 227-253.

45. Hopkins, E. J., Keener, E. R., Louis, P. T. (1970). "Measurements of Turbulent Skin Friction on a Non-Adiabatic Flat Plate at M - 6.5 and Comparison with Eight Theories." NASA TN D - 5675.

46. Hopkins, E. J., Inouye, M. (1971). "An Evaluation of Theories for Predicting Turbulent Skin Friction and Heat Transfer on Flat Plates at Supersonic and Hypersonic Mach Numbers." AIAA J. 9. pp. 993 - 1003.

47. Johnson, C. B., Bushnell, D. M. (1970). "Power-Law Velocity Profile Exponent Variations with Reynolds Number, Wall Cooling and Mach Number in a Turbulent Boundary Layer." NASA TN D-5753.

48. Kays, W. M. (c. 1966). Convective Heat and Mass Transfer. McGraw-Hill Book Company

49. Kessler, W. C., Reilly, J. F., Mockapetris, L. J. (1970). "Supersonic Turbulent Boundary Layer Interaction with an Expansion Ramp and a Compression Corner." MDC EO 264, McDonnell Douglas, U.S.

50. Kirk, F. N. (1959). "An Approximate Theory of Base Pressure in Two Dimensional Flow at Supersonic Speeds." R.A.E. Tech. Note Aero. No. 2377.

51. Klebanoff, P. S. (1955). NACA-Rep. 1247.

52. Korst, H. H., Chow, W. L. and Zumwalt, G. W. (1959). "Research on Transonic and supersonic Flow of a Real Fluid at Abrupt Increases in Cross Section (with special consideration of base drag problems), Final Report." Univ. of IL, ME-TN-392-5.

53. Kuen, D. M. (1959). "Experimental Investigation of the Pressure Rise Required for the Incipient Separation of Turbulent Boundary Layers in Two-Dimensional Supersonic Flow," NASA Memo 1-21-59A.

54. Kuehn, D. M. (1961). "Turbulent Boundary Layer Separation Induced by Flares on Cylinders at Zero Angle of Attack." NASA TR R-117.

55. Laderman, A. J., Demetriades, A. (1974). "Mean and Fluctuating Flow Measurements in the Hypersonic Boundary Layer over a Cooled Wall." JFM vol. 63, pp. 121 - 144.

56. Laderman, A. J., Demetriades, A. (1979). AIAA J vol. 17, no. 7 "Turbulent Shear Stresses in Compressible Boundary Layers."

57. Law, H. C. (1974). "Supersonic Turbulent Boundary Layer Separation." AIAA J vol. 12, no. 6.

58. Law, H. C. (June, 1975). "Two-Dimensional Compression Corner and Planar Shock Wave Interactions with a Supersonic, Turbulent Boundary Layer," ARL-75-0157.

59. Van Le, N. (1953). "Transformation Between Compressible and Incompressible Boundary Layer Equations." JAS, vol. 20, pp. 583 - 584.

60. Locke, F.W.S., Jr. (June 1952). "Recommended Definition of Turbulent Friction in Incompressible Fluid." DR Rept. 1415, Navy Dept., Bureau of Aeronautics Research Div.

61. Ludwieg, J. and Tillman, W. (1950). "Investigations of the Wall Shearing Stress in Turbulent Boundary Layers." NACA T.M. no. 1285.

62. Mager, A., (1956). "On the Model of the Free, Shock Separated Turbulent Boundary Layer." J. Aero Sci. vol. 23, p. 181.

63. Mager, A. (1958). "Transformation of the Compressible and Incompressible Boundary Layer Equations," JAS, vol. 25, pp. 305 - 311.

64. Maskell, E. C. (1951). R.A.E. Rep. Aero. No. 2443.

65. Meller, G. L. and Gibson, D. M., (1966). "Equilibrium Turbulent Boundary Layers." J.F.M., Vol. 24, pp. 225 - 253.

66. McDonald, H., (1964). "Turbulent Shear Layer Re-attachment with Special Emphasis on the Base Pressure Problem." Aero. Quart., vol. 15, p. 247 - 280.

67. McDonald, H. (1965). "A Study of the Turbulent Separated Flow Region Occurring at a Compression Corner in Supersonic Flow." JFM, vol. 22, part 3, pp. 481 - 505.

68. Mikulla, V. and Horstman, C. C. (Jan. 20-22, 1975). "The Measurement of Shear Stress and Total Heat Flux in a Nonadiabatic Turbulent Hypersonic Boundary Layer." AIAA paper. 75-119 13th Aerospace Sciences Meeting, Pasadena, CA. See also AIAA paper No. 76-162.

69. Narasimha, R. and Viswanath, P. R. (1975). "Reverse Transition at an Expansion Corner in Supersonic Flow." AIAA J vol. 13, no. 5.

70. Nash, J. F. (1962). "an Analysis of Two-Dimensional Turbulent Base Flow, Including the Effect of the Approaching Layer," ARC 24000, R & M 3344.

71. Needham, D. A. (1965). "Laminar Separation in Hypersonic Flows." Ph.D. Thesis, University of London.

72. Needham, D. A., Elfstrom, G. M. and Stollery, J. L. (May, 1970). "Design and Operation of the Imperial College Number 2 Hypersonic Gun Tunnel." I.C. Aero Report 70-04, Imperial College. Also available as ARC 32,569.

73. Owen, F. K., and Horstman, C. C. (1972). "On the Structure of Hypersonic Turbulent Boundary Layers." JFM vol. 53, part 4, pp. 611 - 636.

74. Page, R. H., Sernas, V. (1970). "Apparent Reverse Transition in an Expansion Fan." AIAA J. 2, 189.

75. Pate, S. R. and Schueler, C. J. (1969). "Radiated Aerodynamic Noise Effects on Boundary Layer Transition in Supersonic and Hypersonic Wind Tunnels." AIAA J vol. 7, no. 3, pp. 450 - 457.

76. Popinsky, Z. and Ehrlich, C. F. (1966). "Development Design Methods for Predicting Hypersonic Aerodynamic Control Characteristics." USAF Technical Report AFFDL-TR-66-85, Wright-Patterson AFB, Ohio.

77. Potter, J. L. and Whitfield, J. D. (1960). "Effect of Unit Reynolds Number, Nose Bluntness, and Roughness on Boundary Layer Transition." AEDC-TR-60-5; also JFM, Vol. 12, 1962, pp. 501-535.

78. Probstein, R. F., Elliot, D. (1956). "The Transverse Curvature Effect in Compressible Axially Symmetric Laminar Boundary Layer Flow." J. Aero Sc. 23, pp. 208 - 224.

79. Pullin, D. (1974). Private Communication.

80. Ray, A. K. (1962). "Estimation of the Critical Pressure Rise for Separation in Two-Dimensional Shock Boundary Layer Interaction Problems." Z. Flugwiss 10, Heft 6.

81. Reshotko, E. and Tucker, M. (1955). "Effect of a
    Discontinuity on Turbulent Boundary Layer Thickness
    Parameters with Application to Shock Induced
    Separation." NACA TN 3454.

82. Richards, R. E. and Stollery, J. L. (1966). "Further
    Experiments on Transition Reversal at Hypersonic
    Speeds," AIAA J, vol. 4, no. 12, pp. 2224 - 2226.

83. Robinson, M. L. (1974) "Boundary Layer Effects in
    Supersonic Flow over Cylinder-Flare Bodies." Australian
    Defense Scientific Service. WRE-Report-1238.

84. Rose, W. C. (1973). "The Behaviour of a Compressible
    Turbulent Boundary Layer in a Shock-Wave-Induced
    Adverse Pressure Gradient." NASA TN D-7092.

85. Roshko, A. and Tomke, G. J. (1966). "Correlations for
    Incipient Separation Pressure," DAC-59800 Douglas
    Aircraft Co.

86. Roshko, A. and Thomke, G. J. (1969). "Supersonic
    Turbulent Boundary Layer Interaction with a
    Compression Corner at Very High Reynolds Number,"
    presented at Symposium on "Viscous Interaction
    Phenomena in Supersonic and Hypersonic Flow." USAF
    ARL, OH. Dayton Press, pp. 109 - 138.

87. Roshko, A., and Tomke, G. J. (Jan., 1975). "Flare-Induced
    Separation Lengths in Supersonic Turbulent Boundary
    Layers," AIAA Paper 75-6.

88. Rubesin, M. W. (1951). "The Effect of an Arbitrary Surface
    Temperature Variation Along a Plat Plate on the
    Convective Heat Transfer in an Incompressible
    Turbulent Boundary Layer." NACA-TN-2345.

89. Sanders, F. and Crabtree, L. F. (1961). "A Preliminary
    Study of Large Regions of Separated Flow in a
    Compression Corner." RAE Tech Note No. Aero 2571.

90. Schultz, D. L., Jones, T. V. (1973). "Heat Transfer
    Measurements in Short Duration Hypersonic Facilities,"
    AGARD-AG-165.

91. Settles, G. S. and Bogdonoff, S. M. (July, 1973),
    "Separation of a Supersonic Turbulent Boundary Layer
    at Moderate to High Reynolds Numbers,"
    AIAA Paper 73-666.

92. Settles, G. S., and Bogdonoff, S. M., Vas, I.E., (Jan.,
    1975). "Incipient Separation of a Supersonic Turbulent
    Boundary Layer at Moderate to High Reynolds
    Numbers," AIAA Paper 75-7.

93. Settles, G. S. and Bogdonoff, S. M., Vas, I.E., (Jan., 1976). "Incipient Separation of a Supersonic Turbulent Boundary Layer at High Reynolds Numbers," AIAA J, vol. 14, no. 1.

94. Sivasegaram, S. (1971). "The Evaluation of Local Skin Friction in Compressible Flow," Roy. Aero. Soc. Aero J. 75, p. 793.

95. Sommer, S. C., Short, B. J. (1955). "Free Flight Measurements of Turbulent Boundary Layer Skin Friction in the Presence of Severe Aerodynamic Heating at Mach Numbers 2.8 to 7." NACA TN 3391.

96. Spaid, F. W., Frishett, J. C. (1972). "Incipient Separation of a Supersonic, Turbulent Boundary Layer, Including Effects of Heat Transfer," AIAA J 10, p. 915.

97. Spalding, D. B., Chi, S. W. (1964). "The Drag of a Compressible Turbulent Boundary Layer on a Smooth Flat Plate With and Without Heat Transfer." J. Fluid Mech. 18, pp. 117 - 143.

98. Sterrett, J. R. and Emery, J. C. (1962). "Experimental Separation Studies for Two-Dimensional Wedges and Curved Surfaces at Mach Numbers of 4.8 to 6.2," NASA TN D-1014, 1962.

99. Todisco, A. and Reeves, B. L. (1969). "Turbulent Boundary Layer Separation and Reattachment at Supersonic and Hypersonic Speeds," Paper Presented at Symposium on "Viscous Interaction Phenomena in Supersonic and Hypersonic Flow," Hypersonic Research Laboratory, USAF ARL, OH.

100. Wagner, R. D., Maddalon, D. V., Weinstein, L. M. and Henderson, A. (1969). "Influence of Measured Free-Stream Disturbances on Hypersonic Boundary Layer Transition," AIAA 69-704.

101. Walker, G. K. (1960). "A Particular Solution to the Turbulent Boundary Layer Equations," J. Aero Sci. 27, p. 715.

102. Watson, E. C., Murphy, J. D. and Rose, W. C. (1969). "Investigation of Laminar and Turbulent Boundary layers Interacting with Externally Generated Shock Waves," NASA TN D-5512.

103. White, R. A. (1963). "Turbulent Boundary Layer Separation from Smooth-Convex Surfaces in Supersonic Two-Dimensional Flow." Ph.D. Thesis, Univ. of IL.

104. Winterwerp, J. C. (June, 1975). "An Experimental Study of Flap-Induced Separation of a Compressible Turbulent Boundary Layer." VK1. Project Report 1975-5.

105. Zukoski, E. E. (1967). "Turbulent Boundary Layer Separation in Front of a Forward-Facing Step." AIAA J, vol. 3, no. 10, pp. 1746 - 1753.
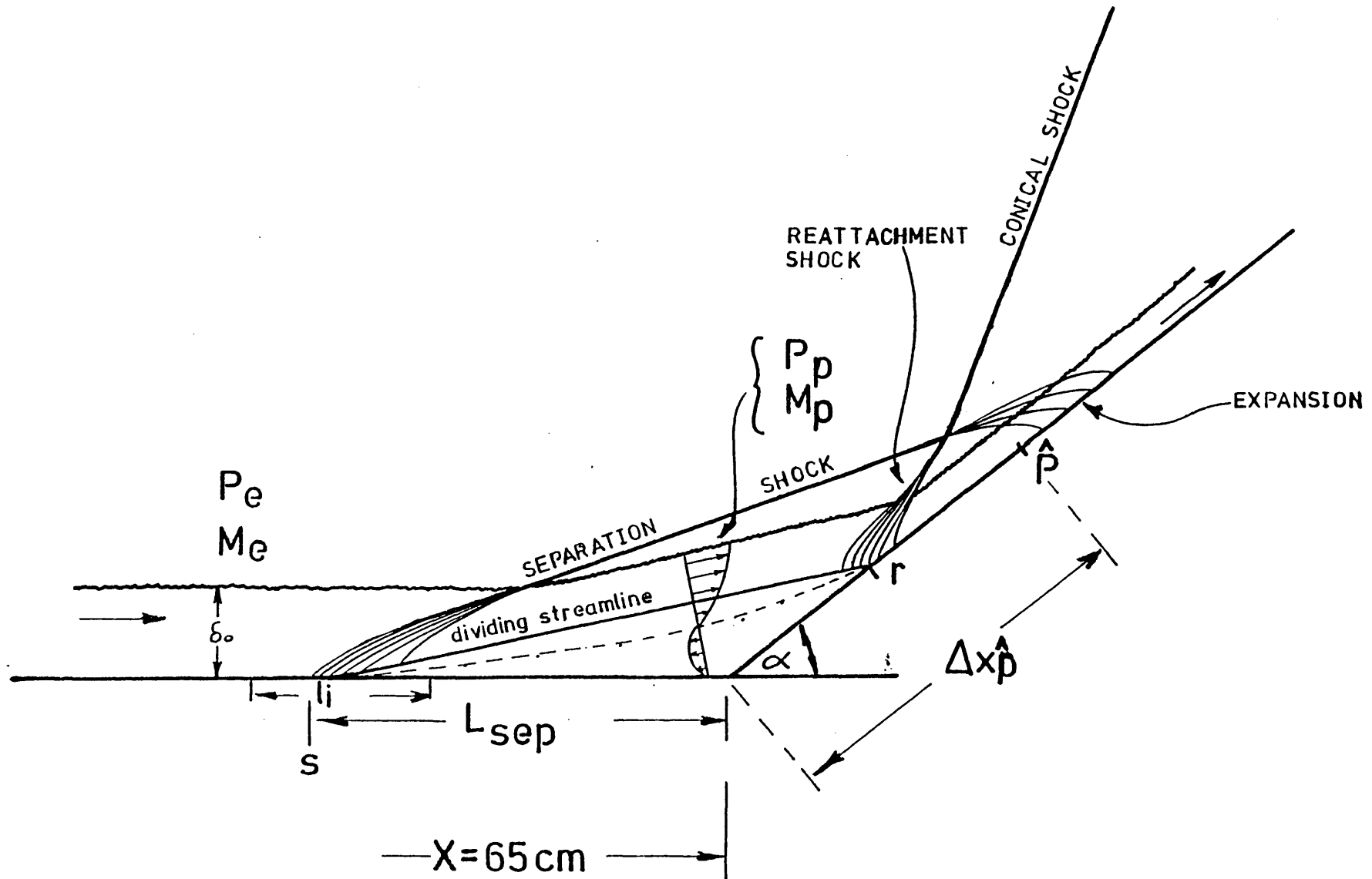
FIG 1   FLOW-FIELD CONSTRUCTION
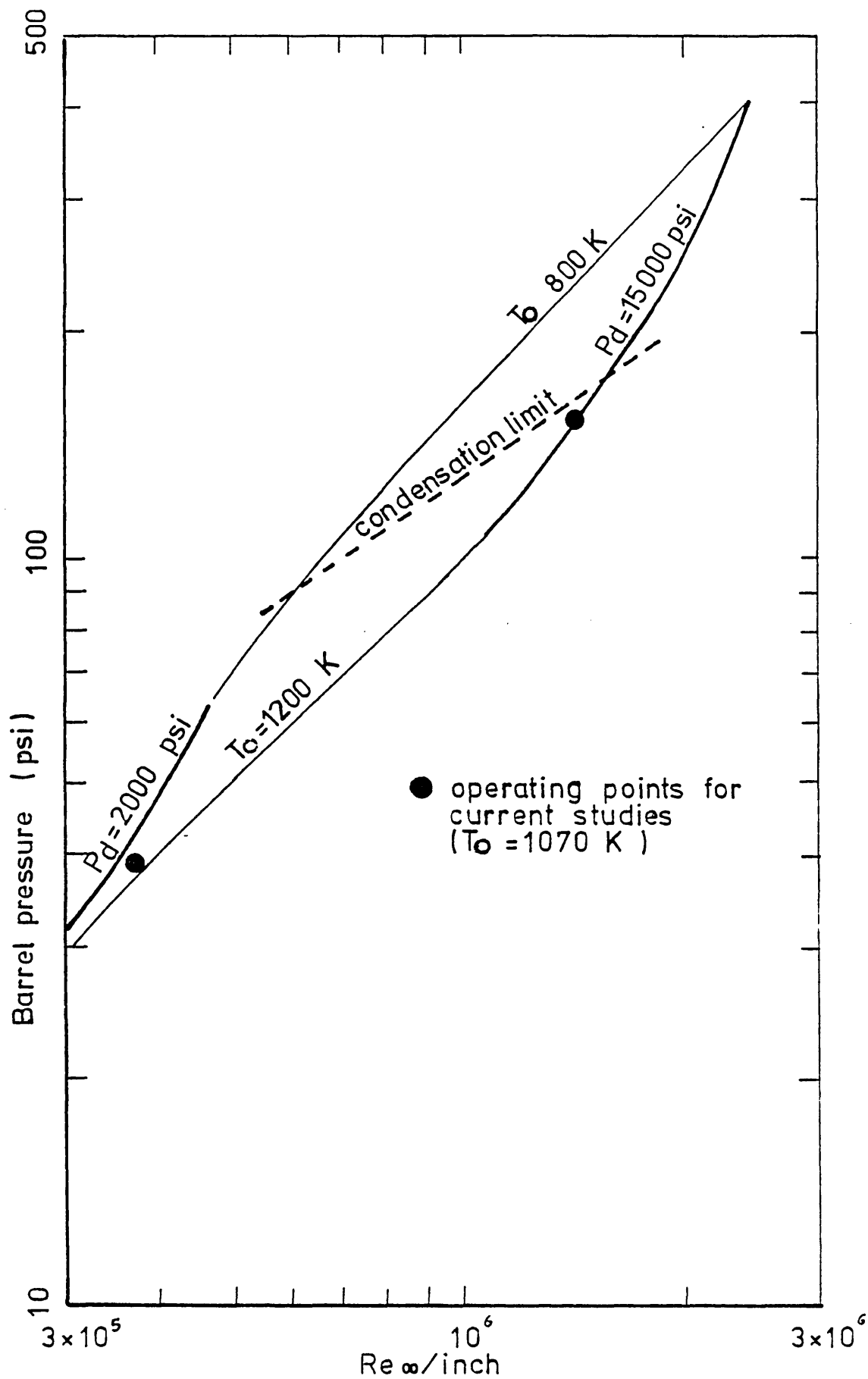
FIG 2   Performance envelope for
         Mach 9 nozzle
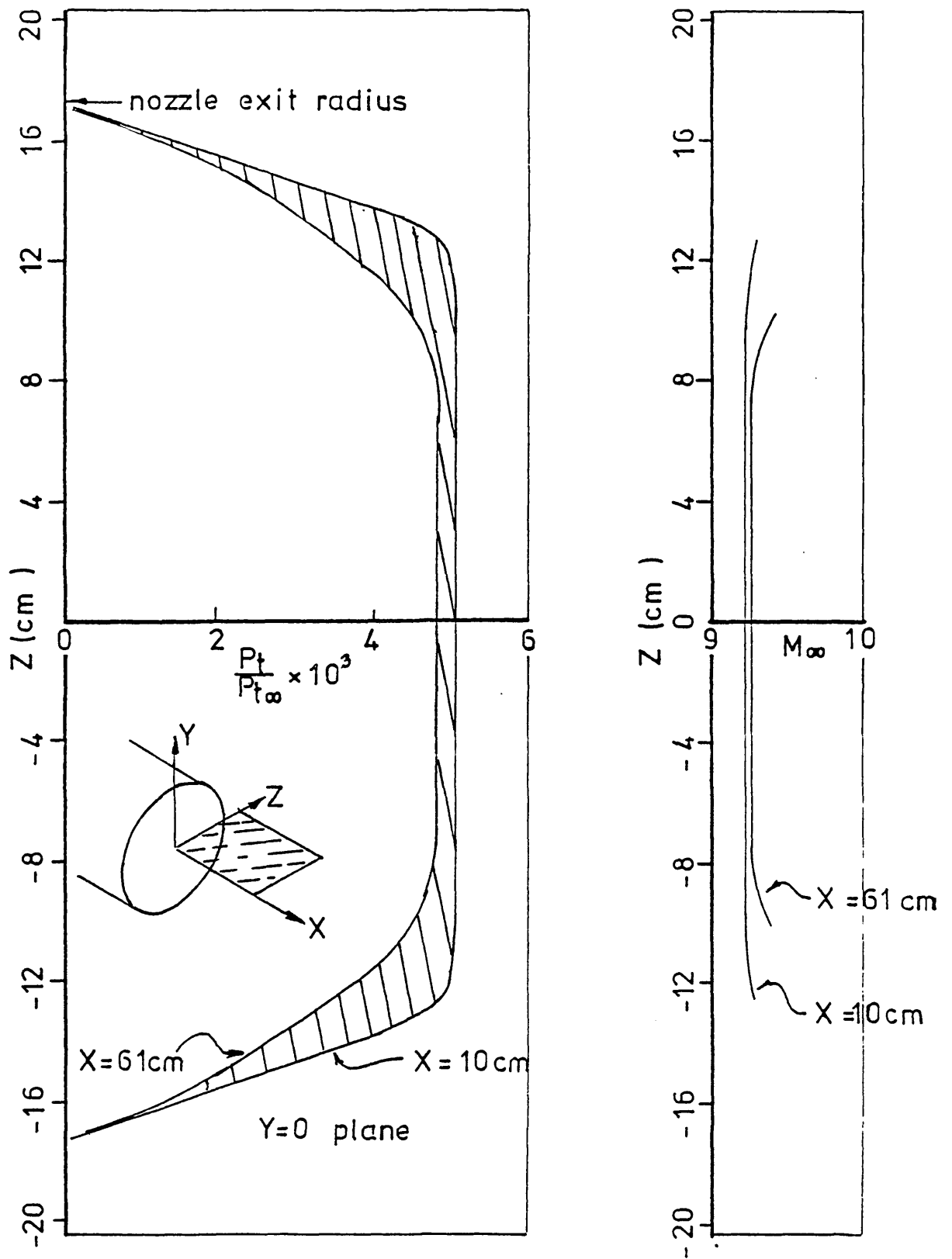
FIG 3   Test core uniformity $Re\infty/cm = 5.17 \times 10^{5}$

Reservoir pressure

2125 psia. Nom

surface pressure

0·1 / 6·7 psia

pitot pressure

·2 G / 12·1 psia

Re∞/cm =1·29×10⁵

9515 psia. Nom

0·36 / 4·6 psid.

surface pressure

2·1 / 61 psia

pitot pressure

3·98 / 90·4 watts/cm²

heat transfer

Re∞/cm =5·17×10⁵

5 ms
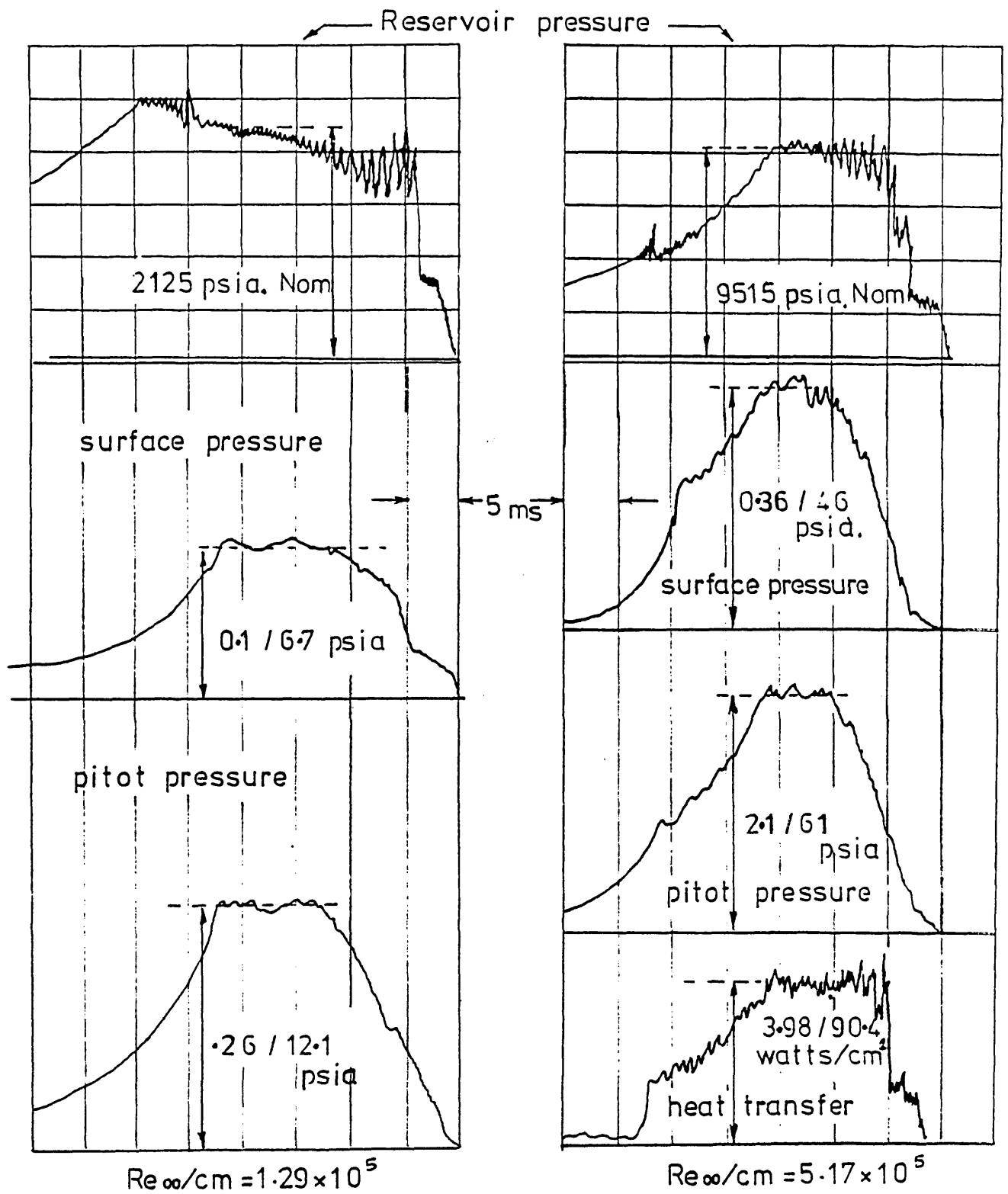
FIG 4   Typical instrumentation response
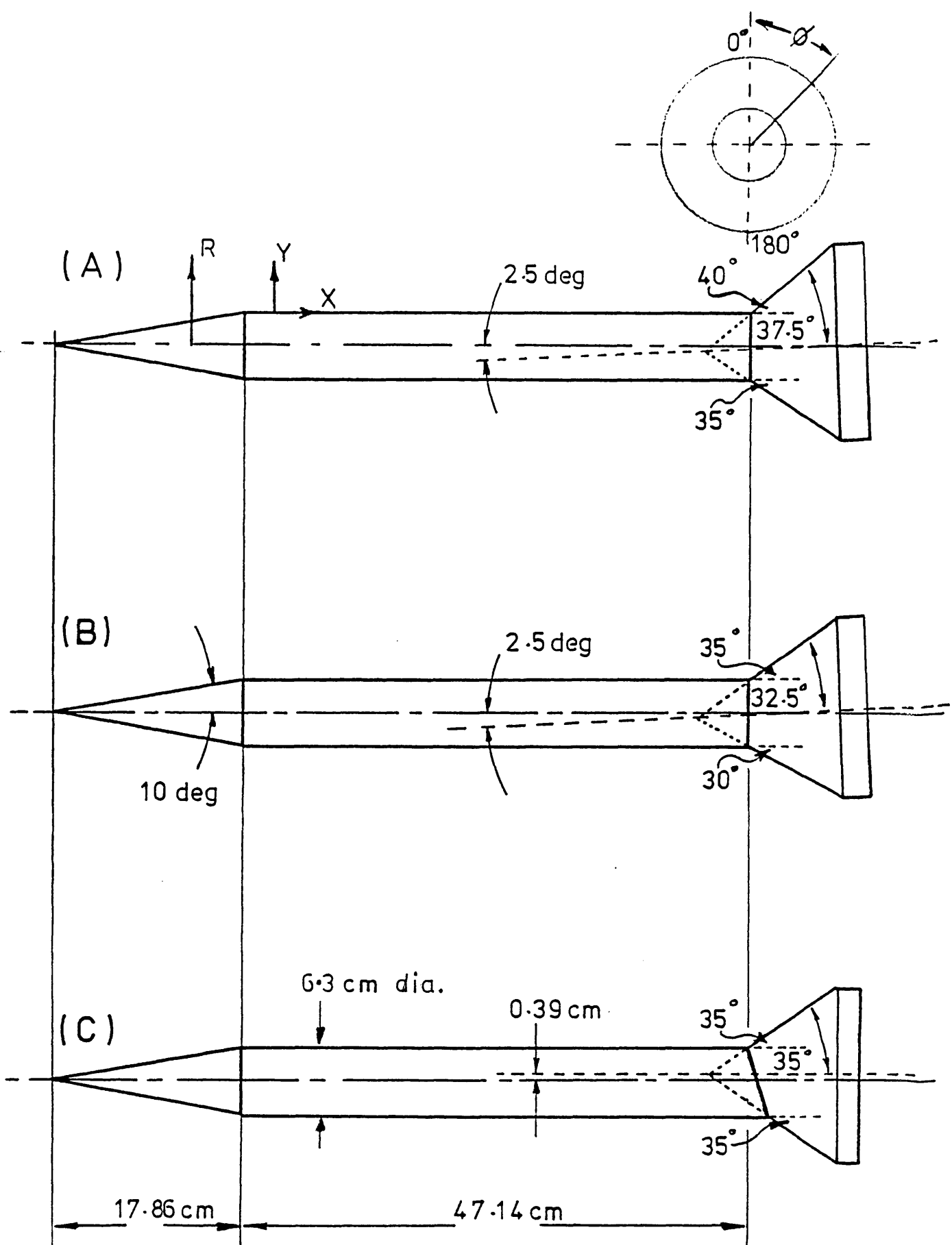
FIG 5 Basic asymmetric geometries

geometry (B) - full scale

Flare Positions
Datum
Datum -0.25cm
Datum -0.50cm

shims

heat transfer

static pressure
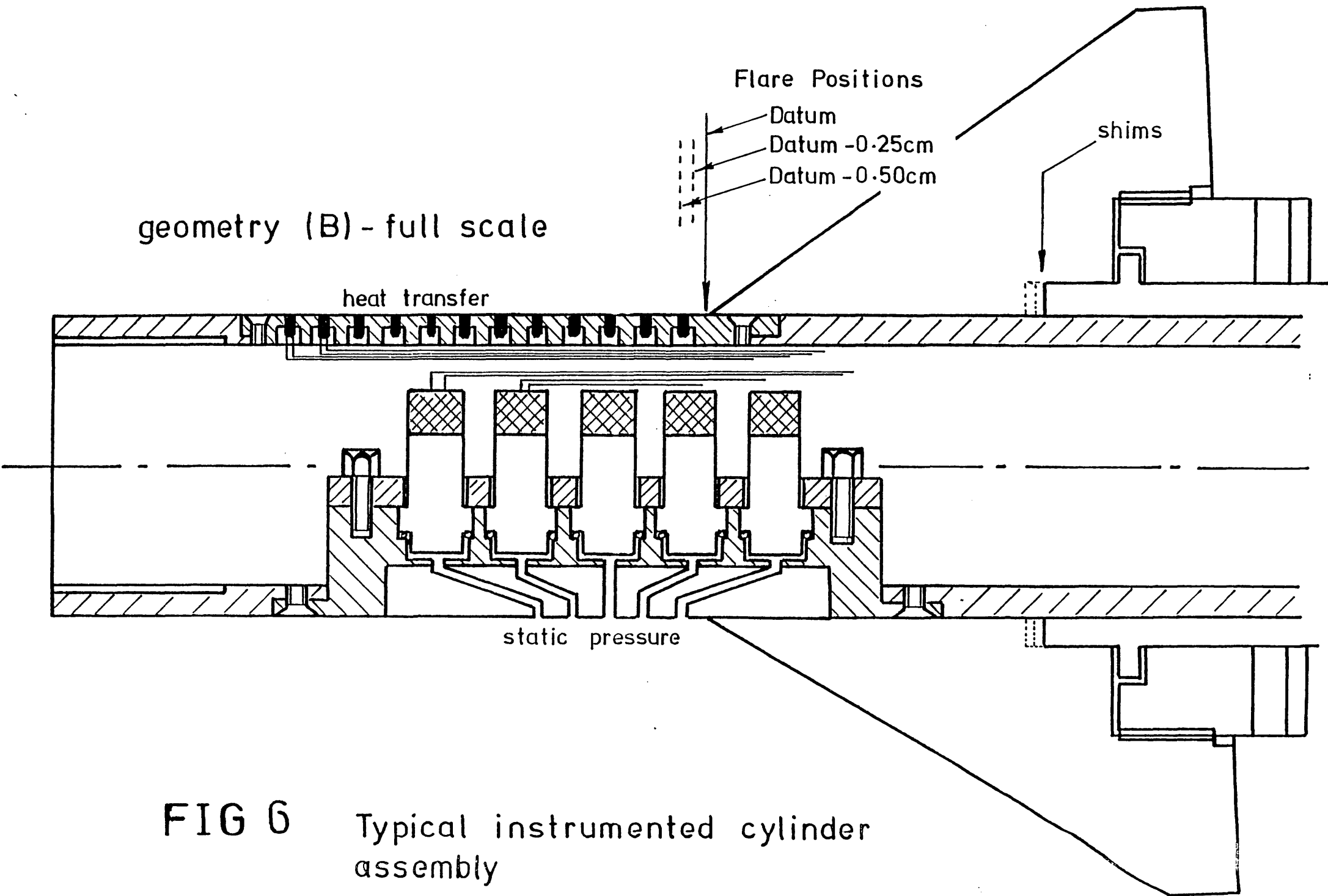
FIG 6   Typical instrumented cylinder
assembly

aprox 3 μm sputtered Platinum

3 mm

Qartz

silver paste

Heat Transfer Gauge Construction

geometry (B) - full scale

heat transfer module

sliding fit

flare mandrel

cylinder mandrel

static pressure tapings
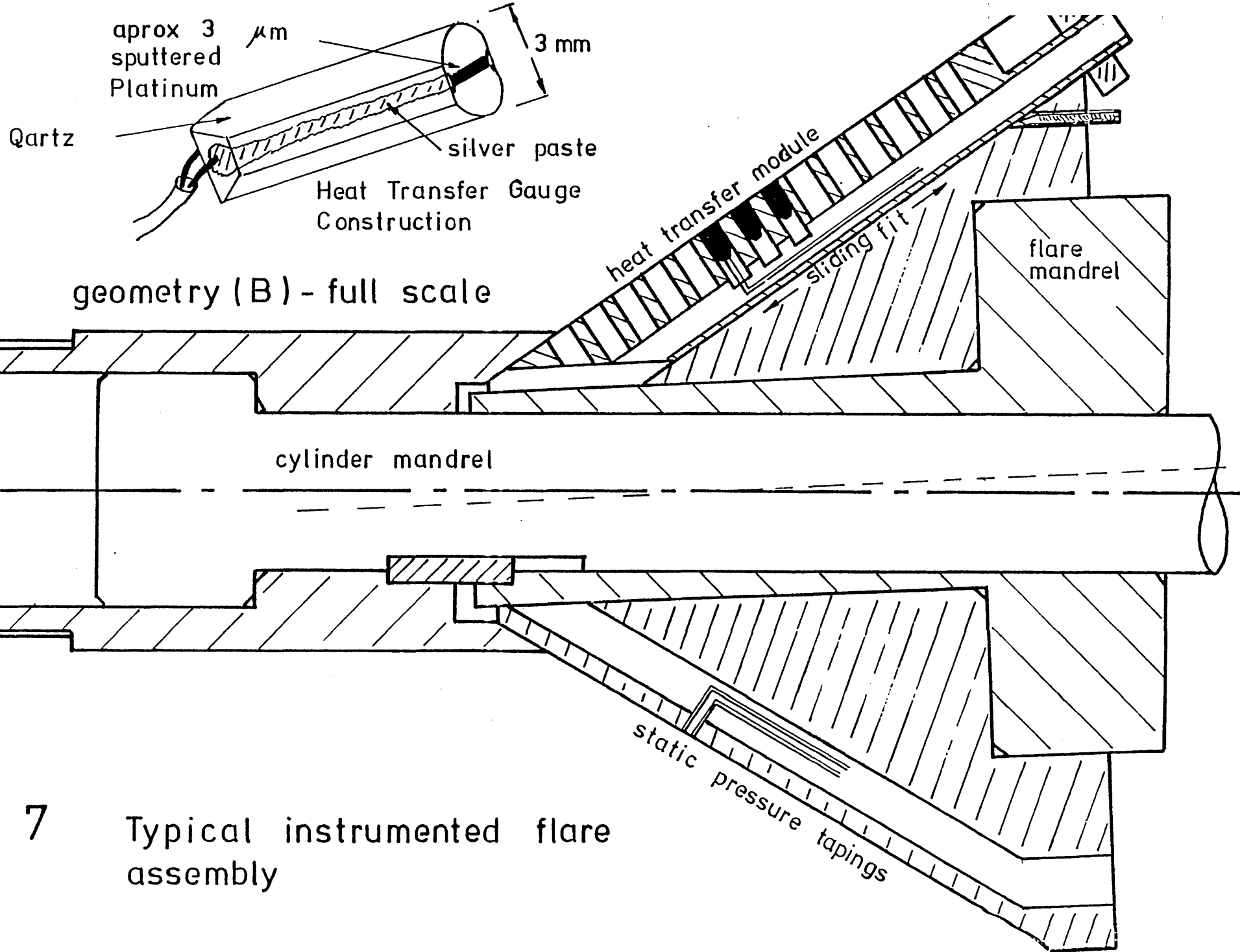
FIG 7   Typical instrumented flare assembly
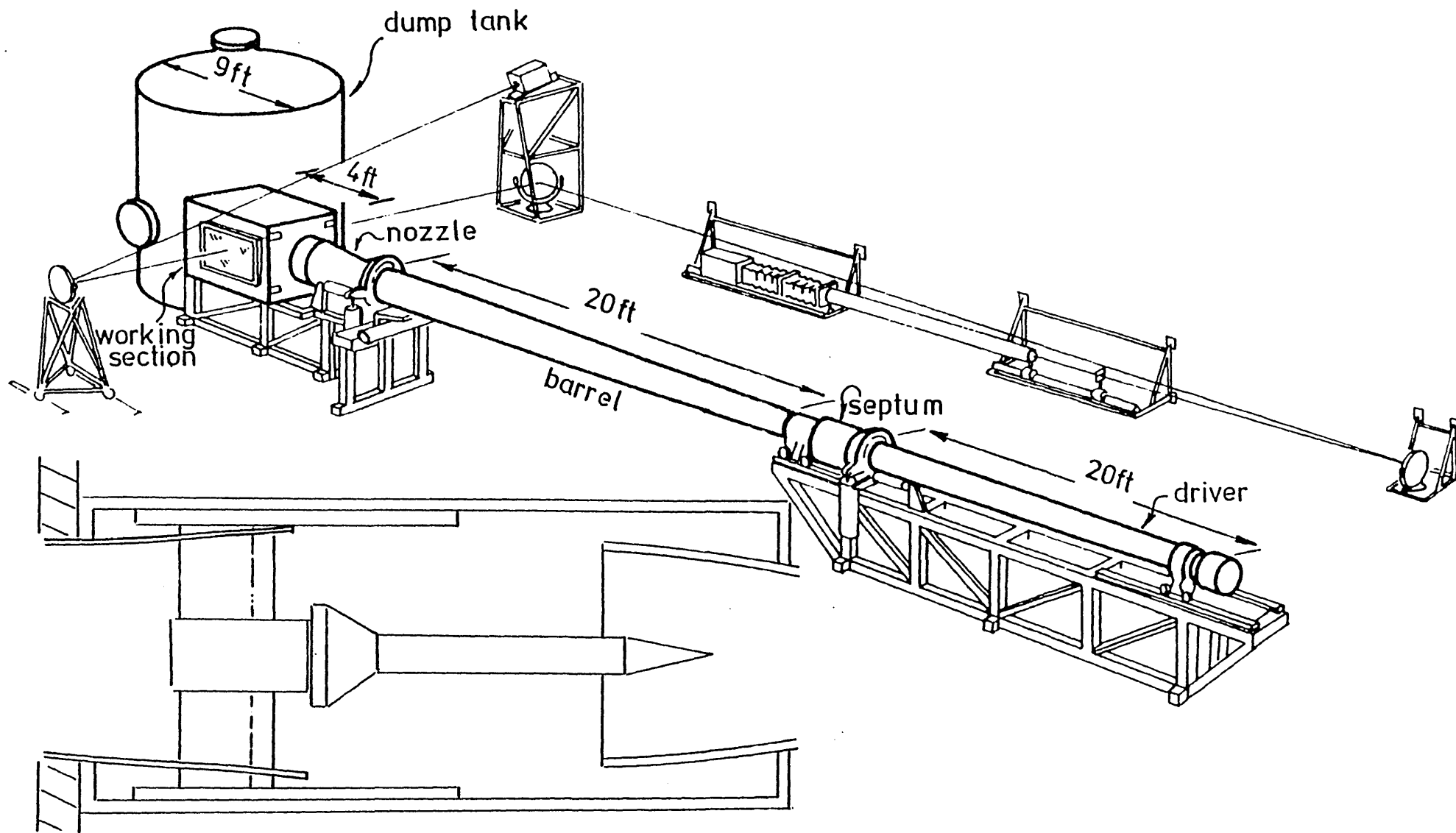
FIG 8   Experimental facility
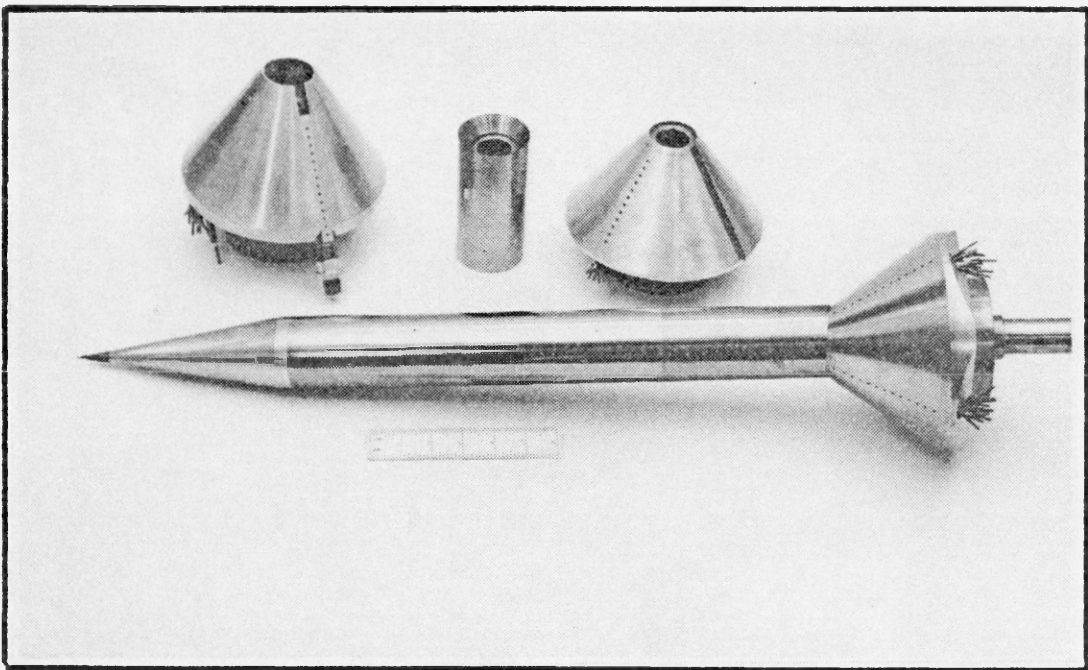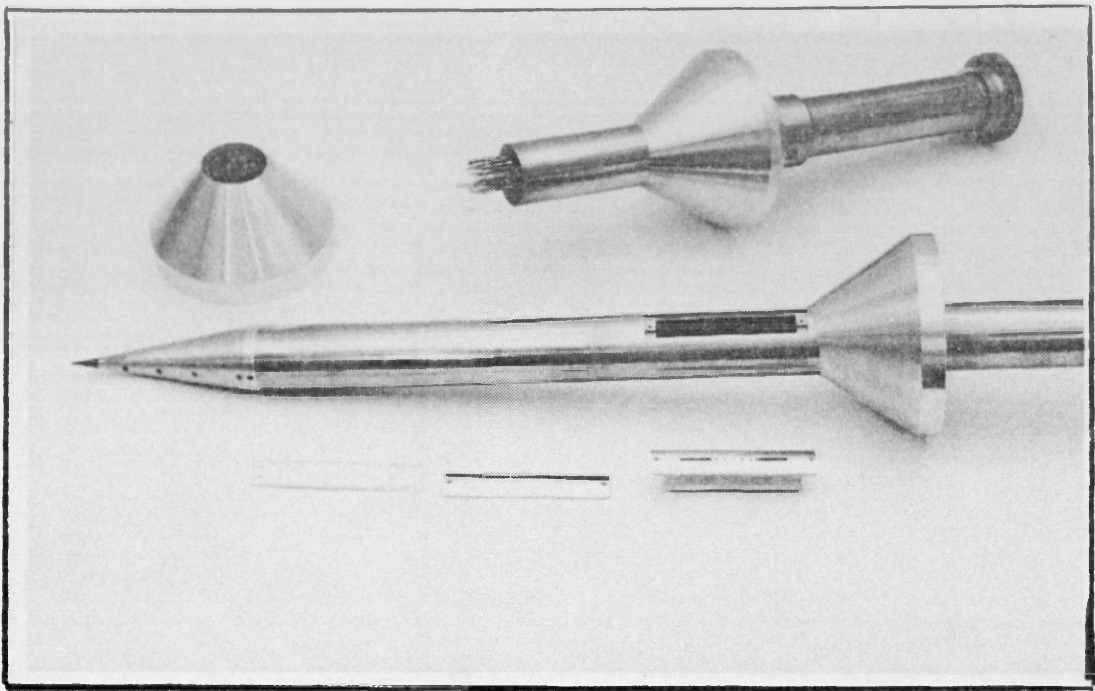
FIG 9   Selected Model Components
(cone-cyl-asymmetric flares only)
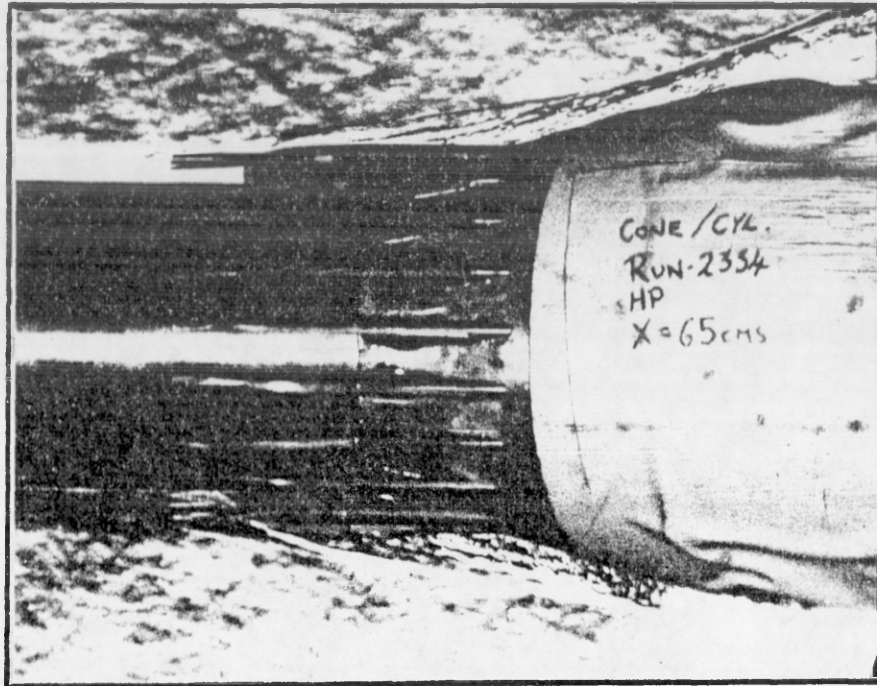
Simultaneous Schlieren/flash exposure

Probe details

0·060" stainless tube (o/d)

0·015"

Inside dimension

3·85 cms

(To support intersection line)
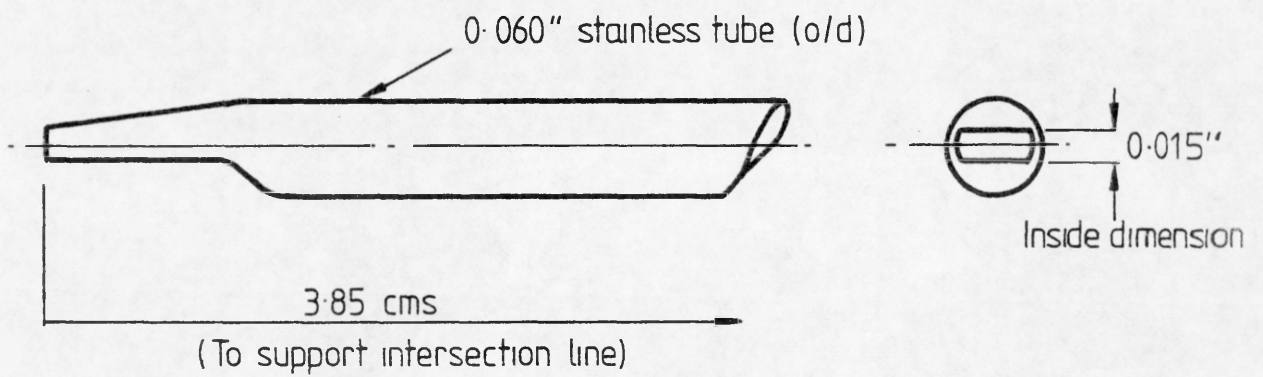
PITOT RAKE DURING OPERATION
(M_e = 9·31, $Re\infty$/cm = 5·17 × 10^5)

FIG 10
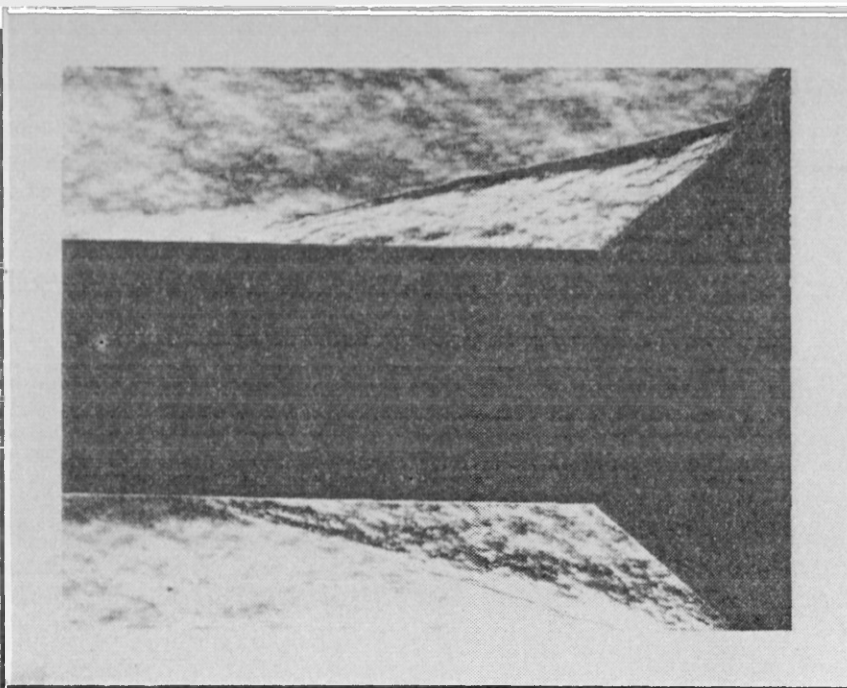
$\alpha = 40$ deg.
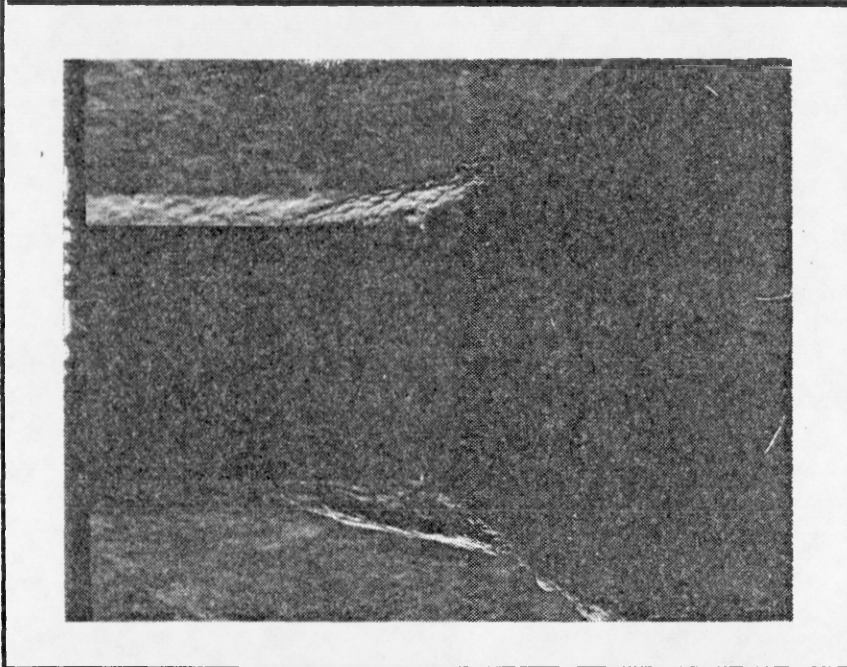
$\alpha = 35$ deg.
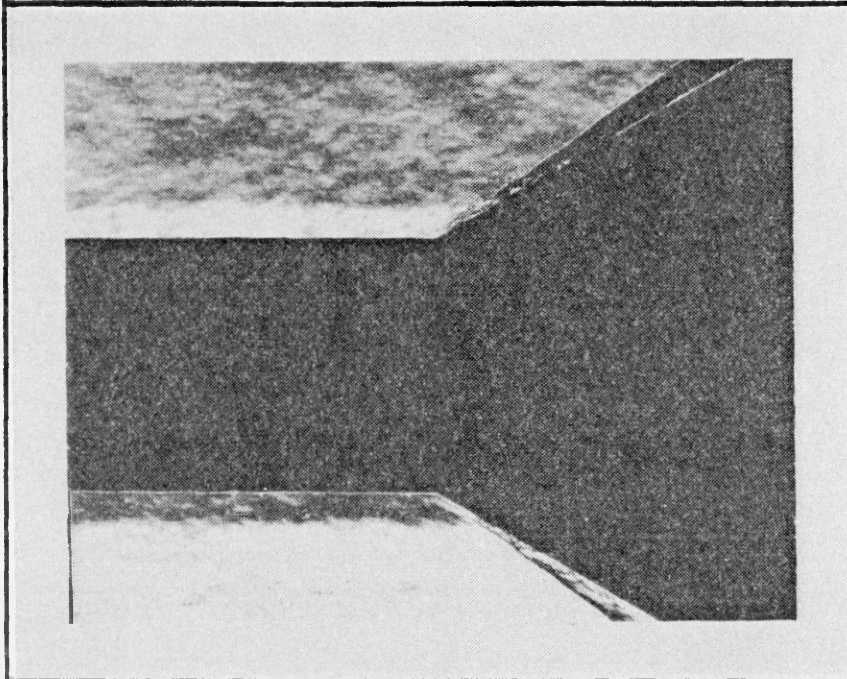
$\alpha = 30$ deg.

FIG 11   Schlieren Photographs

(axisymmetric flow, $M_\infty = 9.31$, $Re_\infty/cm = 5.17 \times 10^5$)
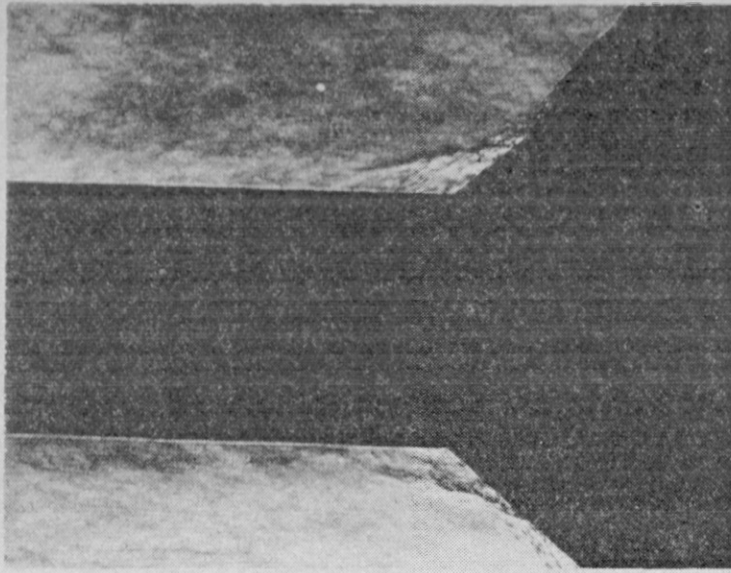
$\alpha = 40$ deg.
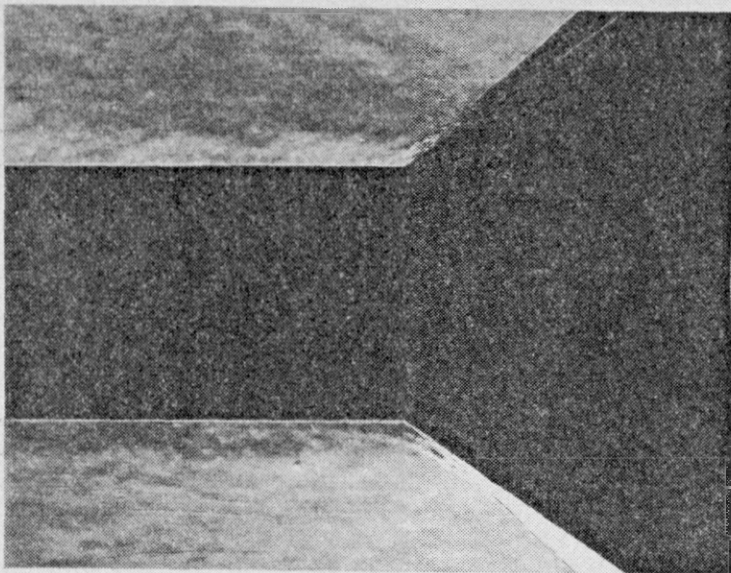
$\alpha = 35$ deg.
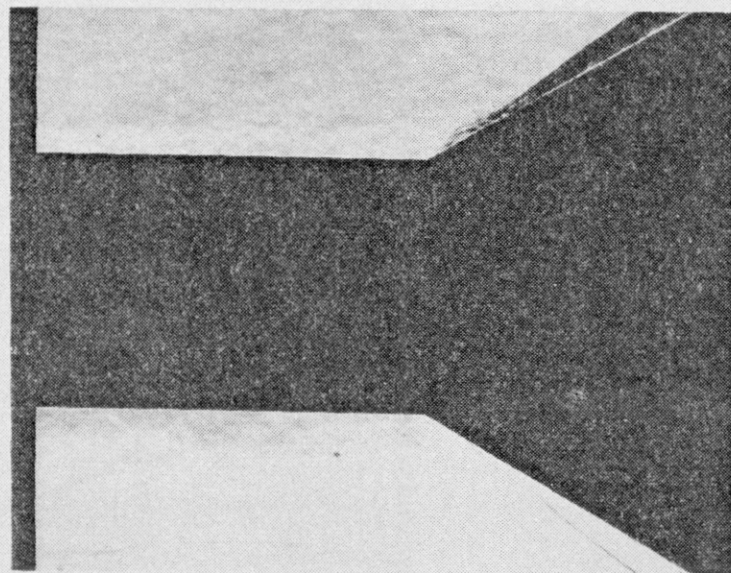
$\alpha = 30$ deg.

FIG 12   Schlieren Photographs
(axisymmetric flow, $M_\infty = 8.93$, $Re_\infty/cm = 1.29 \times 10^5$)

$M_\infty = 9 \cdot 31$

$P_\infty = 2490 \ N/m^2$

$(0 \cdot 36 \ psia)$

$\dfrac{Pe - Pw}{Pw} = 0 \cdot 02$

EXPANSION FAN
(region of strong
normal pressure
gradient)
$\dfrac{Pe - Pw}{Pw} > 2\%$

shock curvature

FLOW

ENTROPY LAYER

IRROTATIONAL FLOW

CONICAL SHOCK

OBSERVED BOUNDARY LAYER
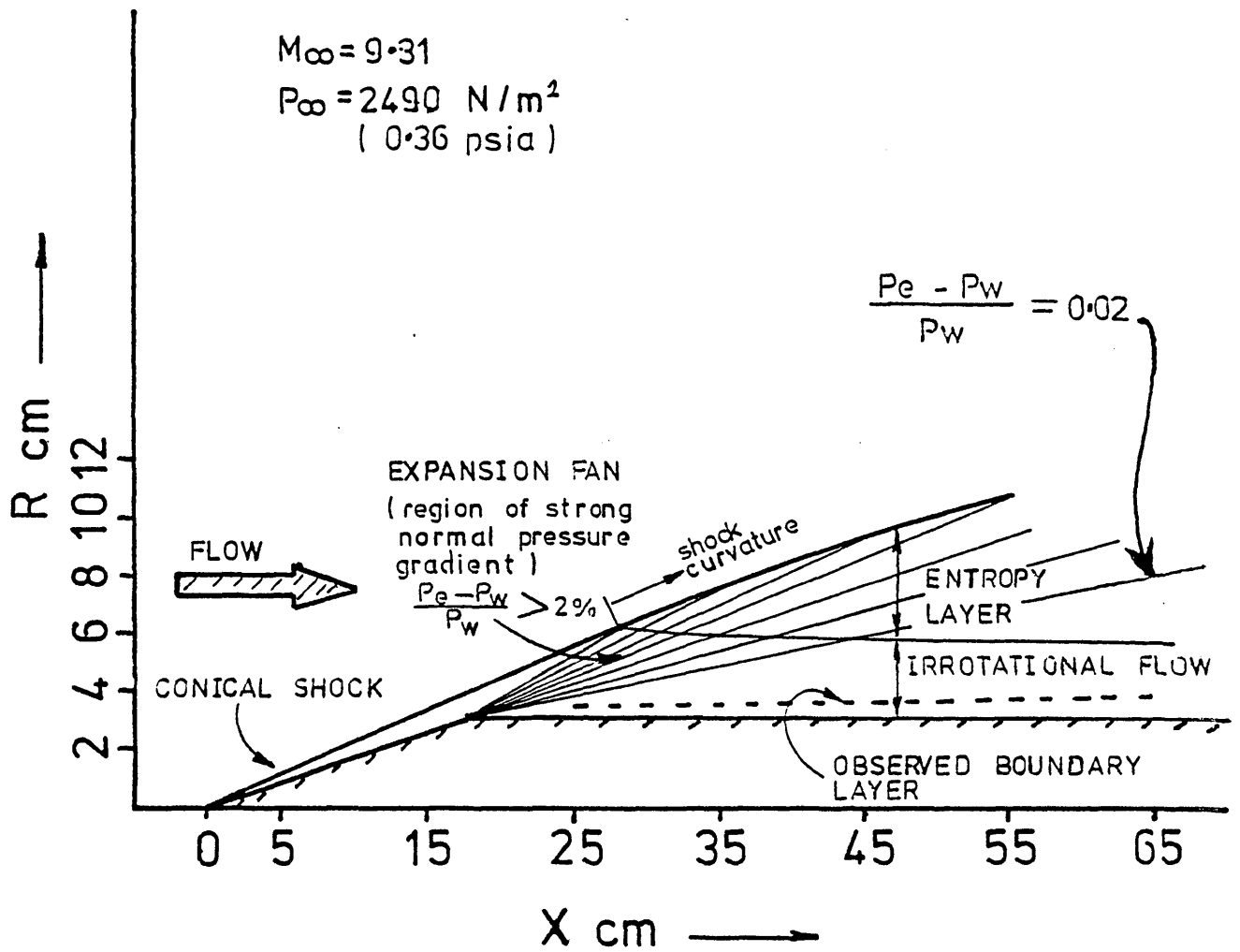
NOTE: AXES   NOT TO SAME SCALE

FIG 13

FOREBODY FLOW FIELD — COMPUTER
PREDICTION

Re$_\infty$/cm = 5.17×10^5
M$_\infty$ = 9.31

+ ——— COLEMAN
——— METHOD OF CHARACTERISTICS
O ——— EXPERIMENT

CONE SHOULDER
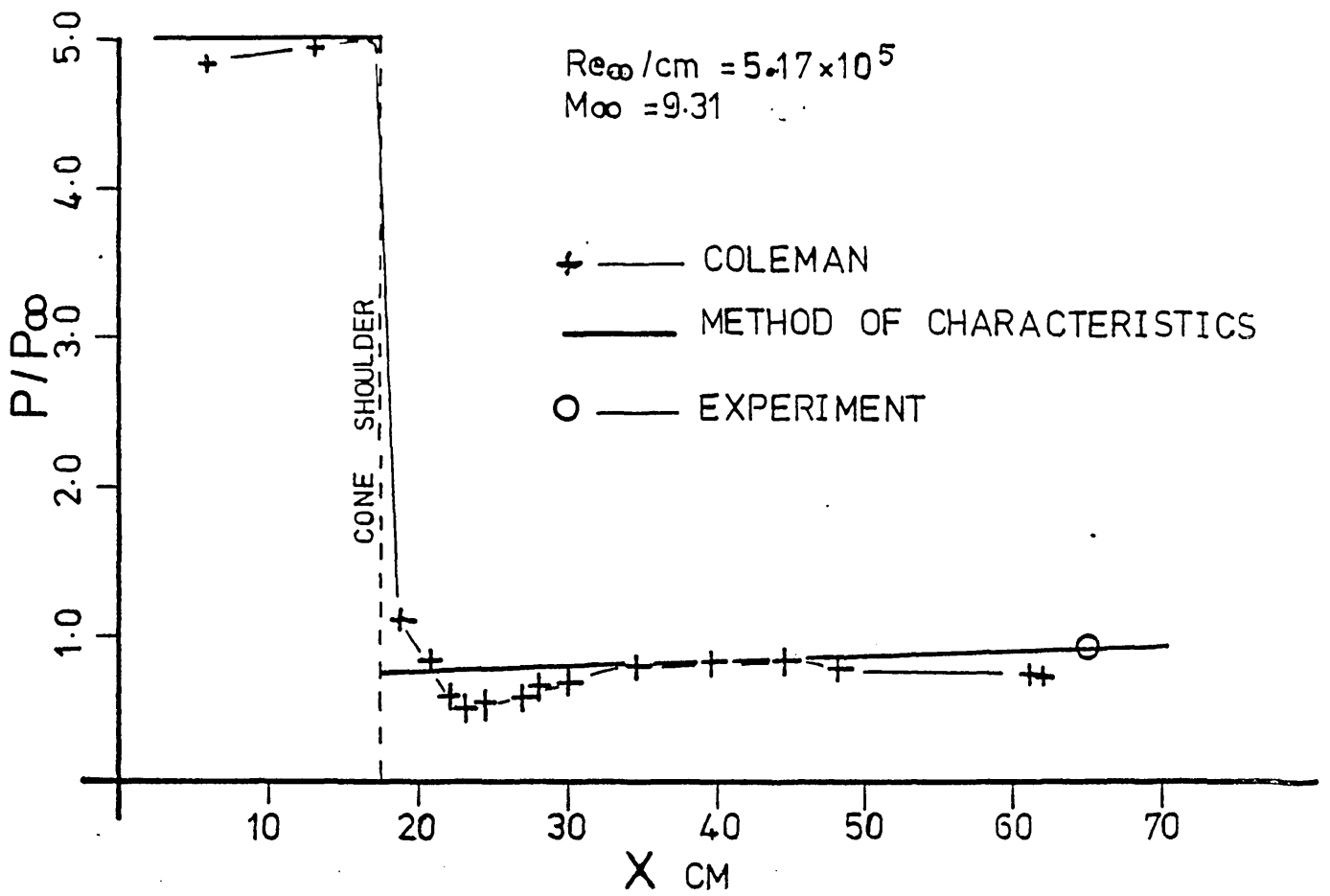
FIG 14 STATIC PRESSURE (CONE-CYLINDER ONLY)

METHOD OF CHARACTERISTICS

$\hat{P}$
M$_\infty$ = 9.31
Re$_\infty$/cm = 5.17×10^5

FLARE SURFACE (extreme case)

40°

CYLINDER SURFACE

$P_{oe}/P_{o\infty}$ (THEORY)
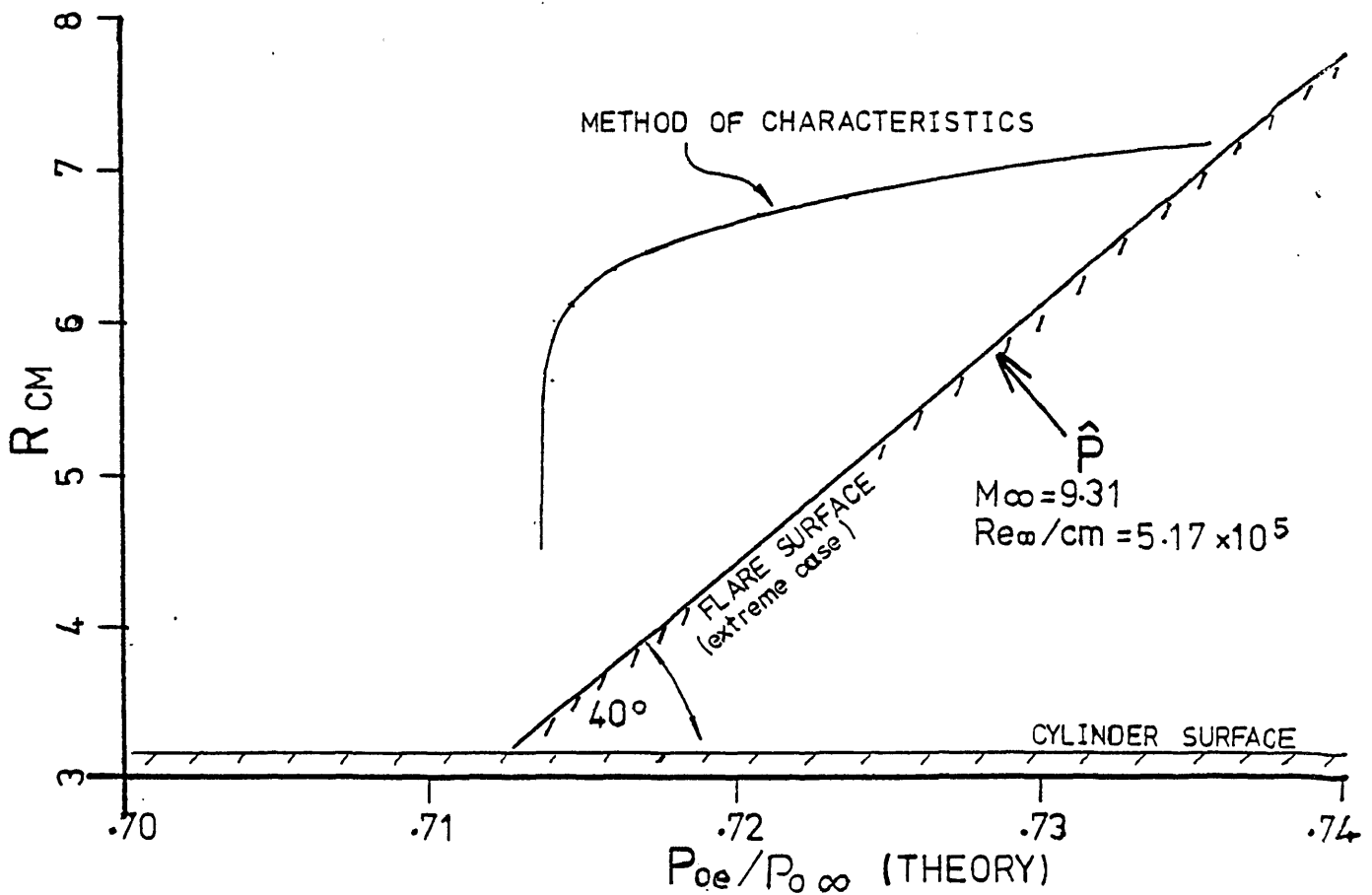
FIG 15 TOTAL PRESSURE AT X = 65 CM
(CONE-CYLINDER ONLY)
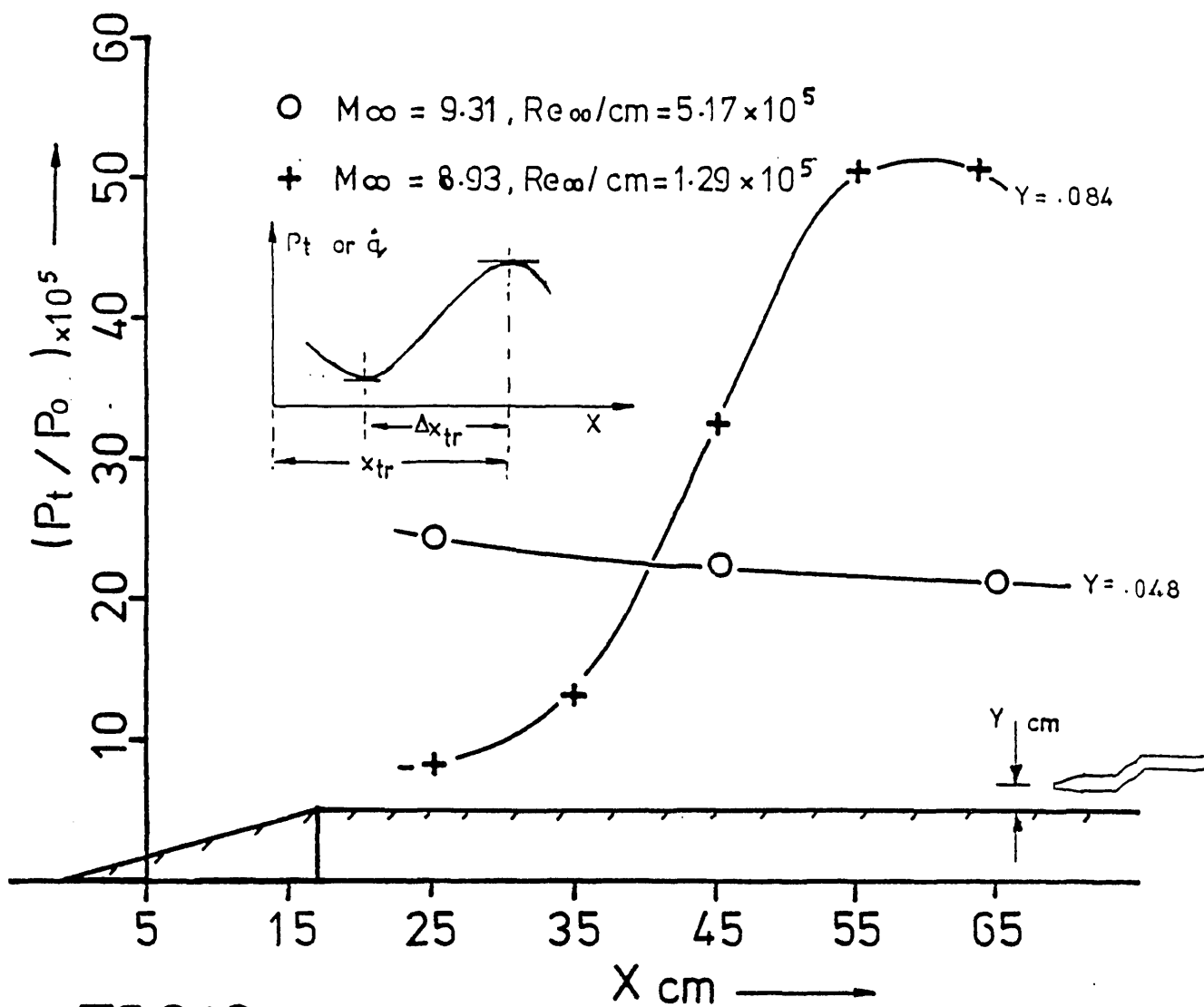
FIG16a SURFACE PITOT DISTRIBUTIONS
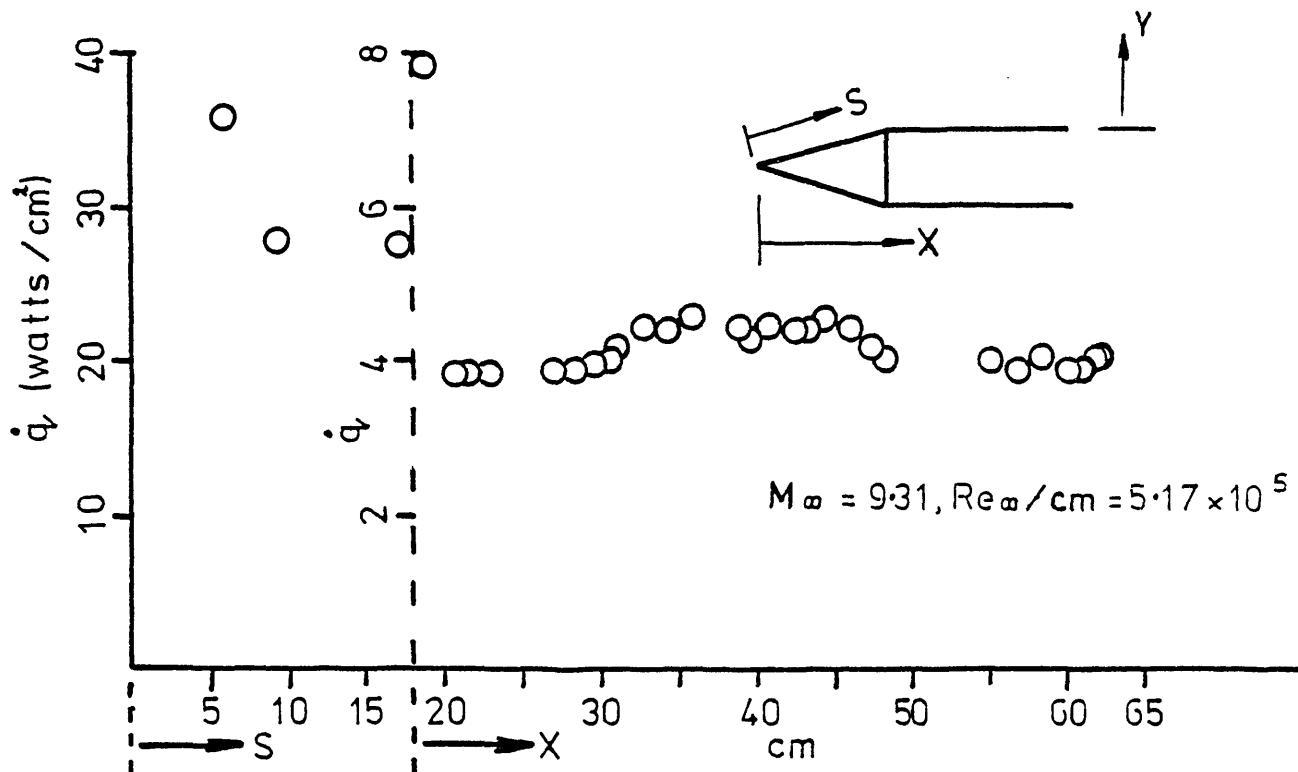
FIG 16b HEAT TRANSFER DISTRIBUTION
(COLEMAN 1973)

Y cms →

Probe ht

(03)　　(02)　　(01)

$$\left[\frac{Pt}{P_{o\,\infty}} - \begin{pmatrix} 01 \\ 02 \\ 03 \end{pmatrix} \right] \times 10^{-3} \longrightarrow$$

Station	X cm
01	25
02	45
03	$\begin{cases} 63{\cdot}6 - LP \\ 65 \quad - HP \end{cases}$

$M_\infty = 8{\cdot}93$

$M_e = 8{\cdot}40$

$Re_\infty / cm = 1{\cdot}29 \times 10^5$
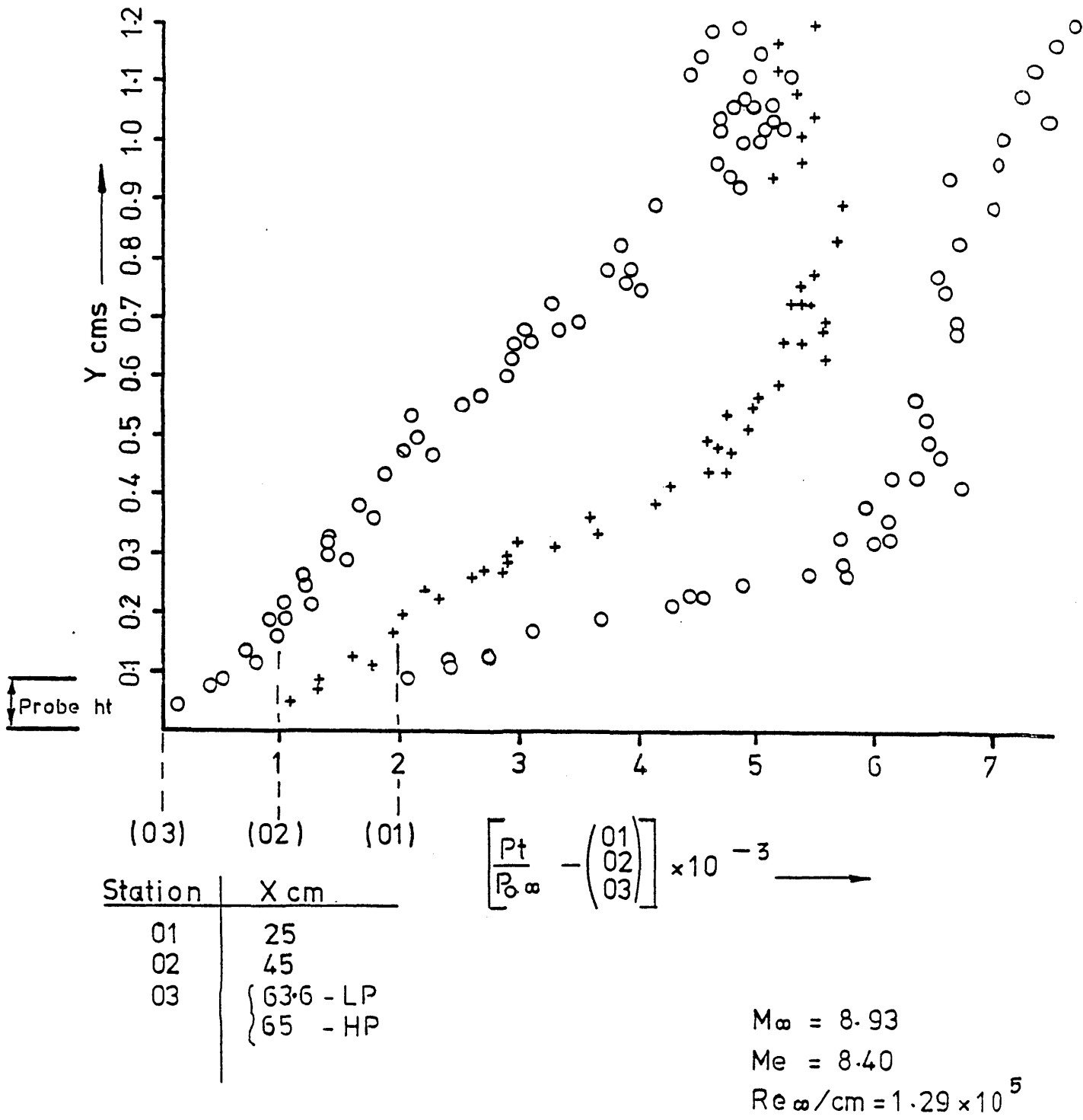
FIG 17　Pitot Profiles　Cone-Cyl
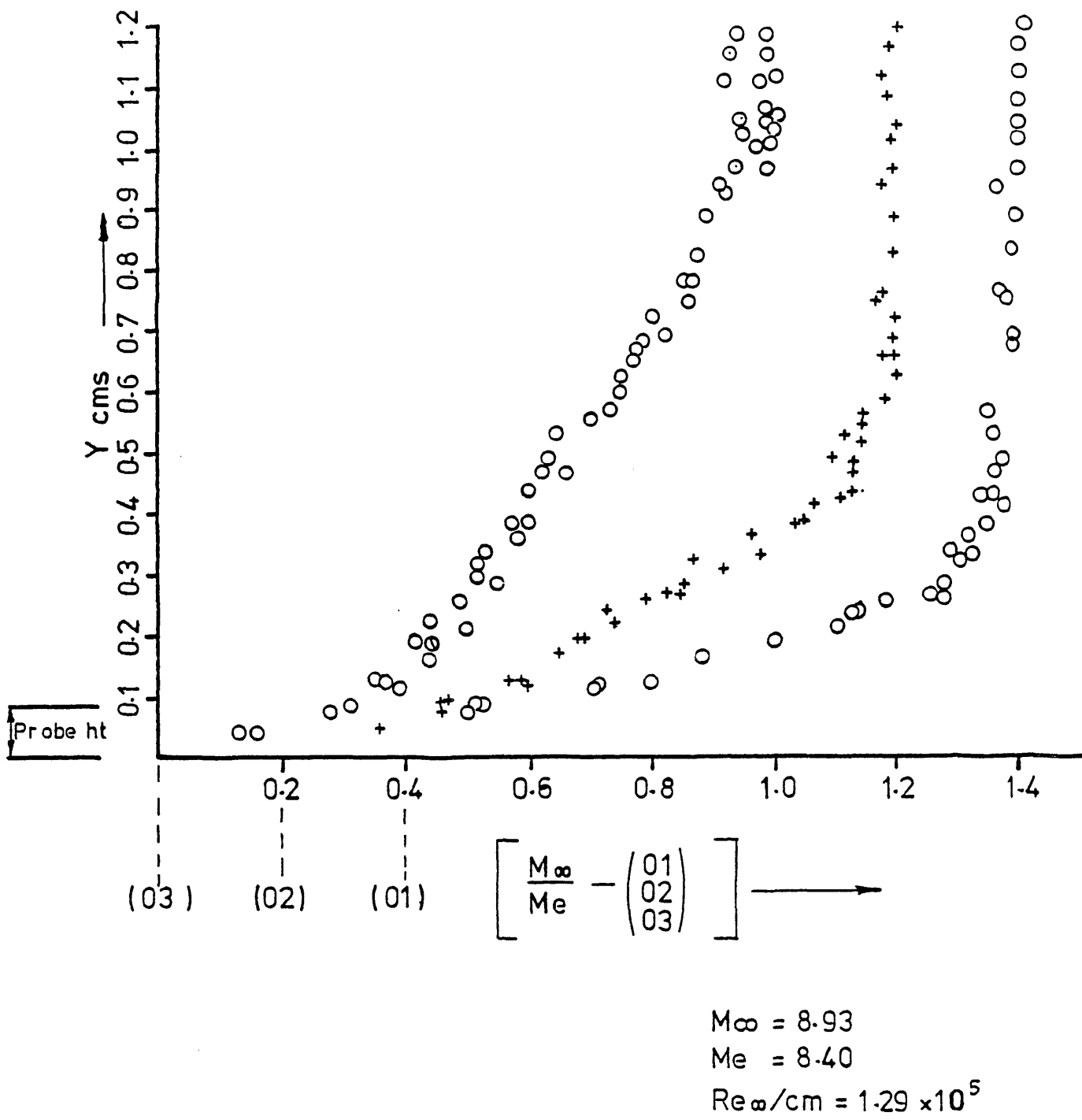
FIG 18   Mach Number Profiles

$M_\infty = 8.93$

$M_e = 8.40$

$Re_\infty/cm = 1.29 \times 10^5$
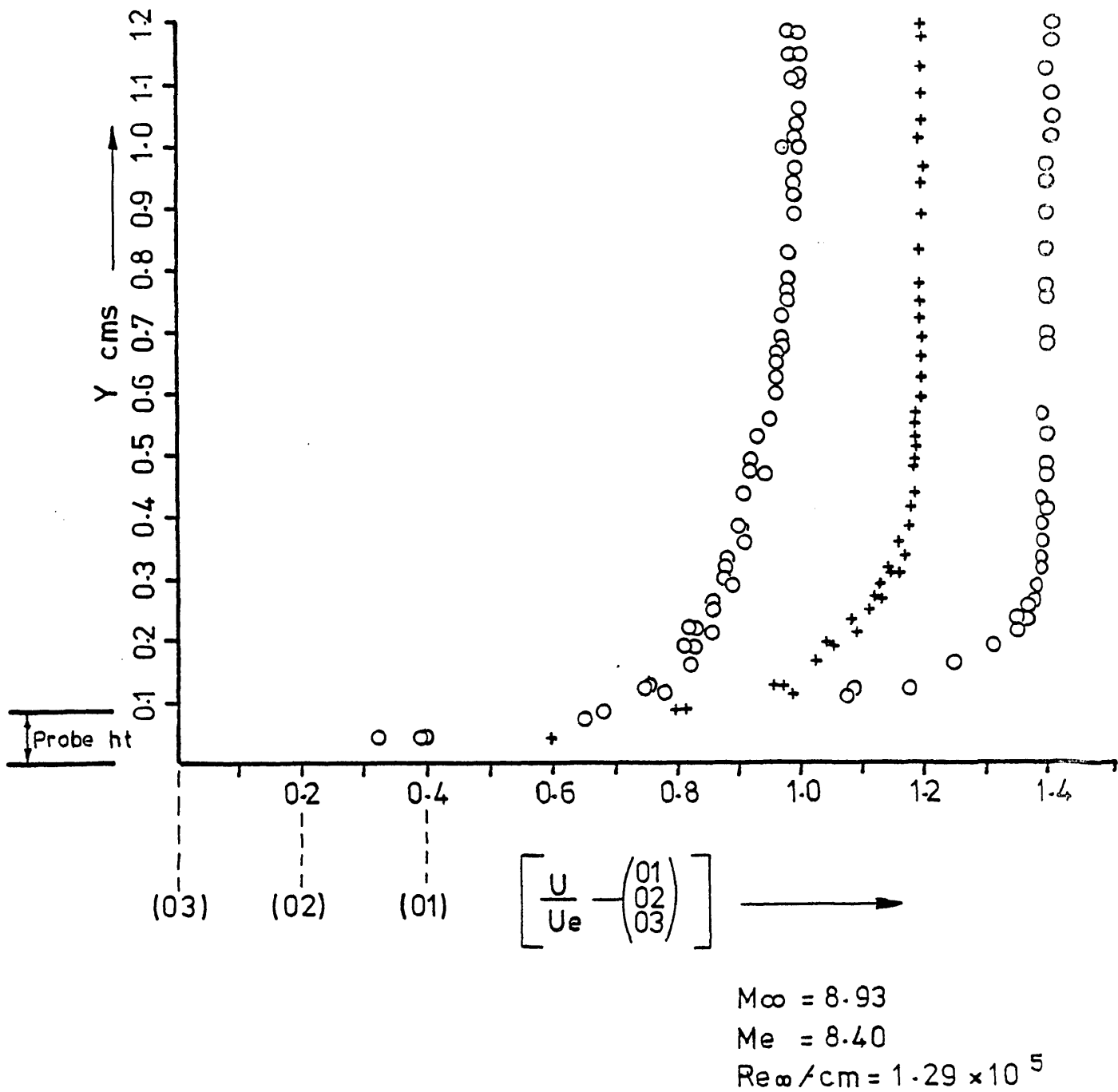
FIG 19   Velocity Profiles
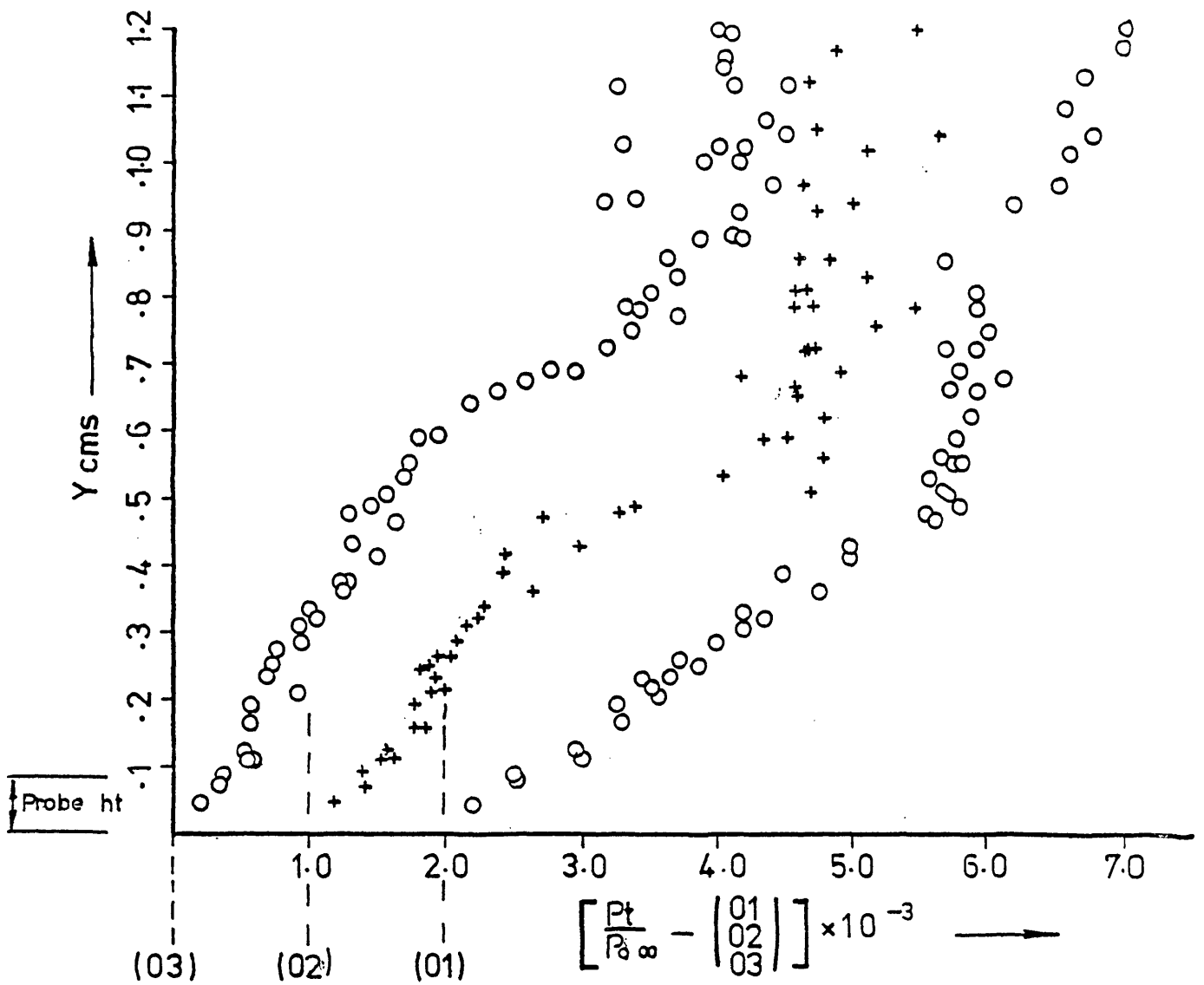
FIG 20   Pitot Profiles   (CONE-CYL)
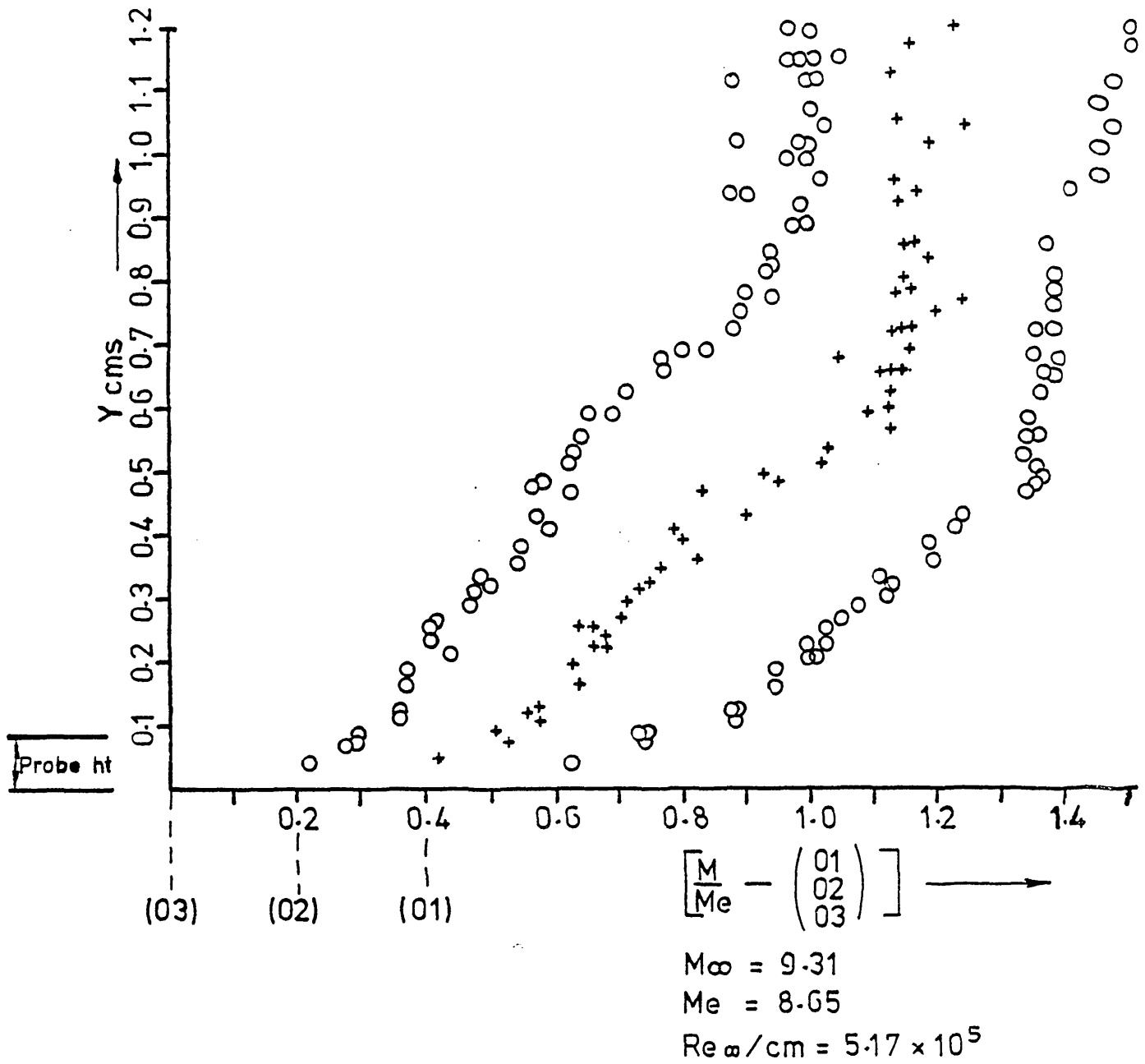
FIG 21   Mach Number Profiles

FIG 22   Velocity   Profiles

EXAMPLE :
X = 63·6
M∞ = 8·93
Me = 8·4
Re∞/cm = 1·29×10⁵

$P_t / P_{0\infty} \times 10^{-3}$ ⟶
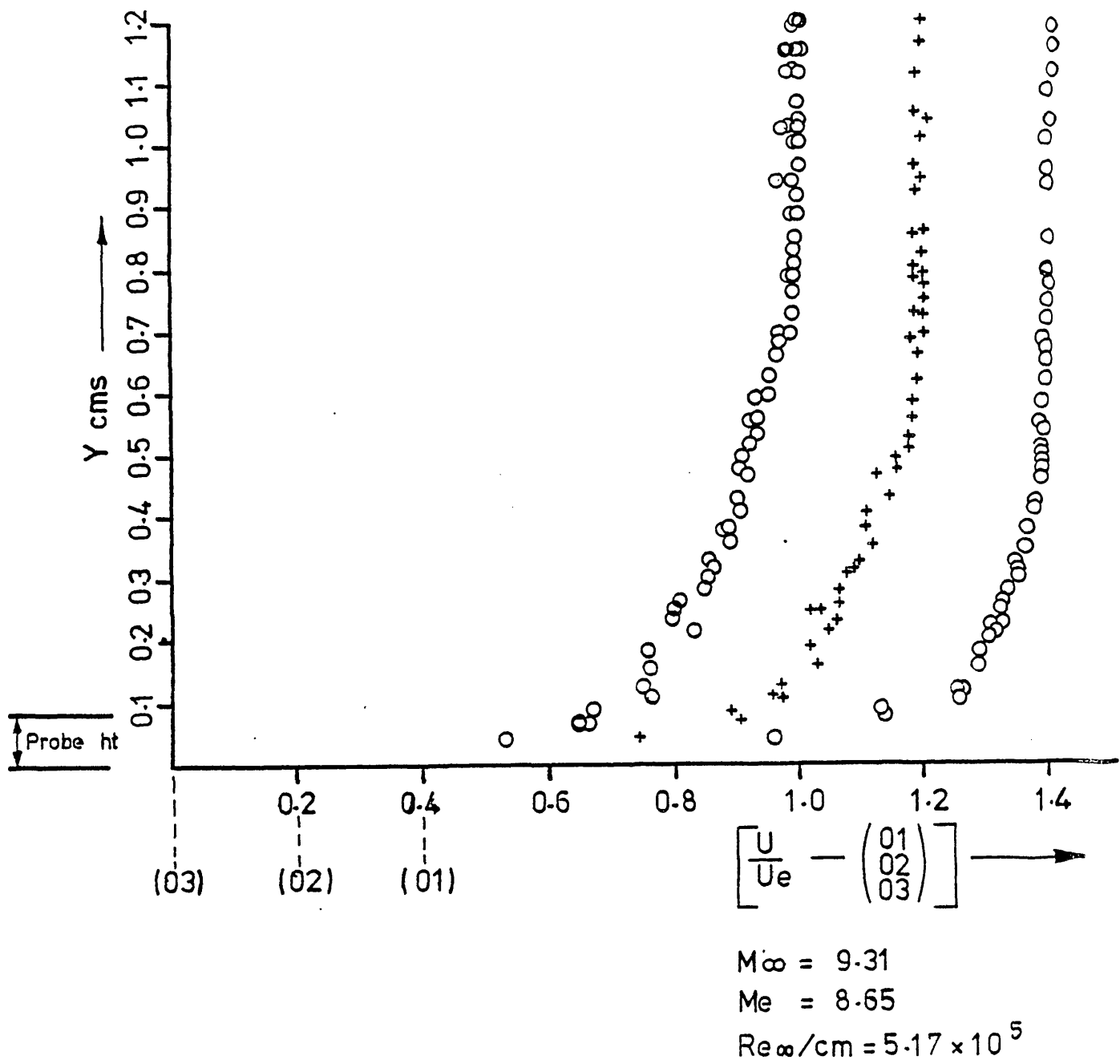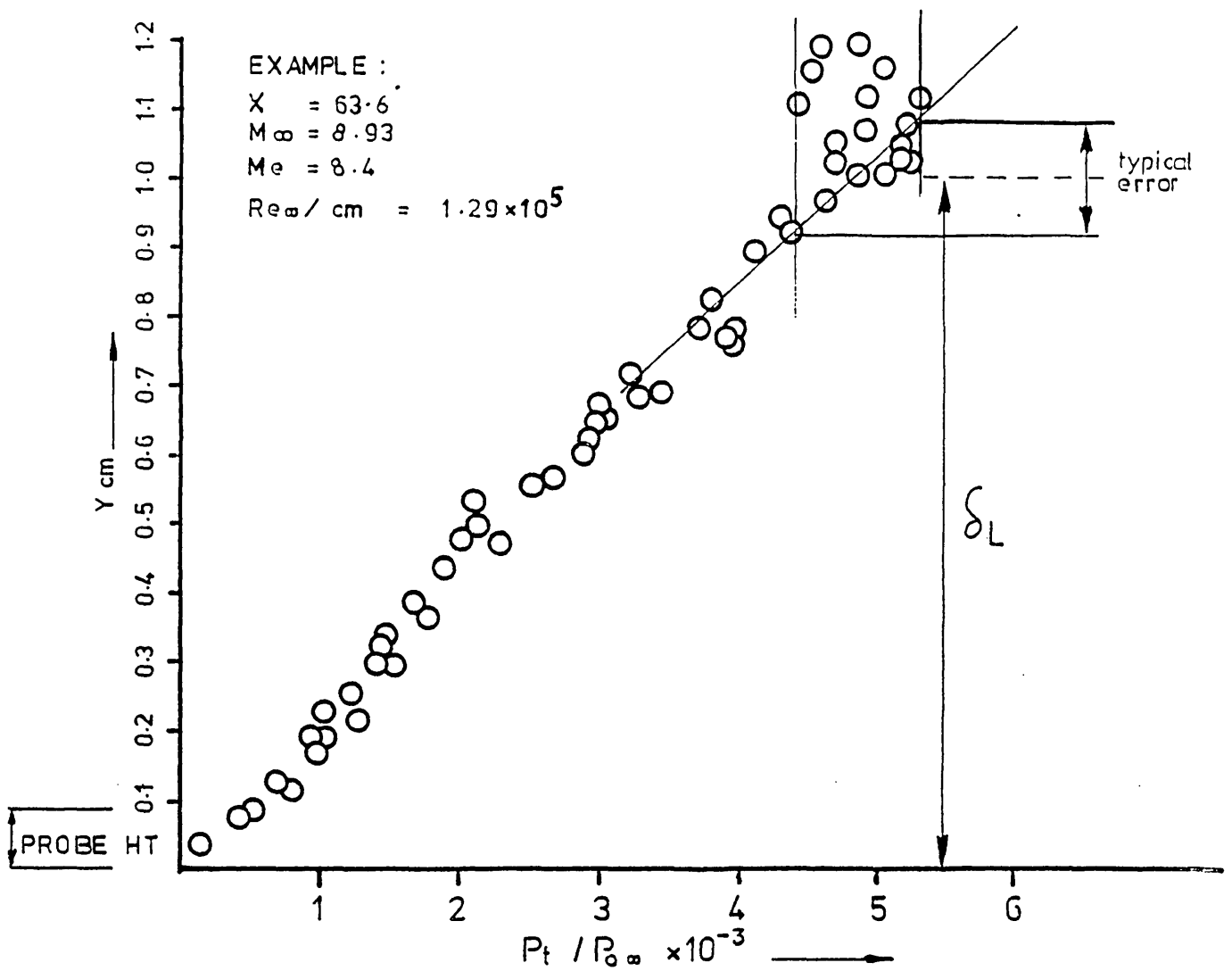
TABLE OF δ_0 VALUES

AUTHOR	MODEL	M∞	METHOD / δ_L cm	
			SCHL	PITOT
ELFSTROM	FLAT PLATE	8·93	0·76	
		9·31	0·72	
COLEMAN	HOLLOW CYLINDER	8·93	0·93	
		9·31	0·46	
LOWDER	CONE CYLINDER	8·93	0·86	1·00
		9·31	0·89	0·97

forced transition

FIG 23 ESTIMATION OF BOUNDARY LAYER HEIGHT
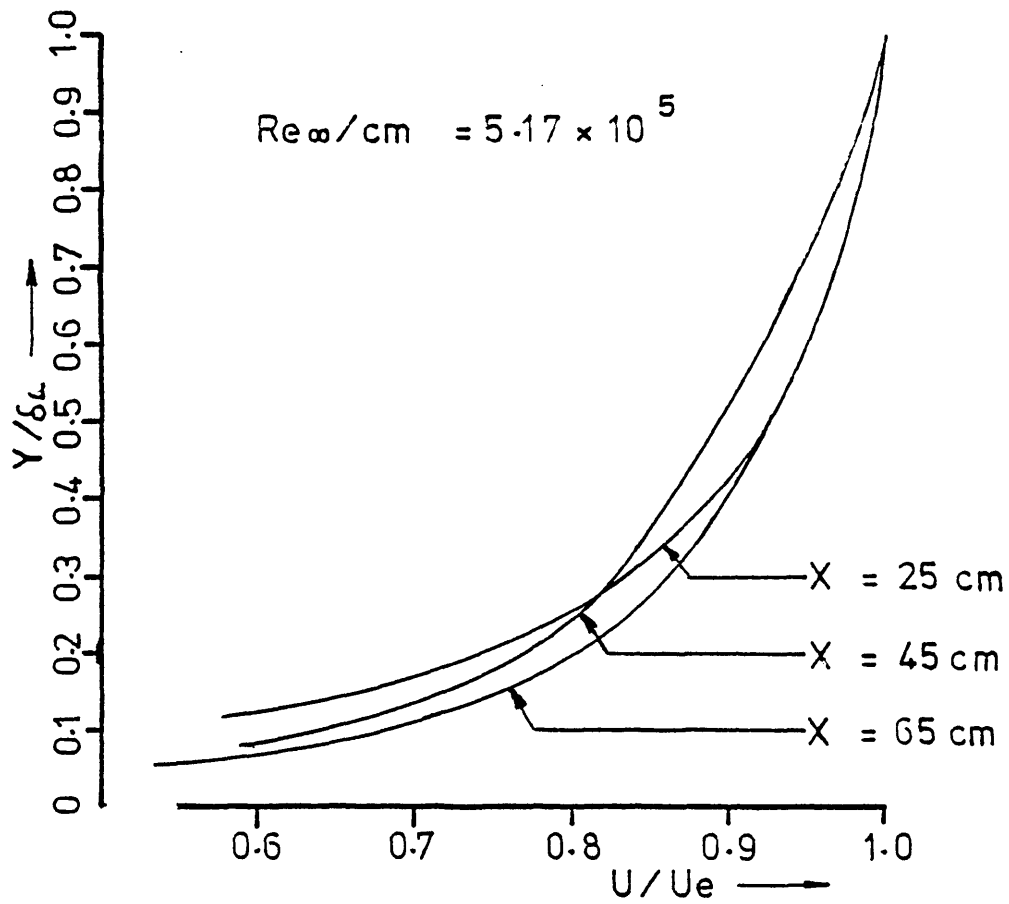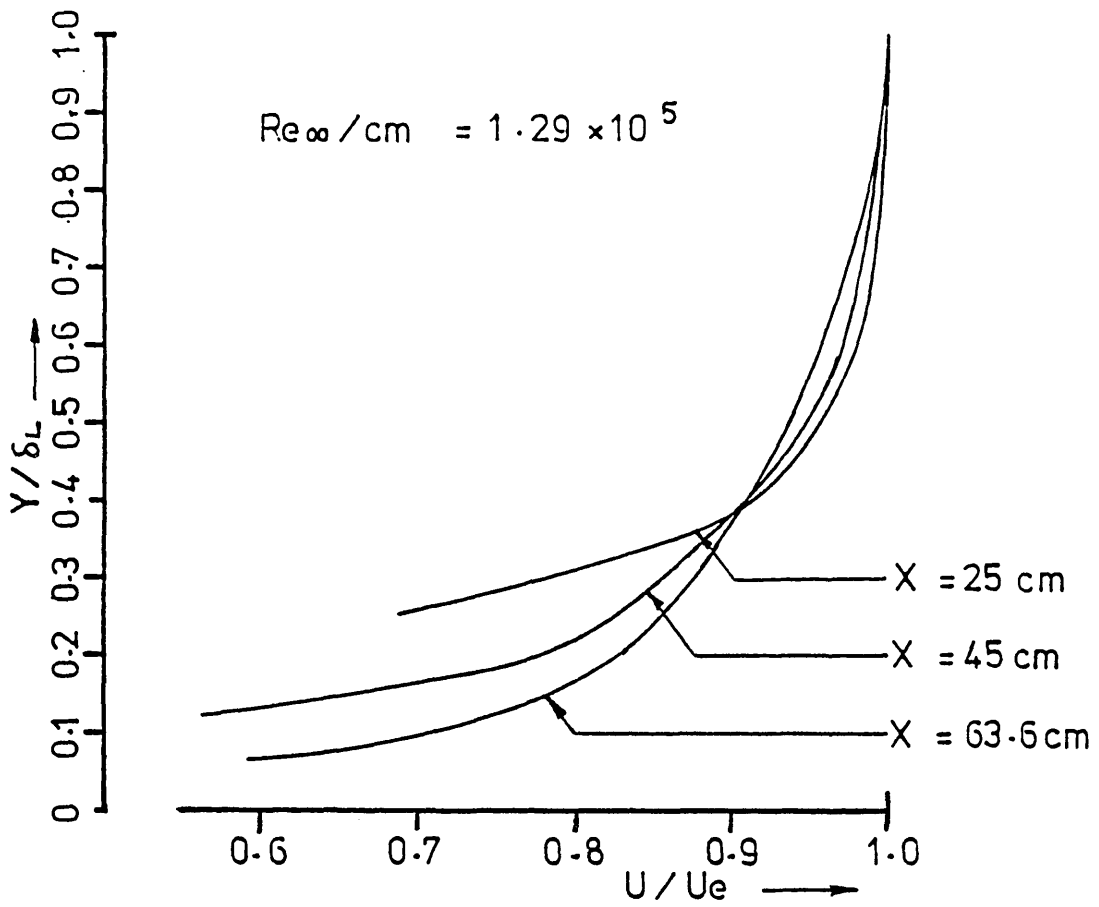
FIG 24   Profile Development
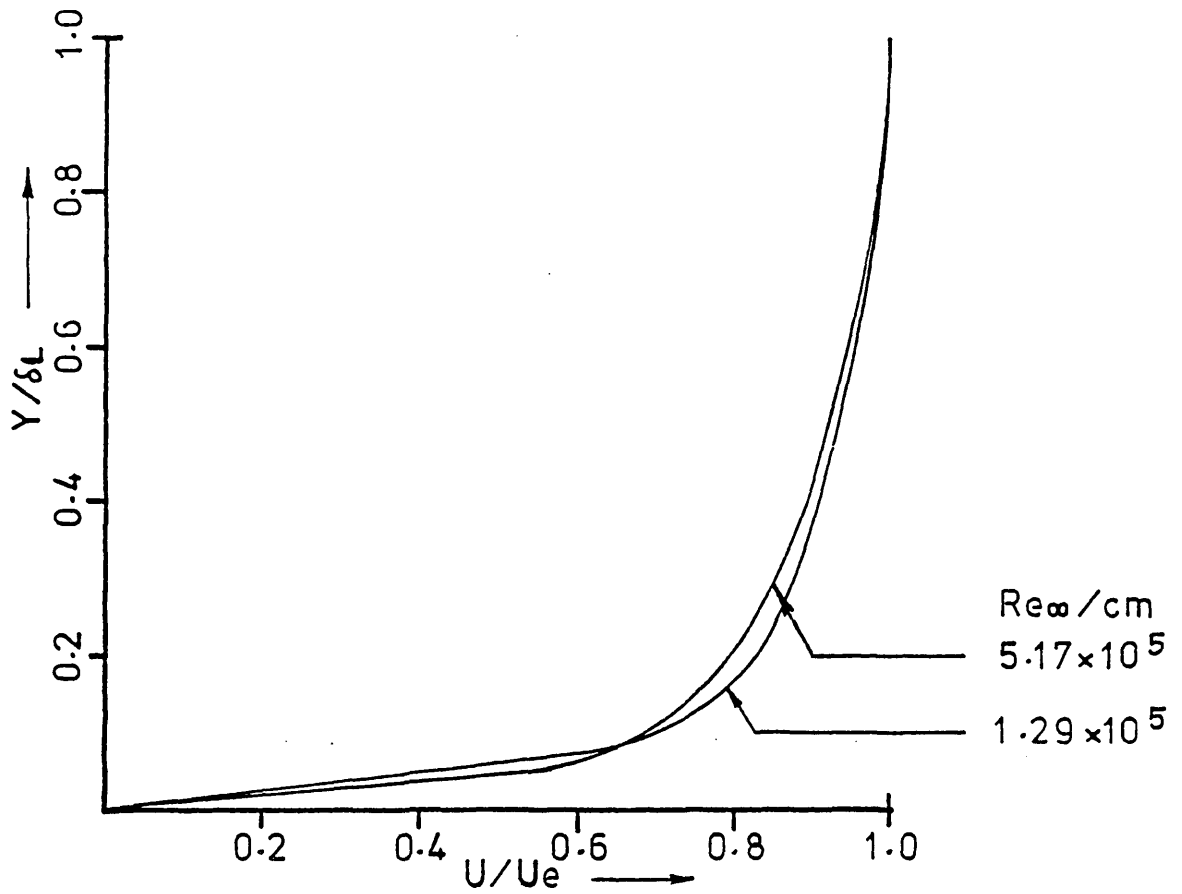
FIG 25   Profile Comparison
(flare intersection line)

Top plot:

CCF – X = 63·6 cm
Re∞/cm = 1·29×10⁵
Re_θ = 3250
R̄ = 350
π = 0·18 (theory)

(COLES)

Middle plot:

CCF – X = 65 cm
Re∞/cm = 5·17×10⁵
Re_θ = 130 50
R̄ = 1140
π = ·49

Bottom plot:

FP – Bartlett (1978) X = 56 cm
Re∞/cm = 5·17×10⁵
Re_θ = 11300
R̄ = 1090
π = ·49
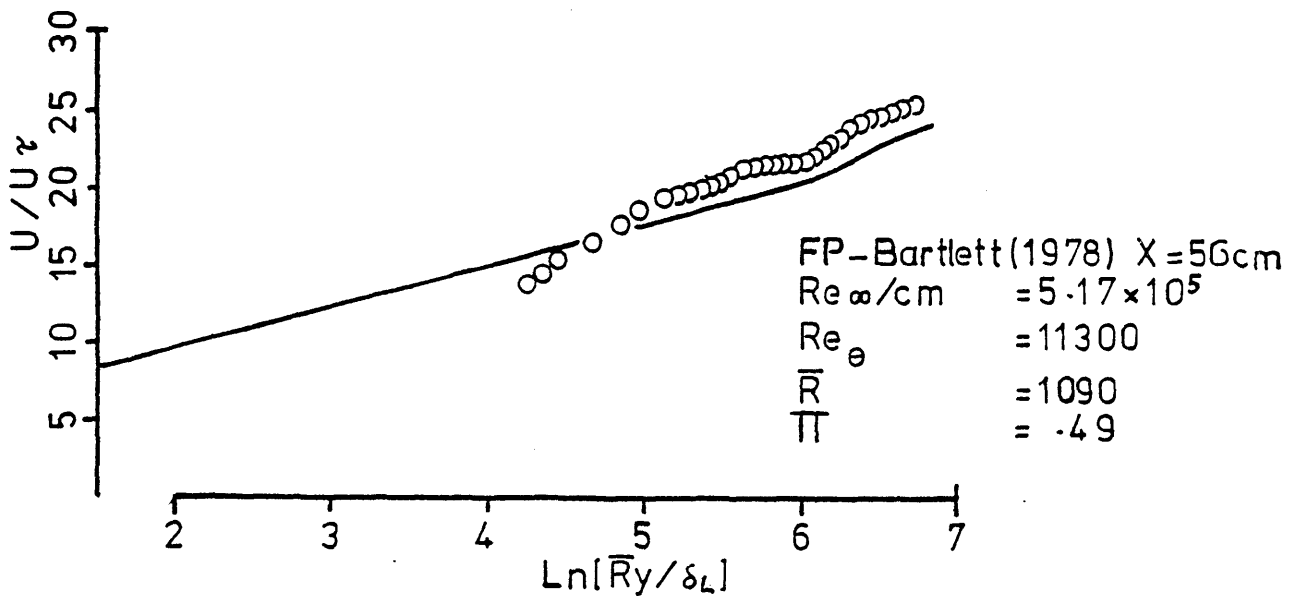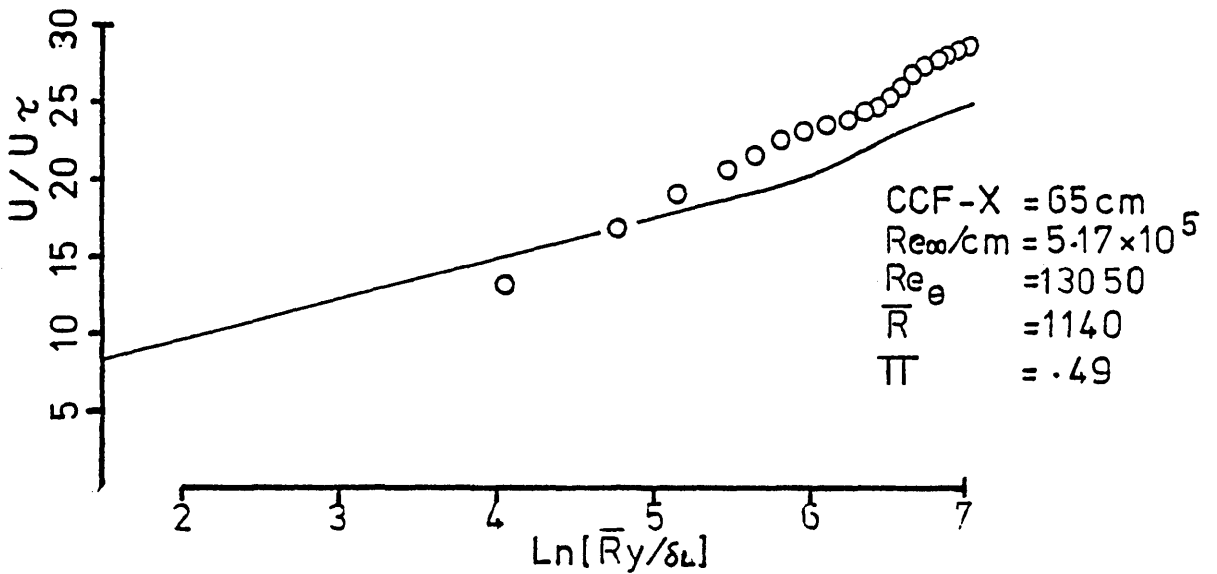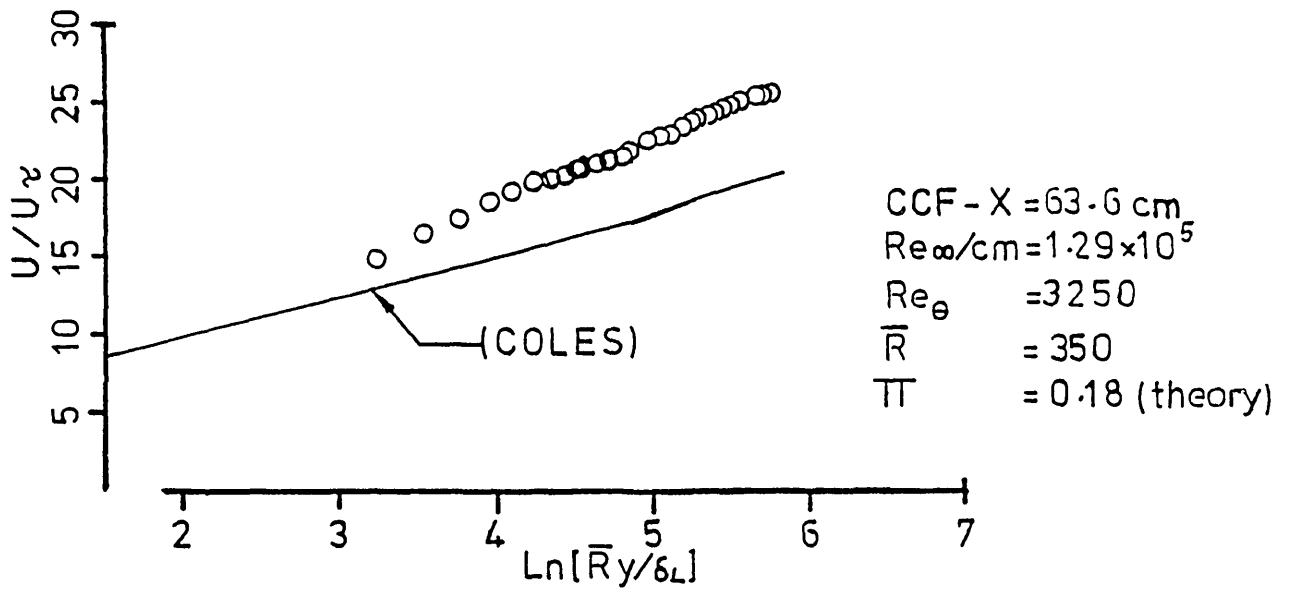
FIG 26   Transformed Profiles
(Comparison With 2D Theory)
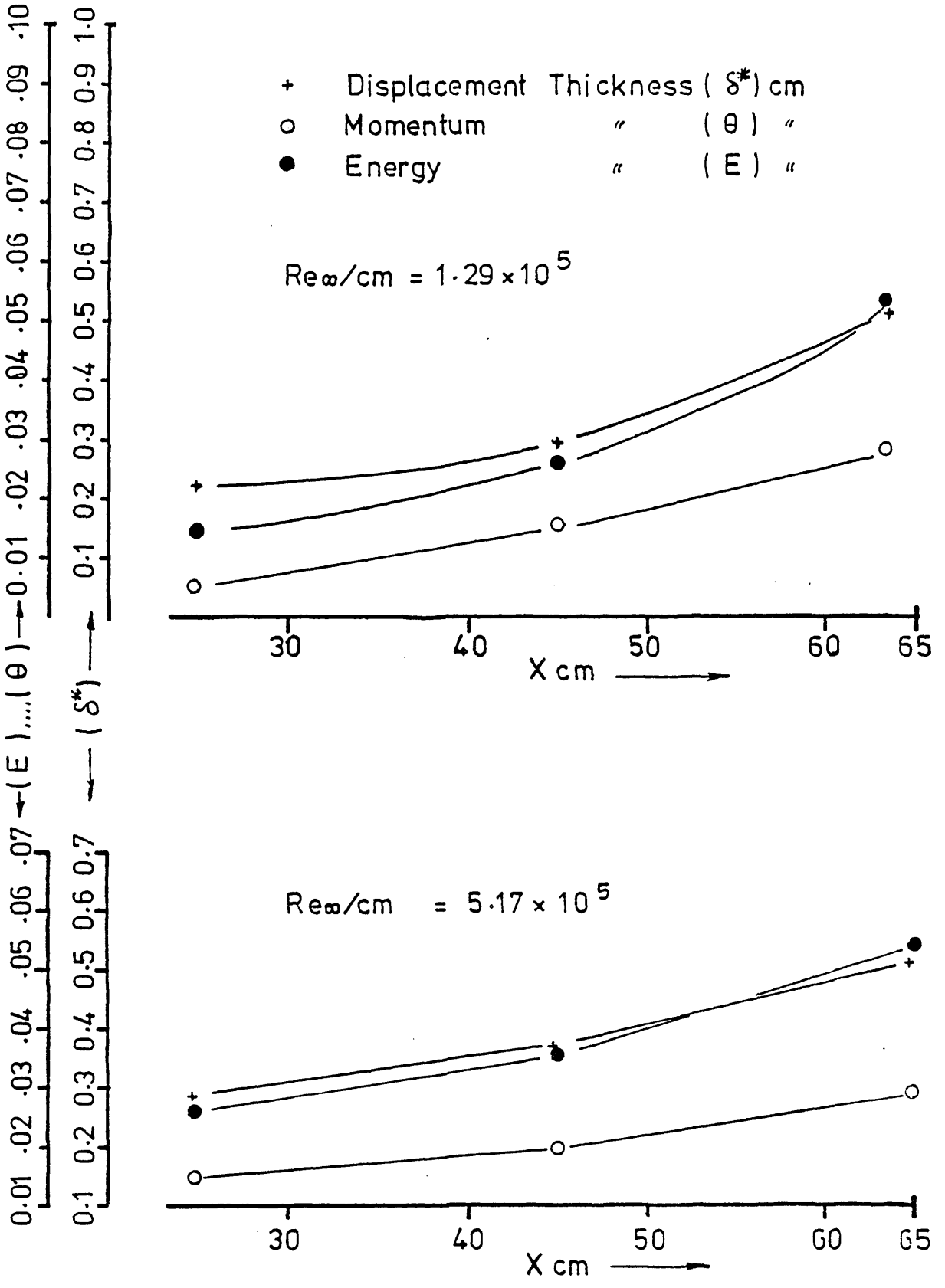
FIG 27   Thickness Parameters
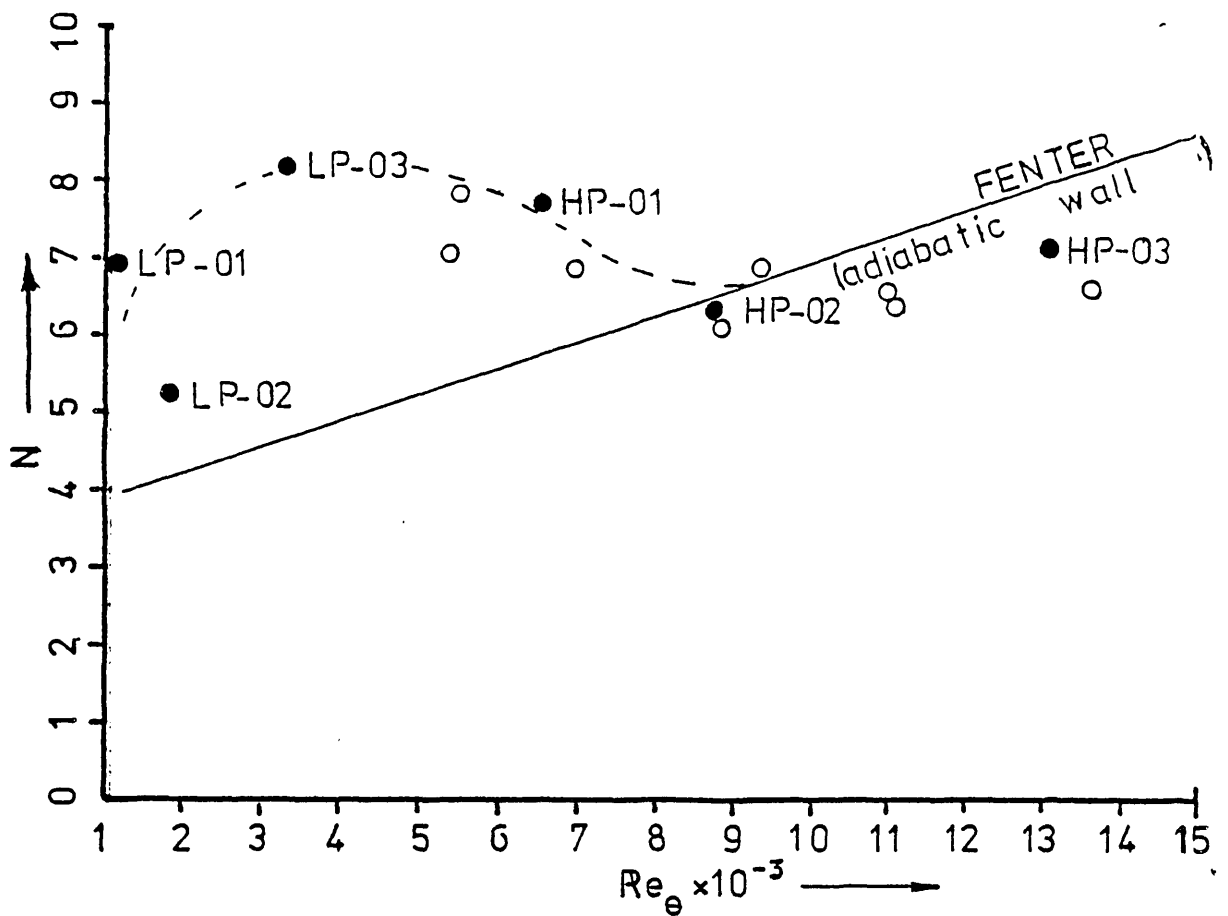
FIG 28   Power Law Exponent Trends
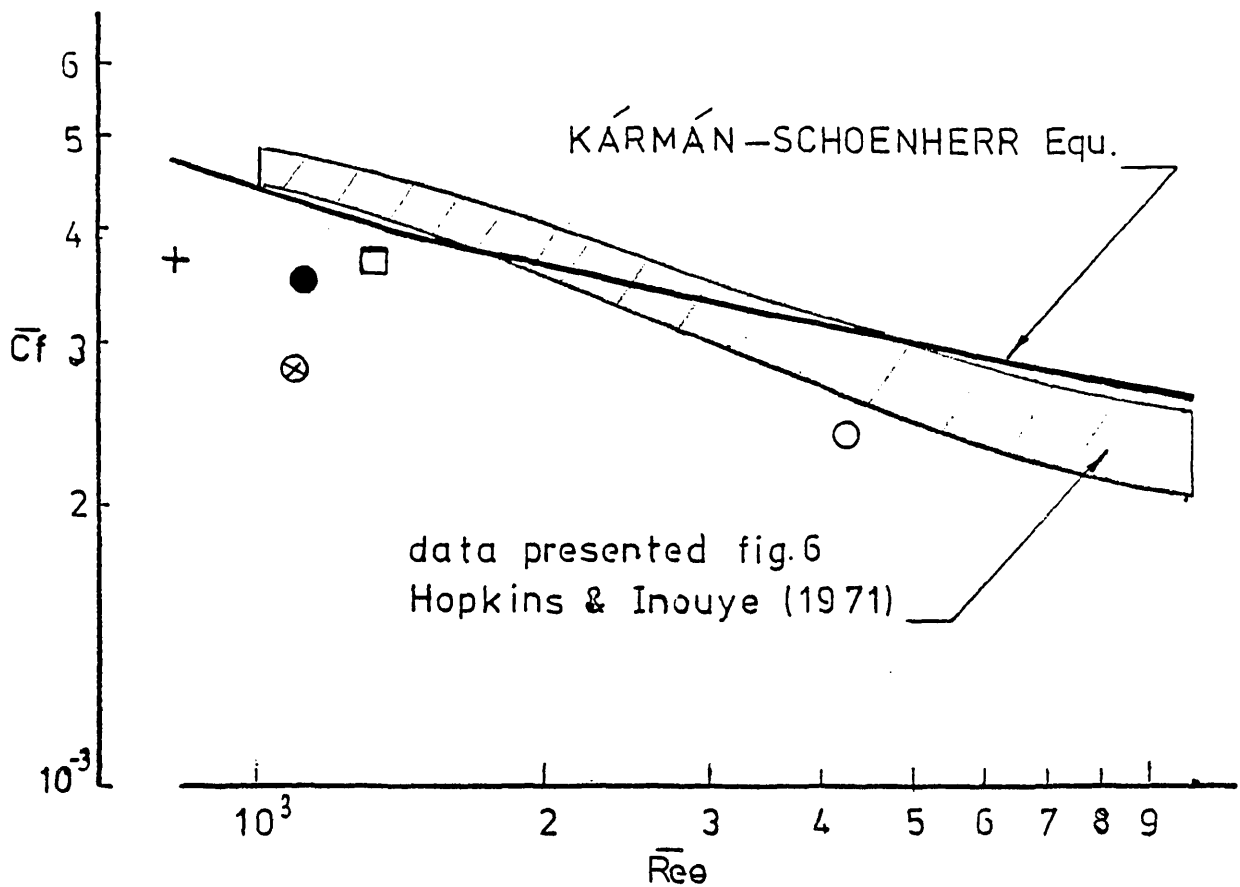
SYMB.	MODEL	tunnel cond. $Re_\infty/cm \times 10^{-5}$	AUTHOR
□	F P	5·17	COLEMAN
+	H C	1·29	"
●	H C	5·17	"
⊗	C C	1 29	EXPERIMENT
○	C C	5 17	"

FIG 29   Skin Friction
(according to van Driest 11)

FIG 30
AXISYMMETRIC PRESSURE DISTRIBUTIONS
(COLEMAN-1973)

Re∞/cm = 1.29×10^5
M∞ = 8.93

FORCED TRANSITION

○   ∝ = 15
+   ∝ = 30
×   ∝ = 35
□   ∝ = 40

P/P∞

(X − L) cms

L

X
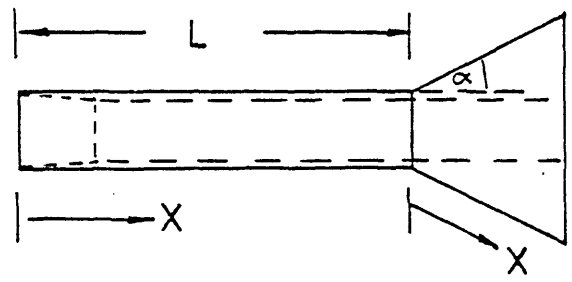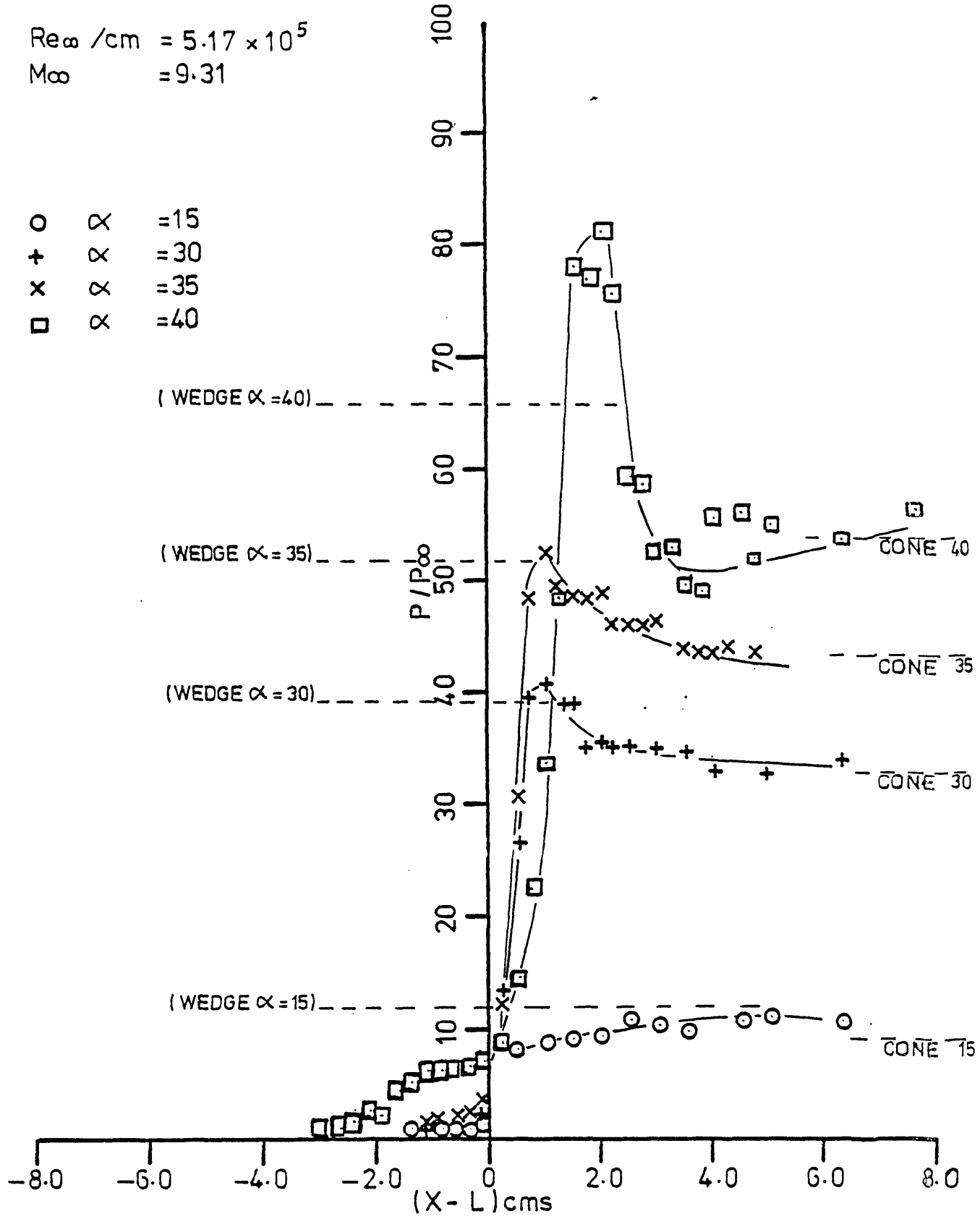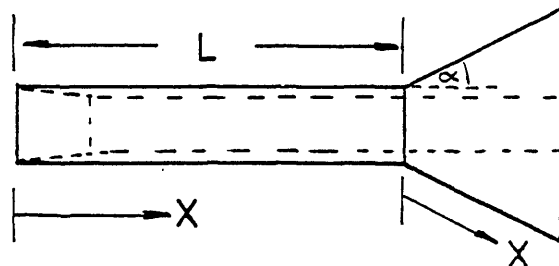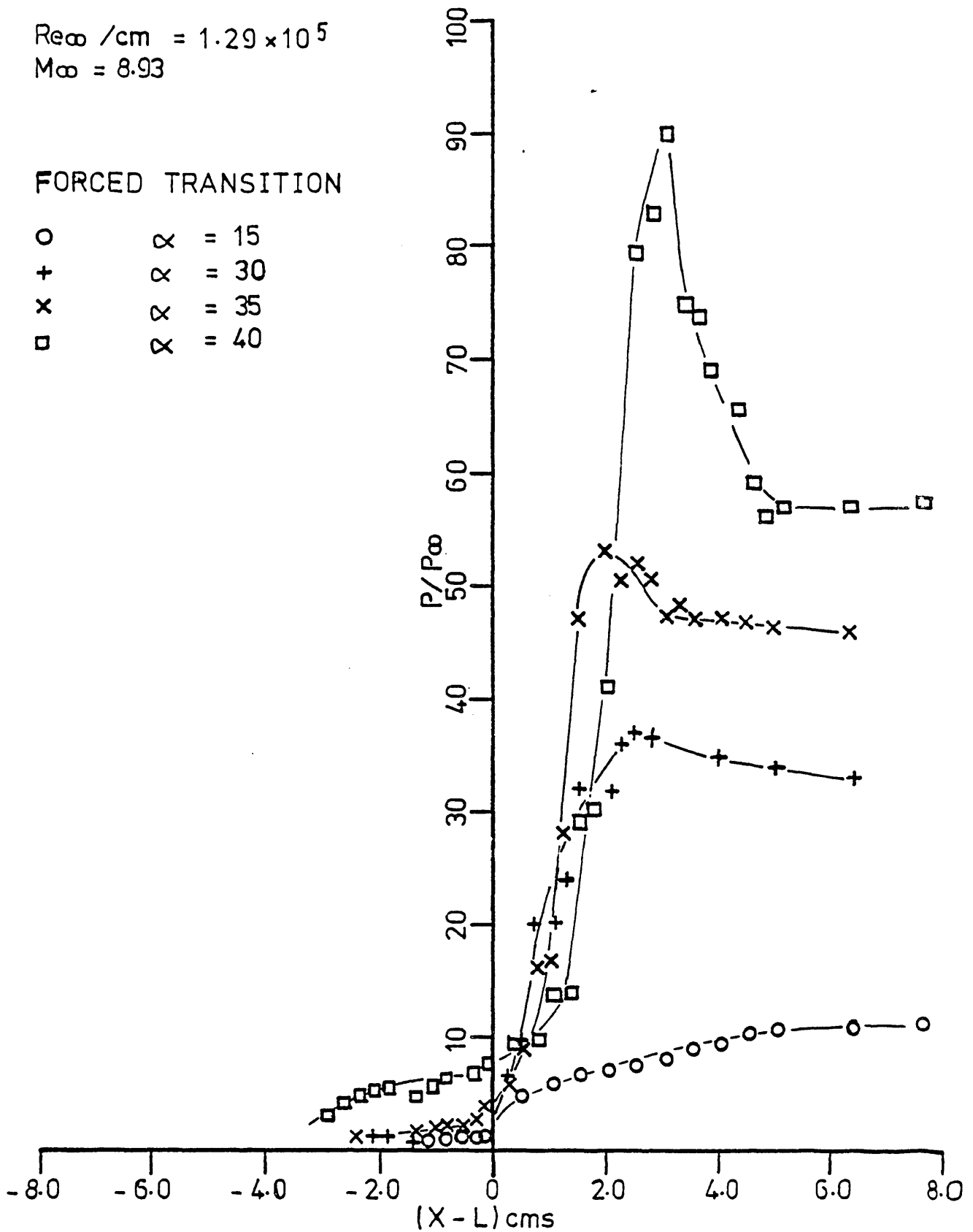
HOLLOW-CYLINDER-FLARE

FIG 31 AXISYMMETRIC PRESSURE DISTRIB-
UTIONS (COLEMAN -1973)

$M_\infty = 9.31$
$Me = 8.65$
$Re_\infty/cm = 5.17 \times 10^5$

+	15	
×	30	} COLEMAN 1973
○	35	
●	40	EXPERIMENT

------ THEORY
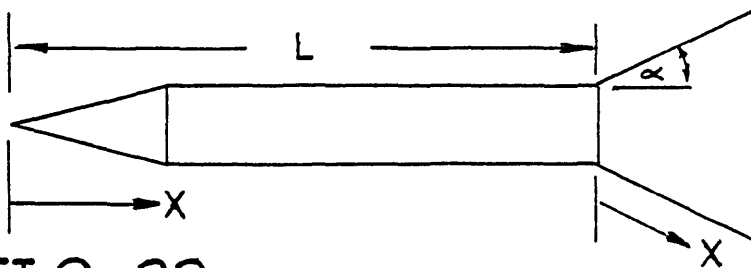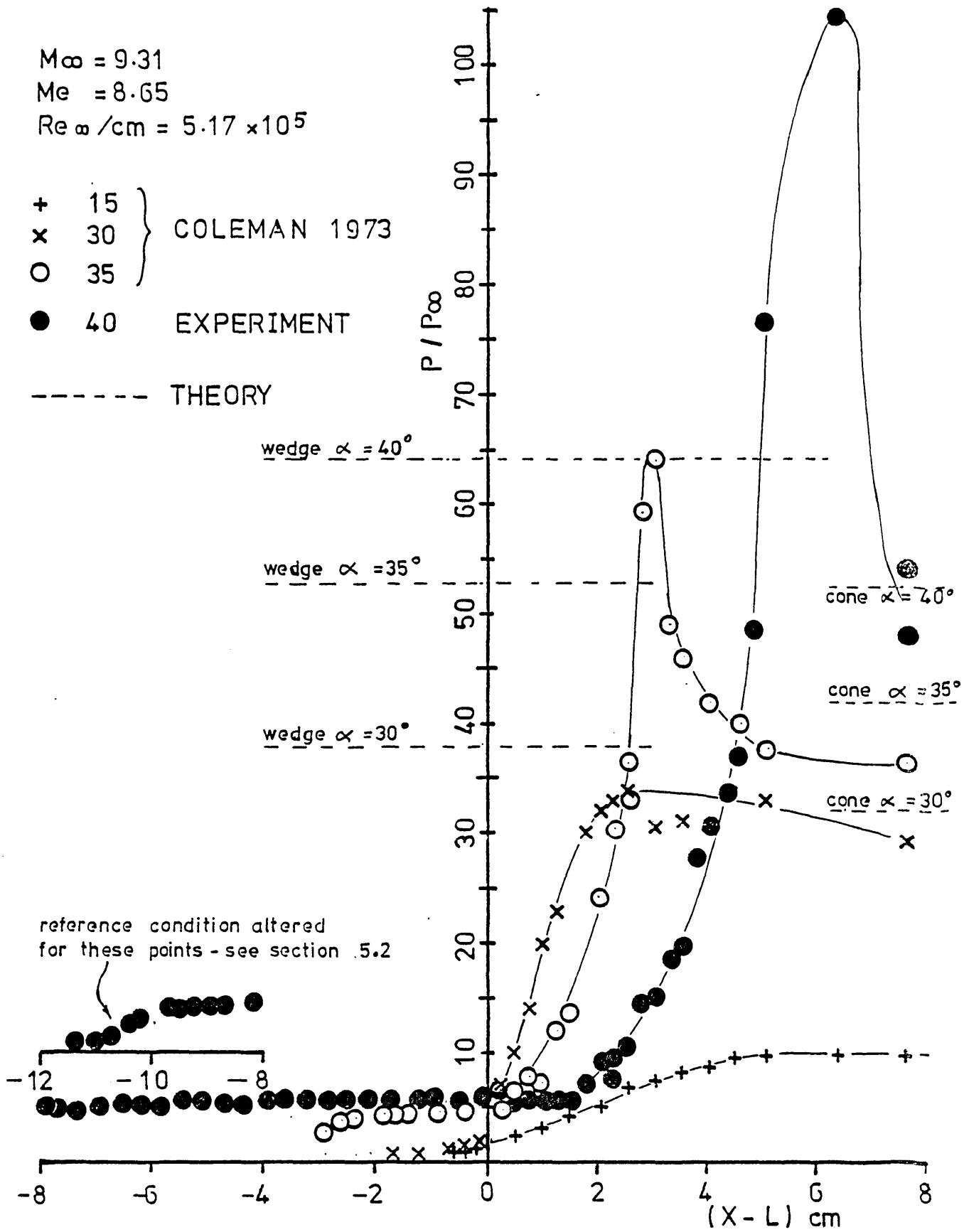
wedge $\alpha = 40°$

wedge $\alpha = 35°$

wedge $\alpha = 30°$

cone $\alpha = 40°$

cone $\alpha = 35°$

cone $\alpha = 30°$

reference condition altered
for these points - see section 5.2

P/P∞

(X - L) cm

FIG 32

AXISYMMETRIC PRESSURE DISTRIBUTIONS
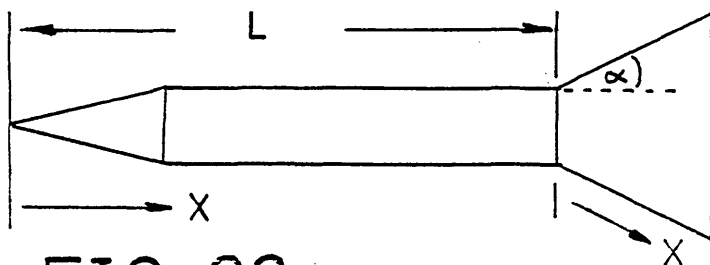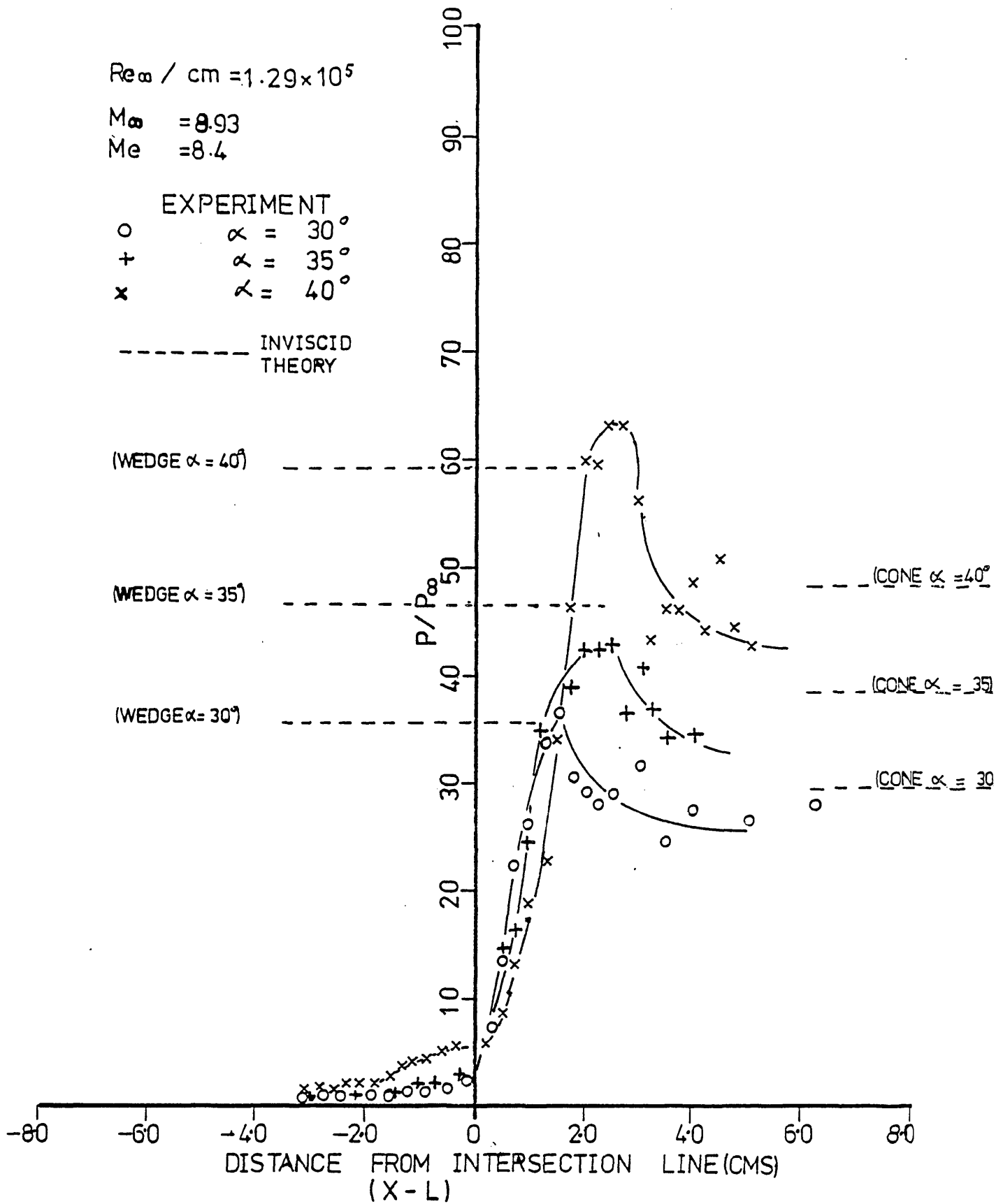
FIG 33

AXISYMMETRIC PRESSURE DISTRIBUTIONS
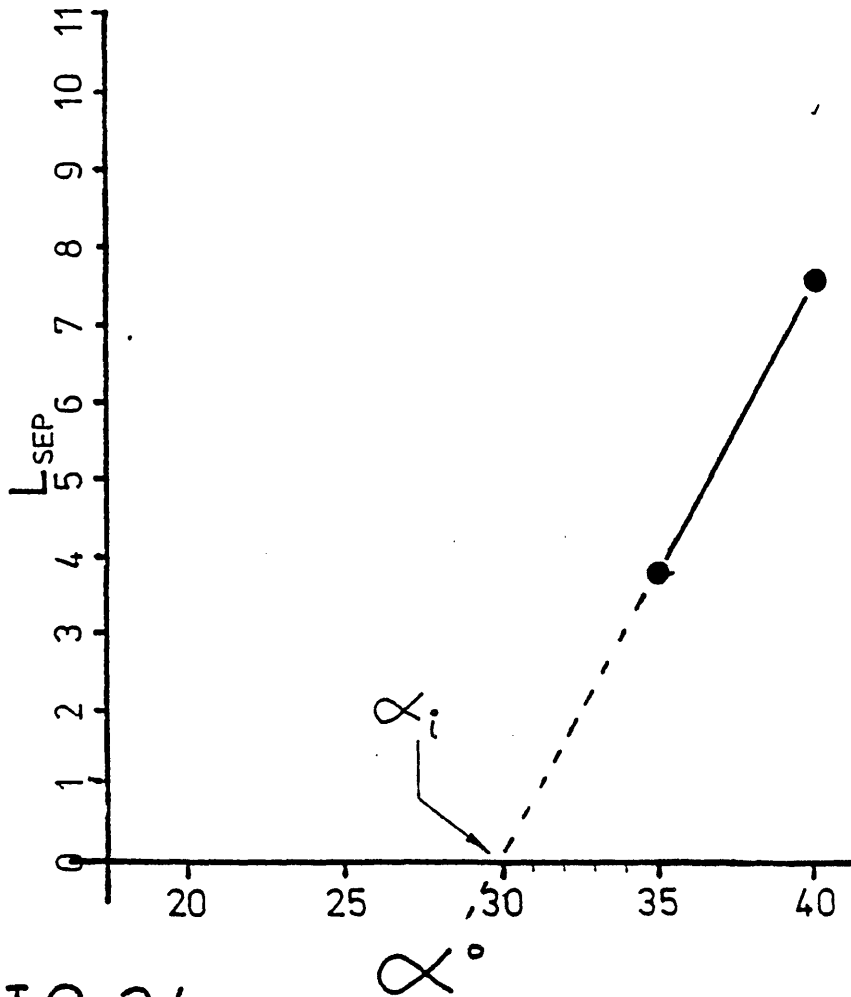
FIG 34
EXTRAPOLATION OF L_{SEP} TO ZERO
(Axisymmetric -CCF, $Re_\infty = 5.17 \times 10^5$)
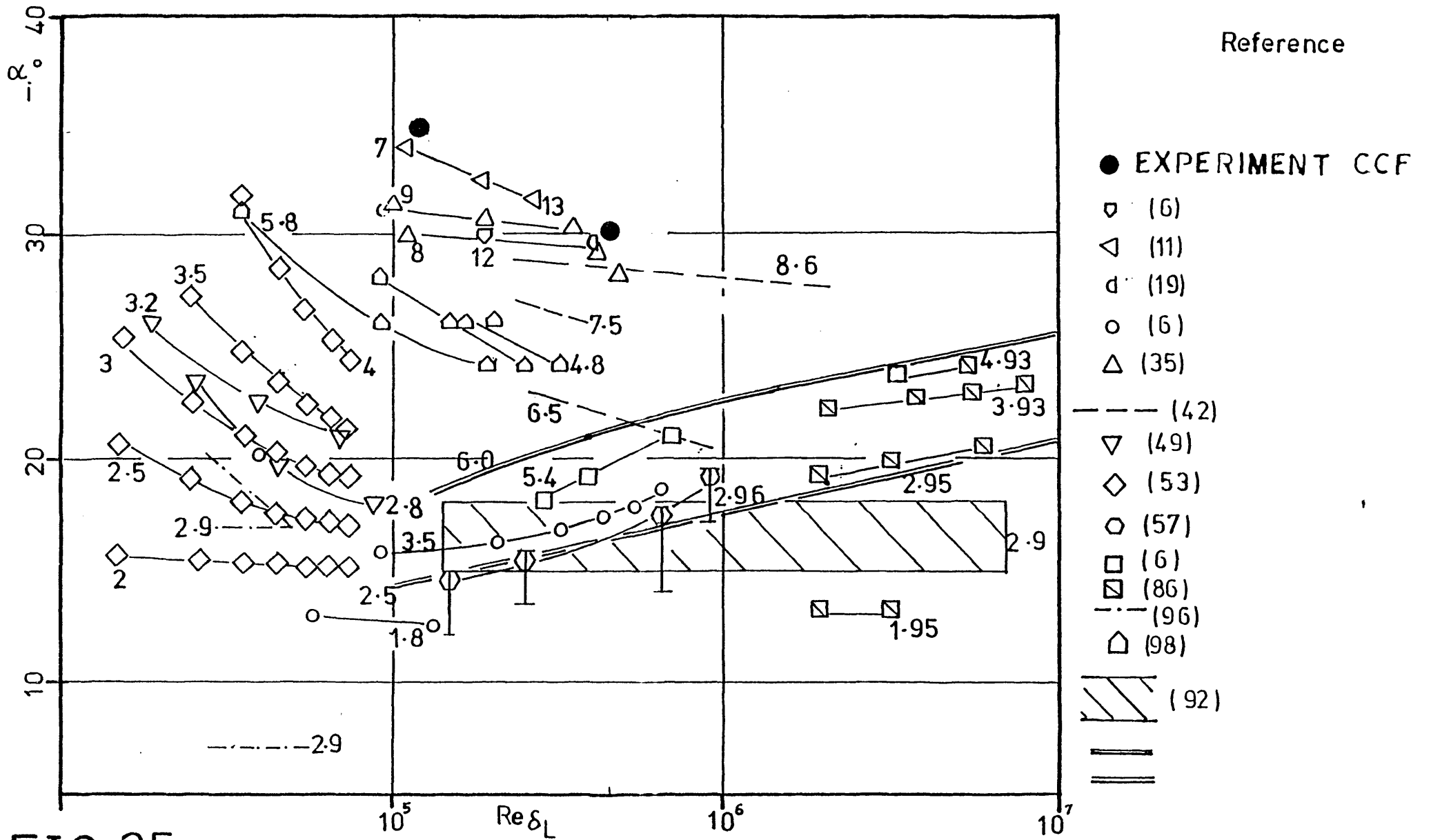
FIG 35   Incipient Separation Angles
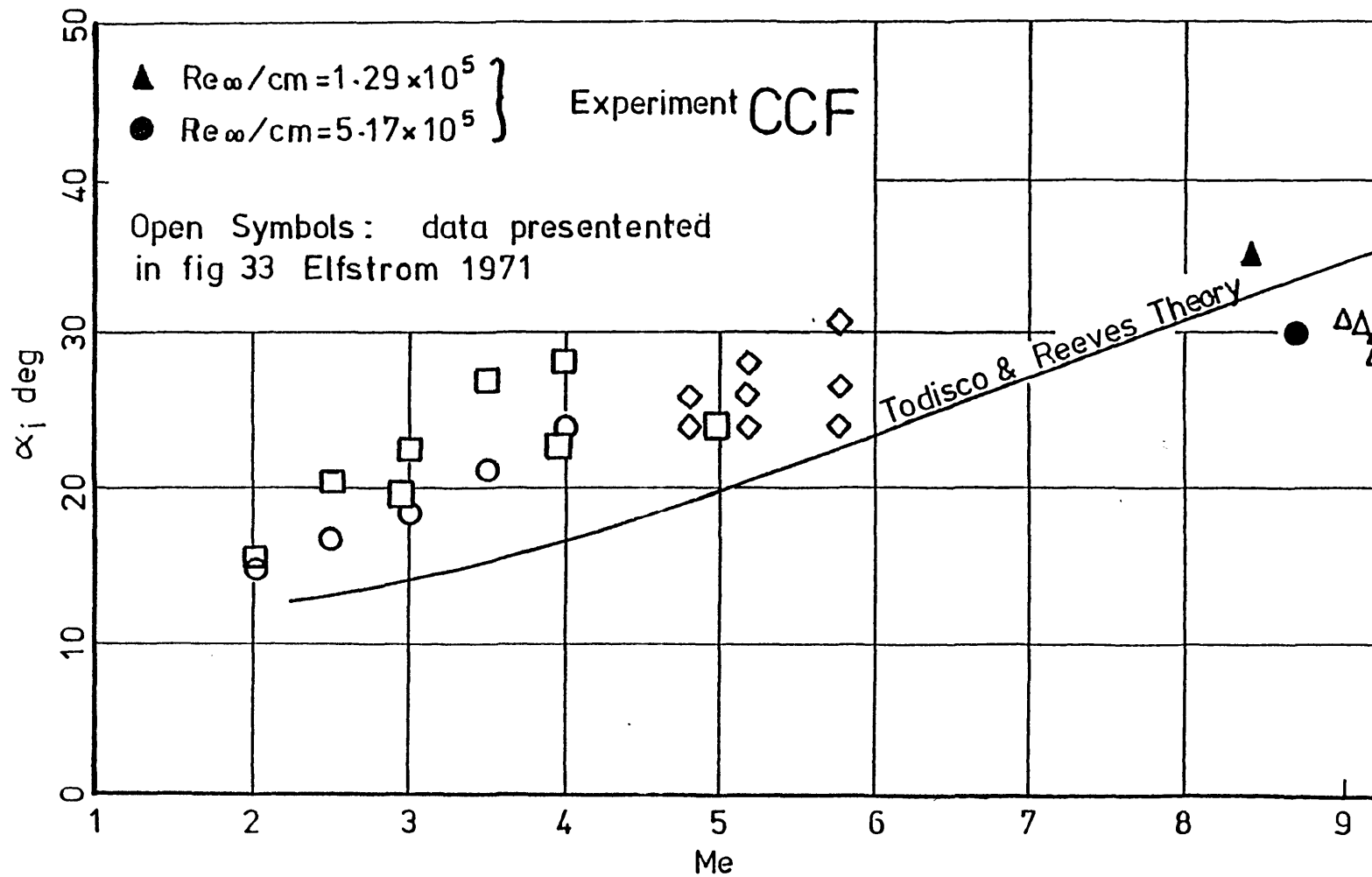
FIG 36   Todisco & Reeves prediction of incipient separation
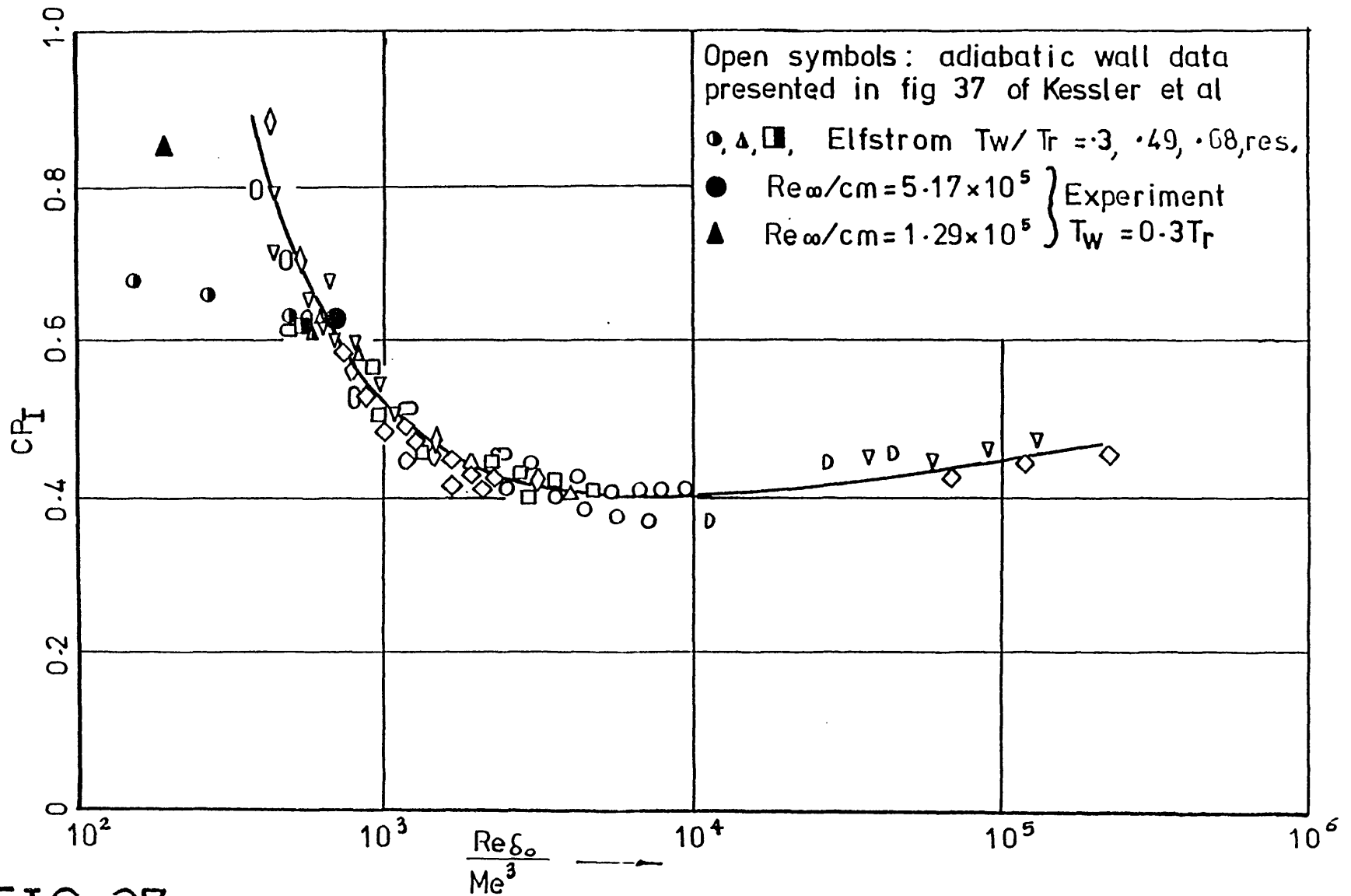
FIG 37 Correlation   of Kessler et al for incipient separation
(wedge compression corner)
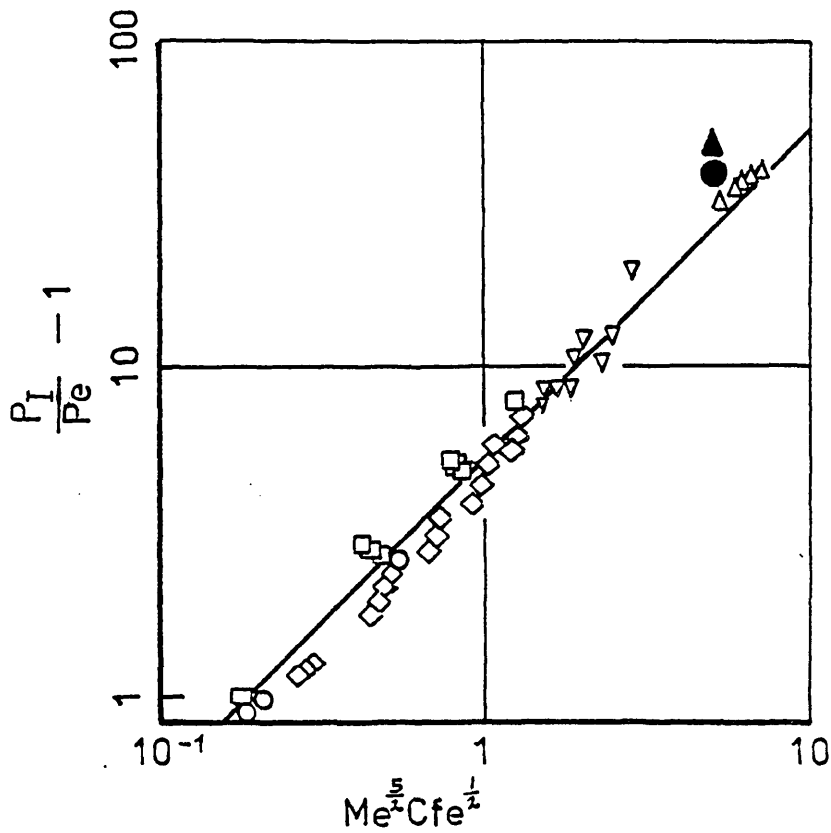
Open symbols: data presented in fig 36, Elfstrom

● $Re\infty/cm = 5.17 \times 10^5$ ⎫
                                    ⎬ Experiment
▲ $Re\infty/cm = 1.29 \times 10^5$ ⎭

FIG 38   Incipient separation pressure rise
correlation due to Roshko & Thomke (1969),
modified by Elfstrom (1971)
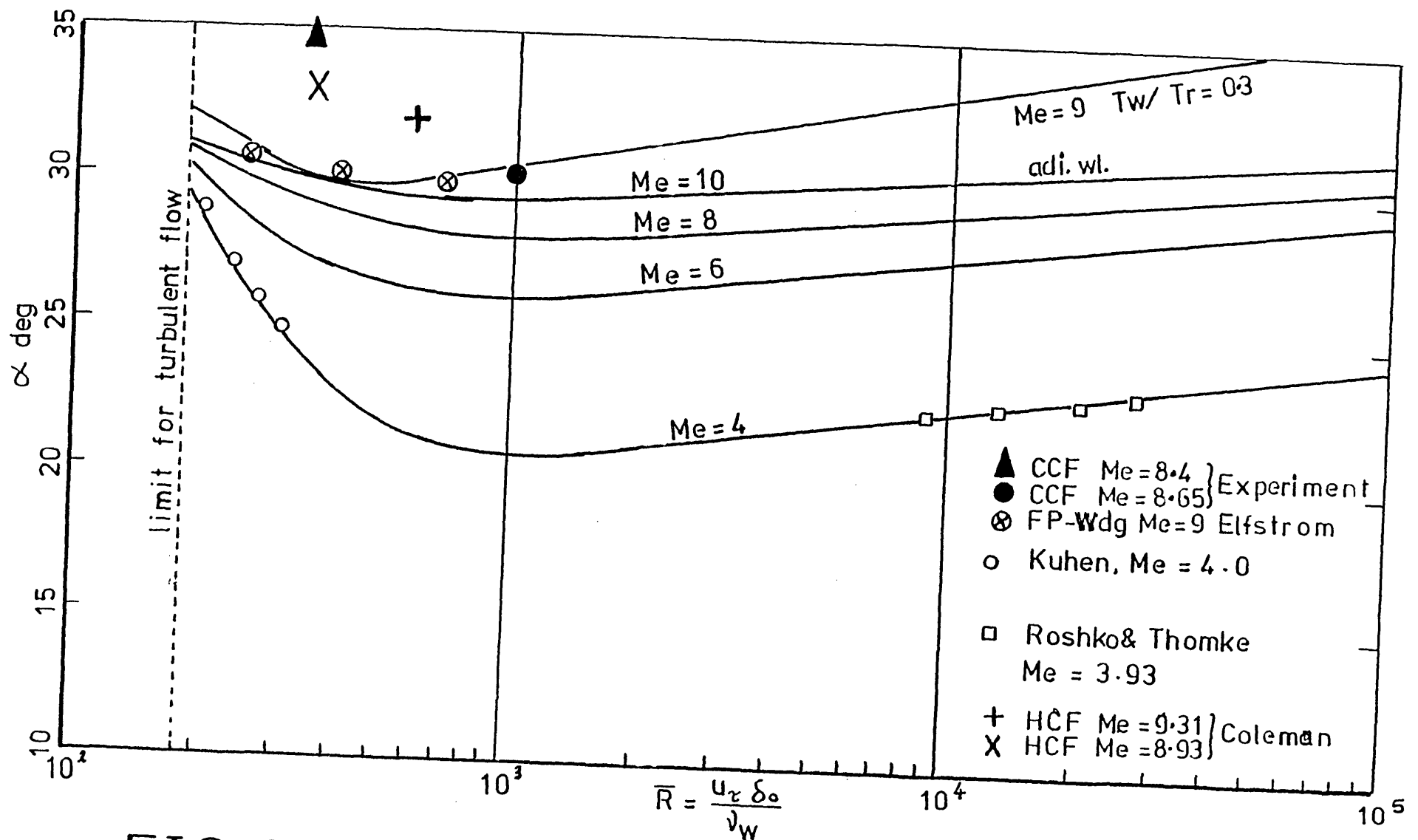
FIG 39   Correlation of adiabatic and cold wall incipient
separation after Elfstrom '1971'
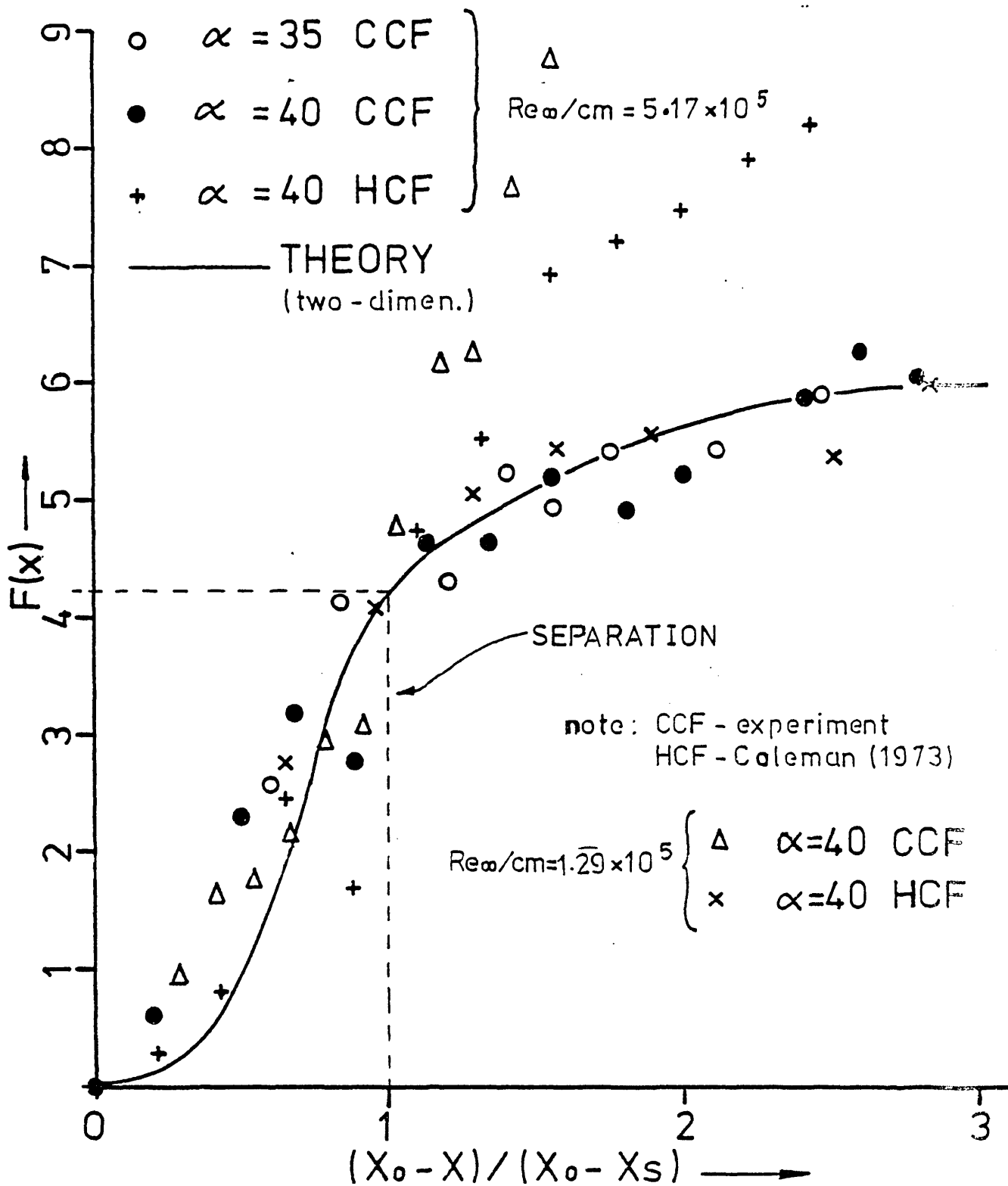
$$F(x) = Cp\,(Me^2-1)^{1/4}/\ (2Cfe)^{1/2}$$

where $\quad Cp = (P-Pe)/\tfrac{1}{2}\,\gamma Pe Me^2$

FIG 40
PRESSURE RISE AT SEPARATION-AXISYMM-ETRIC FLOW,(UNIVERSAL CORRELATION OF ERDOS AND PALLONE).
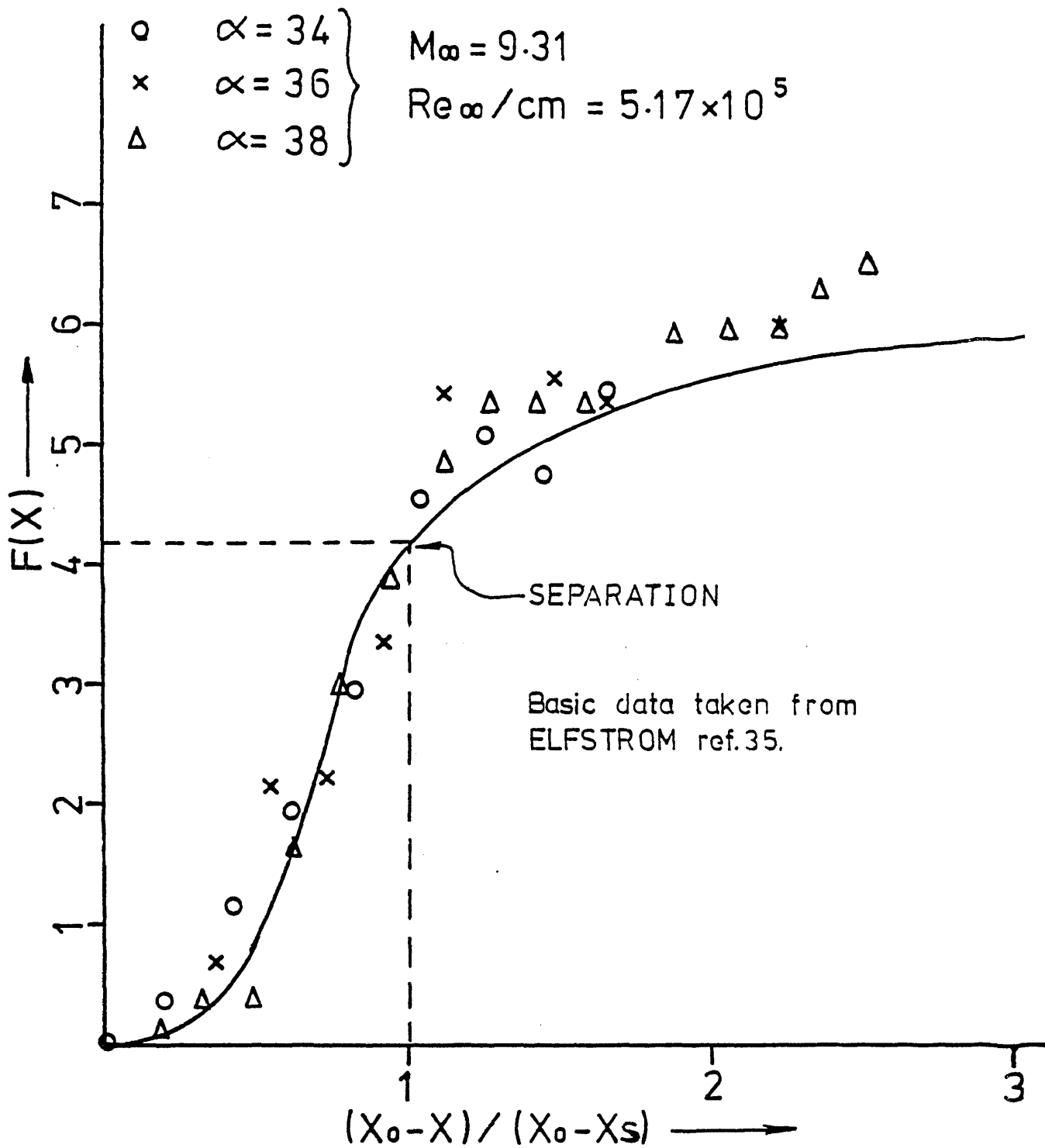
FIG 41

PRESSURE RISE AT SEPARATION-2D FLOW,

(UNIVERSAL CORRELATION OF ERDOS AND PALLONE)
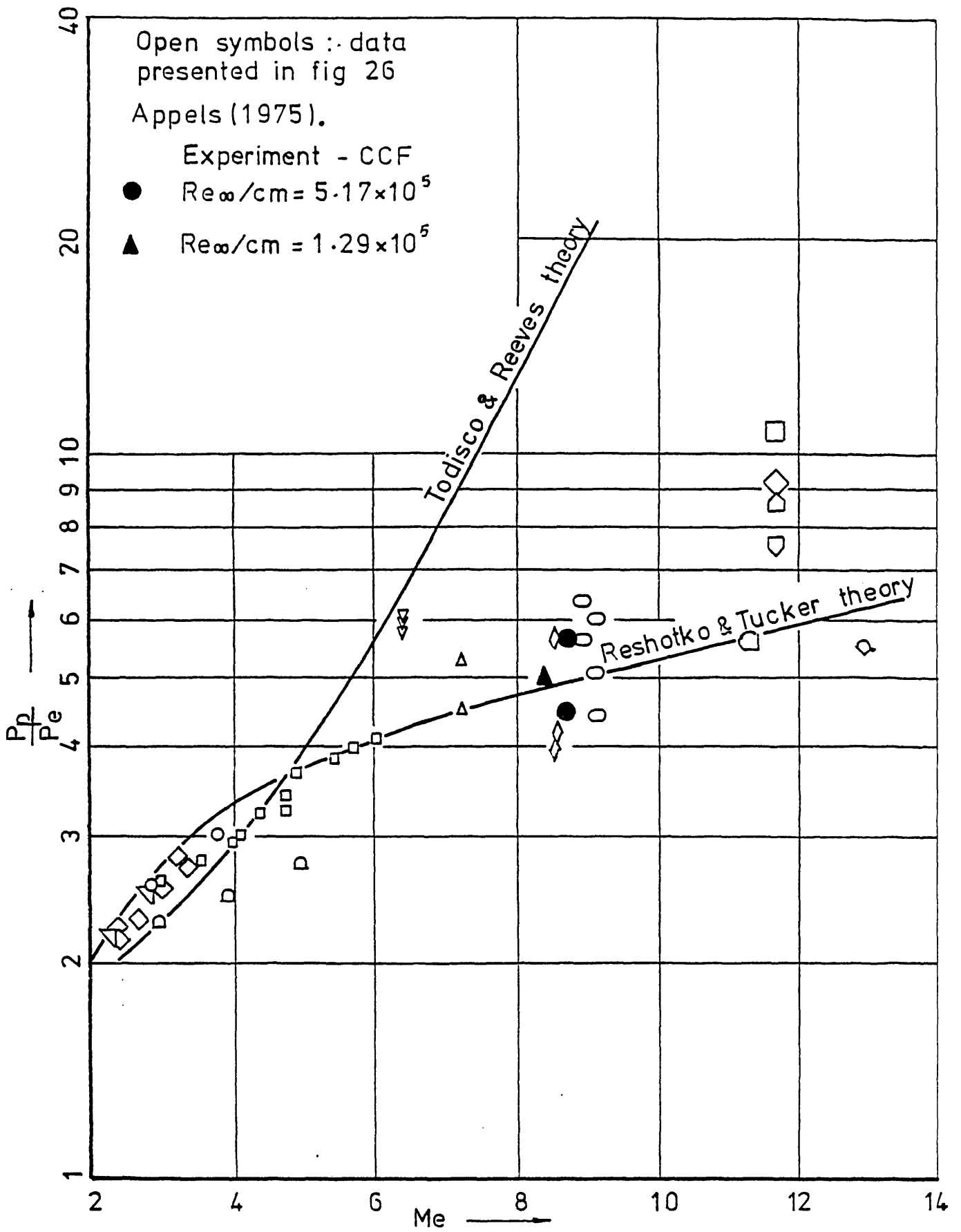
FIG 42   Plateau pressure correlations
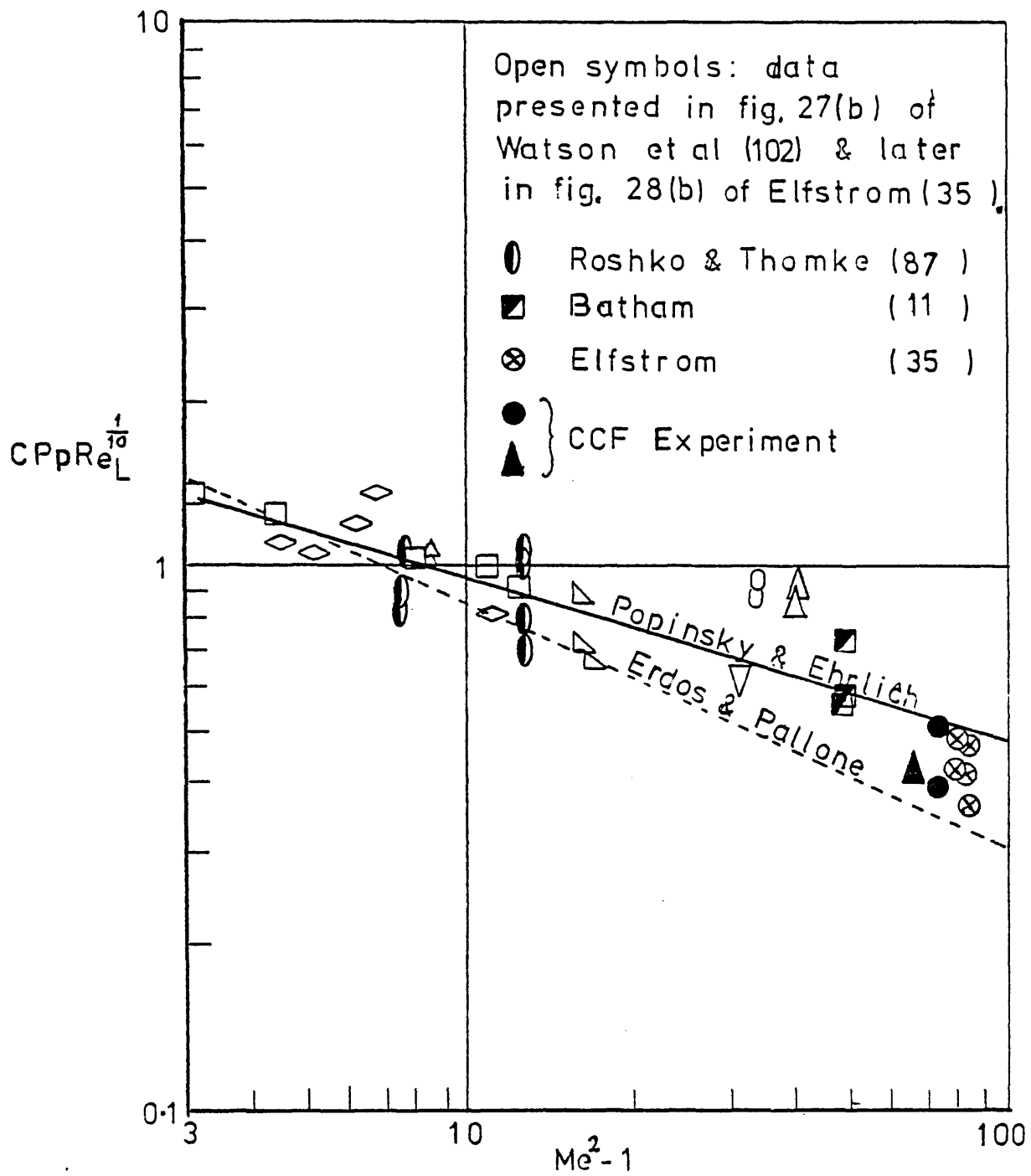
FIG 43 Free interaction prediction methods
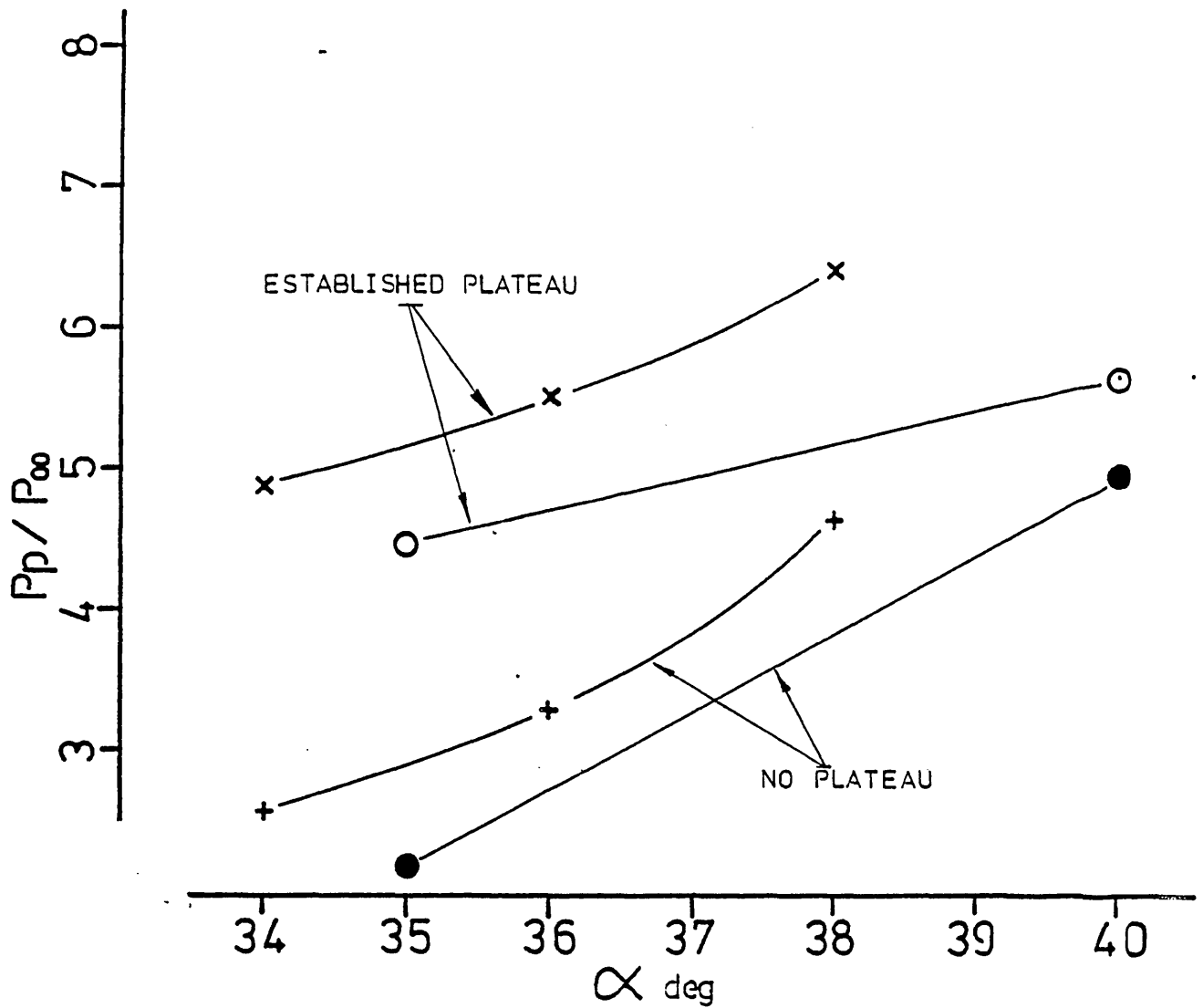
FIG 44

MEAN PRESSURE AHEAD OF COMPRESSION CORNER
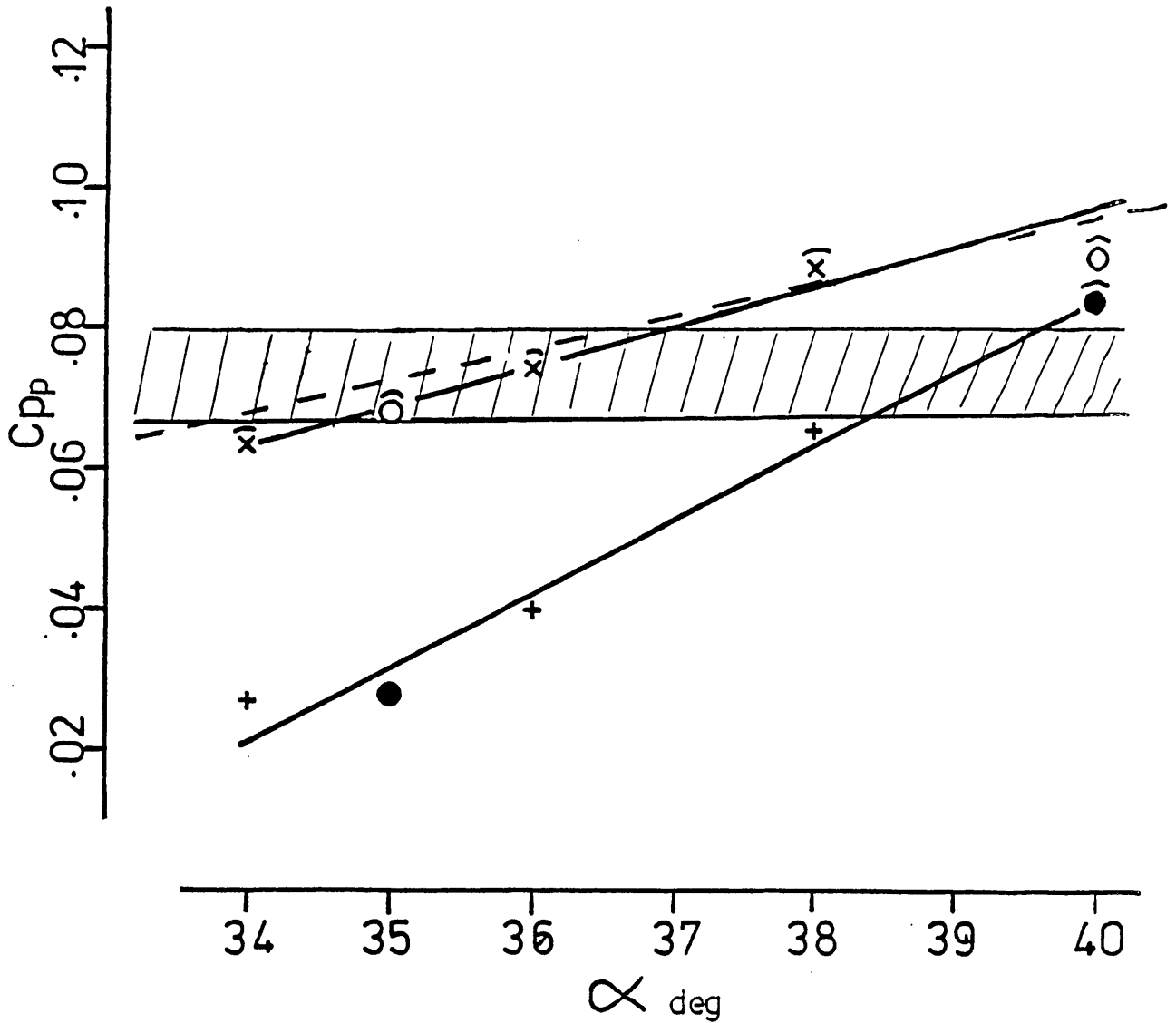
x 2D WEDGE } $M_\infty = 9.31$
o CCF   } $Re_\infty/cm = 5.17 \times 10^5$

+ 2D WEDGE } $M_\infty = 8.93$
● CCF   } $Re_\infty/cm = 1.29 \times 10^5$

⌒ PRESSURE DISTRIBUTION EXHIBITS FREE INTERACTION BEHAVIOUR

///// REGION PRESCRIBED BY THE ERDOS AND PALLONE UNIVERSAL CORRELATION

— — — — — EMPIRICAL PREDICTION FIG 46

FIG 45
MEAN PRESSURE COEFFICIENT AHEAD OF COMPRESSION CORNER (COMPARISONS WITH THEORY)
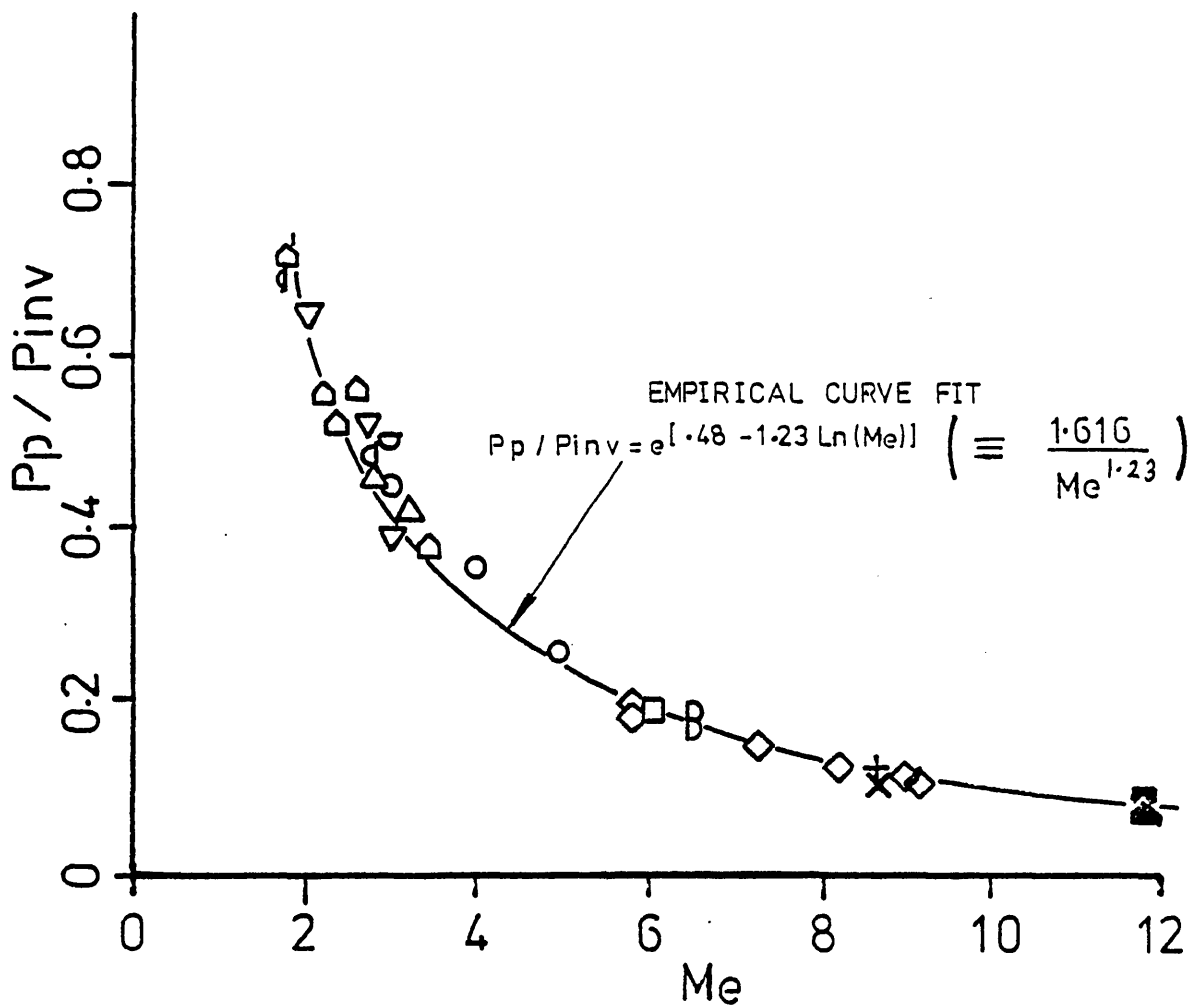
Open symbols : Data presented in Fig. 12
of ELFSTROM (ref. 36)

APPELS (ref. 6)

+ α =35 CCF ⎫ Experiment
× α =40 CCF ⎬ $M_\infty = 9\cdot31$, $Re_\infty/cm = 5\cdot17 \times 10^5$
⎭ $Me = 8\cdot65$

FIG 46

PLATEAU PRESSURE (CORRELATION DUE TO ELFSTROM - 1972)

Inv. Solution For A Strong
Detached Corner Shock

α_i min
Elfstrom

θ$_s$ ⟶ deg

Me ⟶

α deg

●   Experiment, CCF, 35°, 40°

◒   Kuhen, FPW, 30°

⊗   Law, FPW, 25°

□   Batham, FPW, 36·5°

△   Settles, CCF, 20°

◊   Elfstrom, FPW, 34°, 36°, 38°
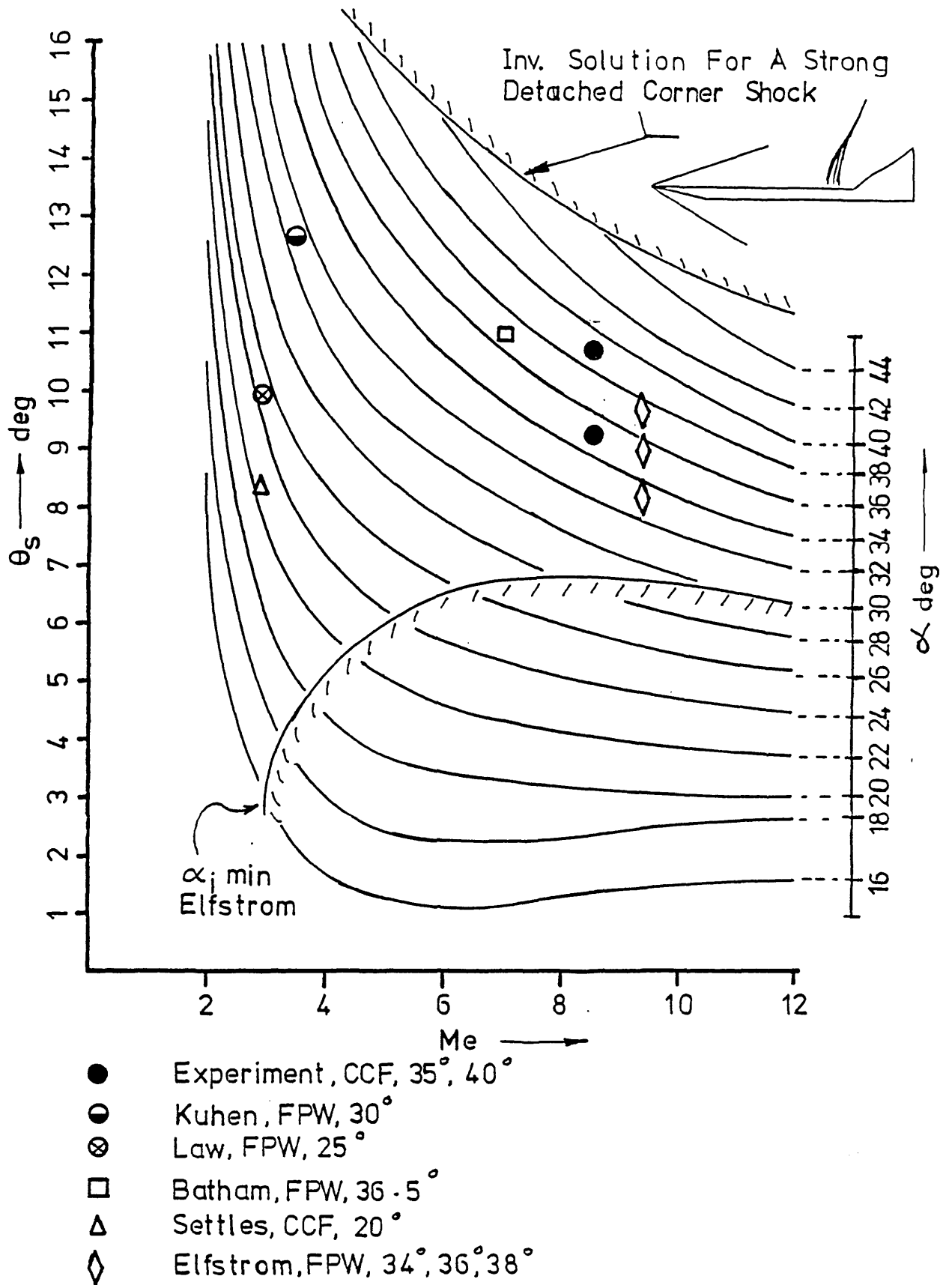
FIG 47   Prediction of θ$_s$ from Fig 46
assuming double wedge flow

FIG 48

REATTACHMENT CORRELATION OF BATHAM

The figure shows a plot of Cpr (y-axis, from 0 to .30) versus Mp (x-axis, from 0 to 7).

Legend:
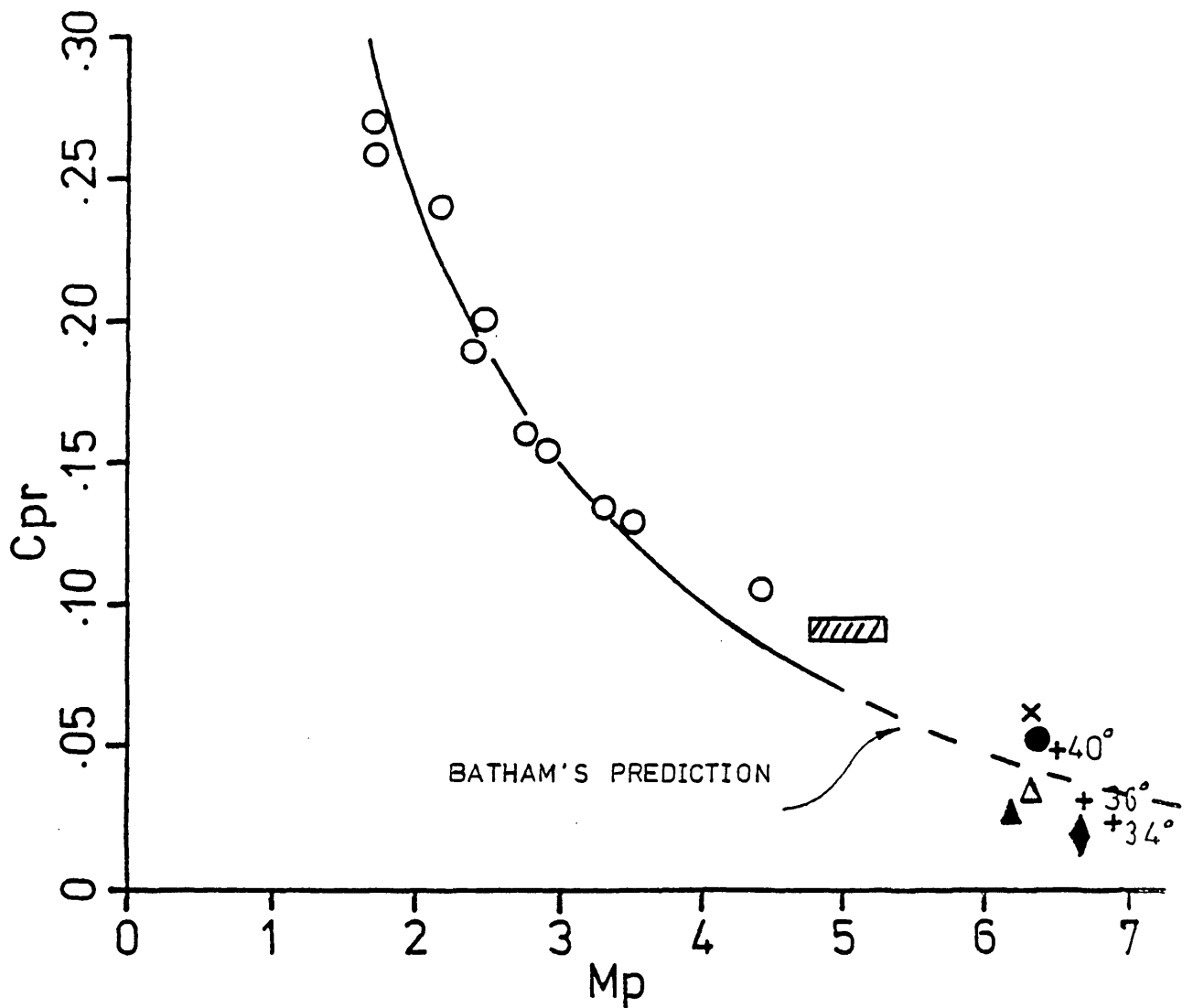
O ▨ RESULTS GIVEN BY BATHAM (ref 10)

+ 2D-WEDGE ELFSTROM

AXISYMMETRIC EXPERIMENTS

SYMB	COND'n	MODEL	α deg	
△	LP *	HCF	40	COLEMAN
▲	LP	CCF	40	EXP.
×	HP *	HCF	40	COLEMAN
●	HP	CCF	40	EXP.
◆	HP	CCF	35	EXP.

THEORY (BATHAM) ----$Cpr \propto [Cfj / (Mp^2-1)^{\frac{1}{2}}]^{\frac{1}{2}}$
where Cfj is evaluated at the jet boundary

* LP — ($M\infty$ = 8.93, $Re\infty/cm$ = 1.29 × 10^5)
  HP — ($M\infty$ = 9.31, $Re\infty/cm$ = 5.17 × 10^5)
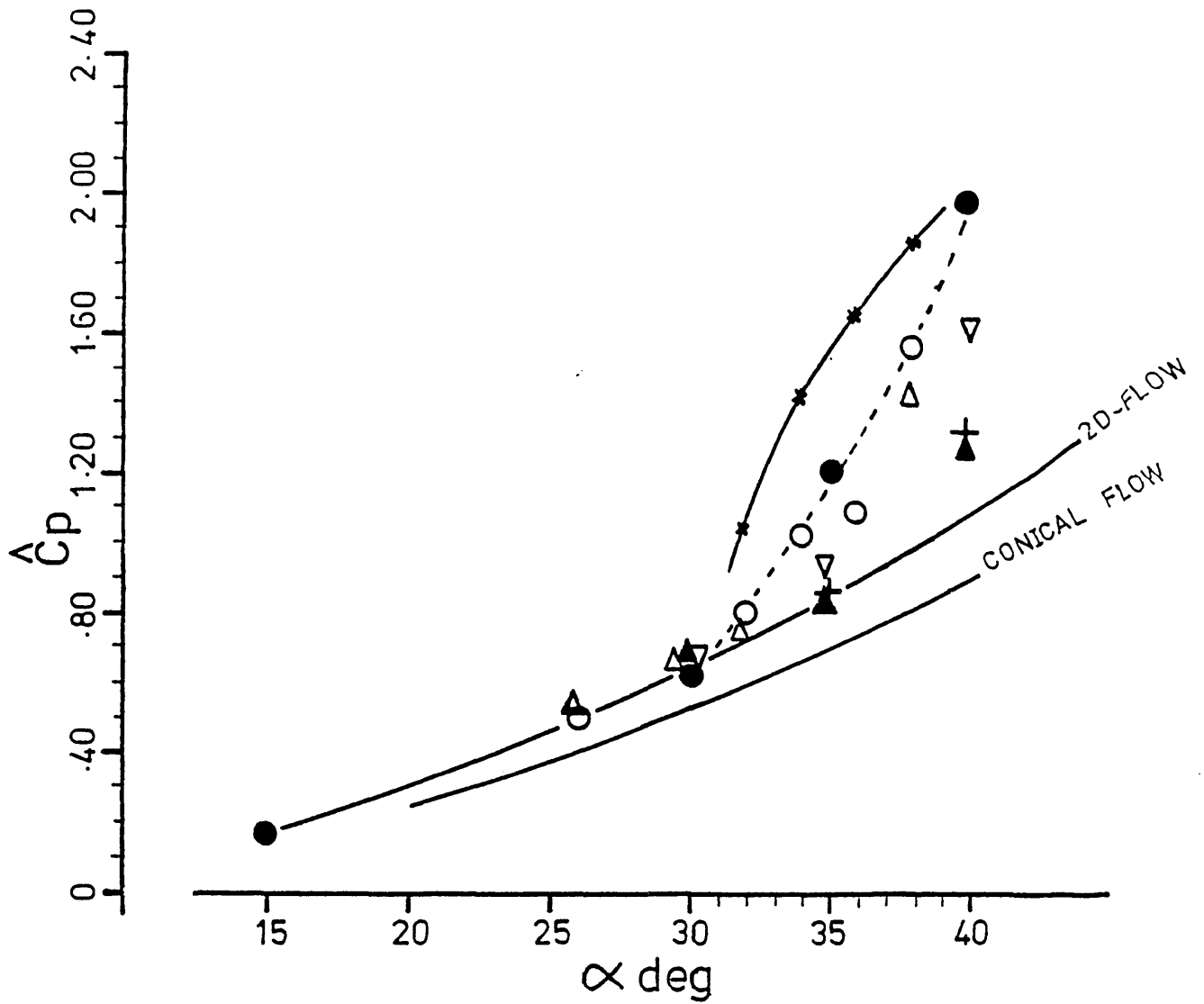
SYMBOL	MODEL	CONDITION
O	2D-WEDGE	$M\infty = 9.31$
●	CCF	$Re\,\infty/cm = 5.17 \times 10^5$
▽	HCF	
△	2D-WEDGE	$M\infty = 8.93$
▲	CCF	$Re\,\infty/cm = 1.29 \times 10^5$
+	HCF	

—*—*—*—*— INVISCID PREDICTION --(DOUBLE WEDGE)

————————— ATTACHED FLOW

FIG 49
REATTACHMENT PRESSURE OVERSHOOT
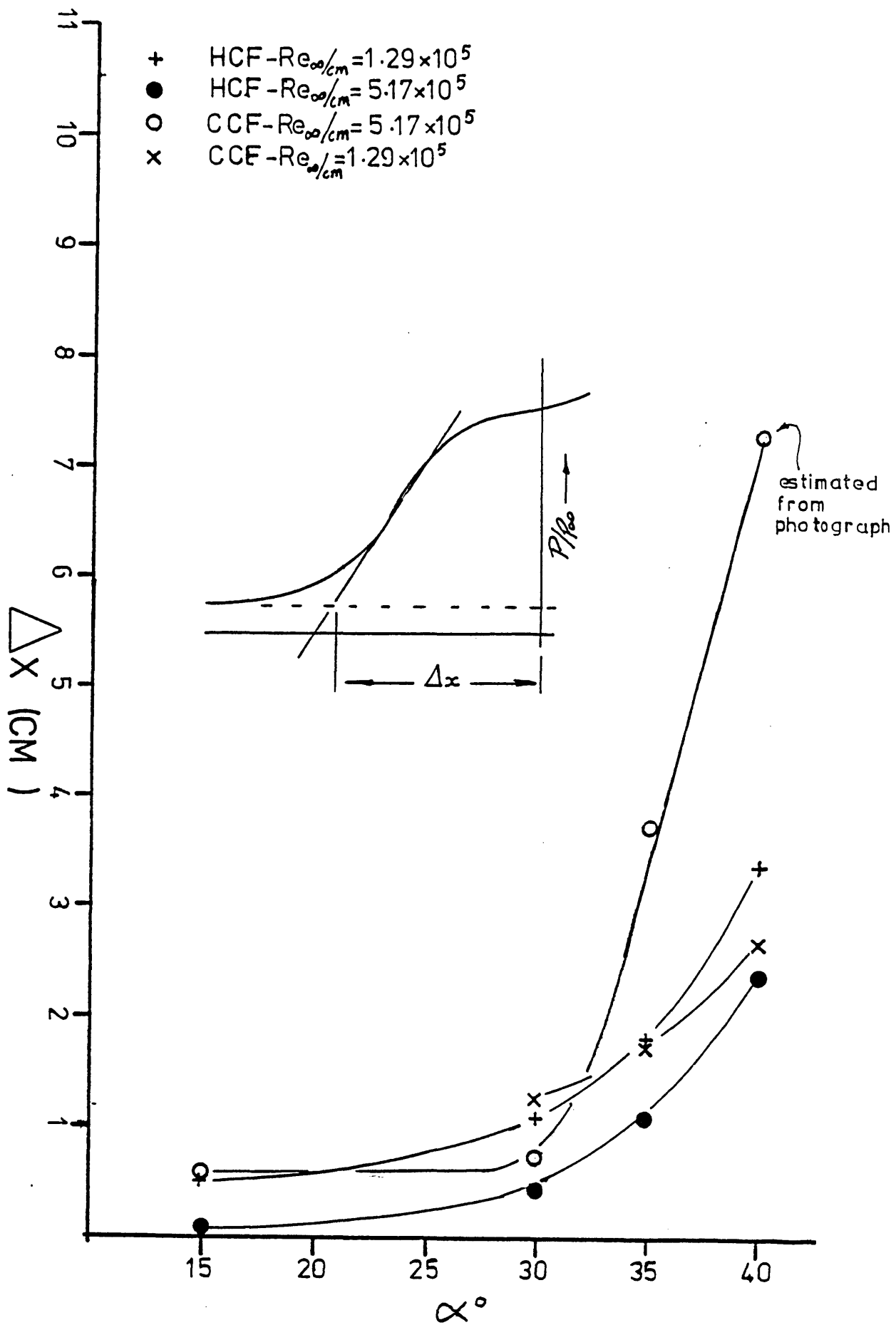
FIG 50

UPSTREAM INFLUENCE - AXISYMMETRIC
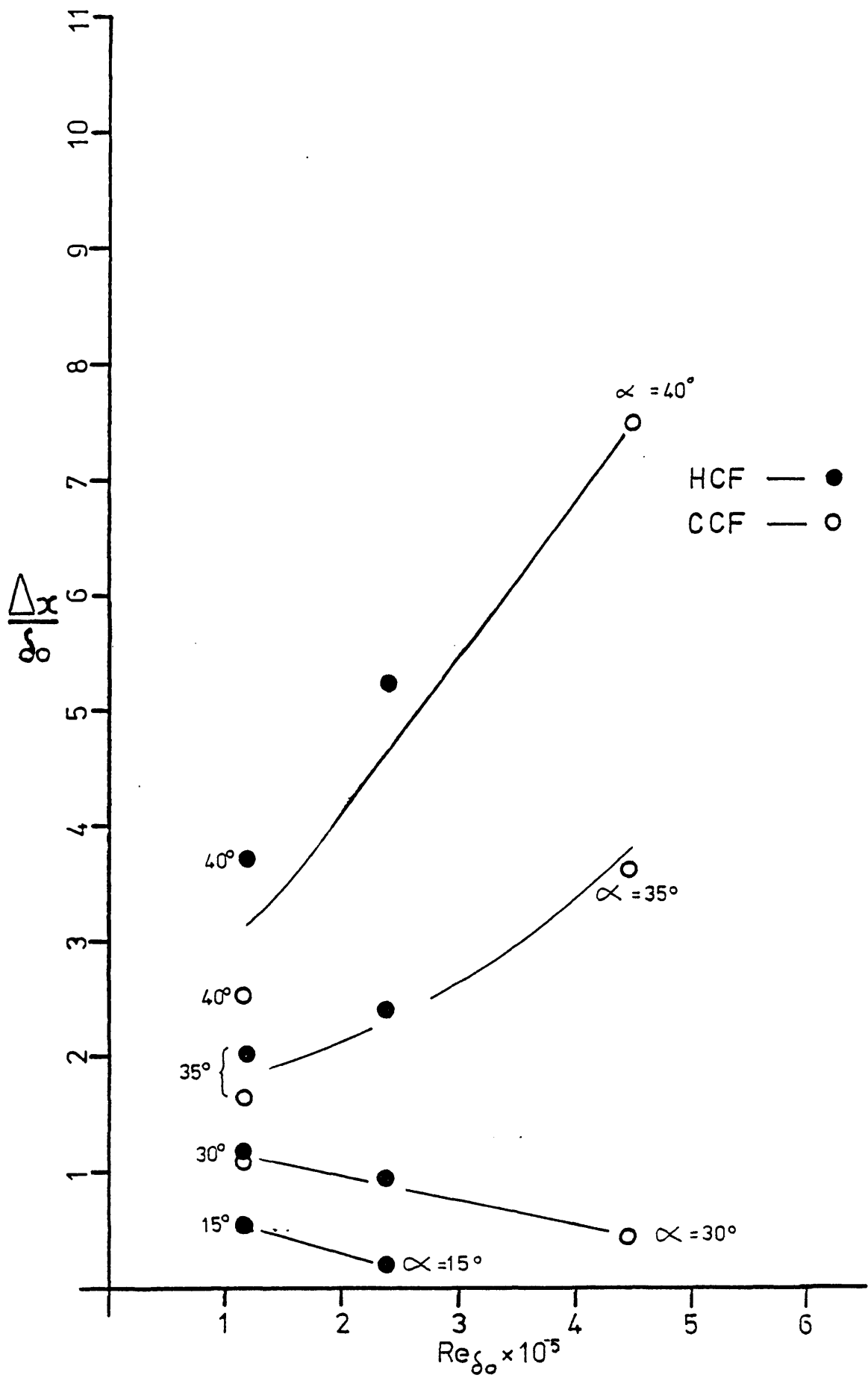
FIG 51 EFFECT OF Re$_{\delta_0}$ ON $\dfrac{\triangle x}{\delta_0}$

(AXISYMMETRIC FLOW)

FIG 52 EFFECT OF Re_{δ_0} ON $\dfrac{\triangle x}{\delta_0}$
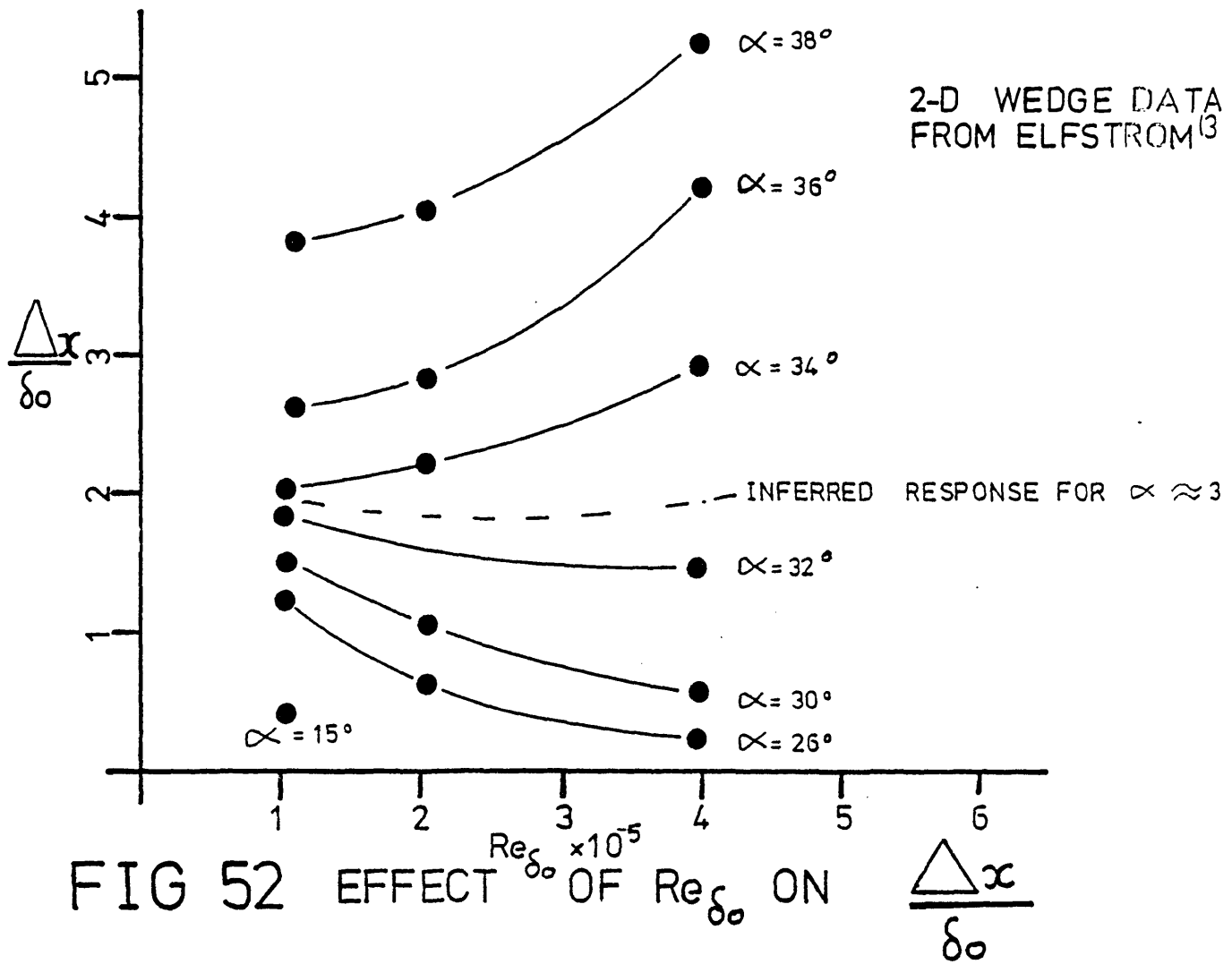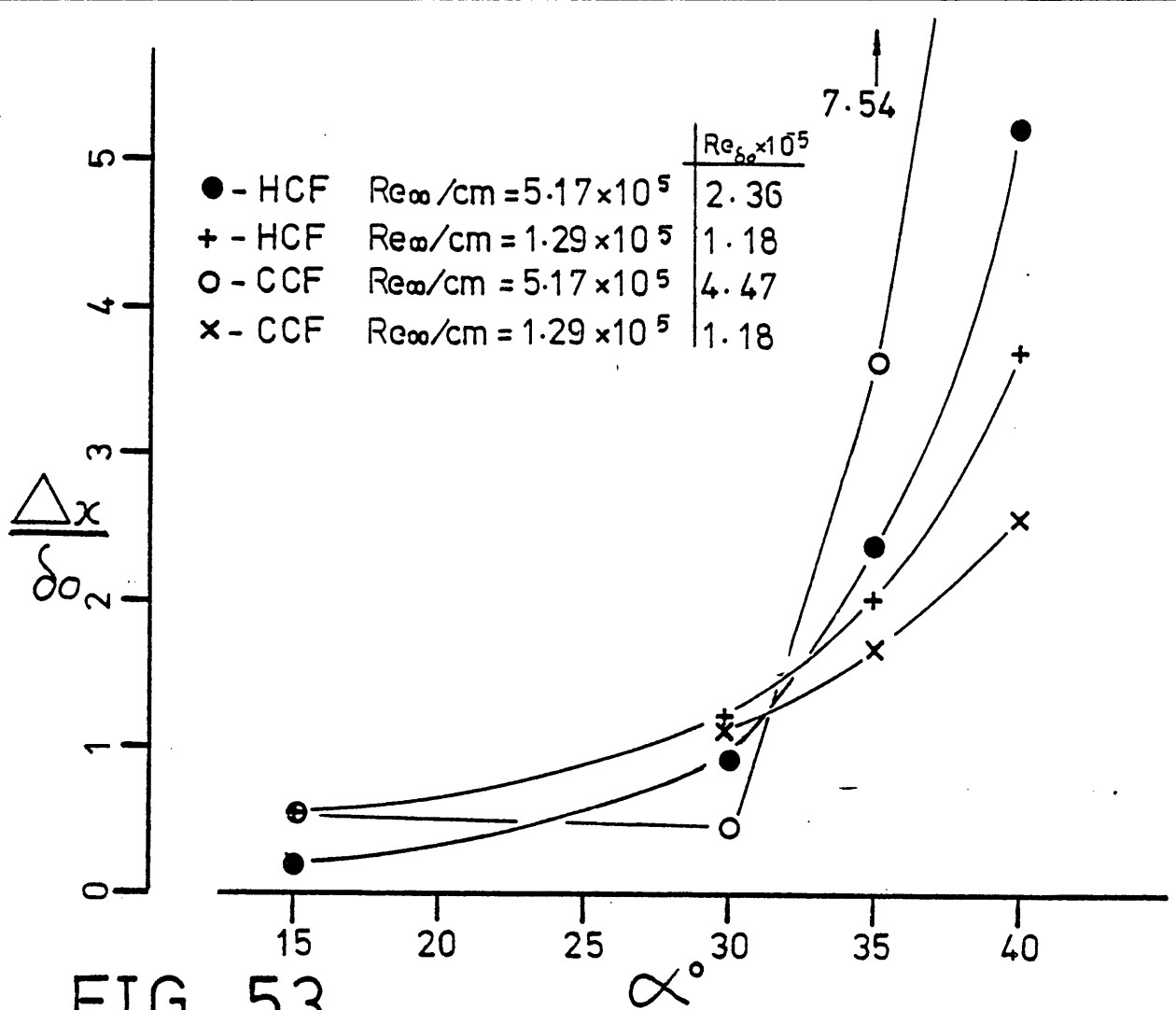
FIG 53

NORMALISED UPSTREAM INFLUENCE vs.
FLARE ANGLE (CCF-exp. & data from Coleman 1973)

Legend (Fig 53):

		Re_∞/cm	$Re_{\delta_0}\times10^5$
●	– HCF	$Re_\infty/cm = 5.17\times10^5$	2.36
+	– HCF	$Re_\infty/cm = 1.29\times10^5$	1.18
○	– CCF	$Re_\infty/cm = 5.17\times10^5$	4.47
×	– CCF	$Re_\infty/cm = 1.29\times10^5$	1.18

7.54

Axis: $\dfrac{\Delta x}{\delta_0}$, α°
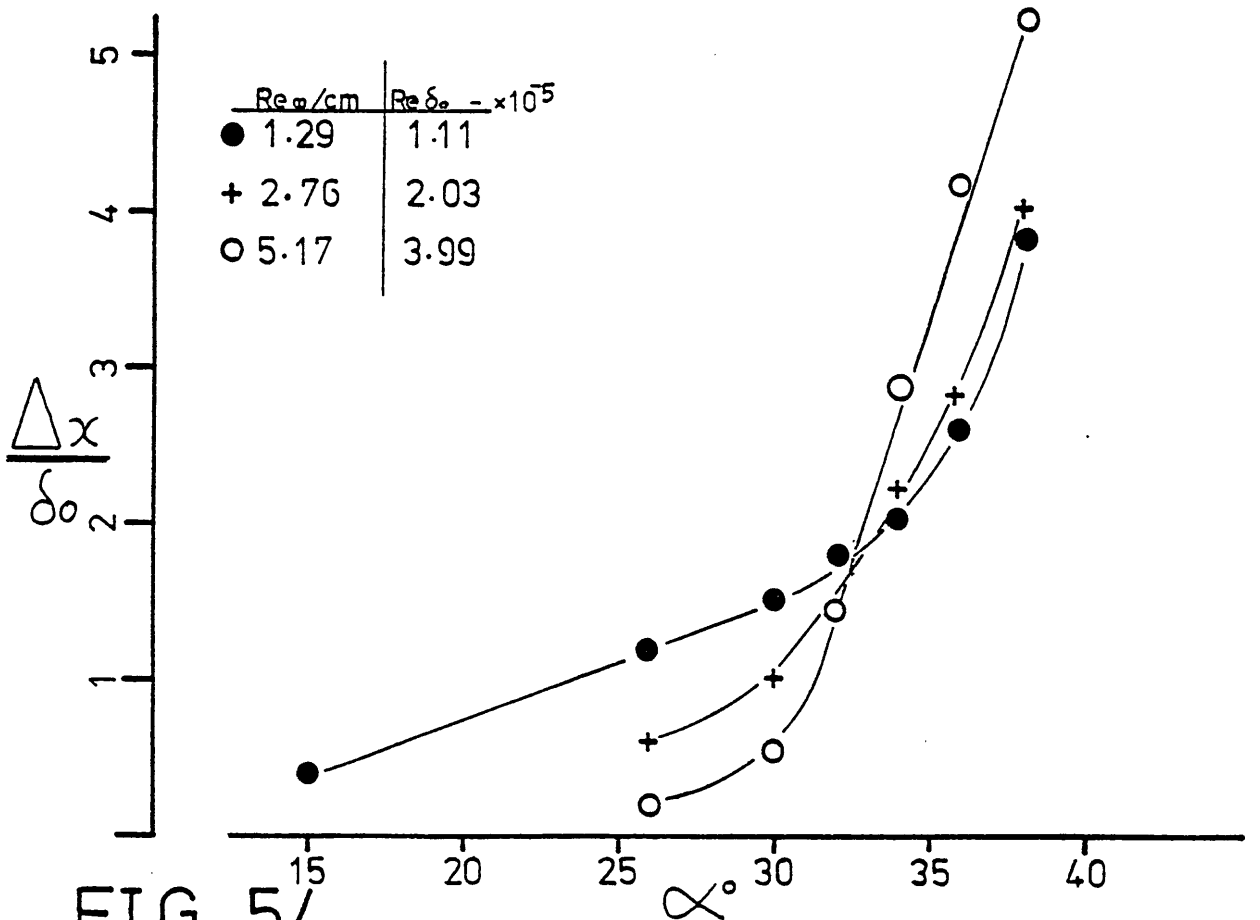
FIG 54

NORMALISED UPSTREAM INFLUENCE vs.
WEDGE ANGLE (data from Elfstrom 1971)

Legend (Fig 54):

	Re_∞/cm	$Re_{\delta_0}\times10^5$
●	1.29	1.11
+	2.76	2.03
○	5.17	3.99

Axis: $\dfrac{\Delta x}{\delta_0}$, α°
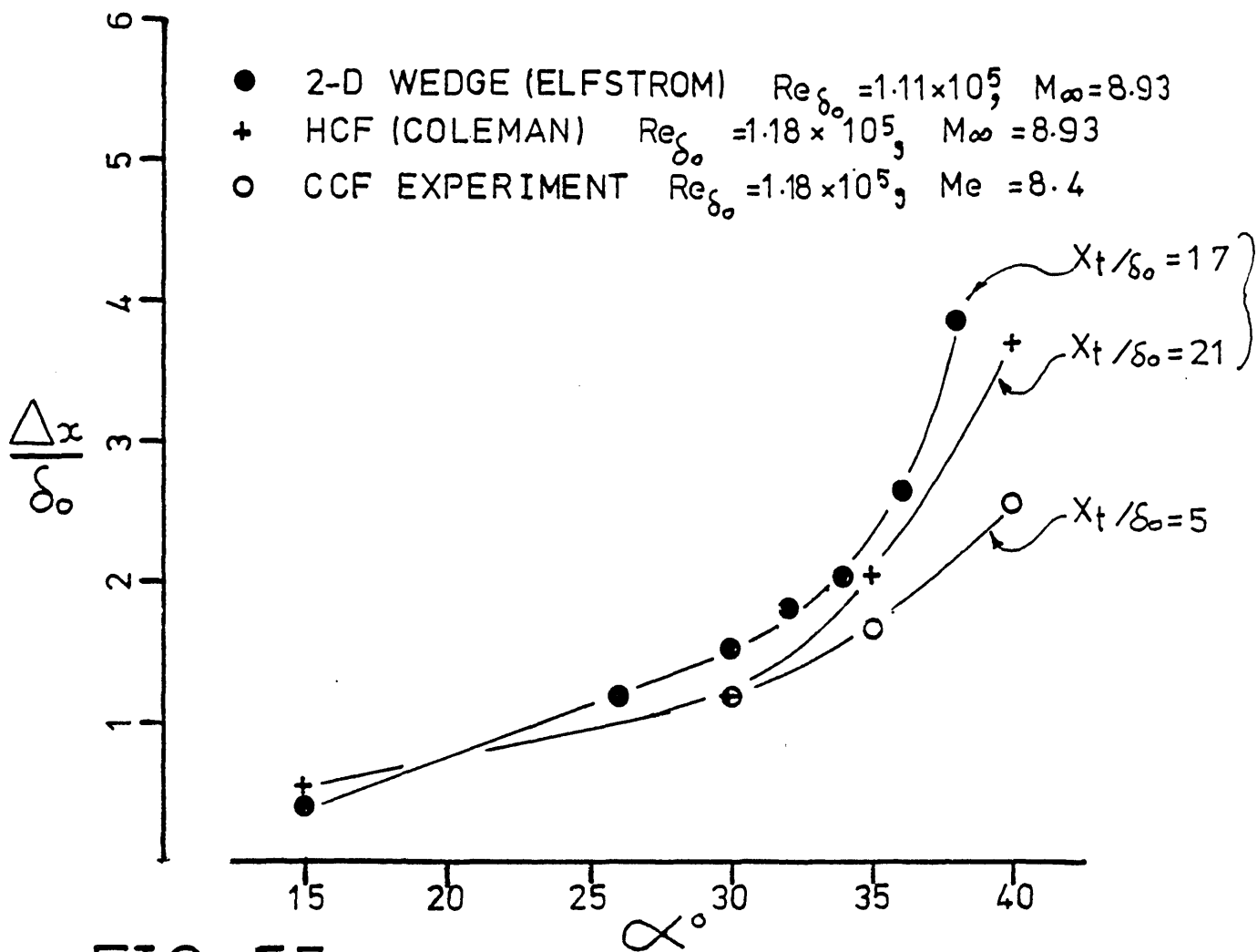
FIG 55 UPSTREAM INFLUENCE
(COMPARISON OF 2-D AND AXISYMMETRIC DATA)

$$\ell/\delta_o = 10^3 \left(\frac{\alpha}{18 \cdot 29}\right)^{2 \cdot 81} \left[Cfe - 10^{-3}(1 \cdot 0 - 0 \cdot 001189 \, \alpha^2)\right]$$

Data from Law (1975)

$Re_{\delta_o} \times 10^{-5}$

◯	1·5
△	2·8
◻	6·0
◇	9·0

$(\ell/\delta_o) \longrightarrow$

α deg $\longrightarrow$
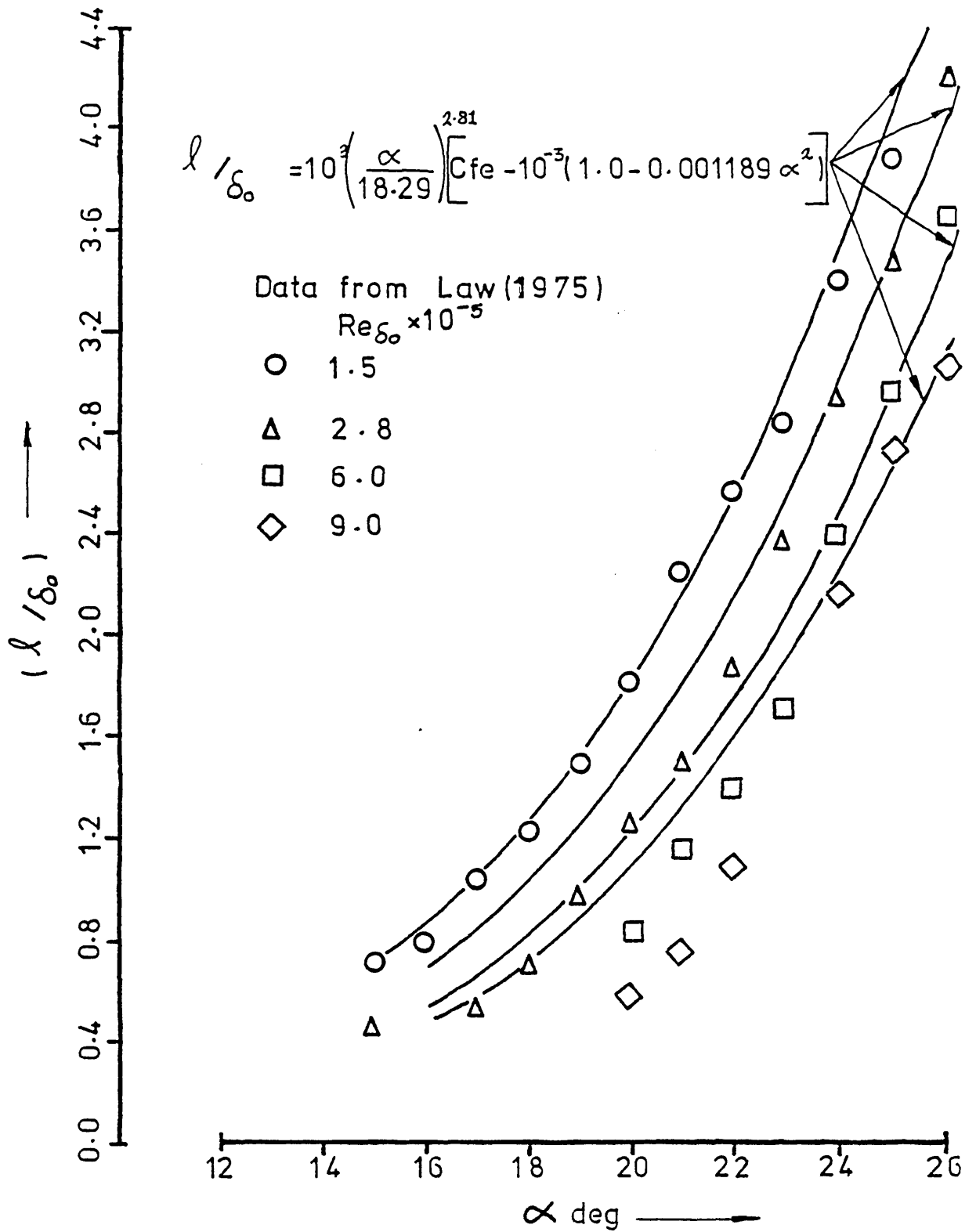
FIG 56   Correlation of Roshko & Thomke after Law

FIG 57

A CORRELATION FOR INTERACTION SCALE
(M∞ ⩾ 5·8)
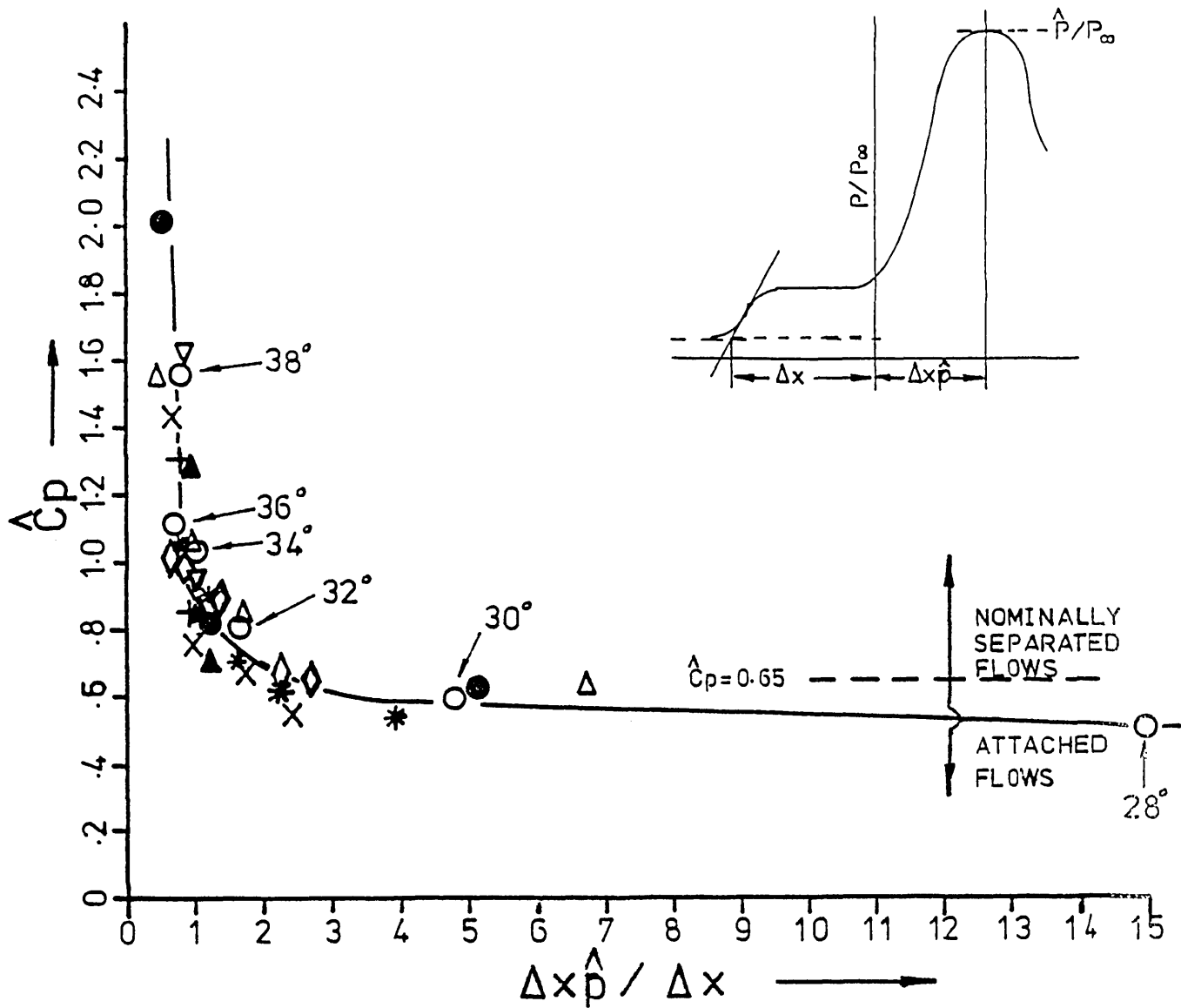
SYMBOL	MODEL	MACH NO M_∞	Rex	Re_{δ_0} ×10^{-5}	ref
●	CCF	9·31		4·47	EXPERIMENT
▲	CCF	8·93		1·18	EXPERIMENT
○	2D-Wdg	9·31		3·99	ELFSTROM (35)
✕	2D-Wdg	8·93		1·11	ELFSTROM (35)
+	HCF	8·93		1·18	COLEMAN (22)
▽	HCF	9·31		2·36	COLEMAN (22)
△	2D-Wdg	11·70	3·66		APPELS (6)
✳	2D-Wdg	5·80		2·00	STERRET + EMERY (98)
◊	2D-Wdg	7·00	95·0 155· }		BATHAM (11)
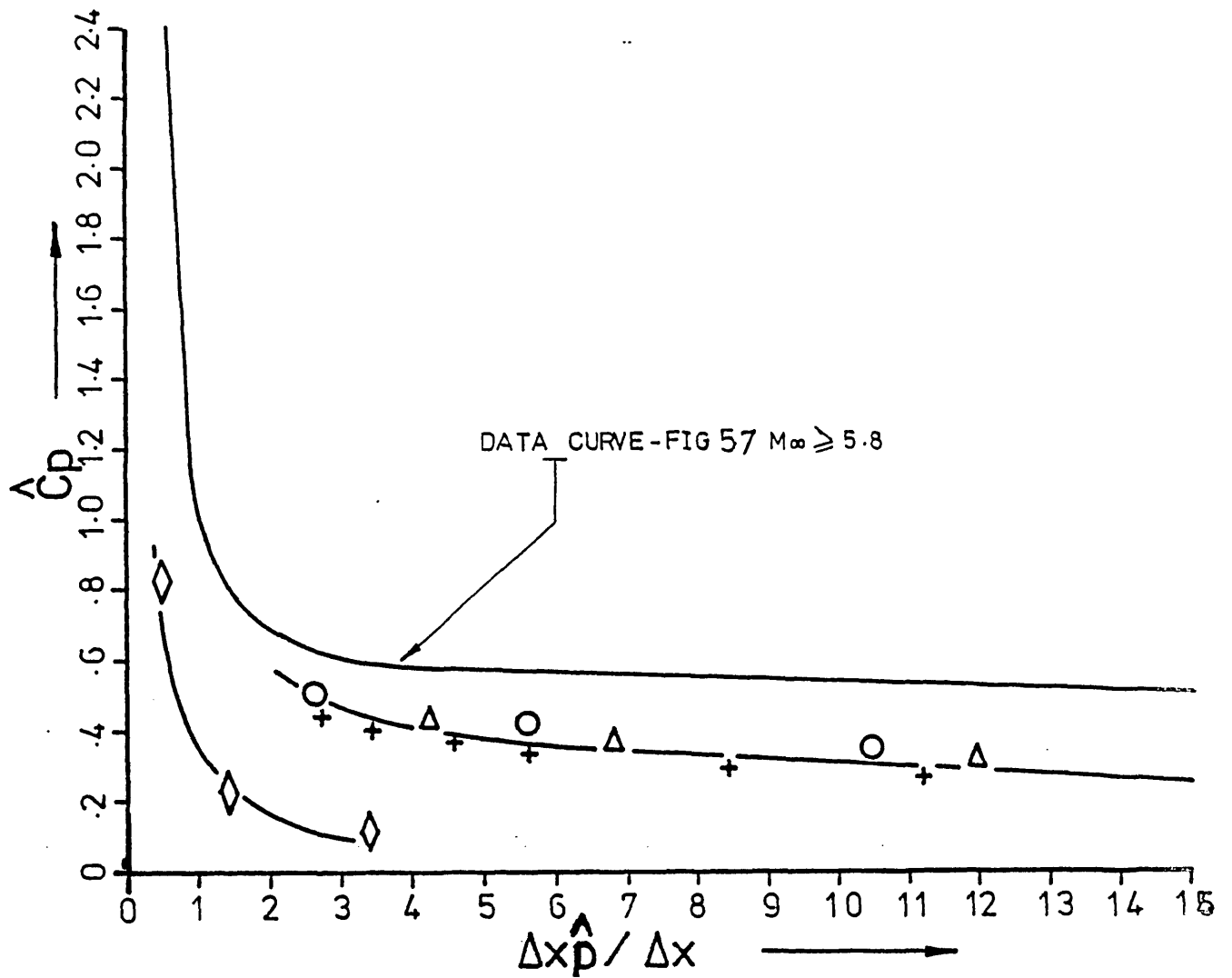
SYMBOL	MODEL	MACH NO M_∞	Re_x Re_{δ_0} $\times 10^{-5}$	ref
O	HCF	3·96	290·0	ROSHKO and THOMKE (86)
Δ	2D-Wdg	2·95	7·80	SETTLES et al (92)
+	2D-Wdg	2·93	0·363	SPAID and FRISHETT (96)
◇	2D-Wdg	8·00	35·81	JOHNSON-transitional ( ) data

FIG 58

INTERACTION SCALE -(EFFECT OF MACH NUMBER AND REYNOLDS NUMBER)
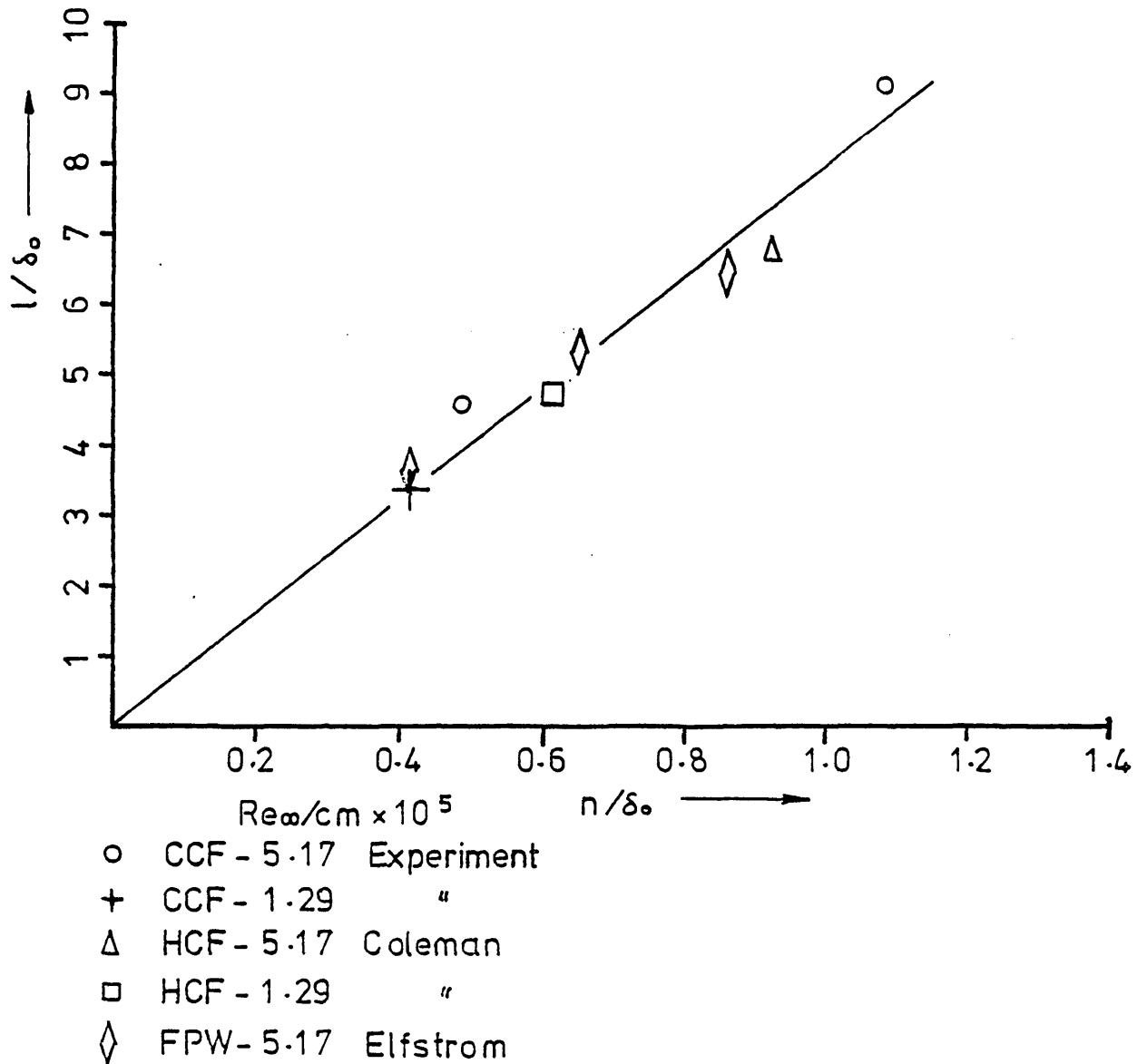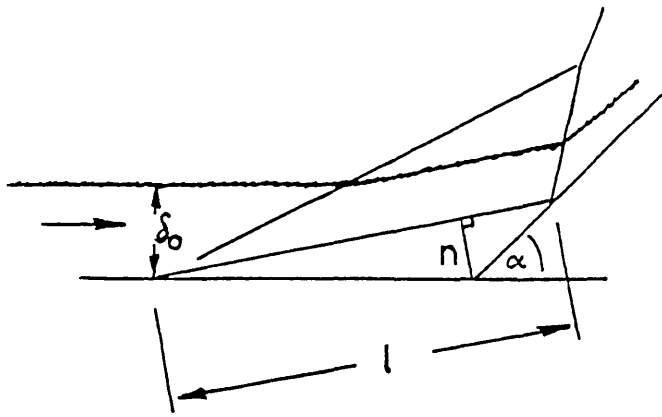
FIG 59   Cavity Geometry
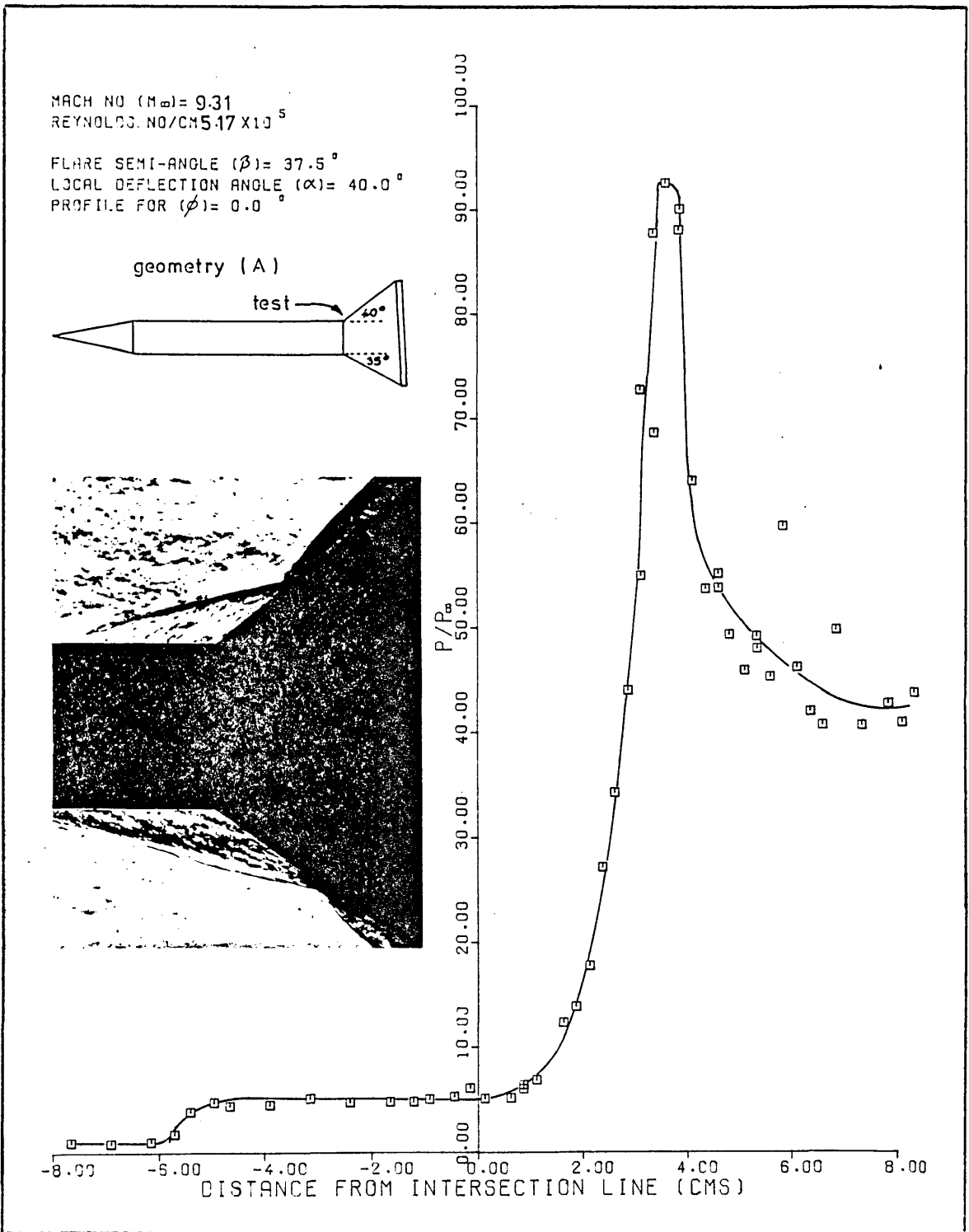
FIG 60 Static pressure-asymmetric geometries

FIG 61 Static pressure-asymmetric geometries

MACH NO (M∞)=9.31
REYNOLDS NO/CM5.17×10^5

FLARE SEMI-ANGLE (β)= 37.5$^°$
LOCAL DEFLECTION ANGLE (α)= 35.0$^°$
PROFILE FOR (φ)= 180.0$^°$

geometry (A)

test

P/P∞
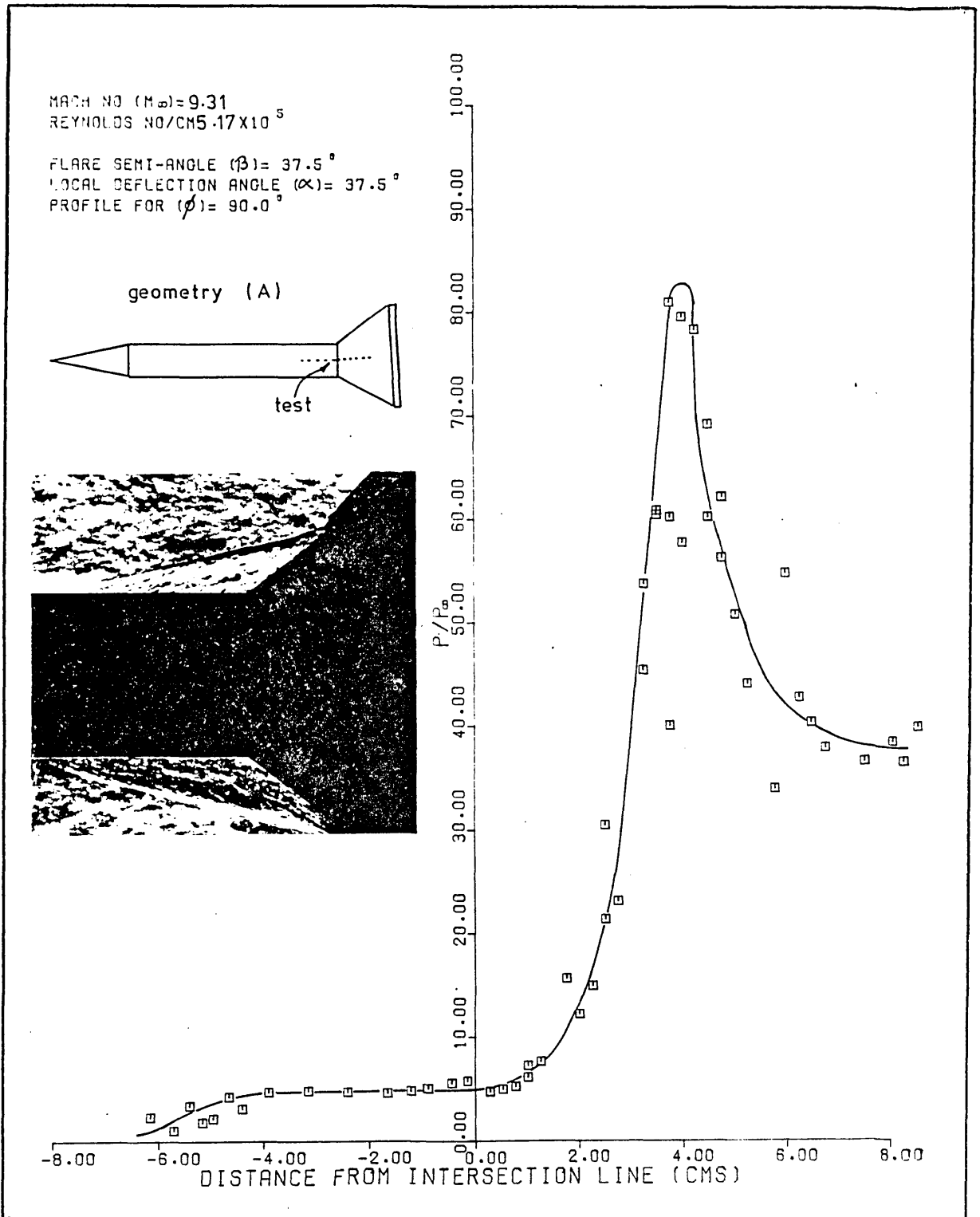
DISTANCE FROM INTERSECTION LINE (CMS)
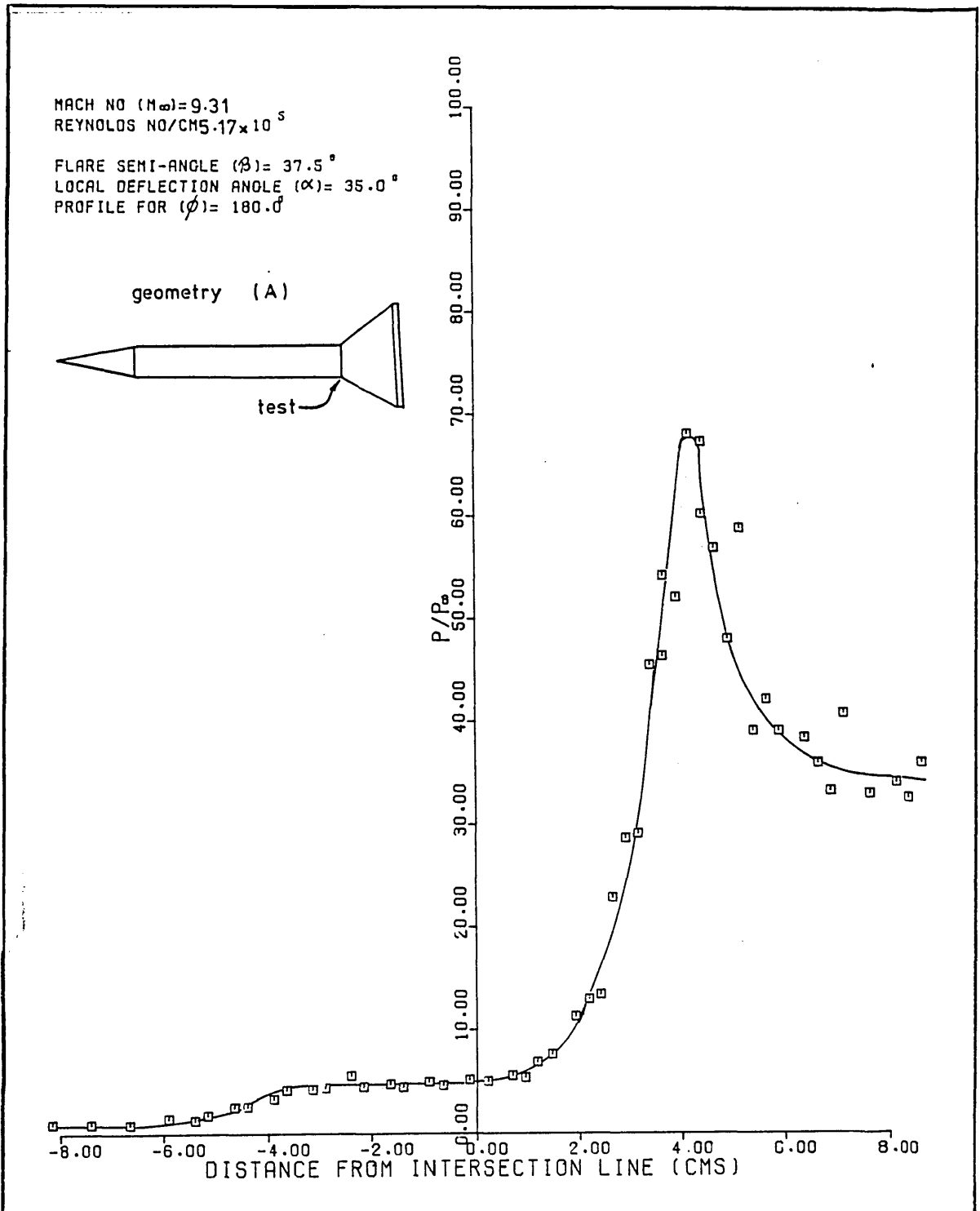
FIG 62 Static pressure-asymmetric geometries
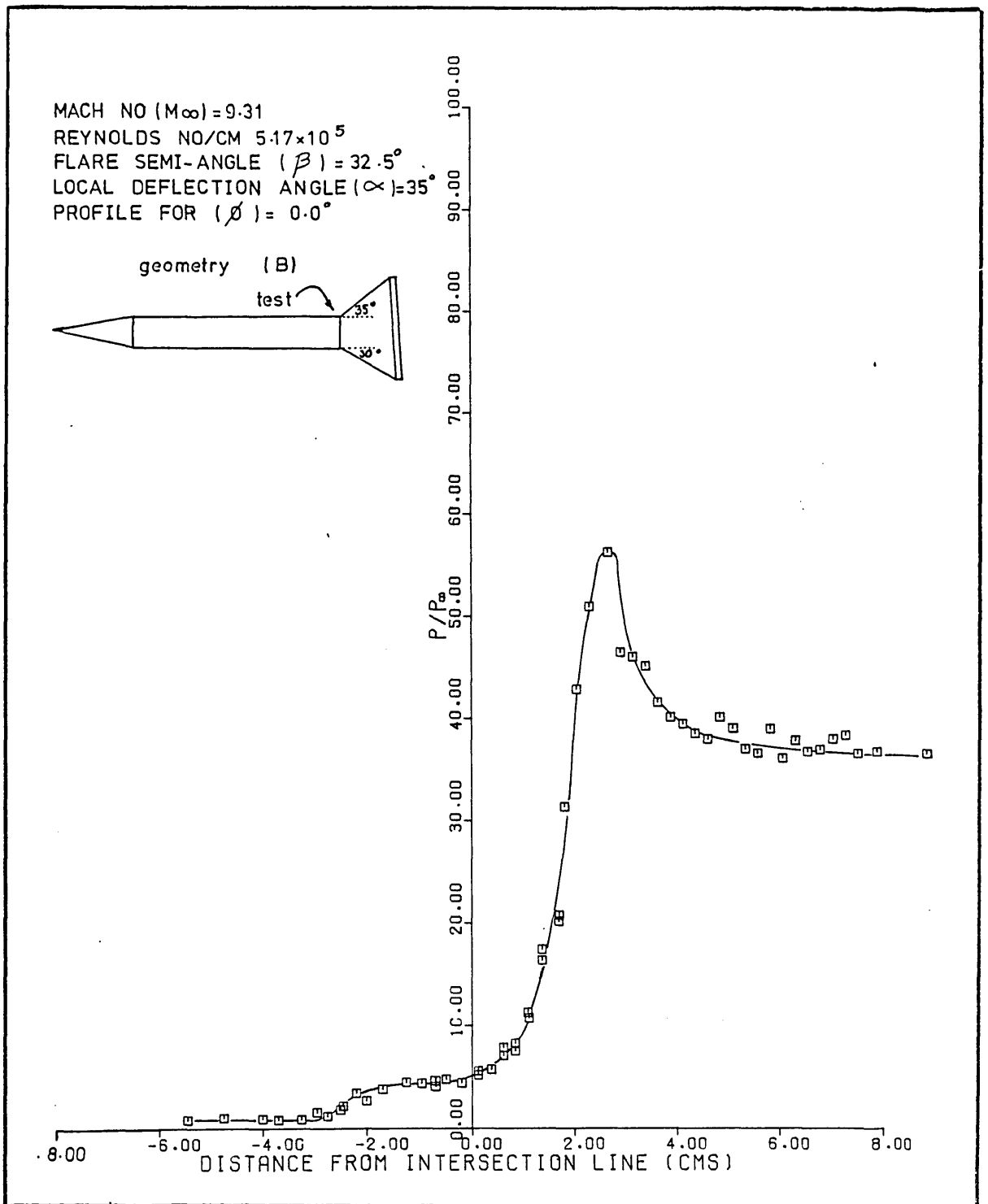
FIG 63 Static pressure-asymmetric geometries

FIG 64 Static pressure-asymmetric geometries

MACH NO (M∞)=9·31
REYNOLDS NO/CM 5·17×10 ^{5}

FLARE SEMI-ANGLE (β)= 32.5 $^{°}$
LOCAL DEFLECTION ANGLE (α)= 30.0 $^{°}$
PROFILE FOR (φ)= 180 $^{°}$

geometry [B]

test

P/P∞
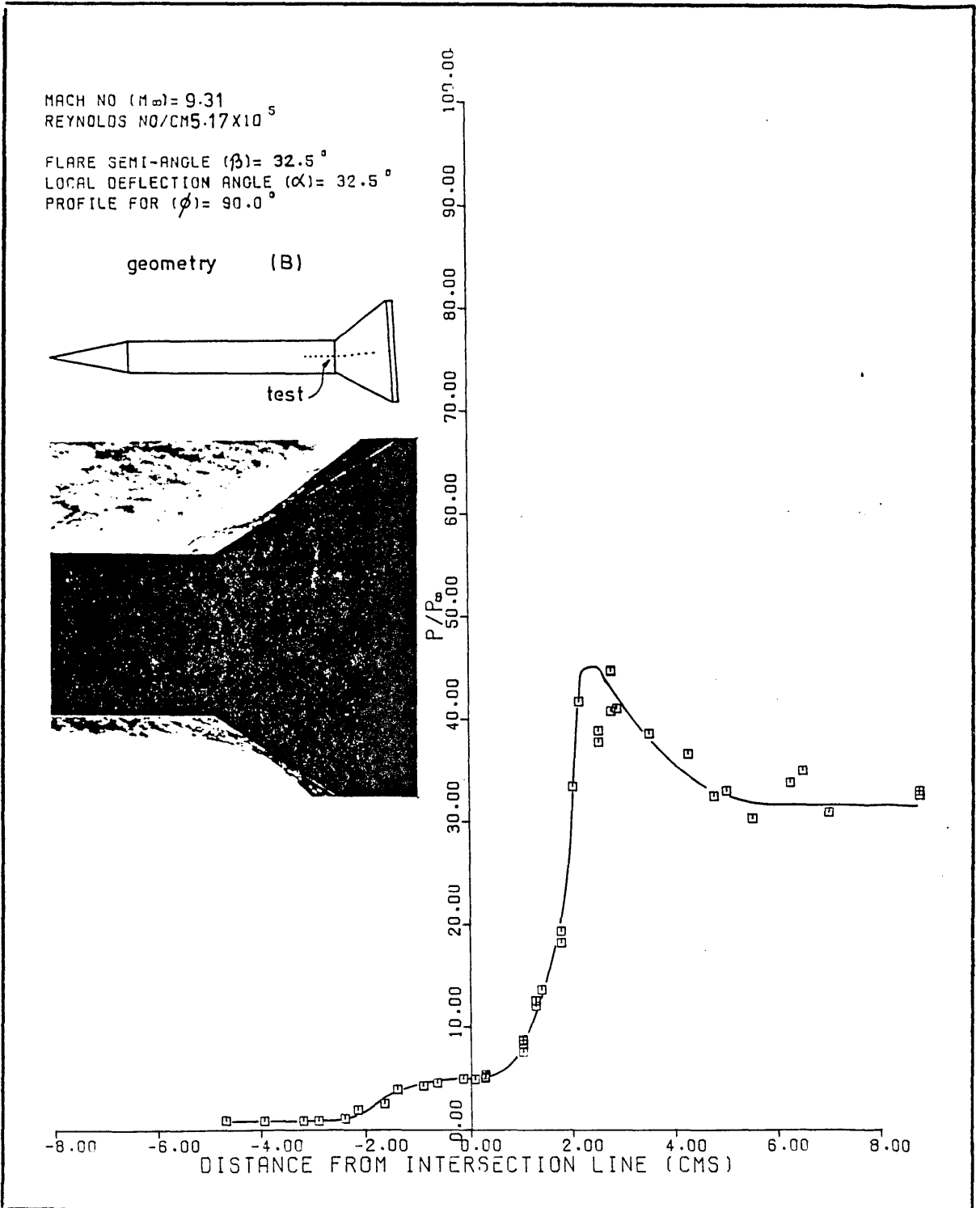
DISTANCE FROM INTERSECTION LINE (CMS)
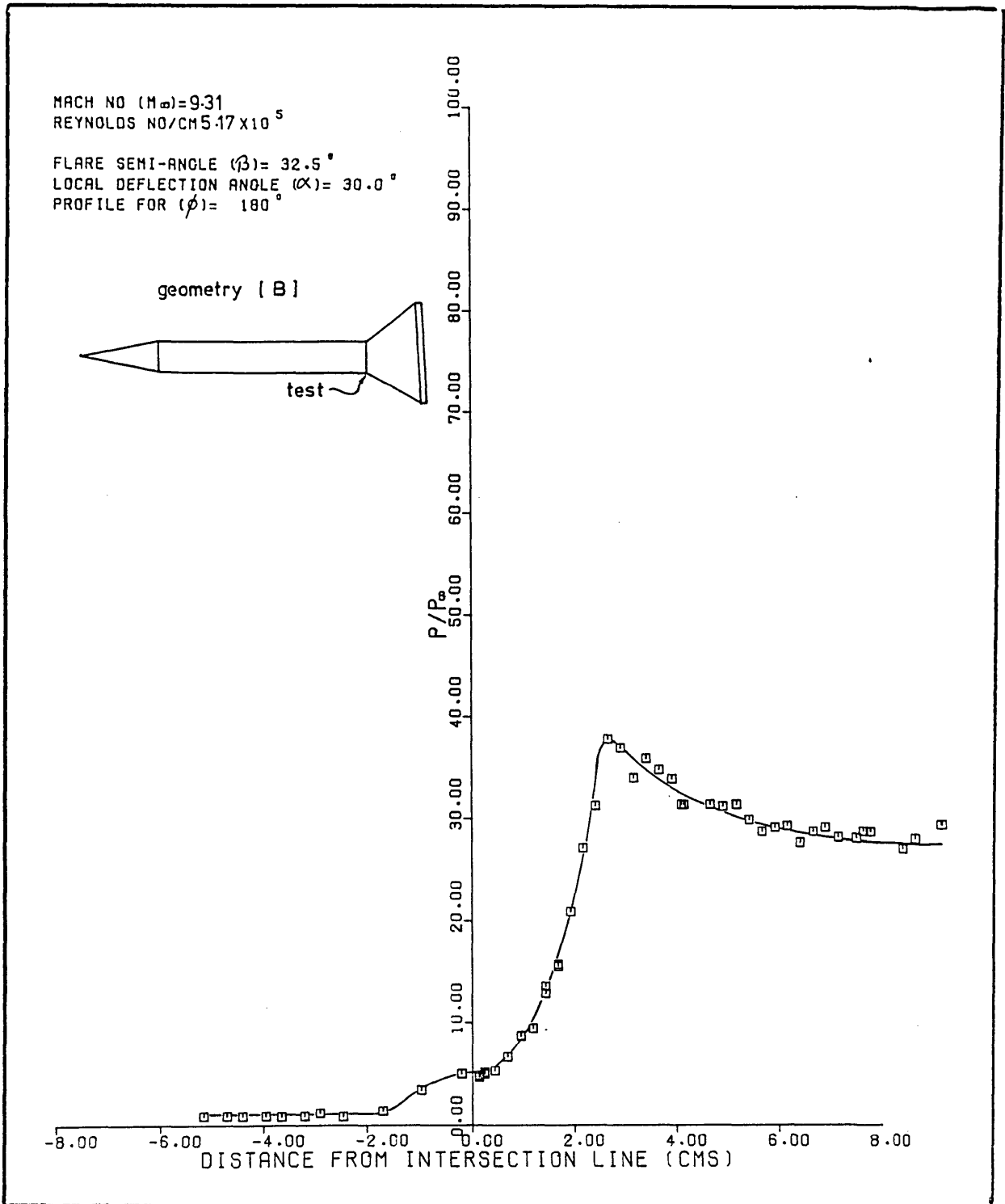
FIG 65 Static pressure-asymmetric geometries
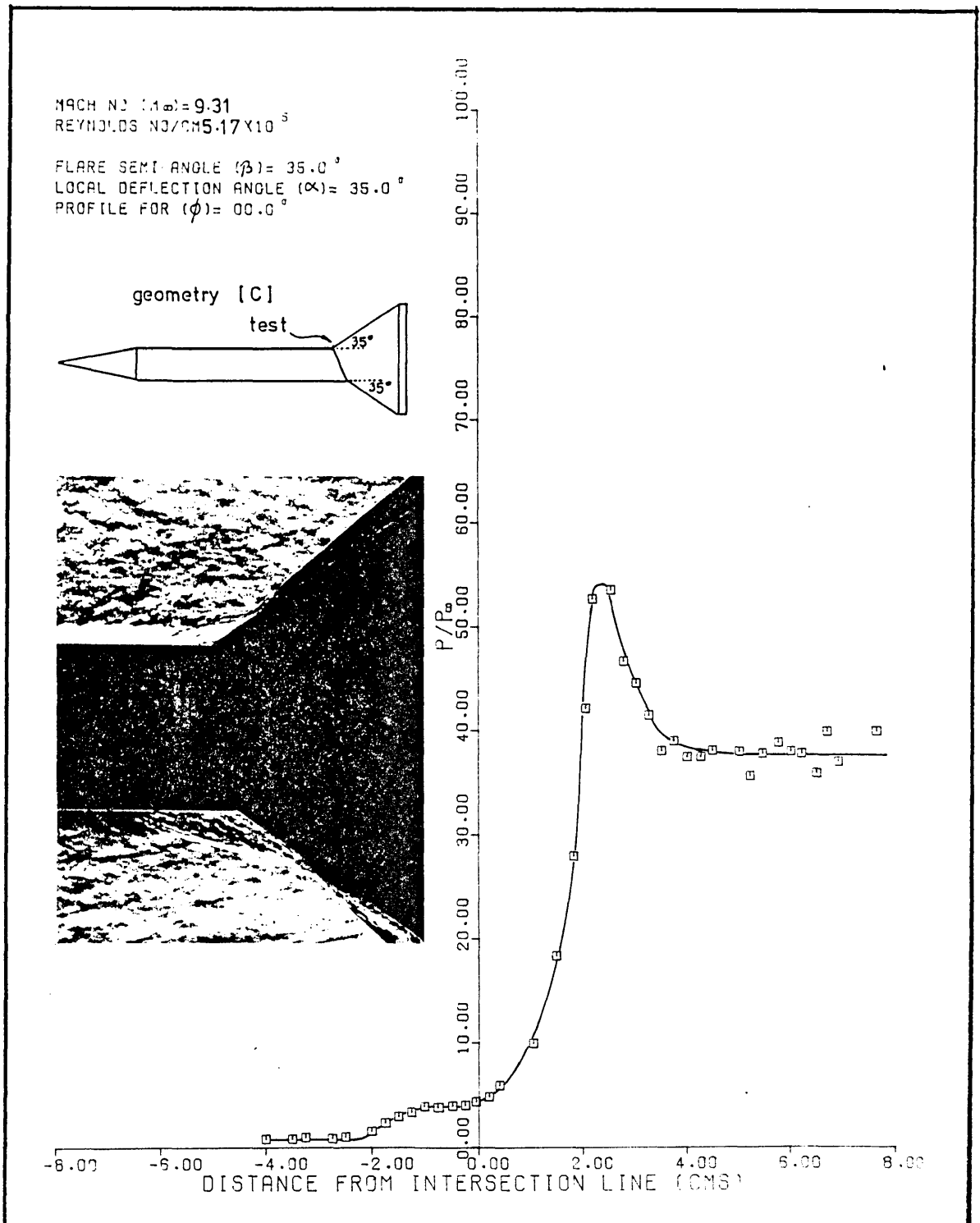
FIG 66 Static pressure-asymmetric geometries
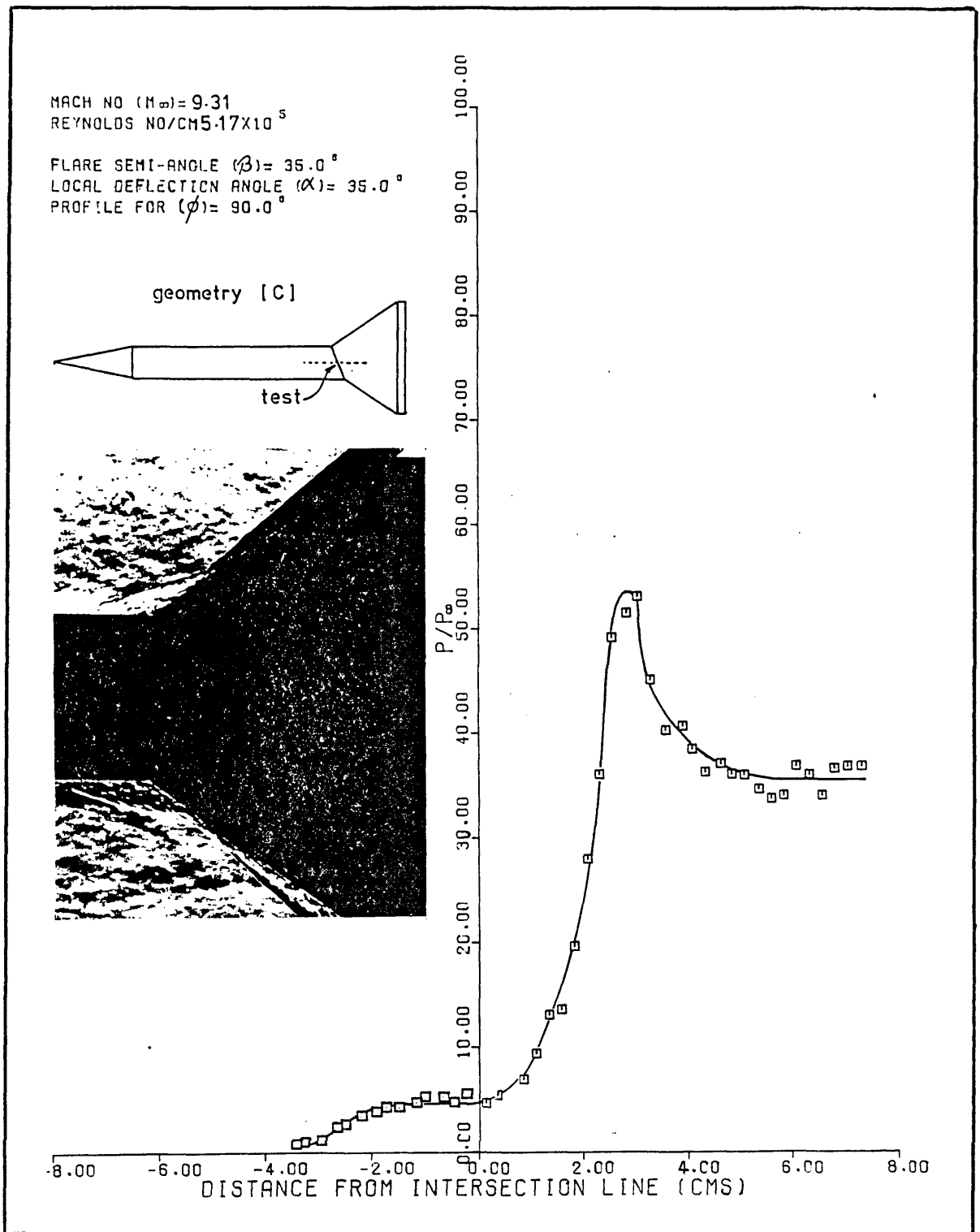
FIG 67 Static pressure-asymmetric geometries
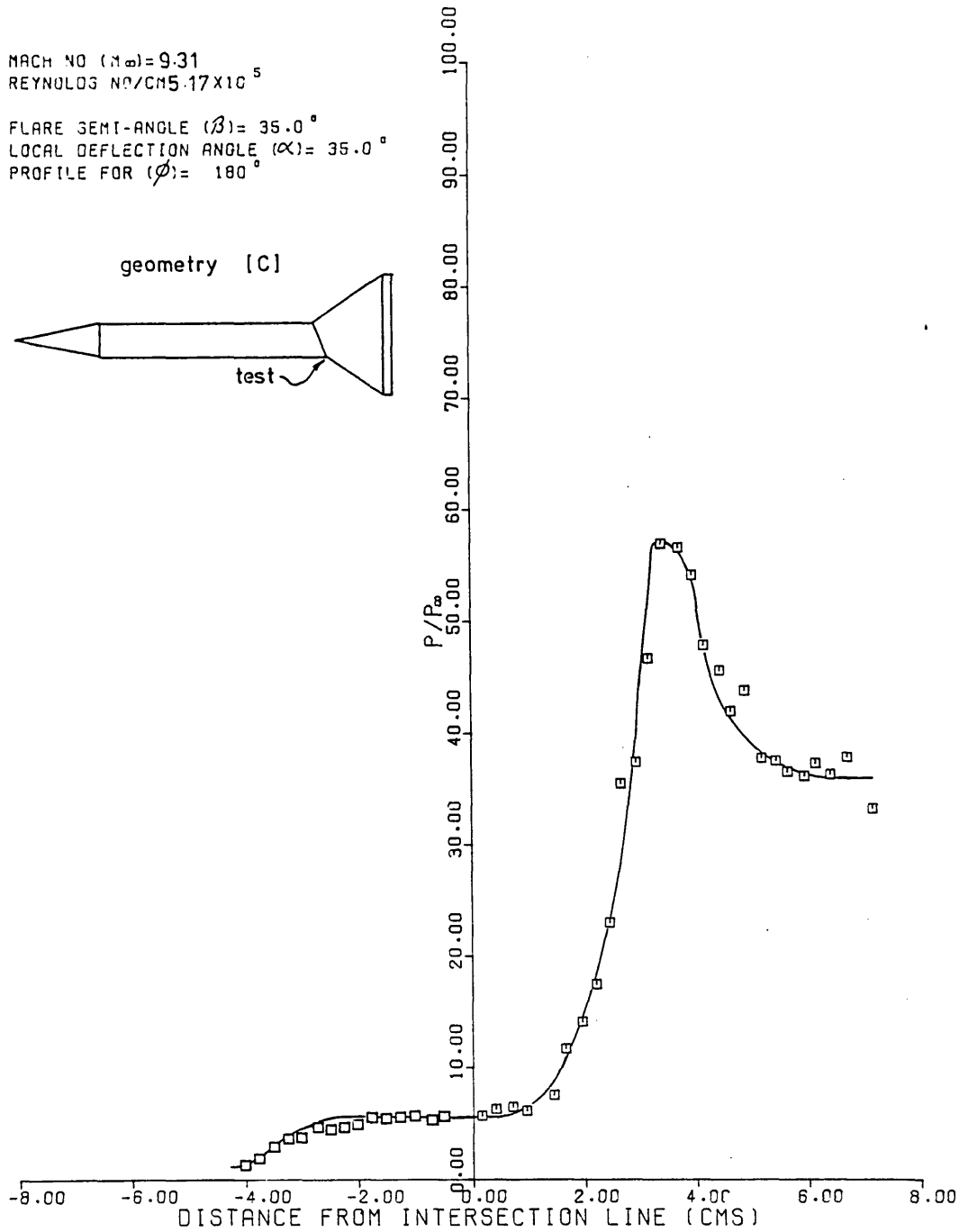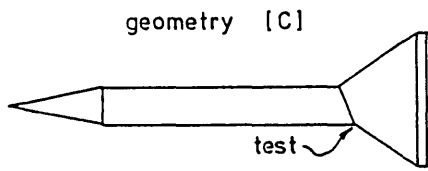
FIG 68 Static pressure-asymmetric geometries

MACH NO (M∞)=8·93
REYNOLDS NO/CM1·29X10^5

FLARE SEMI-ANGLE (β)= 37·5°
LOCAL DEFLECTION ANGLE (α)= 40·0°
PROFILE FOR (ϕ)= 0·0°

geometry [A]

test

40°

35°

FIG 69 Static pressure-asymmetric geometries

MACH NO (M∞)=8.93
REYNOLDS NO/CM1.29 X10 ^{5}

FLARE SEMI-ANGLE (β)= 37.5 ^{0}
LOCAL DEFLECTION ANGLE (α)= 37.5 ^{0}
PROFILE FOR (φ)= 90.0 ^{0}

geometry [A]

test

P/P_∞
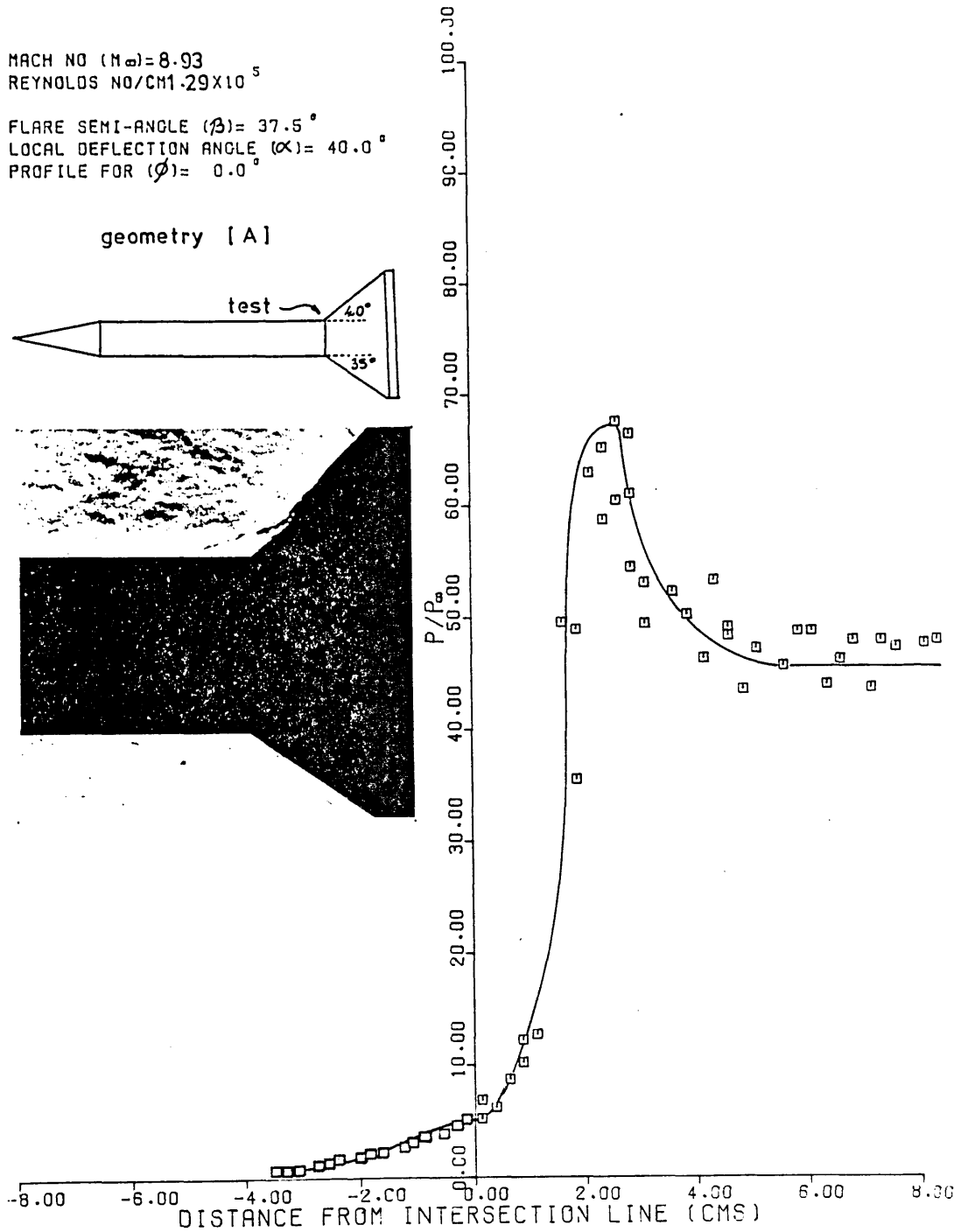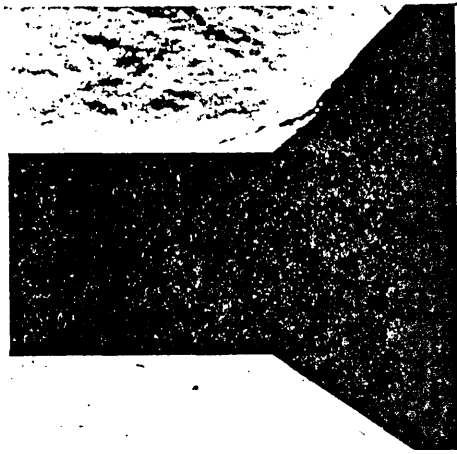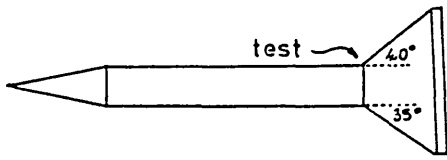
DISTANCE FROM INTERSECTION LINE (CMS)
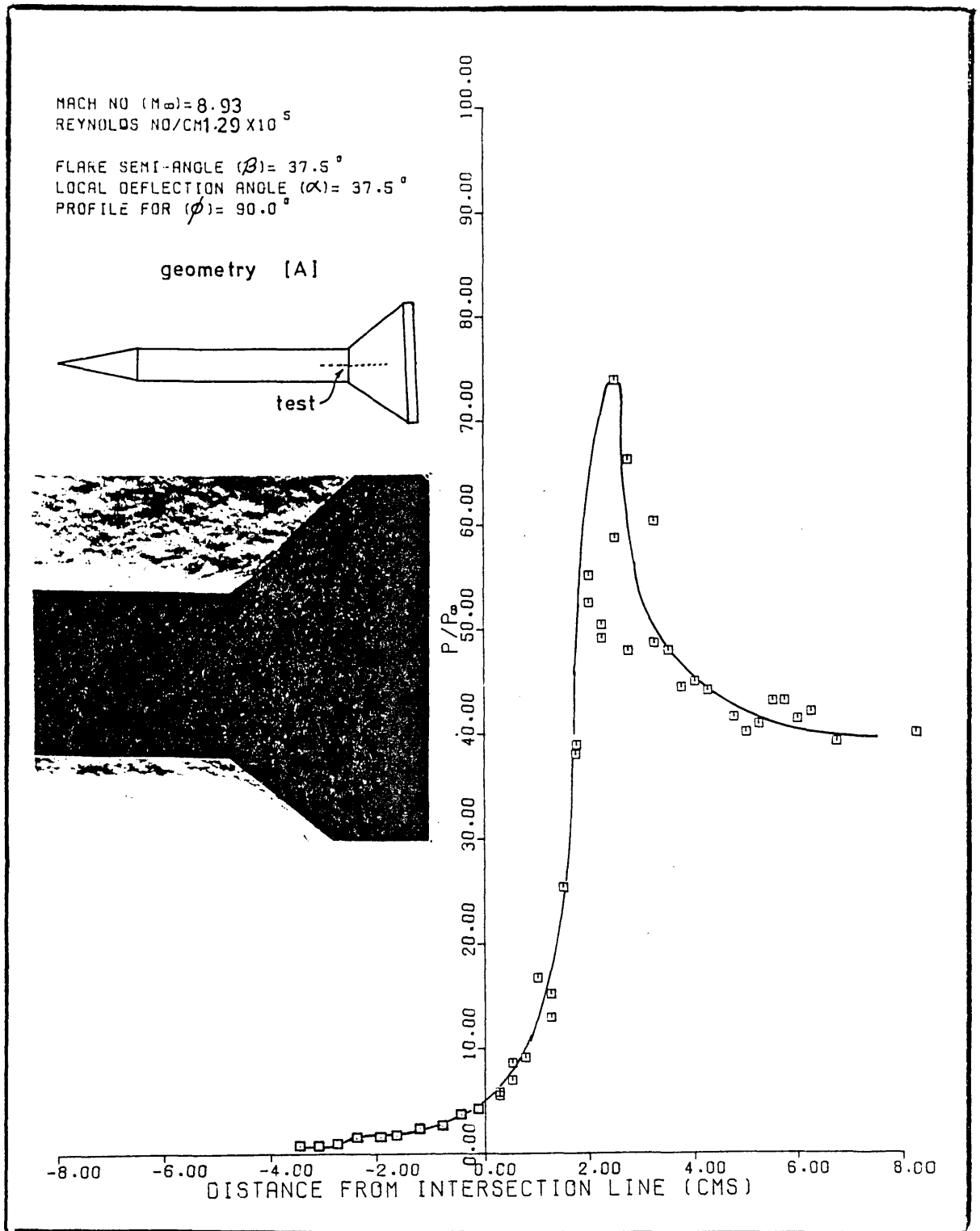
FIG 70 Static pressure-asymmetric geometries

FIG 71 Static pressure-asymmetric geometries
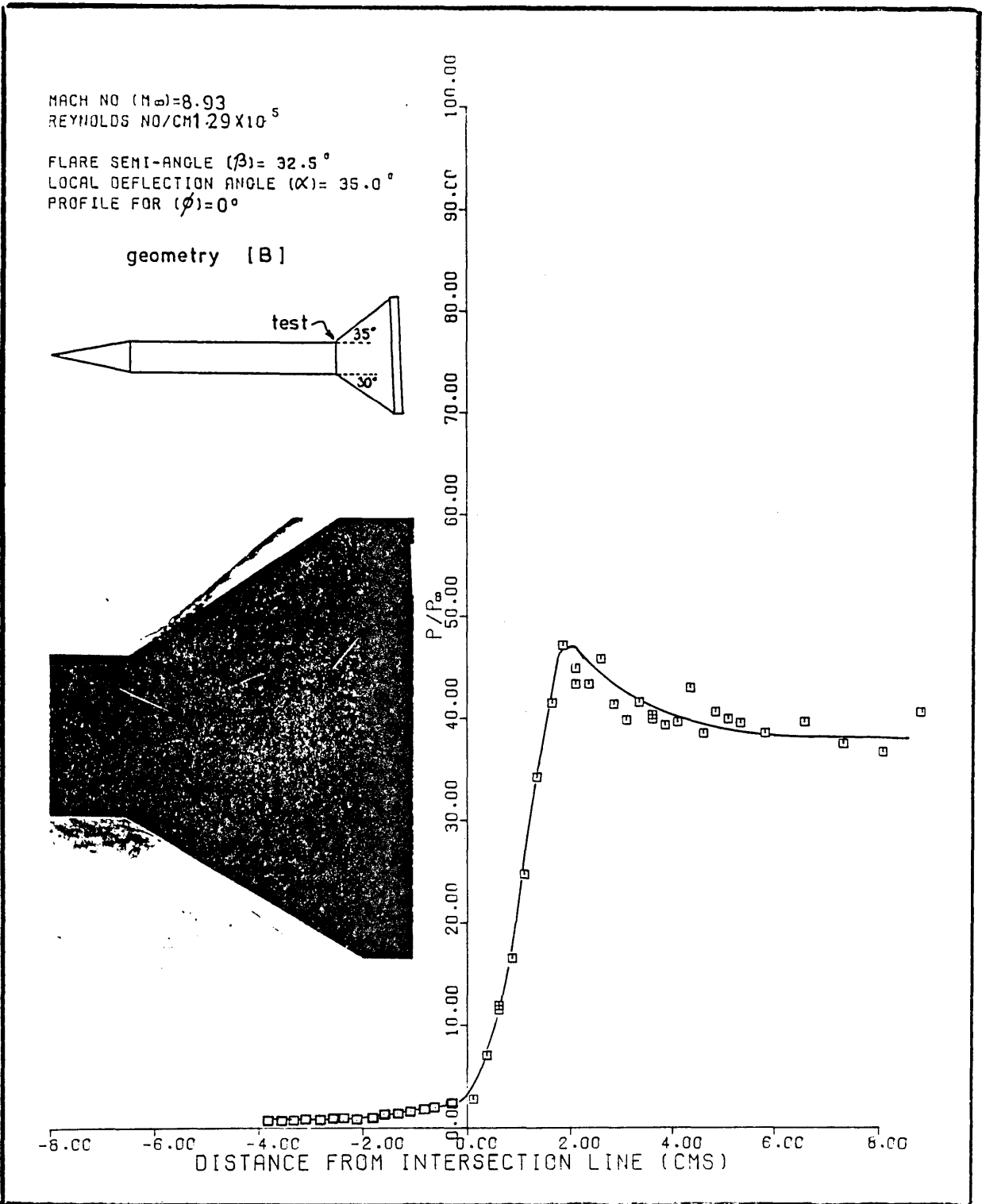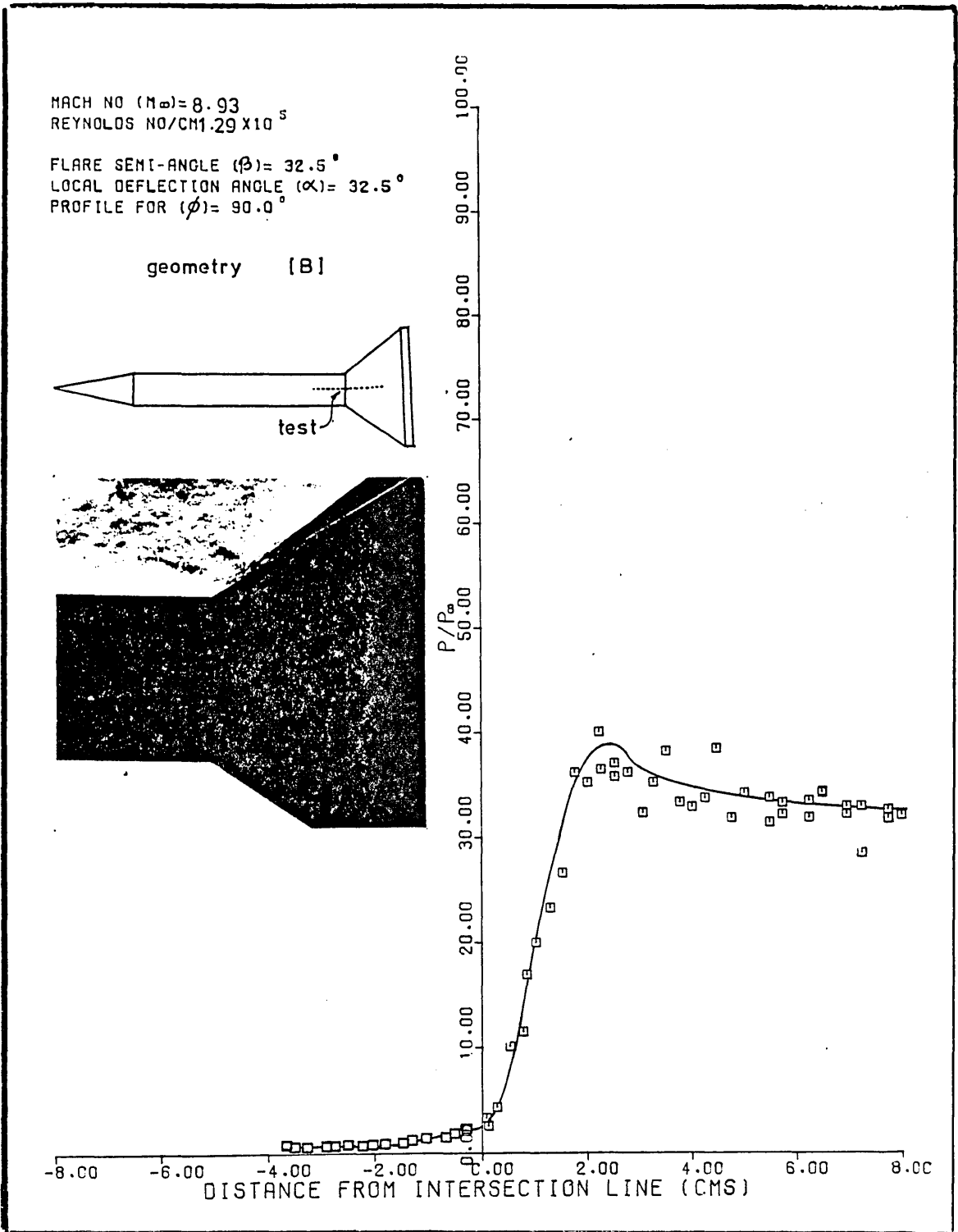
MACH NO (M∞)=8.93
REYNOLDS NO/CM1·29×10⁵

FLARE SEMI-ANGLE (β)= 32.5°
LOCAL DEFLECTION ANGLE (α)= 35.0°
PROFILE FOR (φ)=0°

geometry [B]

FIG 72 Static pressure-asymmetric geometries

MACH NO (M∞)= 8.93
REYNOLDS NO/CM 1.29 X 10 ^{5}

FLARE SEMI-ANGLE (β)= 32.5 °
LOCAL DEFLECTION ANGLE (α)= 32.5 °
PROFILE FOR (φ)= 90.0 °

geometry   [B]

test

FIG 73 Static pressure-asymmetric geometries

MACH NO (M∞)=8.93
REYNOLDS NO/CM 1·29 × 10⁵

FLARE SEMI-ANGLE (β)= 32.5°
LOCAL DEFLECTION ANGLE (α)= 30.0°
PROFILE FOR (φ)=180°

geometry   [B]

test

P/P∞

DISTANCE FROM INTERSECTION LINE (CMS)
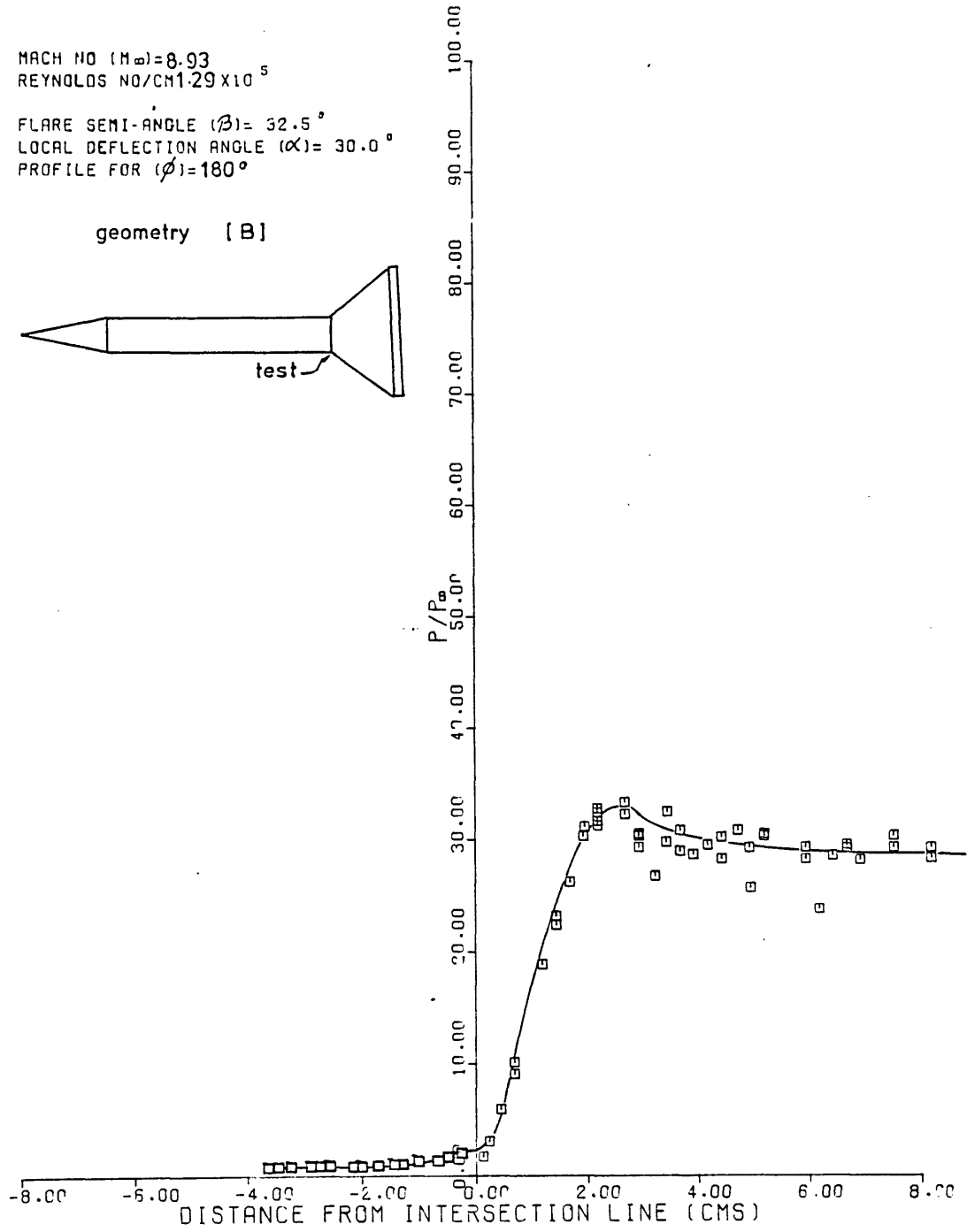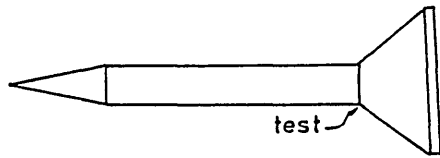
FIG 74 Static pressure-asymmetric geometries
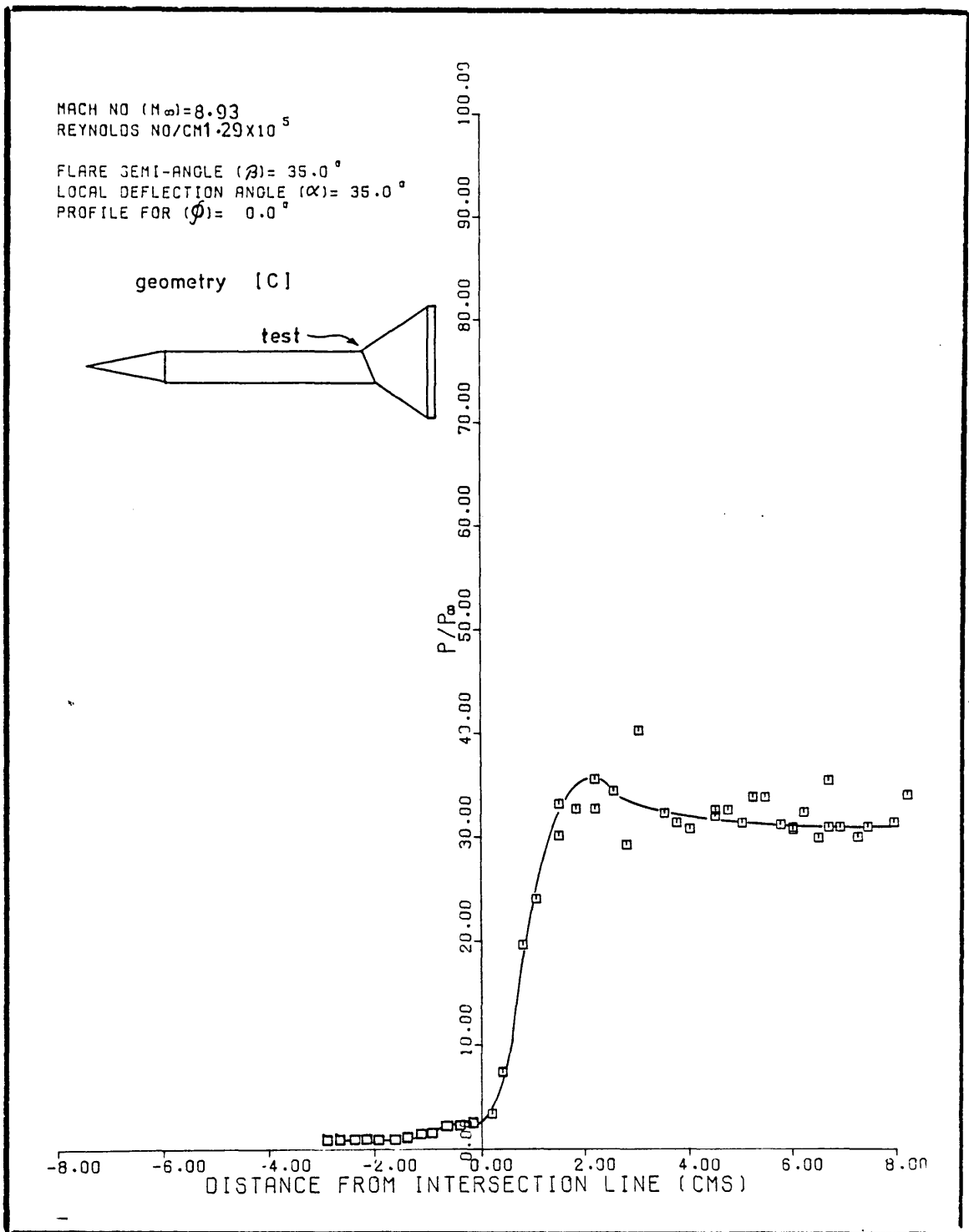
FIG 75 Static pressure-asymmetric geometries

MACH NO (M∞)=8·93
REYNOLDS NO/CM 1·29 X 10 ^{5}

FLARE SEMI-ANGLE (β)= 35·0 °
LOCAL DEFLECTION ANGLE (α)= 35·0 °
PROFILE FOR (φ)= 90·0 °

geometry [C]

test

FIG 76 Static pressure-asymmetric geometries

MACH NO (M∞)=8.93
REYNOLDS NO/CM1.29 X10 ^{5}

FLARE SEMI-ANGLE (β)= 35.0 °
LOCAL DEFLECTION ANGLE (α)= 35.0 °
PROFILE FOR (ø)= 180 °

geometry [C]

test
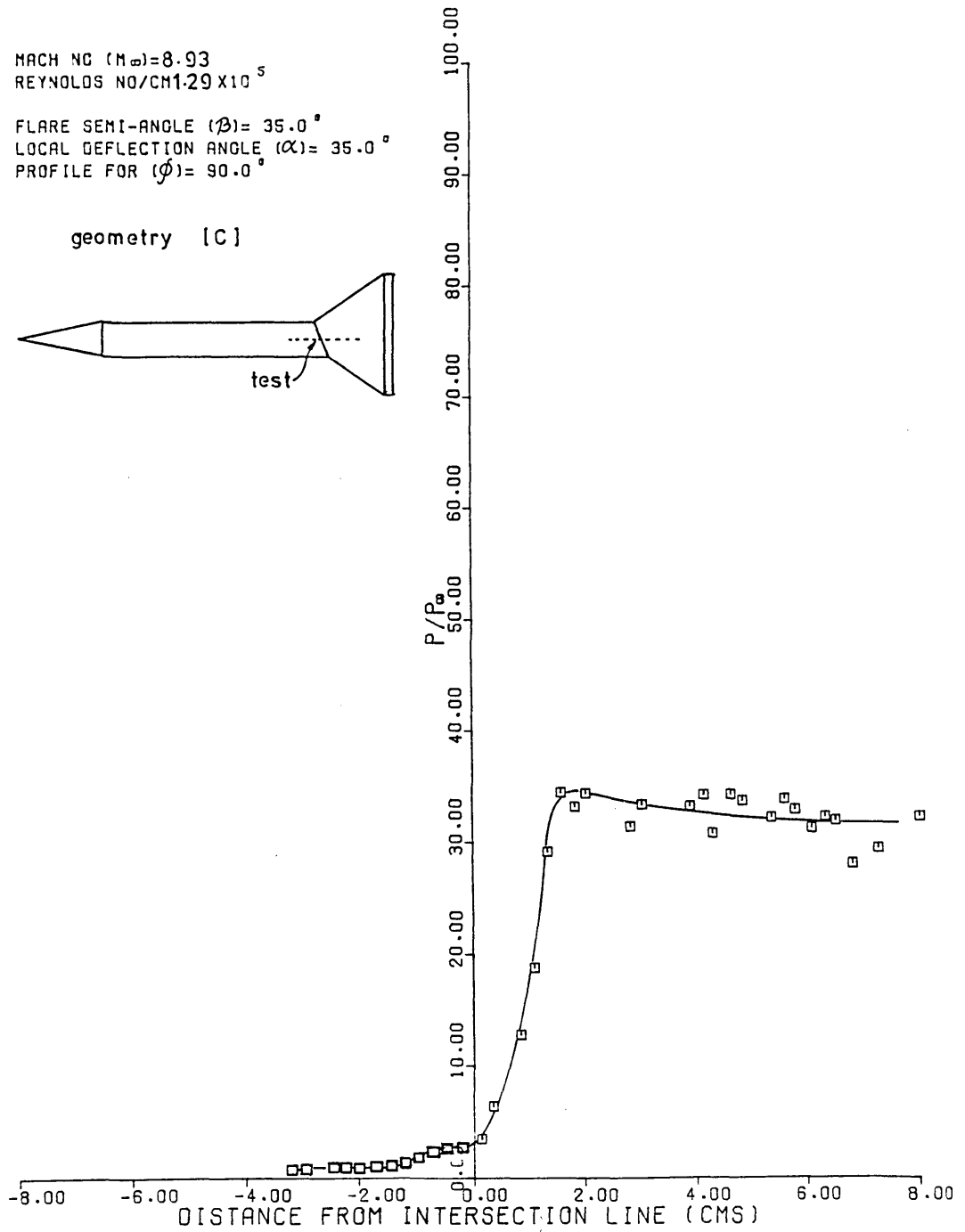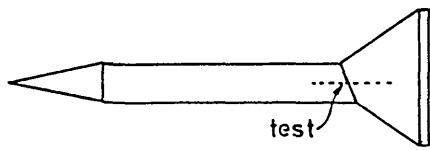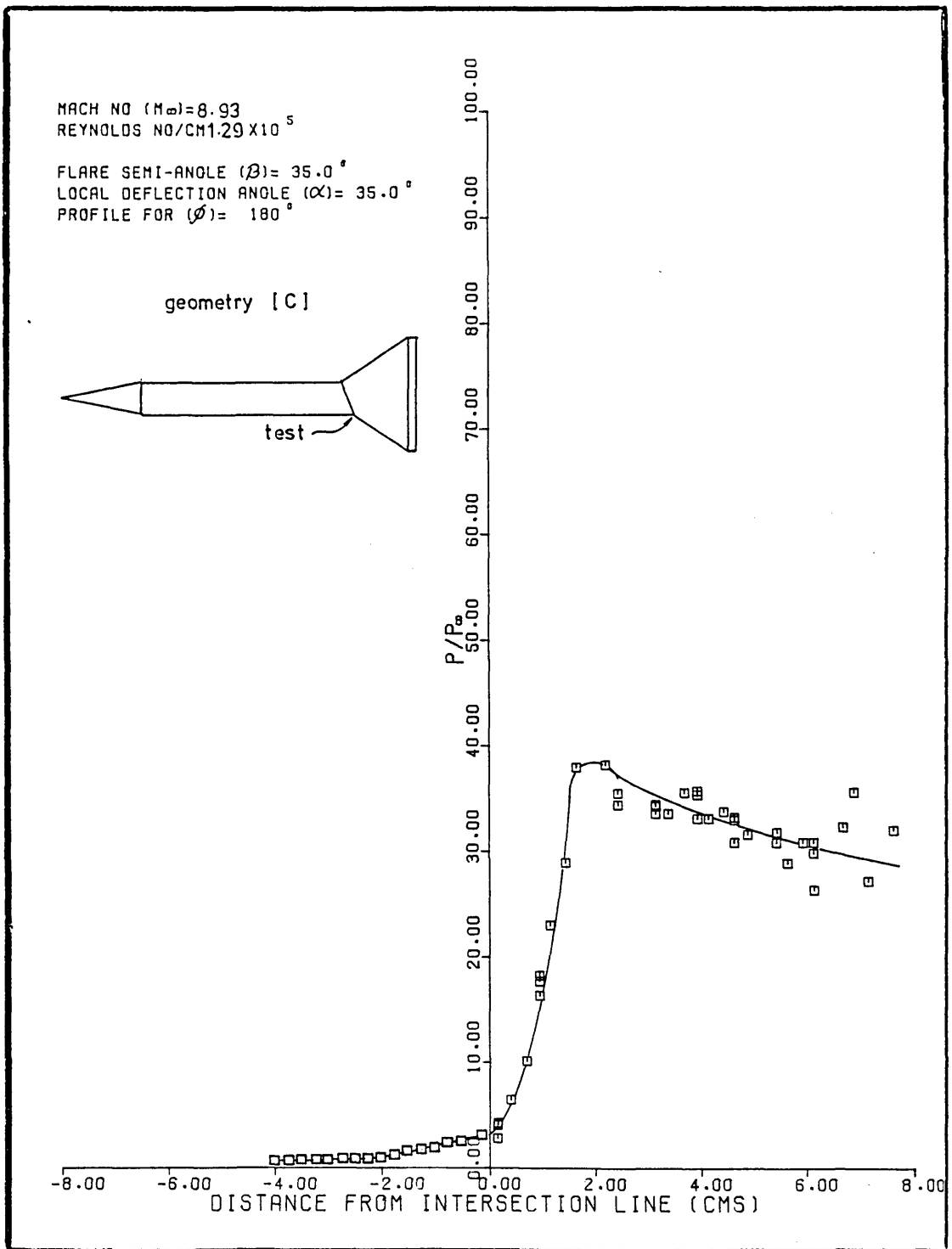
FIG 77 Static pressure-asymmetric geometries

$Re_\infty/cm = 5.17 \times 10^5$ $Re_\infty/cm = 1.29 \times 10^5$

geometry
A

B

C
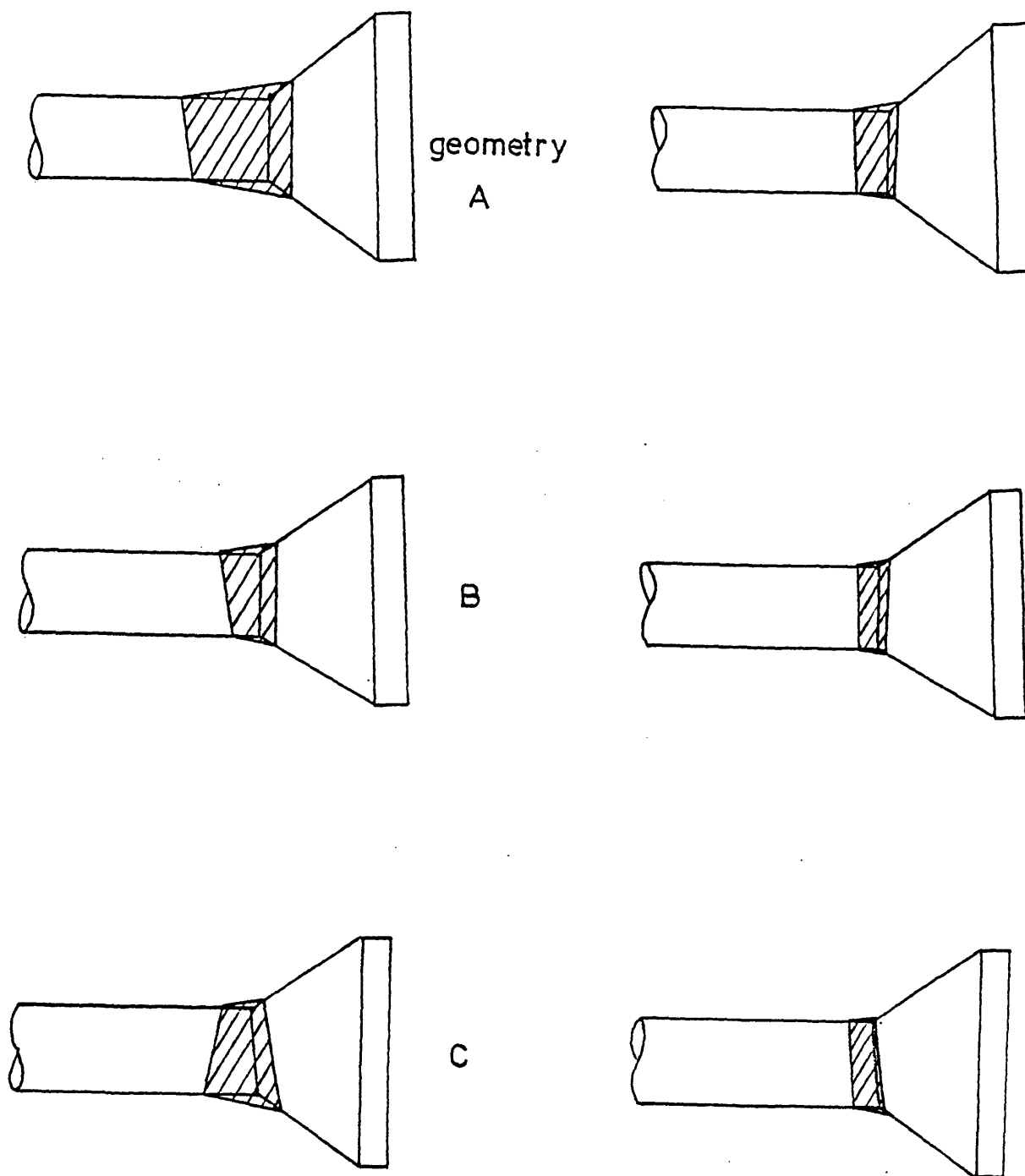
FIG 78   Cavity geometries
(inferred from plateau conditions)

Graph: P/P∞ (y-axis, 1 to 6) versus (X − Xo) cm (x-axis, 0 to 6)

$Re\infty/cm = 5.17 \times 10^5$
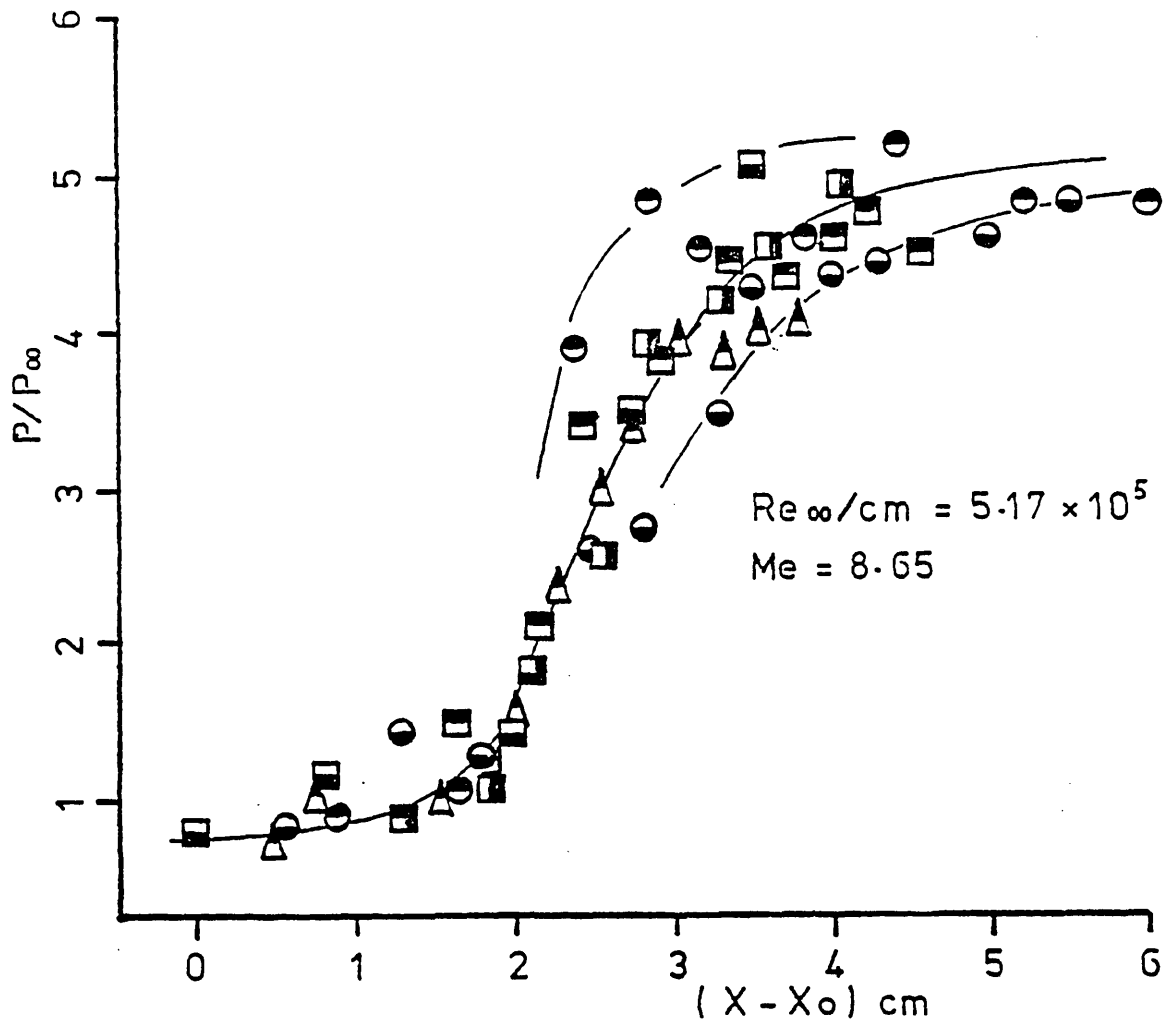
$Me = 8.65$

Table 7

Asymmetric CCF - Notation & Symbols (Figures 79 onwards)*

$Me = 8.65$, $Re\infty = 5.17 \times 10^5$		$Me = 8.4$, $Re\infty = 1.29 \times 10^5$	
A/40/0 - HP	◐	A/40/0 - LP	◠
A/37.5/90 - HP	◑	A/37.5/90 - LP	D
A/35/180 - HP	⊖	A/35/180 - LP	◡
B/35/0 - HP	▣	B/35/0 - LP	⊡
B/32.5/90 - HP	◧	B/32.5/90 - LP	⊞
B/30/180 - HP	⊟	B/30/180 - LP	⊓
C/35/0 - HP	◭	C/35/0 - LP	△
C/35/90 - HP	◮	C/35/90 - LP	▷
C/35/180 - HP	▲	C/35/180 - LP	▽

FIG 79 Pressure rise at separation asymmetric flows

* unless otherwise stated

PRESSURE RISE AT
SEPARATION
$M_\infty = 9.31$
$M_e = 8.65$
$Re_\infty/cm = 5.17 \times 10^5$

——— ERDOS/PALLONE
FREE INTERACTION THEORY.

CORRELATION FOR CONE CYLINDER
WITH ASYMMETRIC FLARES

EXPERIMENT

⊙	BETA= 37.5°	PHI= 0.0°
△	BETA= 37.5°	PHI= 90.0°
+	BETA= 37.5°	PHI= 180°
×	BETA= 32.5°	PHI= 0.0°
◇	BETA= 32.5°	PHI= 90.0°
↑	BETA= 32.5°	PHI= 180°
✕	BETA= 35.0°	PHI= 00.0°
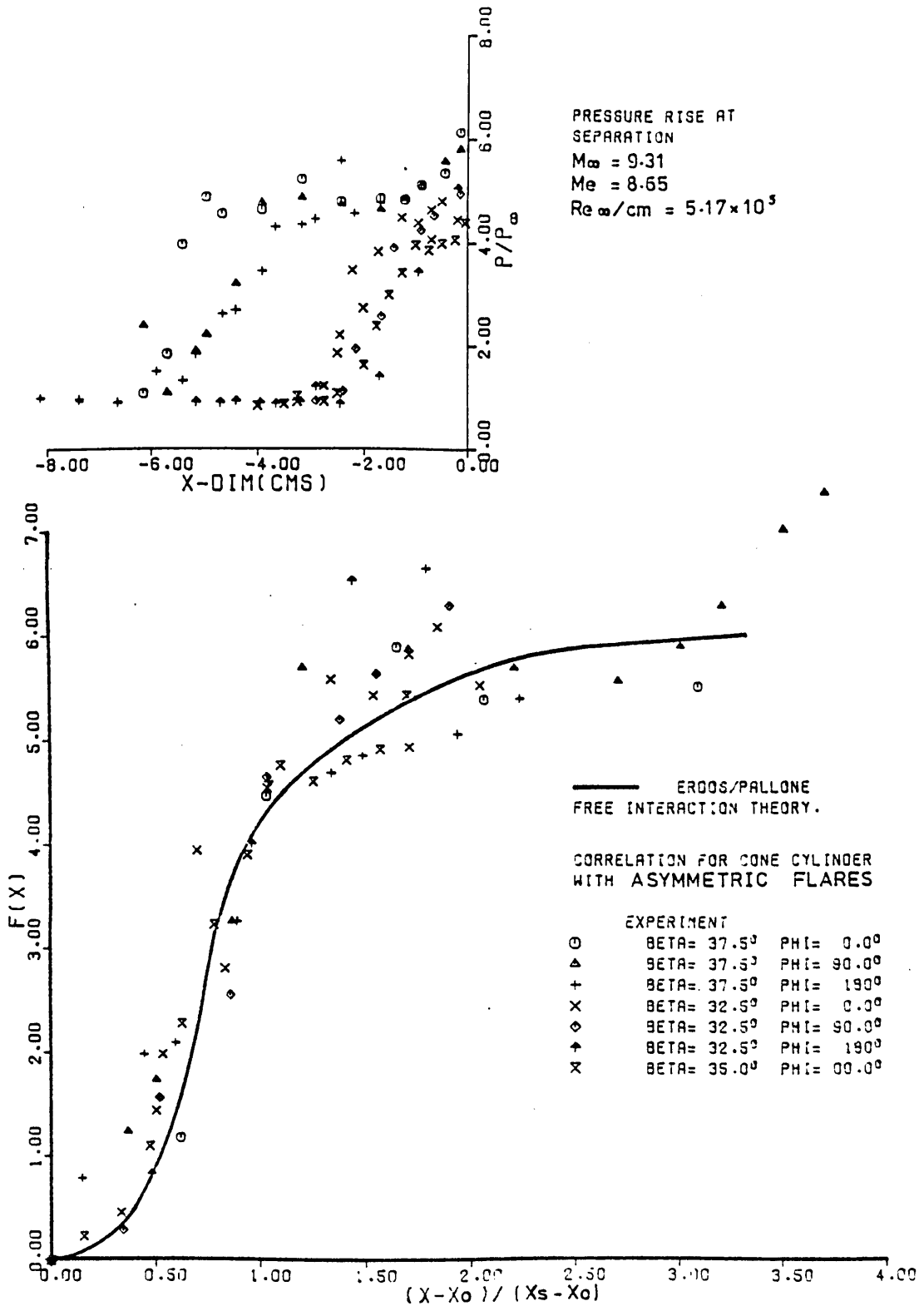
FIG 80   Free   Interaction
comparison with   2D theory
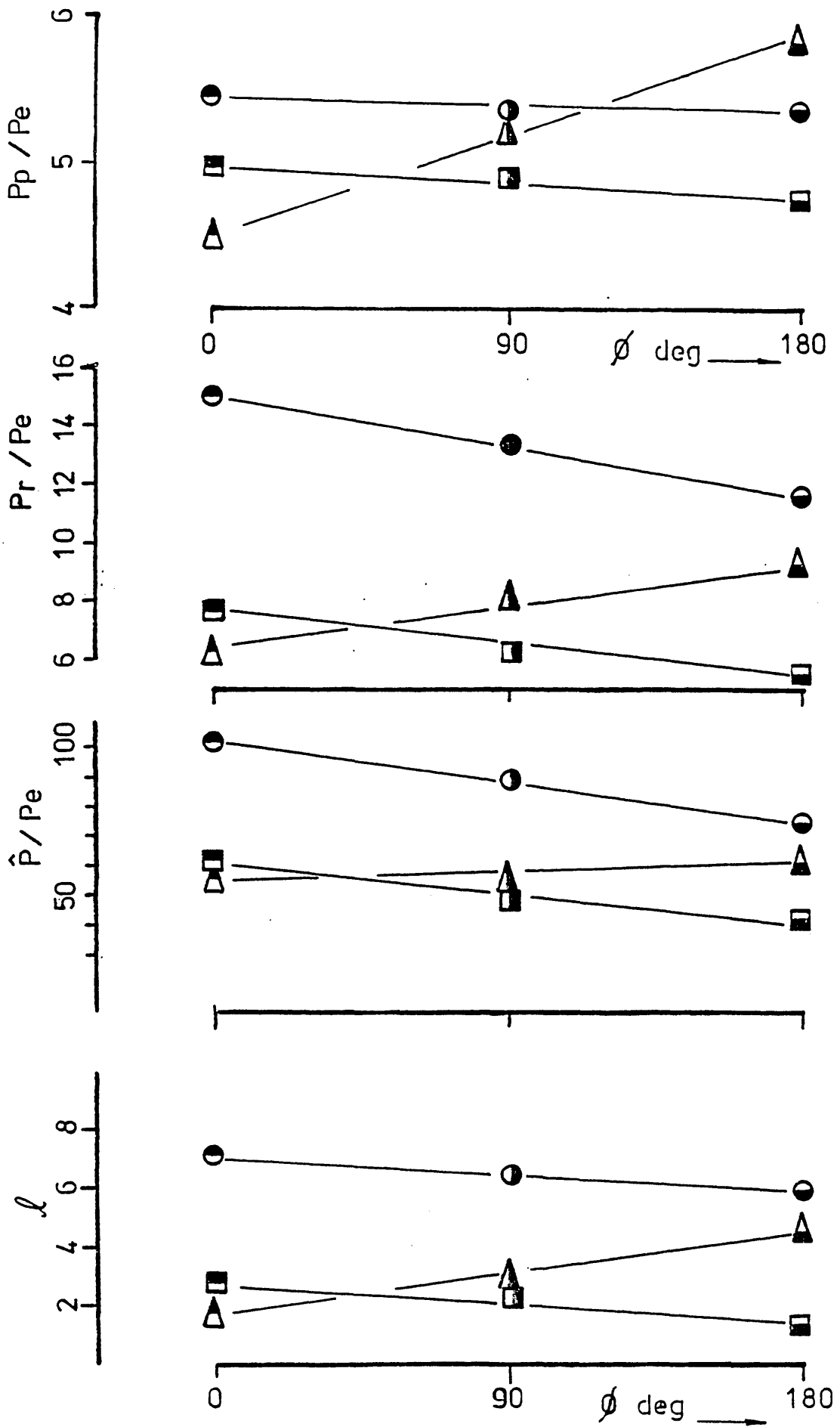
FIG 81 Selected cavity parameters

(a)

prediction for Me = 8.65 (3D case)
$$Cp_p = \left[\frac{P_{INV}}{Pe} \cdot e^k - 1\right] / (\tfrac{1}{2}.\gamma.Me^2)$$

geom(A)

prediction for α = 37.5 deg
(axisymmetric flow)

geometry

(A)   (B)   (C)

$$\frac{Pp}{P_{INV}} = EXP(.48 - 1.23 Ln(Me))$$
(2D case)
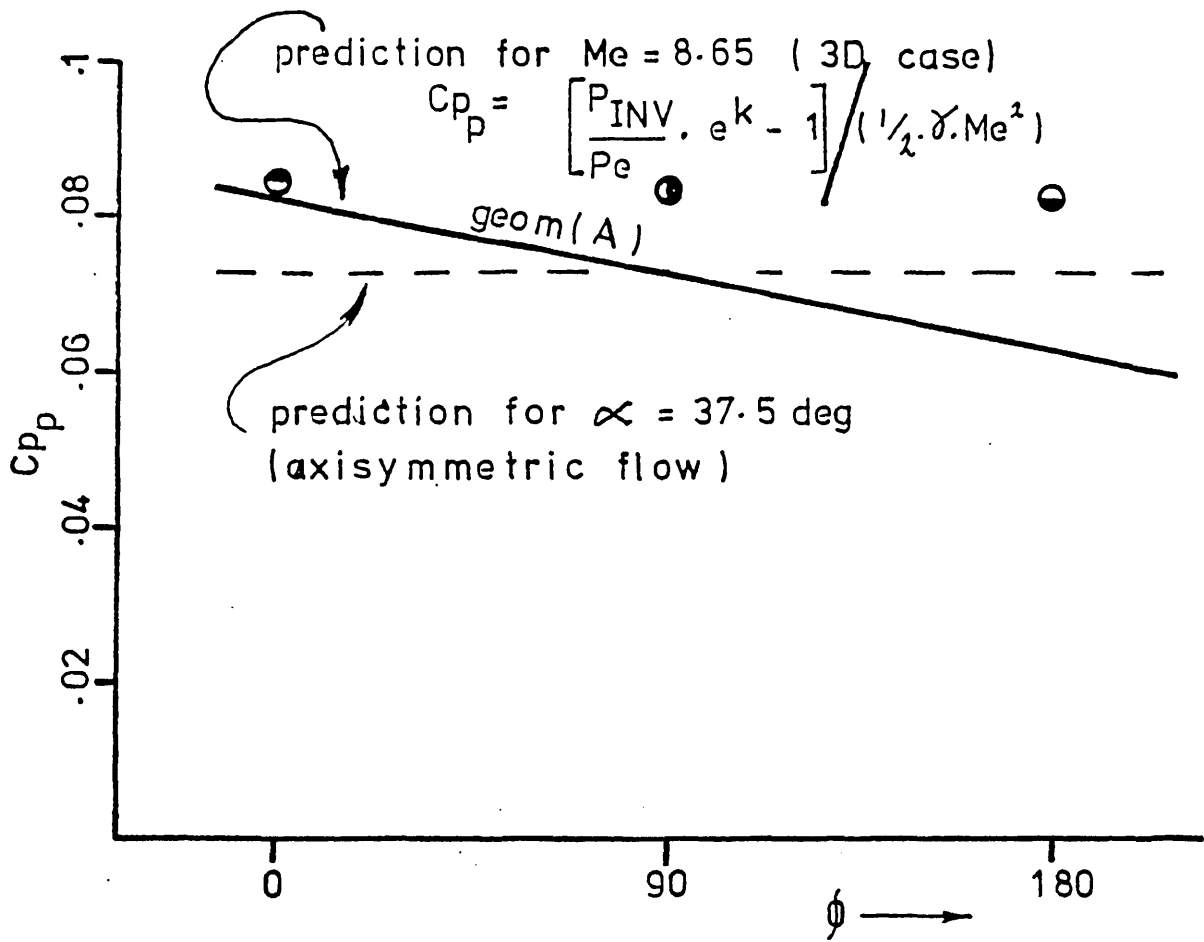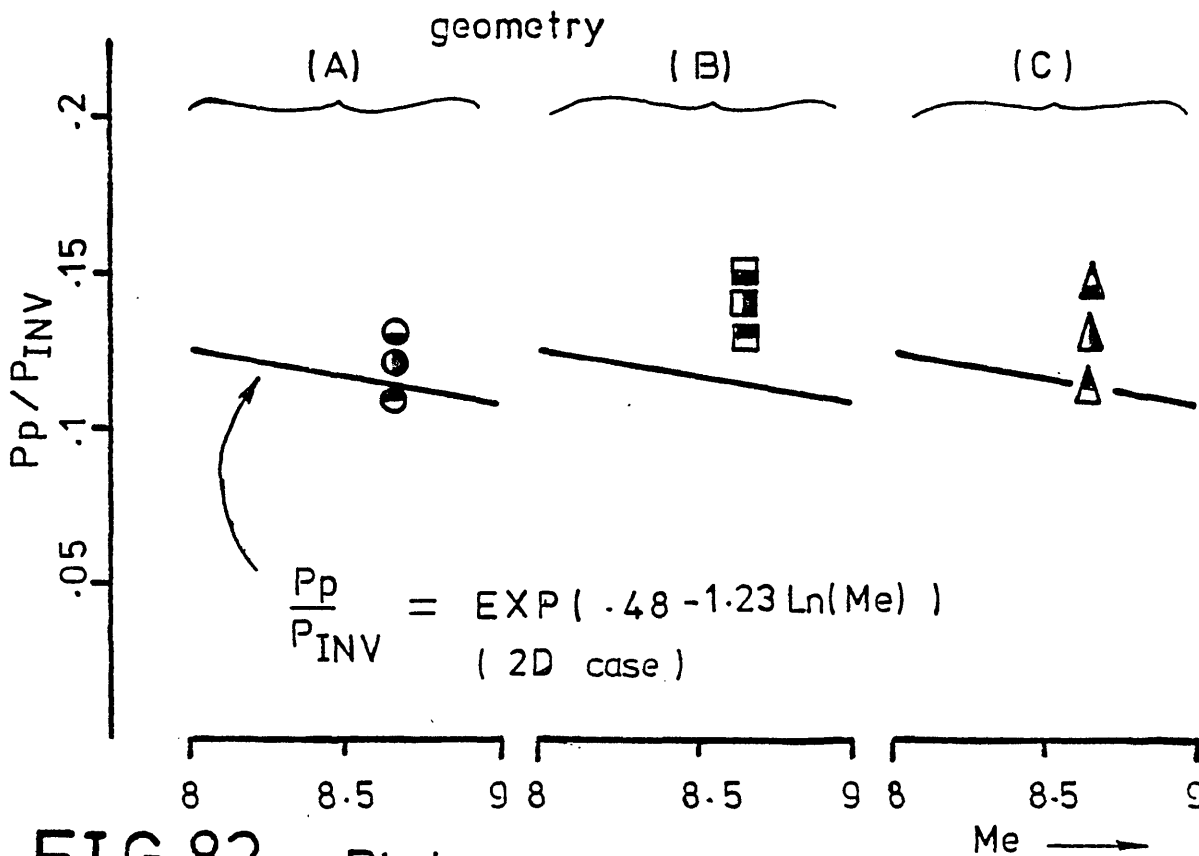
(b)

FIG 82   Plateau pressure
comparison with modified
Elfstrom correlation
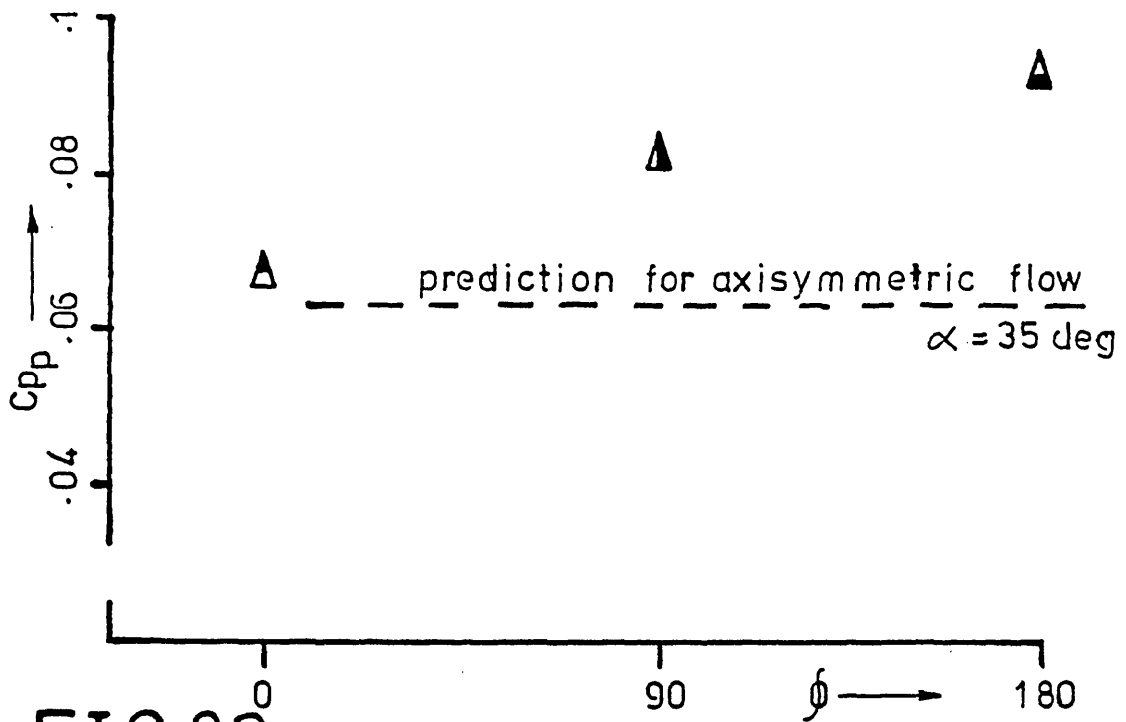
FIG 83 Plateau pressure comparison for geometry (C)
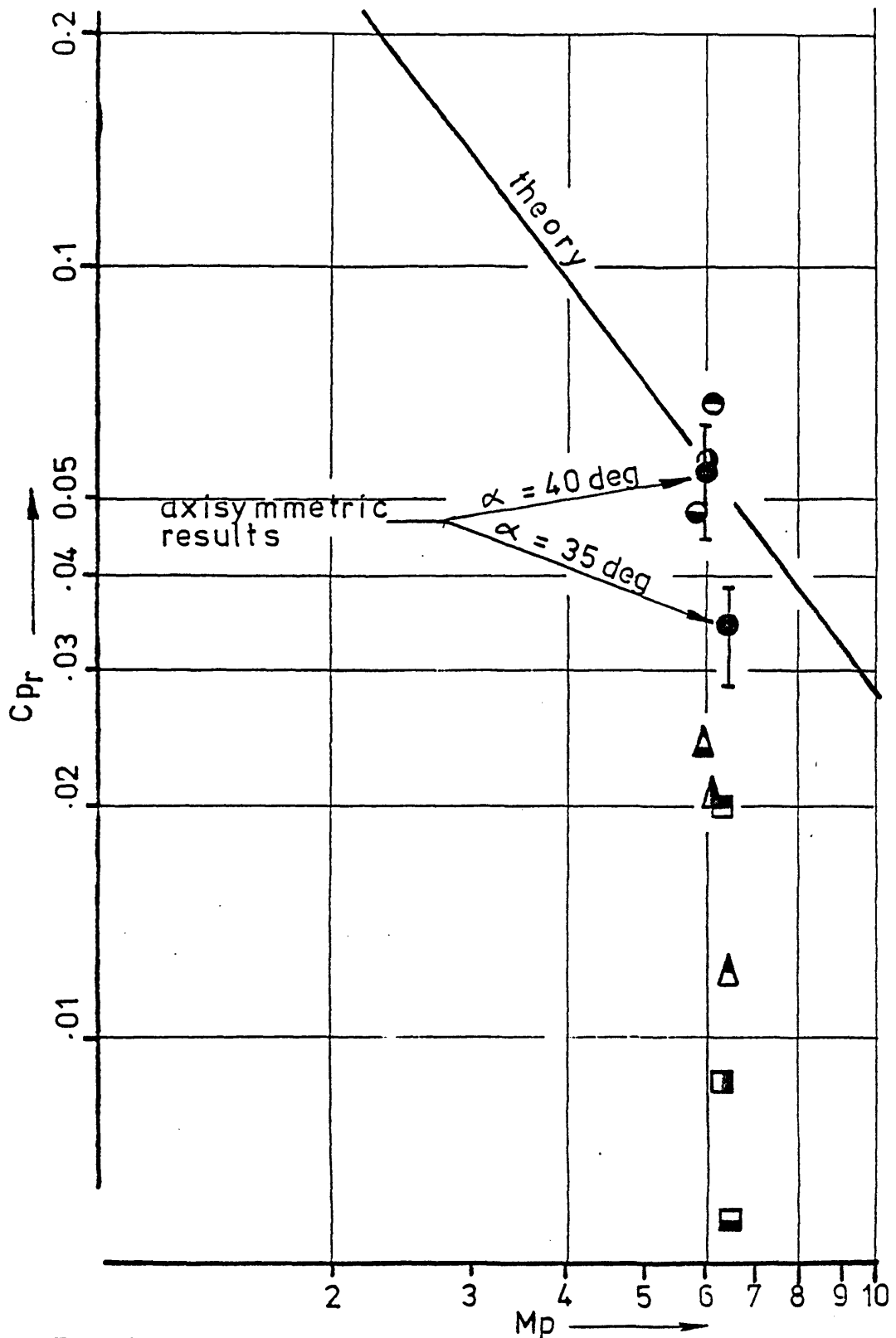
FIG 84   Reattachment pressure
comparison with Batham's
2D theory
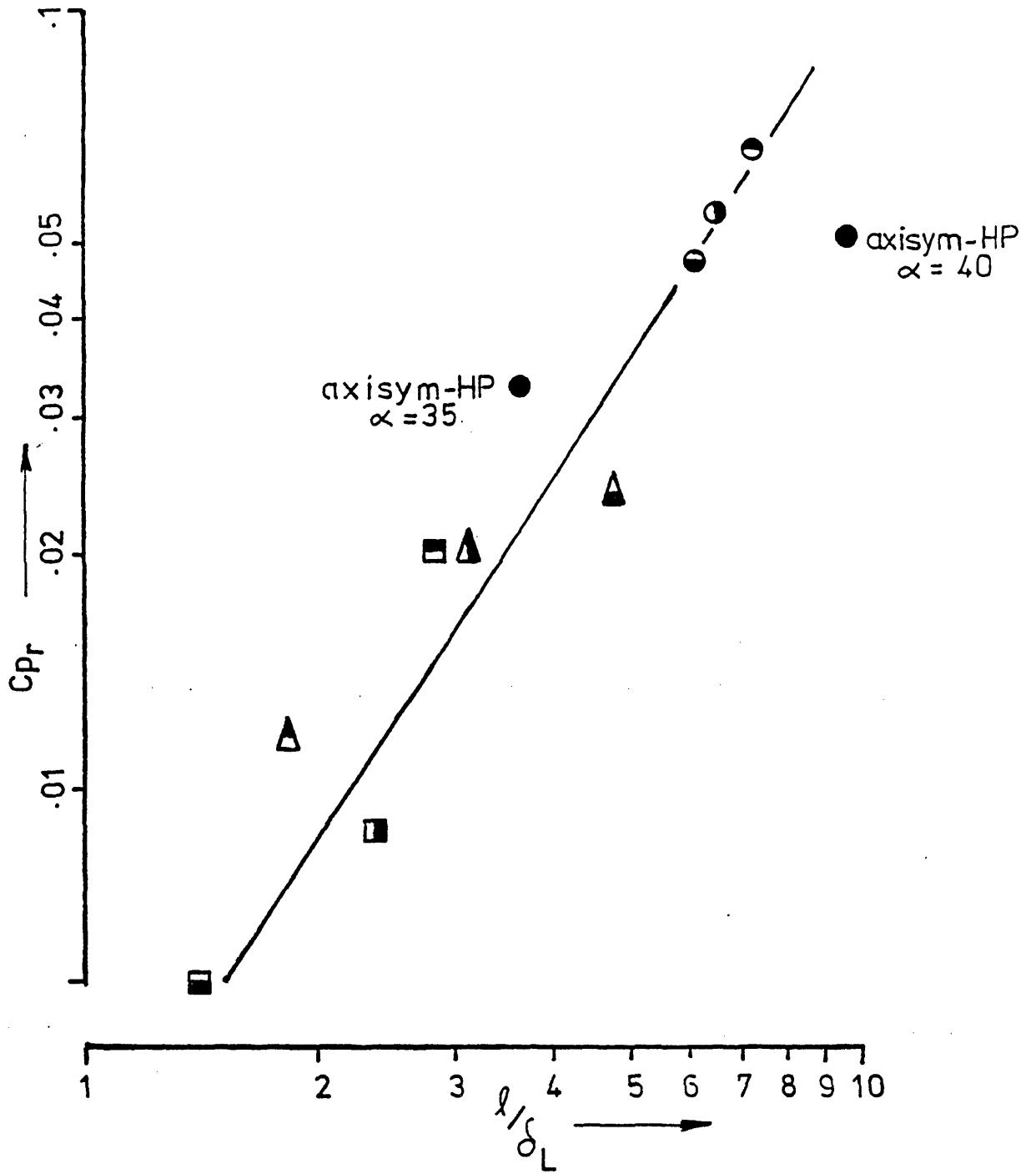
FIG 85 Implicit link between cavity
development length and
reattachment pressure
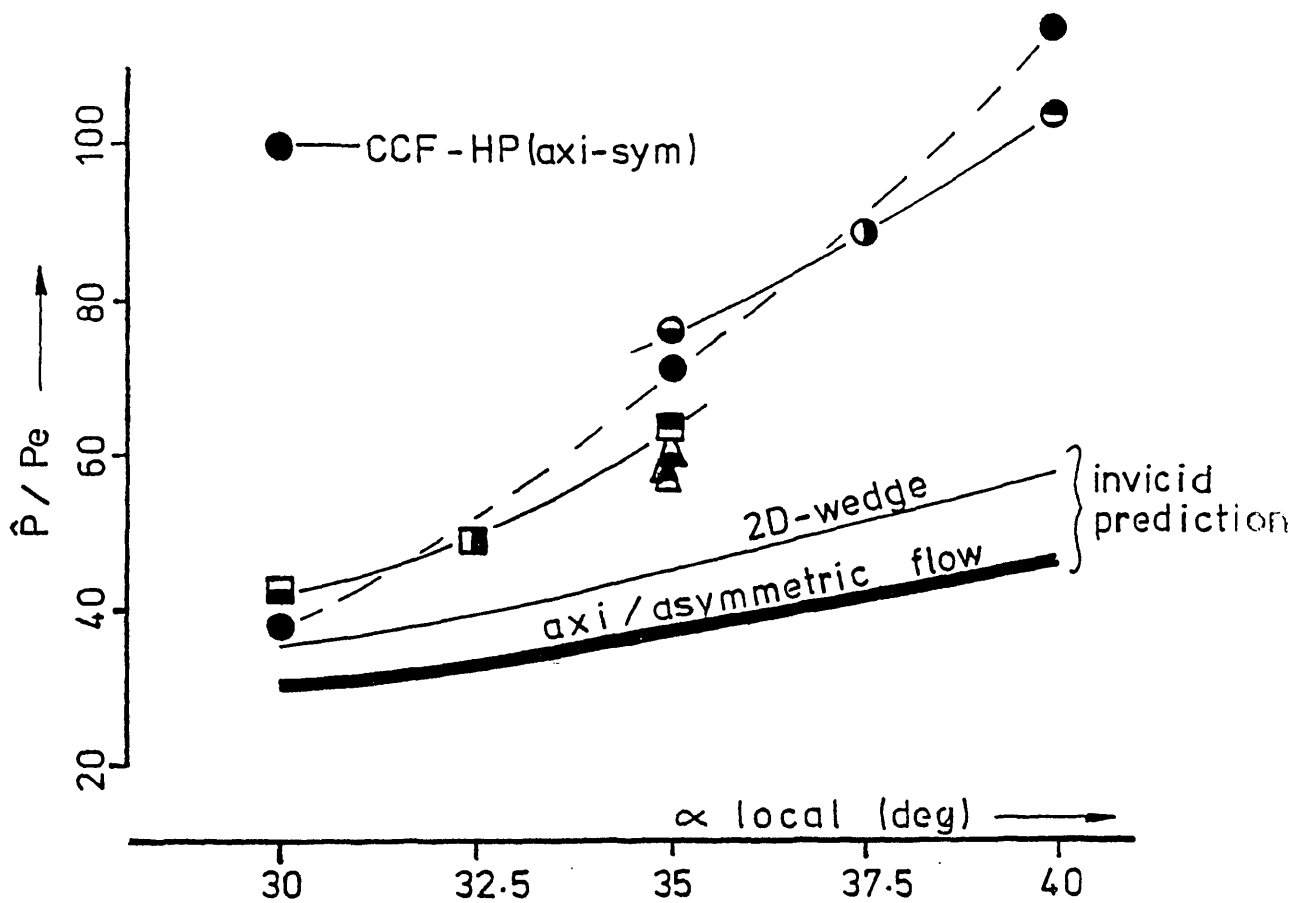
FIG 86 Reattachment pressure overshoot
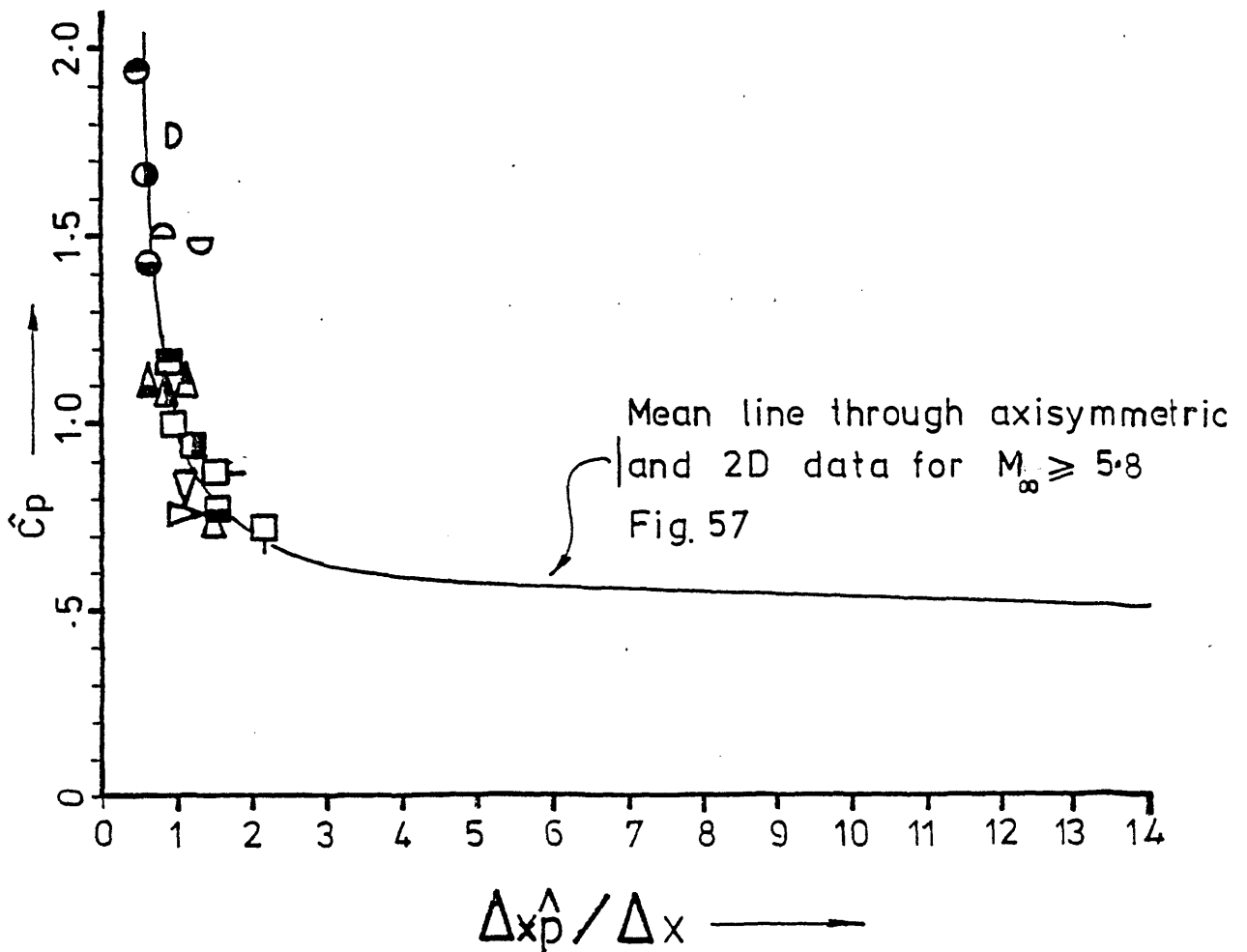
FIG 87 Overshoot pressure coefficient for asymmetric flows
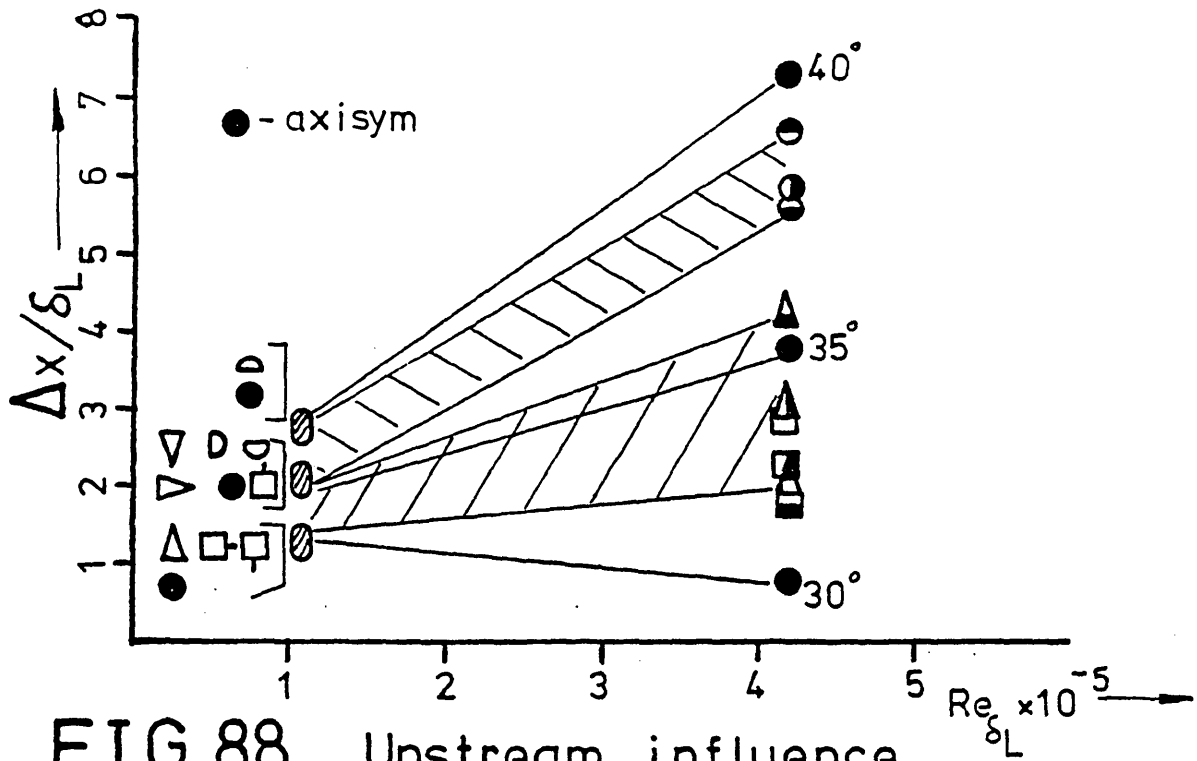
FIG 88 Upstream influence
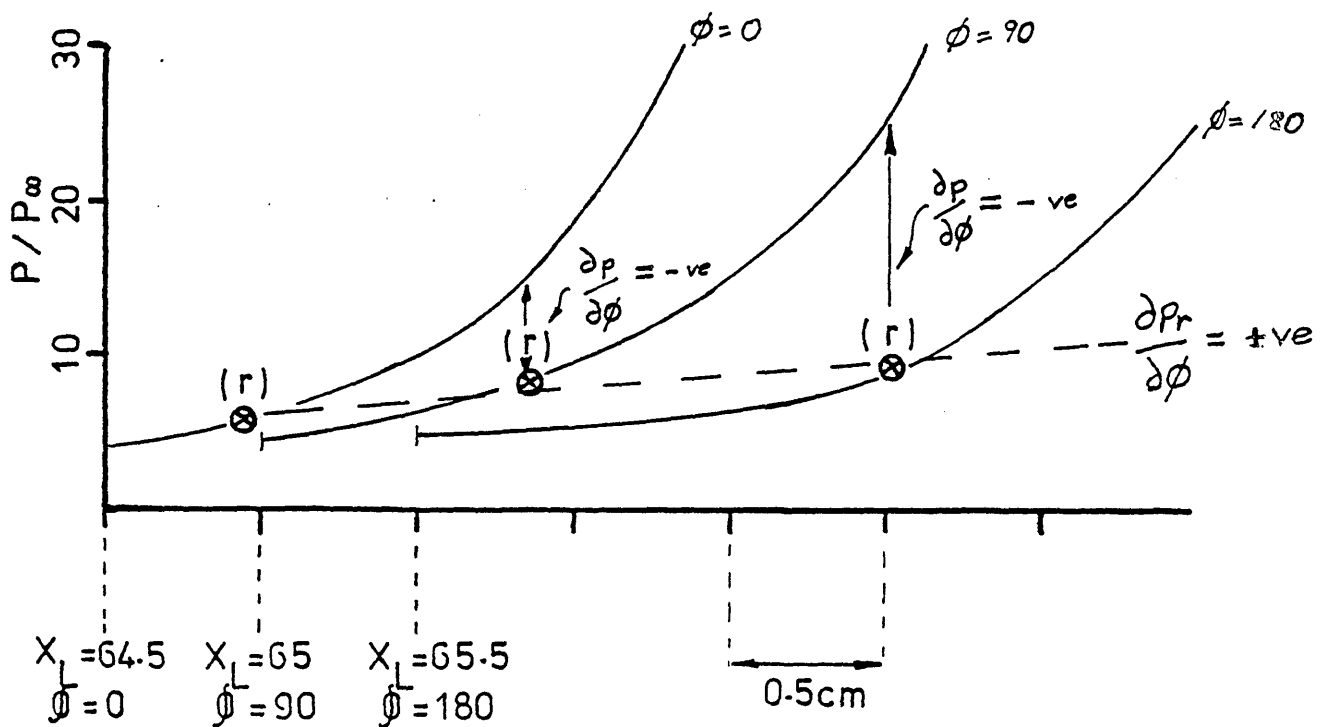
FIG 89 Absolute disposition of reattachment, geometry (C)
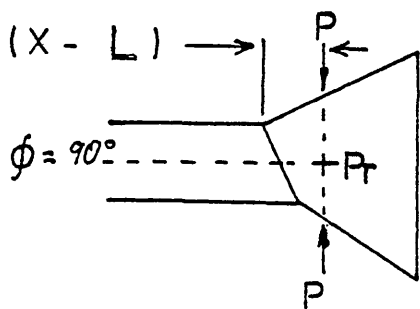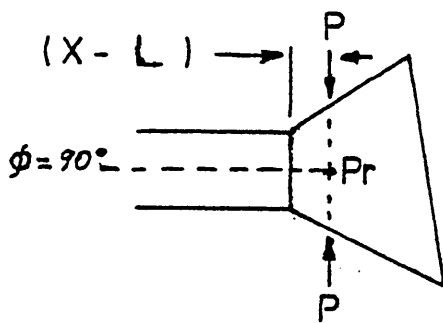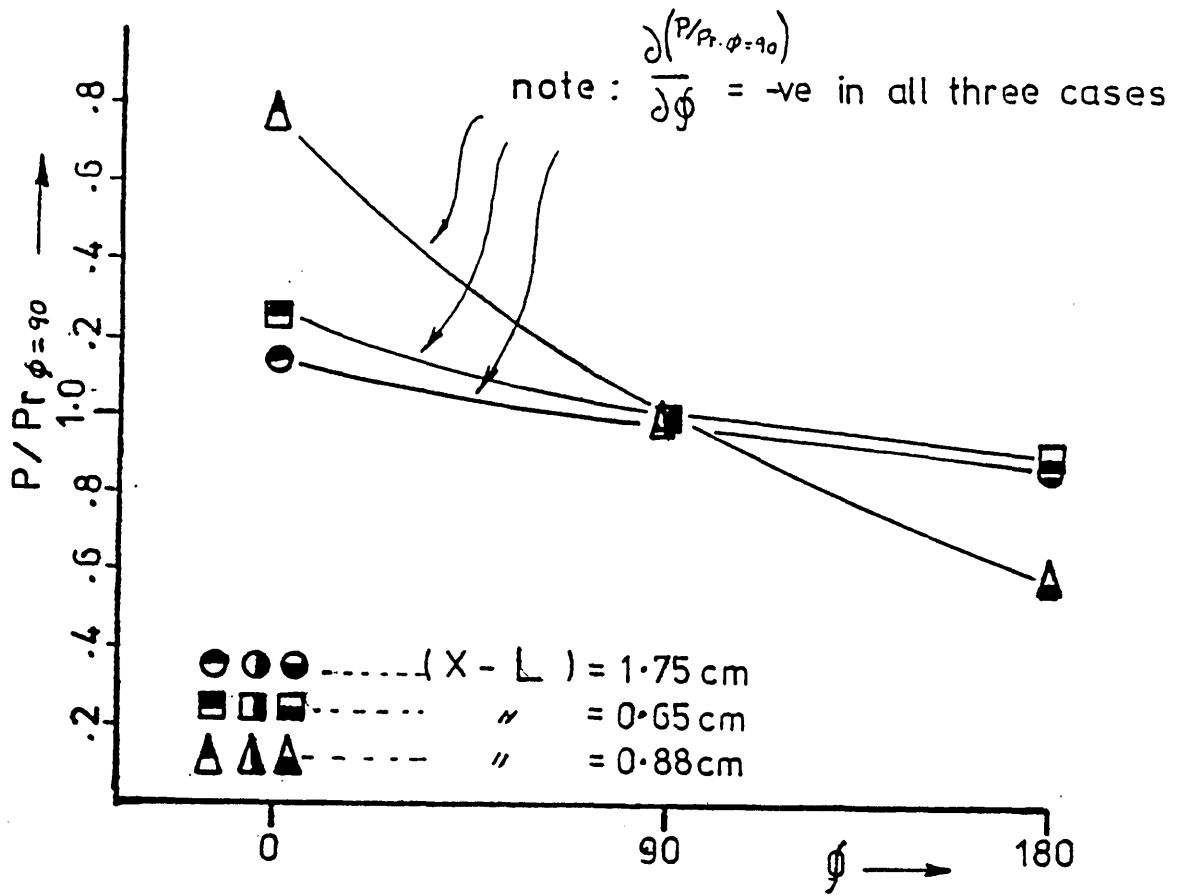
FIG 90 Transverse pressure gradient
in the vicinity of reattachment

$M_\infty = 9.31$
$Me = 8.65$
$Re_\infty/cm = 5.17 \times 10^5$

○ $\alpha = 35$ deg

+ $\alpha = 30$ deg

$\dot{q}$ (watts/cm^2)

(X - L)cm
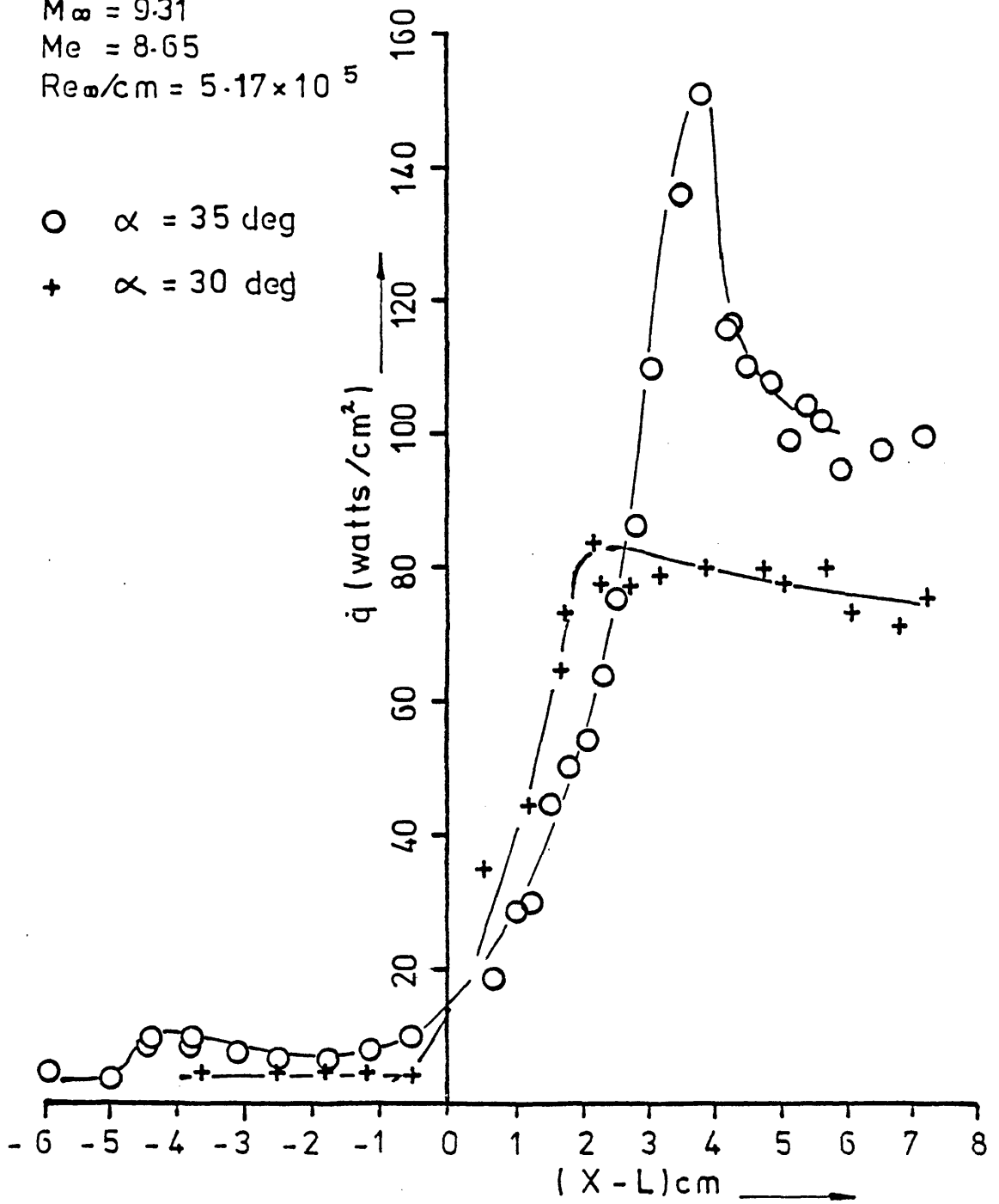
FIG 91 Heat transfer - axisymmetric flow (COLEMAN - 1973)

Moo = 9.31
Me = 8.65
Re∞/cm = 5.17 ×10⁵

Flare semi-angle = 37.5 deg

O ∝ local = 40 deg

+ ∝ local = 35 deg

geometry [A]

$\dot{q}$ (watts/cm²)

(X - L) cm
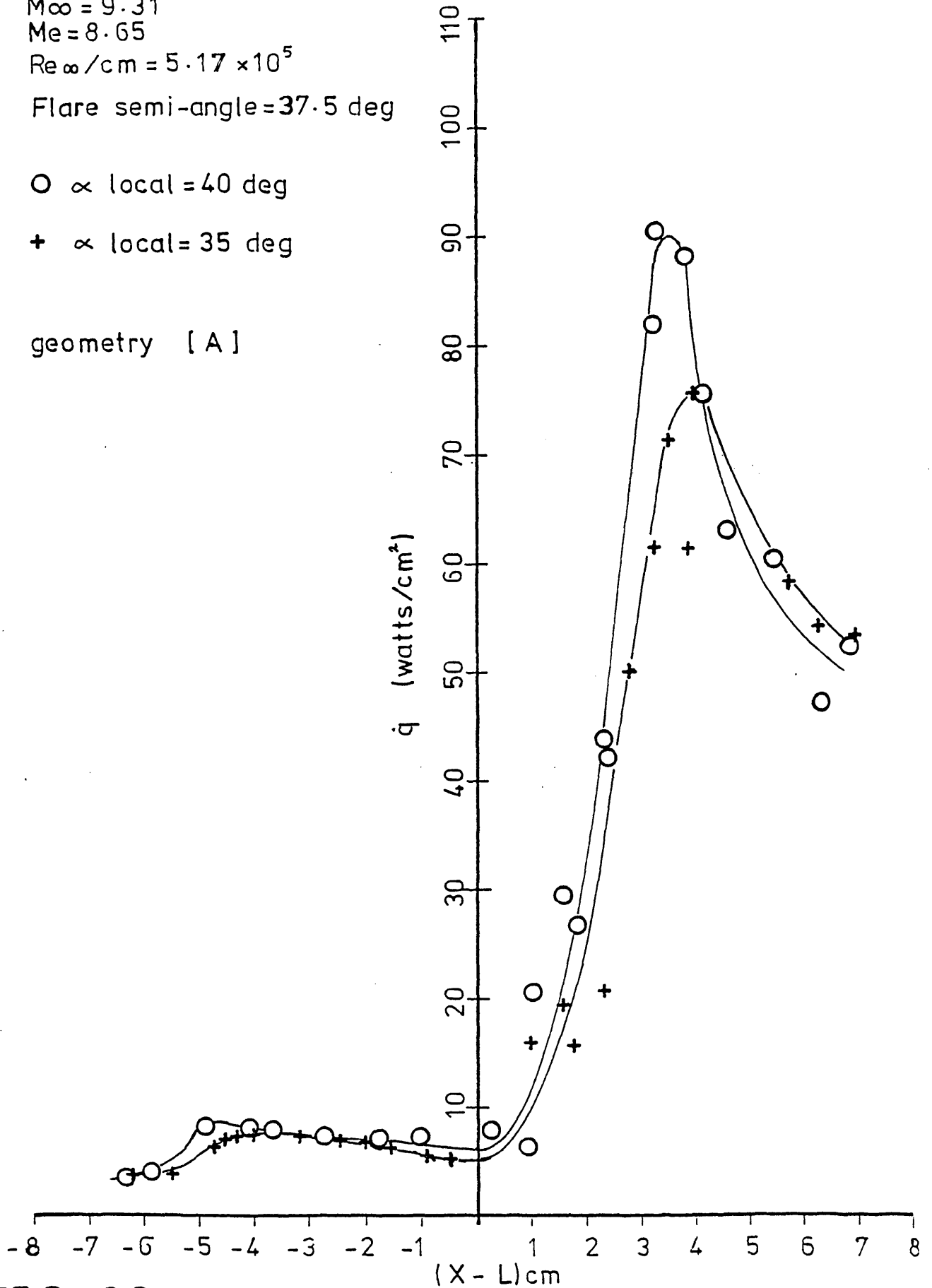
FIG 92 Heat transfer - asymmetric flares

$M_{\infty} = 9.31$

$Me = 8.65$

$Re_{\infty}/cm = 5.17 \times 10^5$

Flare semi-angle = 32.5 deg

O $\propto$ local = 35 deg

+ $\propto$ local = 30 deg

geometry [B]

$\dot{q}$ (watts/cm)

(X - L) cm
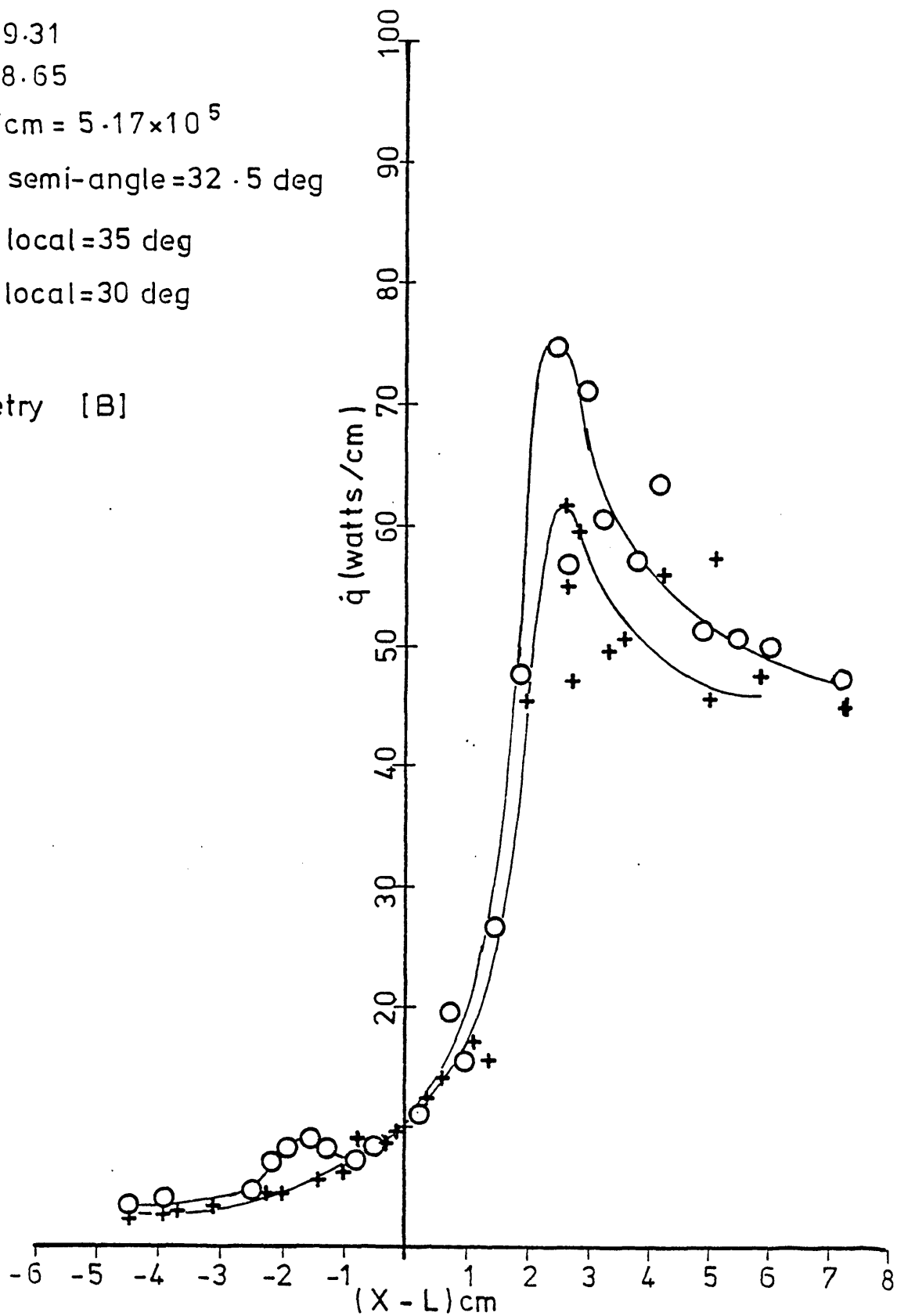
FIG 93 Heat transfer - asymmetric flares

$M_\infty = 9.31$
$M_e = 8.65$
$Re_\infty /cm = 5.17 \times 10^5$
Semi-angle = 35 deg

$+$ ϕ = 0 deg

$\circ$ ϕ = 180 deg

geometry [C]
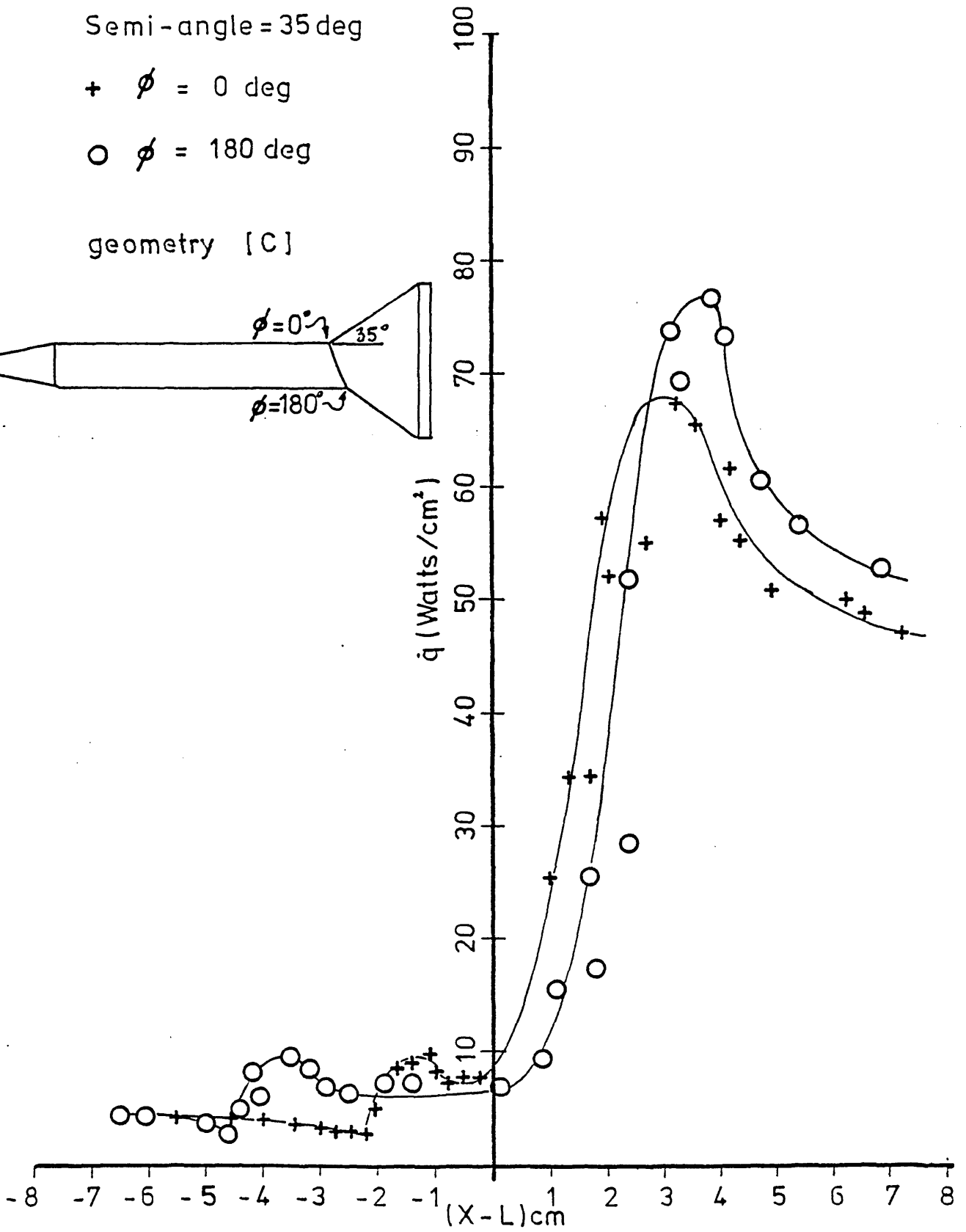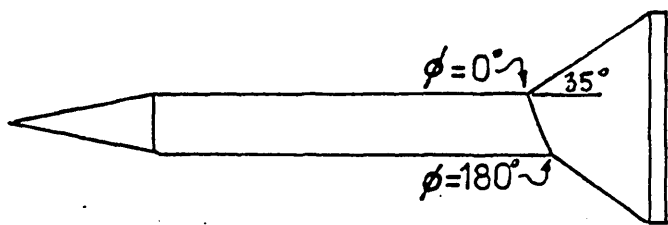
FIG 94   Heat transfer-asymmetric flares
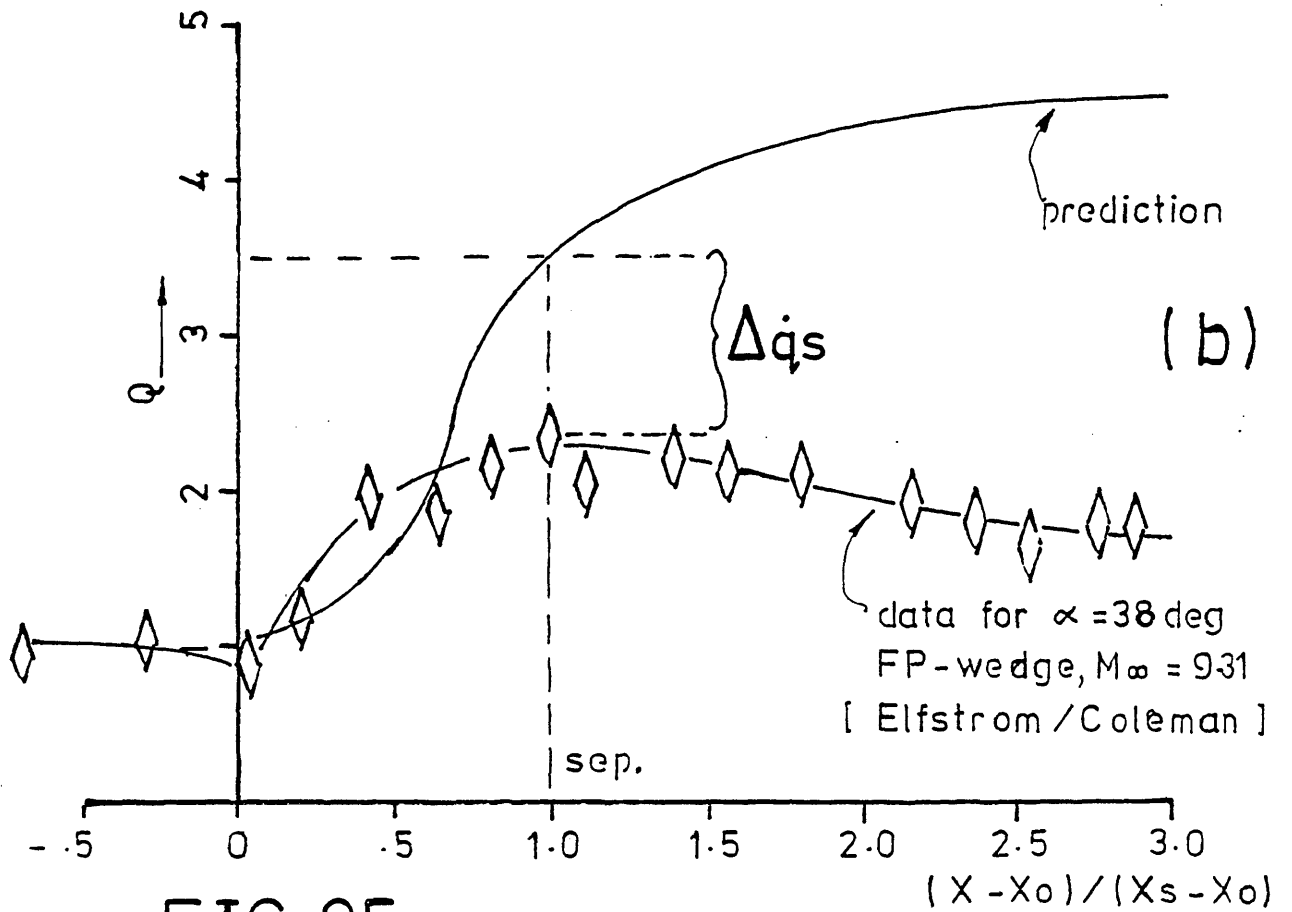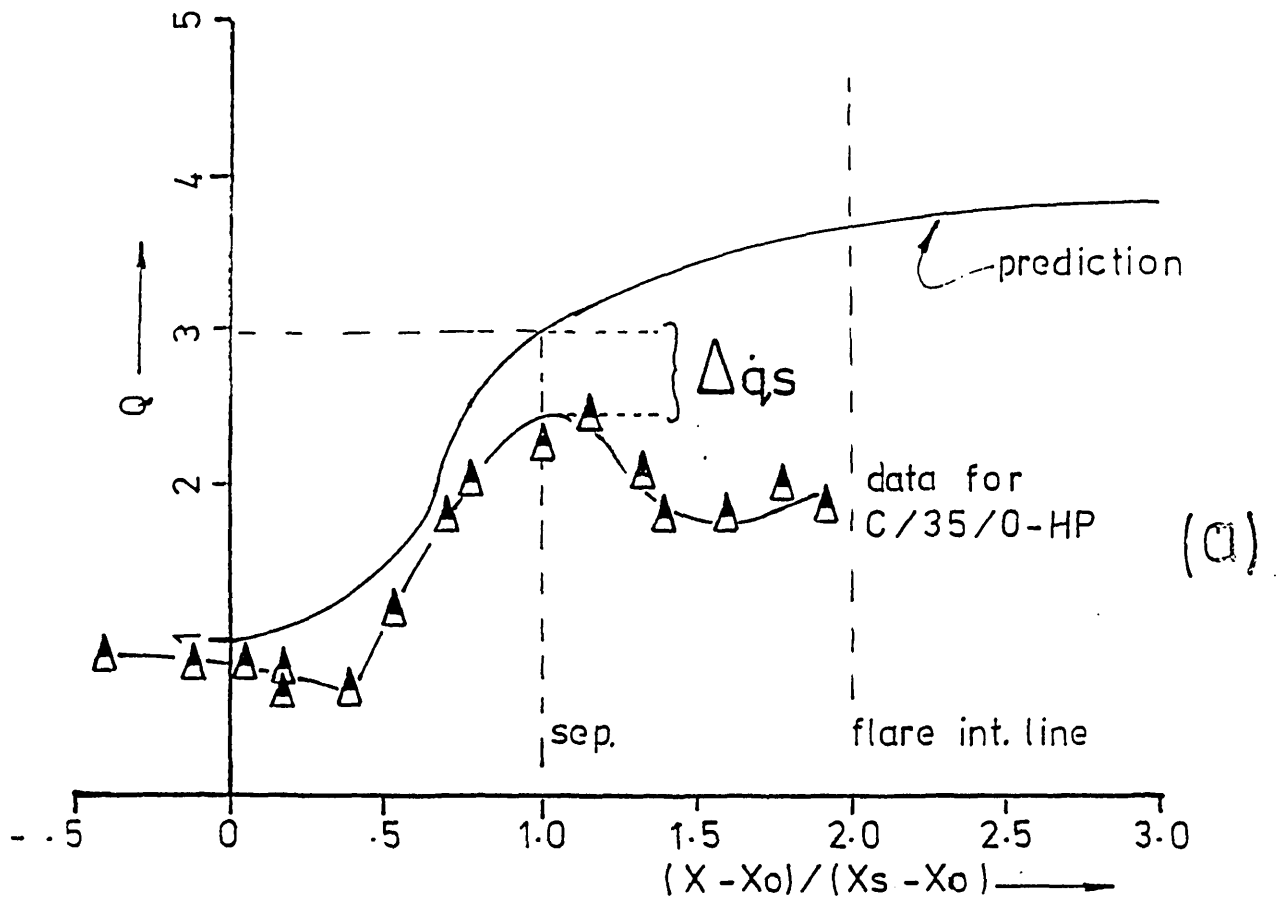
FIG 95 Plateau heating comparison with attached flow theory
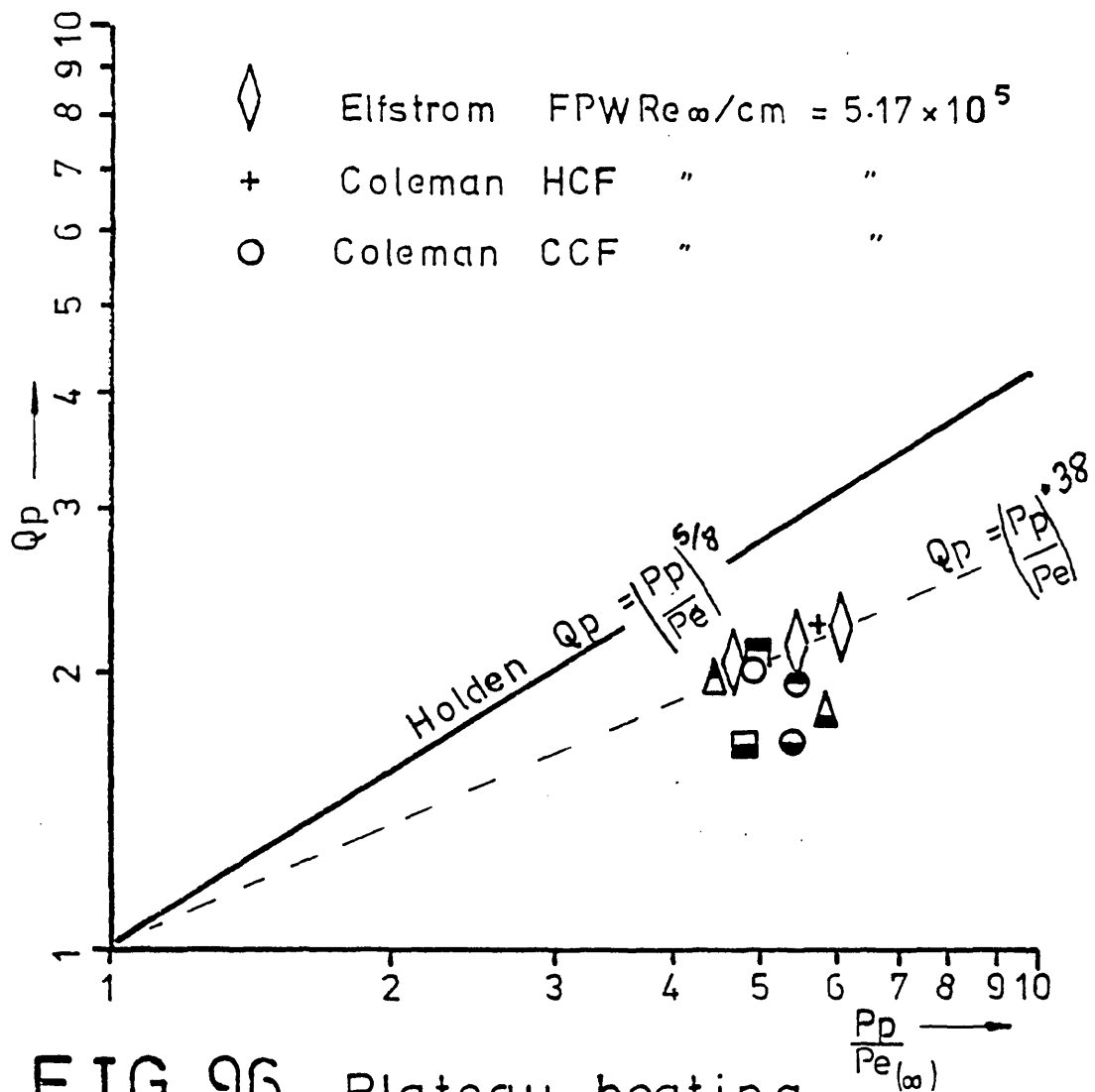
FIG 96 Plateau heating
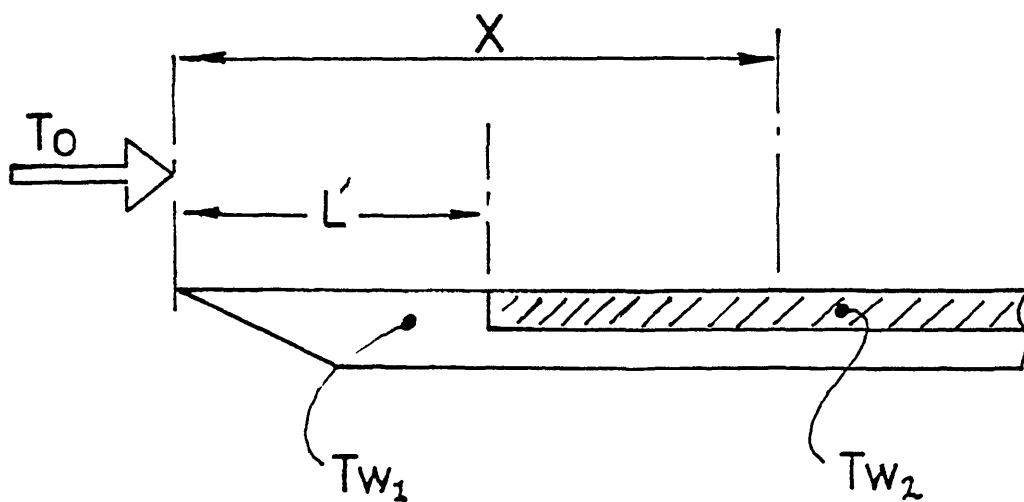
FIG 97 Co-ordinate system for wall temperature discontinuity
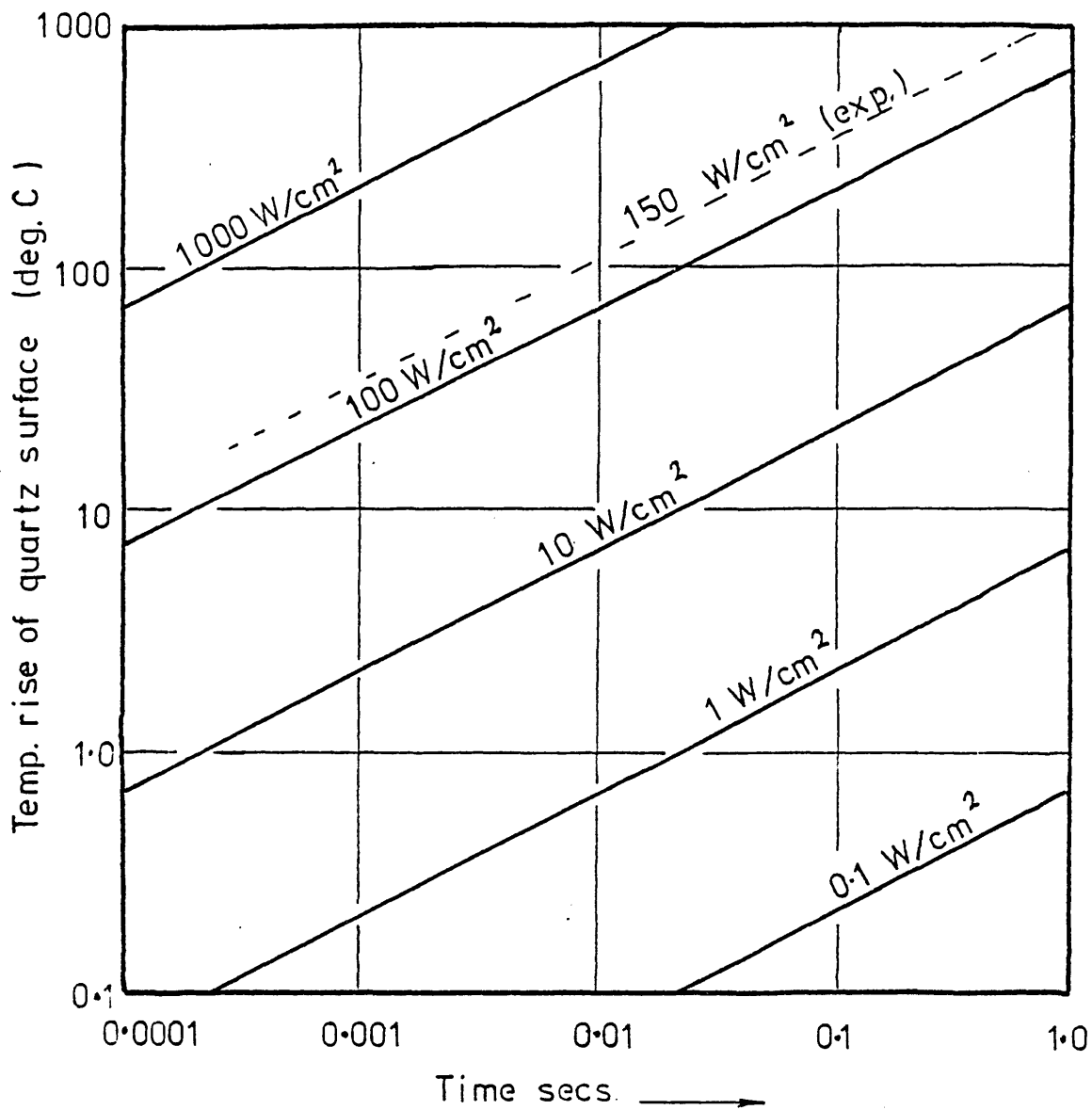
FIG 98

Surface Temperature response of Quartz Semi-infinite Insulators, as a Function of Time for Constant Heat Transfer Rate. (Schultz & Jones 1973).

FIG 99 Correlation of peak heating rates

Experimentally Implied Mean Free Shear Layer Deflection Angle (θs)

Consider the oblique shock solution for a single wedge given by equation (A1.1) below: -

$$\frac{P_2}{P_1} = 1 + \frac{2\gamma}{\gamma+1} \; (Me^2 Sin^2 B_1 - 1) \qquad \text{---(A1.1)}$$

Using this equation, Elstrom's correlating parameter Pp/Pinv can be expressed as follows: -

$$\frac{P_p}{Pinv} = \frac{(\gamma+1) + 2\gamma(Me^2 Sin^2 B_1 - 1)}{(\gamma+1) + 2\gamma(Me^2 Sin^2 B_2 - 1)} \qquad \text{---(A1.2)}$$

where B_1 and B_2 are the separation and attached flow shock angles corresponding to a free stream Mach number (Me). From previous results equation (A1.2) is also known to conform to the function $P_p/Pinv$ = EXP(K). Substituting the empirical function into equation (A1.2) yields equation (A1.3) after some algebra.

$$B_1 = Sin^{-1} \left[\frac{2\gamma Me^2 Sin^2 B_2 (EXP(K)) - (1-EXP(K))(1-\gamma)}{2\gamma Me^2} \right]^{\frac{1}{2}} \quad \text{---(A1.3)}$$

For a given Mach number (Me) and corner angle (α), B_2 can be computed by iteration of the shock relations or direct reference to the tables. B_1 can then be computed from Equation (A1.3) and the notional separation angle (θs) follows from the relation

$$\theta_s = Tan^{-1} \left[\frac{2 \; Cot \; B_1 (Me^2 Sin^2 B_1 - 1)}{Me^2 (\gamma + Cos 2B_1) + 2} \right] \quad \text{---(A1.4)}$$

Prediction of Heat Transfer Rate for Attached Turbulent Flow at Wedge Compression Corner

Reproduced and Modified from Coleman and Stollery (1972)

The energy thickness is defined as:

$$\Gamma = \int_0^\delta \frac{\rho U}{\rho_\ell U_\ell} \cdot \left[\frac{H_\ell - H(y)}{H_\ell - H_w} \right] dy \qquad \text{---(A2.1)}$$

Where the subscript (ℓ) denotes local boundary layer edge conditions. The intergral form of this equation may be written

$$\frac{d}{dx} \left[\rho_\ell U_\ell (H_\ell - H_w) \, \Gamma \right] = \dot{q} \qquad \text{---(A2.2)}$$

To complete the solution, Ambrok (1957) suggested a relation for $\dot{q}$ (Γ) analageous to the skin friction equation in terms of Re_θ, namely

$$St_\ell \sim \left(\frac{\rho_\ell U_\ell}{\mu_\ell} \Gamma \right)^{-\frac{1}{4}} \qquad \text{---(A2.3)}$$

Back and Cuffel found this to be a reasonable description of measurements subsequently made in both accelerating and decelerating flows. Equation (A2.3) may be expressed exactly by the use of the Reynolds analogy factor $\frac{2St}{Cf}$, i.e

$$\frac{\dot{q}}{\rho_\ell U_\ell (H_r - H_w)} = St_\ell = \frac{Cf}{2} \left(\frac{2 St}{Cf} \right) \qquad \text{---(A2.4)}$$

together with Eckert's (1955) reference temperature law

$$\frac{Cf}{2} = 0.013 \, Re_\theta^{-\frac{1}{4}} \left(\frac{\mu^*}{\mu_\ell} \right)^{\frac{1}{4}} \left(\frac{\rho^*}{\rho_\ell} \right) \qquad \text{---(A2.5)}$$

$$\frac{T^*}{T\ell} = 0.5 \left(\frac{Tw}{T\ell} + 1 \right) + 0.44.r. \, M\ell$$

for flat plate flow, provided that the Crocco relation holds

$$\theta = \frac{(H\ell - Hw)(\Gamma)}{\left(\frac{2 \, St}{Cf}\right)(Hr - Hw)} \qquad \qquad ---(A2.6)$$

From equations A2.3, A2.5 and A2.6 together with the assumption of the power law viscosity relation $\mu \sim T^{.76}$

$$\frac{\dot{q}}{\left(\frac{2St}{Cf}\right)\rho\ell U\ell \, (Hr-Hw)} = 0.013 \left[\frac{T^*}{T\ell}\right]^{-0.81} \left[\frac{2St}{Cf} \cdot \frac{(Hr - Hw)}{H\ell - Hw}\right]^{\frac{1}{4}} Re\Gamma^{-\frac{1}{4}}$$

$$---(A2.7)$$

This may be rewritten in the form

$$\dot{q} = \frac{f(x)}{\left[\rho\ell U\ell \, (H\ell - Hw)\Gamma\right]^{\frac{1}{4}}} \qquad \qquad ---(A2.8)$$

substituted in equation A2.2 and integrated to produce an expression for Γ , which may then be introduced into equation (A2.8) The result is

$$\dot{q} = 0.0296 \left(\frac{2St}{Cf}\right) \frac{\rho\ell U\ell \mu\ell^{\frac{1}{4}} (Hr - Hw)^{\frac{5}{4}} \left[\frac{T^*}{T\ell}\right]^{-.81}}{\left[\int_{xv}^{x} \rho\ell U\ell \mu\ell^{\frac{1}{4}} (Hr - Hw)^{\frac{5}{4}} \left[\frac{T^*}{T\ell}\right]^{-.81} dx\right]^{\frac{1}{5}}}$$

$$---(A2.9)$$

For an isothermal wall (Hr-Hw) is constant and may be

cancelled. The variation of $\mu_\ell^{1/20}$ and $(T^*/T_\ell)^{-0.16}$ in the

denominator is usually insignificant so that equation (A2.9) may

be simplified to

$$\frac{\dot{q}}{\rho_\ell U_\ell(Hr - Hw)} = St_\ell = 0.0296 \left[\frac{2St}{Cf}\right] \left[\frac{T^*}{T_\ell}\right]^{-0.65} Rex^{-1/5}$$

$$---(A2.10)$$

where $Rex = \dfrac{\rho_\ell U_\ell x}{\mu_\ell}$ and $\rho_\ell U_\ell x = \displaystyle\int_{xv}^{x}\rho_\ell U_\ell \, dx$

xv being the virtual origine of the turbulent boundary layer.

In order to compute the distribution of $(\dot{q})$ local boundary layer

edge conditions must be specified. In Coleman's study this was

accomplished using Elfstrom's (1973) prediction for the attached

flow distribution over a compression wedge in conjunction with

the isentropic relations for the post corner shock free stream.

The method was found to work quite well and the results can be

seen in Figure 57 of Coleman (1973). In the present discussion

it is more convenient to express equation (A2.10) in terms of the

starting conditions as follows:

$$\frac{\dot{q}}{\dot{q}_L} = \frac{\rho_\ell U_\ell}{\rho e U e} \cdot \frac{\left[\frac{2St}{Cf}\right]\left[\frac{T^*}{T_\ell}\right]^{-.65} Rex^{-1/5}}{\left[\frac{2St}{Cfe}\right]\left[\frac{T^*}{Te}\right]^{-.65} Re_L^{-1/5}} \qquad ---(A2.11)$$

Since Toe = To$_\ell$ for a homenergic external flow and using r = .9

we get

$$\frac{T^*}{T} = 0.5\left[\left[1 + \frac{Tw}{Toe}\right] + \frac{M^2}{5} \cdot \left[0.4 + \frac{Tw}{Toe}\right]\right]$$

and equation (A2.11) becomes A2.4

$$Q = \frac{\dot{q}}{\dot{q}_L} = \frac{\rho \ell U \ell}{\rho e U e} \left[\frac{\left[1 + \frac{Tw}{Toe}\right] + \frac{Me^2}{5}\left[0.4 + \frac{Tw}{Toe}\right]}{\left[1 + \frac{Tw}{Toe}\right] + \frac{Me^2}{5}\left[0.4 + \frac{Tw}{Toe}\right]} \right]^{.65} \left[\frac{\rho e U e L}{\int_{xv}^{x} \rho \ell U \ell dx} \left(\frac{\mu \ell}{\mu \ell}\right) \right]^{\frac{1}{5}}$$

$$\text{---(A2.12)}$$

Coleman pointed out that the last group in this expression is approximately unity since the wedge chord was small in comparison with the undisturbed starting run. His results for equation (A2.12) using the shock relations to give local conditions downstream of the intersection line are shown in Figure (A2.1).

It can be seen that the use of isentropic relations to equate input and recovery conditions also gives fairly good agreement provided the pressure recovery is small. This is indicated by the broken line in the figure. Since the maximum pressure ratio immediately following separation is about 5 the present analysis proceeds on a similar basis to that of Coleman's but using isentropic relations instead of the oblique shock solutions. Hence returning to equation (A2.12), this expression can be simplified by noting that the separation interaction length is small in comparison with the undisturbed run of boundary layer. Hence, as before, the last group will be approximately unity. For the current experiments Tw/Toe = 0.275 and, with the use of the isentropic relations, equation (A2.12) reduces to

$$Q = \left(\frac{P}{Pe}\right)^{.9} \left[\frac{1 - \left(\frac{P}{Pe}\right)^{\frac{\gamma-1}{\gamma}} + 0.2 \, Me^2}{0.2 \, Me^2} \right]^{\frac{1}{2}} \left[\frac{1.276 + 0.135 \, Me^2}{0.6\left(\frac{P}{Pe}\right)^{\frac{\gamma-1}{\gamma}} + 0.675 + 0.135 \, Me^2} \right]^{0.65}$$

$$\text{---(A2.13)}$$

Consequently, together with the approximate form of the free interaction pressure distribution derived from the theory of Erdos and Pallone (1962).

$$\frac{P}{Pe} = 1 + \frac{1}{2}\gamma F(X)Me^{3/2}(2Cfe)^{1/2} \qquad ---(A2.14)$$

the heat transfer distribution for an equivalent, low incidence, attached flow may be computed in terms of the starting conditions. This is shown for the cone-cylinder-flare interactions (assumed two-dimensional) in Figure 95 (a) and for the flate plate conditions studied by Coleman in Figure 95 (b).

FIG A2.1

Correlation of pressure and heat transfer for attached turbulent wedge flows.

APPENDIX 3

PROCESSED DATA FOR CONE - CYLINDER - FLARE GEOMETRIES (PRESSURES AND SCALE)

Ps/P∞ =3.12 (HP), Ps/P∞ =3.25 (LP)

Geometry and Tunnel Condition	θ Deg	Symbol	Me	Pe/P∞	δL cm	Δx cm	P̄p/Pe	β deg.	Θs deg.	Mp	α deg	P̂/Pe	Xo cm	Xs cm	L cm	(Xs-Xo) cm	(L-Xs) cm	xr cm	(xr-L) cm	Θr deg.	ℓ cm	ℓ/δL	Cp̂p x10²	Pr/Pe	Cp̂r x10	Ĉf cm	Λ·p̂ cm	Ĉf x10
Re∞/cm = 5.17 x 10⁵ M∞= 9.31 (A)	0	●	8.65	0.9	0.97	6.0	5.44	14.68	9.59	6.18	40	102.86	58.85	59.48	65	0.63	5.52	66.82	1.82	30.41	7.01	7.23	8.48	15.0	6.57	1.95	1.6	5.41
	90	◐	"	"	"	5.70	5.36	14.57	9.48	6.2	37.5	88.29	58.8	60.0	"	1.20	5.0	66.75	1.75	28.02	6.48	6.68	8.32	13.33	5.52	1.67	4.0	"
	180	◑	"	"	"	5.5	5.32	15.52	10.41	5.98	35	75.48	59.0	60.7	"	1.7	4.3	66.87	1.87	24.59	5.93	6.11	8.25	11.67	4.77	1.42	4.2	"
(B)	0	◼	"	"	"	2.8	4.98	14.05	8.96	6.33	35	62.52	61.75	62.95	"	1.2	2.05	65.73	0.73	26.14	2.68	2.76	7.6	7.78	2.0	1.18	2.7	"
	90	◧	"	"	"	2.2	4.9	13.94	8.85	6.35	32.5	49.68	62.10	63.30	"	1.2	1.70	65.65	0.65	23.65	2.28	2.35	7.45	6.11	0.88	0.93	2.8	"
	180	◨	"	"	"	1.7	4.73	13.7	8.61	6.42	30	42.02	62.5	64.0	"	1.5	1.00	65.41	0.41	21.39	1.37	1.41	7.12	5.5	0.56	0.78	2.7	"
(C)	0	▲	"	"	"	2.1	4.52	13.4	8.31	6.5	35	59.48	62.25	63.1	64.5	0.85	1.40	64.95	0.45	26.69	1.79	1.85	6.72	6.11	1.19	1.12	2.6	"
	90	◭	"	"	"	2.9	5.38	14.6	9.51	6.2	35	58.92	62.0	62.7	65	0.70	2.30	65.88	0.88	25.49	3.07	3.16	8.36	8.33	2.04	1.11	3.1	"
	180	◮	"	"	"	4.0	5.84	15.21	10.11	6.05	35	63.74	61.25	62.05	65.5	0.80	3.45	66.94	1.44	24.89	4.7	4.85	9.24	9.44	2.41	1.19	3.4	"
Re∞/cm = 1.29 x 10⁵ M∞= 8.96 (A)	0	◌	8.4	"	1.0	2.75	4.18	13.28	8.01	6.42	40	75.13	62.0	63.3	65.0	1.30	1.7		0.45	31.99	2.06	2.06	6.44			1.50	2.62	6.6
	90	◍	"	"	"	2.35	3.58	12.32	7.00	6.67	37.5	89.83	62.3	63.8	"	1.50	1.2		0.29	30.5	1.44	1.44	5.22			1.80	2.52	"
	180	◎	"	"	"	2.0	2.95	11.22	5.80	6.97	35	74.46	62.7	64.15	"	1.45	0.85		0.18	29.2	1.00	1.00	3.95			1.40	2.67	"
(B)	0	☐	"	"	"	1.85	2.59	10.54	5.02	7.16	35	52.37	63.0	64.45	"	1.45	0.55		0.10	29.93	0.63	0.63	3.22			1.04	1.88	"
	90	☐	"	"	"	1.45	2.37	10.11	4.51	7.28	32.5	44.52	63.25	64.65	"	1.40	0.35		0.06	27.99	0.4	0.4	2.77			0.88	2.25	"
	180	☐	"	"	"	1.25	2.12	9.59	3.88	7.44	30	37.01				"										0.73	2.69	"
(C)	0	△	"	"	"	1.40	2.55	10.47	4.94	7.18	35	39.42	62.85	63.9	64.5	1.05	0.60		0.10	30.06	0.69	0.69	3.14			0.78	2.20	"
	90	▷	"	"	"	1.70	2.51	10.39	4.84	7.2	35	38.19	63.0	64.3	65	1.30	0.70		0.12	30.16	0.80	0.80	3.06			0.75	2.04	"
	180	▽	"	"	"	1.75	2.72	10.79	5.31	7.09	35	42.32	63.0	64.65	65.5	1.65	0.85		0.16	29.69	0.98	0.98	3.48			0.84	1.93	"
Axl - SYM CCF He = 9.31 Re∞/cm = 5.17 x 10⁵		Various	8.65	"	0.97	7.3	5.99	15.4	10.29	6.01	40	116.00			65		7.30		2.63	29.71	9.48	9.77	9.53	13.89	5.22	0.73	6.35	5.41
			"	"	"	3.8	4.85	13.87	8.78	6.38	35	71.67			"		2.77		0.96	26.22	3.6	3.71	7.35	9.43	3.31	0.48	3.05	"
He = 8.96 Re∞/cm = 1.29 x 10⁵		Various	8.4	"	1.0	2.7	5.21	14.81	9.56	6.66	40	70.09	61.70	62.9	"	1.20	2.10		0.69	30.44	2.66	2.66	8.52			1.4	2.55	6.6
			"	"	"	1.8	2.7	10.76	5.27	7.09	35	46.48	63.15	64.25	"	1.10	0.75		0.14	29.73	0.87	0.87	3.44			0.92	2.00	"

APPENDIX 4

SURFACE PRESSURE AND HEAT TRANSFER DATA

(Cone - Cylinder Forebody After Coleman, 1973)

Conditions

$M_\infty = 9.31$

$Re_\infty/cm = 5.17 \times 10^5$

Surface Pressure	
S cm	P/P_∞
5.9	4.86
13.0	4.95
X cm	P/P_∞
18.4	1.12
20.6	0.80
21.9	0.56
23.1	0.50
24.4	0.51
26.9	0.59
28.2	0.64
30.7	0.65
34.5	0.76
39.6	0.80
44.7	0.80
48.4	0.75
61.3	0.71
62.9	0.70

Heat Transfer			
X cm	$\dot{q}$ W/cm^2	X cm	$\dot{q}$ W/cm^2
18.36	7.9	42.26	4.45
21.06	3.8	43.56	4.35
22.36	3.93	44.86	4.62
23.56	3.91	46.16	4.43
27.36	3.97	47.36	4.18
28.66	3.91	48.66	4.01
29.96	4.08	55.16	4.10
30.56	4.35	56.46	3.92
33.06	4.54	57.76	4.15
34.36	4.44	60.16	3.98
35.66	4.69	60.66	3.91
39.46	4.41	61.46	4.19
39.76	4.38	61.96	4.17
41.06	4.50	62.46	4.12

M_∞ = 8.93
M_e = 8.4
Re_∞/cm = 1.29 x 10^5
Re_e/cm = 1.12 x 10^5
Station x = 25 cm (δ = 0.47cm)

T_w/T_r = 0.28
P_e = 6.894 x 10^2 N/m²
    (0.1 psia)
T_o = 1070K

Y cm	Po N/m² X 10^{-7}	Pt/Po X 10^3	M/Me	U/Ue	Y cm	Po N/m² X 10^{-7}	Pt/Po X 10^3	M/Me	U/Ue
1.202	1.4968	5.72	1.11	1.01	0.361	1.4272	4.11	0.92	0.99
1.176	1.4065	5.50	1.05	1.01	0.335	1.4755	3.73	0.89	0.99
1.125	1.4065	5.35	1.04	1.00	0.335	1.4651	4.15	0.93	0.99
1.084	1.4968	5.27	1.06	1.01	0.323	1.4272	4.01	0.91	0.99
1.047	1.4968	5.45	1.08	1.01	0.289	1.4272	3.78	0.88	0.98
1.014	1.4968	5.19	1.06	1.01	0.269	1.4803	3.46	0.86	0.98
0.965	1.4065	5.05	1.01	1.00	0.269	1.4169	3.80	0.88	0.98
0.947	1.4065	4.62	0.96	1.00	0.259	1.5813	2.88	0.79	0.97
0.892	1.4617	5.02	1.03	1.00	0.236	1.5127	2.46	0.73	0.95
0.831	1.4617	4.72	0.99	1.00	0.236	1.5058	2.56	0.74	0.96
0.772	1.4617	4.53	0.97	1.00	0.219	1.5313	2.30	0.71	0.95
0.752	1.4617	4.61	0.98	1.00	0.193	1.5127	1.69	0.60	0.91
0.694	1.4617	4.70	0.99	1.00	0.168	1.5313	1.10	0.49	0.85
0.681	1.4617	4.71	0.99	1.00	0.124	1.5803	0.47	0.32	0.69
0.566	1.4617	4.31	0.95	0.99	0.124	1.4651	0.78	0.40	0.78
0.531	1.4617	4.44	0.96	1.00	0.117	1.5313	0.46	0.31	0.68
0.490	1.4617	4.49	0.97	1.00	0.091	1.5058	0.11	0.13	0.31
0.470	1.4272	4.55	0.96	1.00					
0.434	1.4651	4.35	0.96	0.99					
0.434	1.4755	4.18	0.94	0.99					
0.414	1.4272	4.73	0.98	1.00					
0.389	1.5803	3.95	0.95	0.99					

TABULATED DATA (PITOT SURVEY)

$M_\infty = 8.93$ $Tw/Tr = 0.28$

$Me = 8.4$ $Pe = 6.894 \times 10^2$ N/m^2

$Re_\infty/cm = 1.29 \times 10^5$ (0.1 psia)

$Re_e/cm = 1.12 \times 10^5$ $To = 1070K$

Station X = 45 cm ($\delta = 0.63$ cm)

Y cm	Po N/m^2 X 10^{-7}	Pt/Po X 10^3	M/Me	U/Ue	Y cm	Po N/m^2 X 10^{-7}	Pt/Po X 10^3	M/Me	U/Ue
1.201	1.4679	4.50	1.01	1.00	0.513	1.4789	3.94	0.95	0.99
1.176	1.5017	4.21	0.99	1.00	0.491	1.4617	3.60	0.90	0.99
1.126	1.5017	4.15	0.98	1.00	0.482	1.4789	3.76	0.93	0.99
1.084	1.4679	4.34	0.99	1.00	0.470	1.4617	3.82	0.93	0.99
1.047	1.4679	4.50	1.01	1.00	0.435	1.4789	3.76	0.93	0.99
1.014	1.4679	4.42	1.00	1.00	0.435	1.4789	3.60	0.91	0.99
0.965	1.5017	4.40	1.01	1.00	0.414	1.4617	3.27	0.86	0.98
0.947	1.5017	4.15	0.98	1.00	0.389	1.4789	3.15	0.85	0.98
0.891	1.3927	4.75	1.01	1.00	0.389	1.4789	3.13	0.84	0.98
0.831	1.3927	4.70	1.00	1.00	0.361	1.4617	2.60	0.76	0.96
0.772	1.3927	4.52	0.98	1.00	0.335	1.4789	2.67	0.78	0.97
0.752	1.3927	4.39	0.97	1.00	0.323	1.4617	2.00	0.67	0.94
0.721	1.4789	4.44	1.00	1.00	0.312	1.4789	2.32	0.72	0.95
0.721	1.4789	4.46	1.00	1.00	0.312	1.4789	2.36	0.73	0.96
0.721	1.4789	4.34	1.00	1.00	0.289	1.4617	1.92	0.66	0.93
0.693	1.3927	4.66	1.00	1.00	0.270	1.4789	1.73	0.63	0.92
0.681	1.4617	4.62	1.02	1.00	0.270	1.4789	1.88	0.65	0.93
0.661	1.4789	4.40	1.00	1.00	0.259	1.4272	1.60	0.59	0.91
0.661	1.4789	4.26	0.98	1.00	0.236	1.4789	1.23	0.53	0.88
0.625	1.4617	4.62	1.02	1.00	0.219	1.4272	1.34	0.54	0.89
0.591	1.4789	4.19	0.98	1.00	0.193	1.4789	1.03	0.48	0.85
0.566	1.4617	4.01	0.95	0.99	0.193	1.4789	1.08	0.49	0.86
0.551	1.4789	3.99	0.95	0.99	0.168	1.4272	0.96	0.45	0.83
0.531	1.4617	3.75	0.92	0.99	0.124	1.4789	0.62	0.37	0.76
					0.124	1.4789	0.68	0.39	0.78
					0.117	1.4272	0.75	0.40	0.79
					0.091	1.4789	0.31	0.26	0.60
					0.091	1.4789	0.34	0.27	0.62
					0.084	1.4272	0.33	0.26	0.61
					0.049	1.4789	0.07	0.09	0.22
					0.049	1.4789	0.14	0.16	0.40

TABULATED DATA (PITOT SURVEY)

M∞ = 8.93   Tw/Tr = 0.28

Me = 8.4   Pe = 6.894 x 10^2 N/m^2

Re∞/cm = 1.29 x 10^5 (0.1 psia)

Re$_e$/cm = 1.12 x 10^5 To = 1070K

Station X = 63.6 cm (δ = 1.00 cm)

Y cm	Po N/m^2 X 10^{-7}	Pt/Po X 10^3	M/Me	U/Ue	Y cm	Po N/m^2 X 10^{-7}	Pt/Po X 10^3	M/Me	U/Ue
1.196	1.4679	4.87	0.97	1.00	1.001	1.4679	4.88	0.97	1.00
1.196	1.4679	4.61	0.94	0.99	0.966	1.4679	4.61	0.94	0.99
1.156	1.4679	5.04	0.99	1.00	0.947	1.4679	4.26	0.91	0.99
1.156	1.4679	4.52	0.93	0.99	0.925	1.4679	4.37	0.92	0.99
1.115	1.4679	5.27	1.01	1.00	0.892	1.4679	4.12	0.89	0.99
1.115	1.4679	4.43	0.92	0.99	0.828	1.4941	3.83	0.87	0.88
1.115	1.4679	4.94	0.98	1.00	0.785	1.4699	3.72	0.85	0.98
1.069	1.4679	4.94	0.98	1.00	0.785	1.4755	3.94	0.87	0.98
1.069	1.4679	5.18	1.00	1.00	0.773	1.4679	3.91	0.87	0.98
1.069	1.4679	4.86	0.97	1.00	0.752	1.3996	4.01	0.86	0.98
1.069	1.4679	4.94	0.98	1.00	0.724	1.4934	3.24	0.80	0.97
1.049	1.4679	4.70	0.95	0.99	0.693	1.4679	3.48	0.82	0.97
1.049	1.4679	5.18	1.00	1.00	0.681	1.3996	3.31	0.78	0.97
1.025	1.4679	5.08	0.99	1.00	0.671	1.4755	3.04	0.77	0.96
1.025	1.4679	5.27	1.01	1.00	0.653	1.4699	3.08	0.77	0.96
1.025	1.4679	5.16	1.00	1.00	0.653	1.4872	2.99	0.76	0.96
1.025	1.4679	4.70	0.95	0.99	0.625	1.4679	2.93	0.75	0.96
1.001	1.4679	5.06	0.99	1.00	0.600	1.4941	2.91	0.75	0.96
1.001	1.4679	4.86	0.97	1.00	0.566	1.5017	2.68	0.73	0.95
1.001	1.4679	4.88	0.97	1.00	0.556	1.4699	2.52	0.70	0.95

PTO – Further data this station

TABULATED DATA (PITOT SURVEY)

$M\infty = 8.93$

$Me = 8.4$

$Re\infty/cm = 1.29 \times 10^5$

$Re_e/cm = 1.12 \times 10^5$

Station $X = 63.6$ cm ($\delta = 1.00$ cm)

continued

$Tw/Tr = 0.28$

$Pe = 6.894 \times 10^2$ N/m^2

(0.1 psia)

$To = 1070K$

Y cm	Po N/m^2 X 10^{-7}	Pt/Po X 10^3	M/Me	U/Ue	Y cm	Po N/m^2 X 10^{-7}	Pt/Po X 10^3	M/Me	U/Ue
0.531	1.5017	2.12	0.64	0.93	0.191	1.4555	0.93	0.42	0.81
0.490	1.3996	2.16	0.63	0.92	0.161	1.5017	1.00	0.44	0.82
0.475	1.4755	2.03	0.62	0.92	0.129	1.4672	0.74	0.37	0.76
0.470	1.4619	2.30	0.66	0.94	0.129	1.4872	0.70	0.36	0.75
0.439	1.4555	1.89	0.60	0.91	0.114	1.4679	0.81	0.39	0.78
0.388	1.4672	1.64	0.60	0.90	0.086	1.4872	0.51	0.31	0.68
0.388	1.4934	1.67	0.57	0.90	0.073	1.4679	0.44	0.28	0.65
0.361	1.4679	1.78	0.58	0.91	0.043	1.4699	0.12	0.13	0.32
0.337	1.4679	1.47	0.53	0.88	0.043	1.4672	0.16	0.16	0.40
0.322	1.4679	1.43	0.52	0.88	0.043	1.4941	0.15	0.16	0.39
0.300	1.4872	1.40	0.52	0.88					
0.290	1.4679	1.58	0.55	0.89					
0.266	1.4934	1.24	0.49	0.86					
0.266	1.4672	1.24	0.49	0.86					
0.254	1.4679	1.24	0.49	0.86					
0.222	1.4755	1.03	0.44	0.83					
0.222	1.4941	1.01	0.44	0.82					
0.219	1.5017	1.27	0.50	0.86					

TABULATED DATA (PITOT SURVEY)

$M_\infty = 9.31$

$M_e = 8.65$

$Re_\infty/cm = 5.17 \times 10^5$

$Re_e/cm = 4.35 \times 10^5$

Station $X = 25$ cm ($\delta = 0.48$ cm)

$T_w/T_r = 0.28$

$P_e = 2.76 \times 10^3$ N/m²

    (0.4 psia – nominal

    value taken for cyl..

    surface)

$T_o = 1070K$

Y cm	Po N/m² $\times 10^{-7}$	Pt/Po $\times 10^3$	M/Me	U/Ue	Y cm	Po N/m² $\times 10^{-7}$	Pt/Po $\times 10^3$	M/Me	U/Ue
1.201	6.437	5.03	1.10	1.01	0.625	6.357	3.92	0.96	1.00
1.176	6.516	5.01	1.10	1.01	0.592	6.321	3.77	0.94	0.99
1.125	6.516	4.70	1.07	1.01	0.566	6.516	3.68	0.94	0.99
1.085	6.437	4.59	1.05	1.00	0.551	6.546	3.81	0.96	1.00
1.046	6.437	4.77	1.07	1.01	0.551	6.536	3.78	0.96	1.00
1.013	6.437	4.60	1.05	1.00	0.531	6.516	3.58	0.93	0.99
0.965	6.516	4.51	1.05	1.00	0.513	6.541	3.71	0.95	.99
0.947	6.516	4.22	1.01	1.00	0.490	6.516	3.82	0.96	1.00
0.856	6.782	3.70	0.97	1.00	0.483	6.782	3.33	0.95	0.99
0.803	6.536	3.93	0.98	1.00	0.470	6.516	3.63	0.94	0.99
0.803	7.546	3.92	0.98	1.00	0.434	6.321	2.98	0.84	0.98
0.785	6.541	3.94	0.98	1.00	0.414	6.198	2.96	0.83	0.98
0.752	6.357	4.03	0.98	1.00	0.389	6.782	2.48	0.79	0.97
0.721	6.536	3.71	0.95	1.00	0.361	6.198	2.77	0.80	0.97
0.721	6.562	3.93	0.98	1.00	0.335	6.321	2.18	0.71	0.95
0.693	6.357	3.80	0.95	0.99	0.323	6.198	2.34	0.73	0.96
0.681	6.357	4.16	0.99	1.00	0.312	6.541	2.18	0.73	0.96
0.663	6.782	3.75	0.97	1.00	0.290	6.198	2.00	0.68	0.94
0.660	6.546	3.94	0.98	1.00	0.269	6.536	1.74	0.65	0.93
					0.259	6.205	1.71	0.63	0.93
					0.236	6.562	1.65	0.63	0.93
					0.236	6.541	1.47	0.60	0.91
					0.221	6.516	1.52	0.61	0.92

TABULATED DATA (PITOT SURVEY)

M_∞ = 9.31   Tw/Tr = 0.28

Me = 8.65   Pe = 2.76 x 10^3 N/m^2

Re$_\infty$/cm = 5.17 x 10^5 (0.4 psia – nominal

Re$_e$/cm = 4.35 x 10^5 value taken for cyl.

Station X = 25 cm (δ = 0.48 cm)   surface)

continued   To = 1070K

Y cm	Po N/m^2 X 10^{-7}	Pt/Po X 10^3	M/Me	U/Ue	Y cm	Po N/m^2 X 10^{-7}	Pt/Po X 10^3	M/Me	U/Ue
0.218	6.205	1.56	0.60	0.91	0.114	6.516	1.02	0.49	0.86
0.218	6.357	1.59	0.61	0.92	0.114	6.516	1.02	0.49	0.86
0.193	6.541	1.26	0.55	0.89	0.091	6.321	0.52	0.34	0.73
0.168	6.205	1.30	0.55	0.89	0.091	6.562	0.53	0.35	0.74
0.124	6.562	0.97	0.48	0.87	0.084	6.205	0.54	0.35	0.74
0.124	6.782	0.98	0.49	0.86	0.048	6.562	0.24	0.23	0.56

TABULATED DATA (PITOT SURVEY)

$M \infty$ = 9.31   Tw/Tr = 0.28

Me = 8.65   Pe = 2.76 x 10^3 N/m^2

Re ∞/cm = 5.17 x 10 ^{5} (0.4 psia)

Re$_e$/cm = 4.35 x 10^5 To = 1070K

Station X = 45 cm (δ = 0.62 cm)

Y cm	Po N/m^2 X 10^{-7}	Pt/Po X 10^3	M/Me	U/Ue	Y cm	Po N/m^2 X 10^{-7}	Pt/Po X 10^3	M/Me	U/Ue
1.201	6.357	4.49	1.03	1.00	0.752	6.389	4.17	1.00	1.00
1.76	6.357	3.90	0.96	1.00	0.722	6.669	3.67	0.95	0.99
1.125	6.357	3.68	0.93	0.99	0.722	6.405	3.69	0.94	0.99
1.052	6.357	3.75	0.94	0.99	0.722	6.677	3.71	0.96	1.00
1.046	6.357	4.65	1.05	1.01	0.693	6.389	3.90	0.96	1.00
1.013	6.357	4.16	0.99	1.00	0.681	6.077	3.17	0.85	0.98
0.966	6.357	3.68	0.93	0.99	0.663	6.669	3.62	0.95	0.99
0.947	6.357	4.01	0.97	1.00	0.663	6.405	3.56	0.92	0.99
0.925	6.357	3.75	0.94	0.99	0.661	6.704	3.57	0.94	0.99
0.856	6.606	3.82	0.97	1.00	0.661	6.414	3.60	0.93	0.99
0.856	6.669	3.80	0.97	1.00	0.624	6.077	3.78	0.93	0.99
0.856	6.405	3.82	0.95	0.99	0.592	6.669	3.52	0.93	0.99
0.856	6.677	3.62	0.95	0.99	0.592	6.405	3.36	0.89	0.99
0.831	6.389	4.13	0.99	1.00	0.567	6.077	3.79	0.93	0.99
0.803	6.606	3.65	0.95	0.99	0.531	6.077	3.05	0.83	0.98
0.803	6.571	3.68	0.95	0.99	0.513	6.704	3.70	0.82	0.98
0.785	6.606	3.71	0.96	1.00	0.490	6.077	2.37	0.73	0.96
0.785	6.571	3.60	0.94	0.99	0.483	6.359	2.29	0.75	0.96
0.772	6.389	4.50	1.04	1.00	0.470	6.389	1.69	0.63	0.93

PTO - Further data this station

TABULATED DATA (PITOT SURVEY)

M ∞ = 9.31   Tw/Tr = 0.28

Me   = 8.65   Pe = 2.76 x 10^3 N/m^2

Re ∞/cm = 5.17 x 10^5 (0.4 psia)

Re$_e$/cm = 4.35 x 10^5 To = 1070K

Station X = 45 cm (δ = 0.62 cm)

continued

Y cm	Po N/m^2 X 10^{-7}	Pt/Po X 10^3	M/Me	U/Ue	Y cm	Po N/m^2 X 10^{-7}	Pt/Po X 10^3	M/Me	U/Ue
0.434	6.704	1.98	0.70	0.95	0.254	6.233	0.91	0.46	0.84
0.434	6.359	1.98	0.70	0.95	0.236	6.571	0.97	0.48	0.86
0.414	6.389	1.48	0.59	0.91	0.219	6.389	0.95	0.47	0.85
0.389	6.571	1.47	0.60	0.91	0.219	6.233	1.00	0.48	0.85
0.360	6.389	1.65	0.62	0.92	0.193	6.414	0.80	0.43	0.82
0.335	6.414	1.31	0.56	0.90	0.160	6.389	0.84	0.44	0.83
0.323	6.389	1.27	0.55	0.89	0.160	6.233	0.86	0.44	0.83
0.313	6.414	1.18	0.53	0.88	0.124	6.606	0.60	0.38	0.77
0.289	6.389	1.10	0.51	0.87	0.114	6.389	0.57	0.36	0.76
0.269	6.677	1.00	0.50	0.87	0.114	6.233	0.65	0.38	0.78
0.269	6.405	1.05	0.50	0.87	0.091	6.571	0.42	0.31	0.69
0.269	6.669	1.01	0.50	0.87	0.074	6.389	0.47	0.33	0.71
0.254	6.389	0.82	0.44	0.82	0.074	6.233	0.48	0.33	0.71
					0.049	6.414	0.22	0.22	0.54

TABULATED DATA (PITOT SURVEY)

M ∞ = 9.31   Tw/Tr = 0.28

Me = 8.65   Pe = 2.76 x 10^3 N/m²

Re ∞/cm = 5.17 x 10 ⁵   (0.4 psia)

Re$_e$/cm = 4.35 x 10^5 To = 1070K

Station X = 65 cm (δ = 0.97 cm)

Y cm	Po N/m² X $\overline{10}^7$	Pt/Po X 10^3	M/Me	U/Ue	Y cm	Po N/m² X $\overline{10}^7$	Pt/Po X 10^3	M/Me	U/Ue
1.196	6.233	4.01	0.97	1.00	0.830	6.389	3.70	0.94	0.99
1.196	6.389	4.17	1.00	1.00	0.802	6.504	3.54	0.93	0.99
1.196	6.389	4.00	0.97	1.00	0.785	6.573	3.42	0.91	0.99
1.155	6.233	4.00	0.96	1.00	0.785	6.602	3.32	0.90	0.99
1.155	6.389	4.00	0.98	1.00	0.773	6.389	3.70	0.94	0.99
1.155	6.389	3.91	0.97	1.00	0.752	6.233	3.38	0.89	0.99
1.115	6.233	3.25	0.87	0.98	0.721	6.609	3.18	0.88	0.99
1.115	6.389	4.51	1.04	1.00	0.693	6.389	2.96	0.84	0.98
1.115	6.389	4.20	1.00	1.00	0.693	6.233	2.77	0.80	0.97
1.070	6.233	4.37	1.00	1.00	0.681	6.233	2.58	0.77	0.97
1.049	6.233	4.51	1.02	1.00	0.662	6.604	2.39	0.77	0.96
1.024	6.389	4.00	0.98	1.00	0.624	6.233	2.19	0.71	0.95
1.024	6.389	4.13	0.99	1.00	0.592	6.573	1.97	0.69	0.95
1.024	6.389	3.28	0.88	0.99	0.592	6.504	1.77	0.65	0.93
1.001	6.389	4.17	1.00	1.00	0.551	6.573	1.70	0.64	0.93
1.001	6.389	3.90	0.96	1.00	0.551	6.602	1.68	0.64	0.93
0.965	6.389	4.40	1.02	1.00	0.531	6.389	1.67	0.63	0.93
0.947	6.389	3.39	0.90	0.99	0.513	6.602	1.57	0.62	0.92
0.947	6.389	3.17	0.87	0.98	0.491	6.389	1.43	0.58	0.90
0.925	6.389	4.13	0.99	1.00	0.482	6.602	1.29	0.56	0.90
0.892	6.389	4.10	0.99	1.00	0.470	6.389	1.64	0.62	0.92
0.892	6.389	4.20	1.00	1.00	0.434	6.609	1.33	0.57	0.90
0.856	6.504	3.63	0.94	0.99	0.414	6.389	1.50	0.59	0.91

TABULATED DATA (PITOT SURVEY)

$M \infty$ = 9.31 Tw/Tr = 0.28

Me = 8.65 Pe = 2.76 x 10^3 N/m^2

$Re \infty/cm$ = 5.17 x 10^5 (0.4 psia)

Re_e/cm = 4.35 x 10^5 To = 1070K

Station X = 65 cm (δ = 0.97 cm)
continued

Y cm	Po N/m^2 X 10^{-7}	Pt/Po X 10^3	M/Me	U/Ue	Y cm	Po N/m^2 X 10^{-7}	Pt/Po X 10^3	M/Me	U/Ue
0.389	6.573	1.24	0.55	0.89	0.218	6.389	0.84	0.44	0.83
0.389	6.609	1.25	0.55	0.89	0.193	6.609	0.58	0.37	0.76
0.361	6.233	1.25	0.54	0.89	0.160	6.389	0.59	0.37	0.76
0.335	6.604	1.00	0.49	0.86	0.124	6.609	0.54	0.36	0.75
0.323	6.389	1.06	0.50	0.87	0.124	6.573	0.54	0.36	0.75
0.323	6.233	1.07	0.50	0.86	0.114	6.389	0.58	0.36	0.76
0.313	6.602	0.97	0.48	0.86	0.114	6.233	0.61	0.37	0.76
0.289	6.389	0.95	0.47	0.85	0.092	6.604	0.38	0.30	0.67
0.270	6.504	0.74	0.42	0.81	0.074	6.389	0.37	0.29	0.66
0.254	6.389	0.73	0.41	0.80	0.074	6.233	0.37	0.28	0.65
0.237	6.504	0.70	0.41	0.80	0.048	6.604	0.21	0.22	0.53

Appendix 6

AXISYMMETRIC SURFACE PRESSURE SURVEY

(Cone-Cylinder-Flare)

Data from Coleman, 1973

$M\infty = 9.31$

$Re\infty/cm = 5.17 \times 10^5$

(X-L)cm	P/P_∞		
	$\alpha = 15°$	$\alpha = 30°$	$\alpha = 35°$
-2.9	--	--	2.70
-2.6	--	0.70	3.70
-2.35	--	0.70	--
-2.1	--	0.71	3.80
-1.85	0.70	--	4.40
-1.60	--	--	4.20
-1.35	--	0.68	4.50
-1.1	0.70	0.68	--
-0.85	--	--	4.50
-0.6	0.75	0.90	--
-0.35	0.91	1.22	4.80
-0.1	1.00	1.80	--
0.25	--	7.00	4.90
0.50	2.50	10.10	6.30
0.75	--	14.30	7.60
1.0	3.00	20.00	6.80
1.25	--	23.80	12.00
1.50	4.20	--	13.70
1.75	--	30.10	--
2.05	5.00	32.50	24.30
2.30	--	33.00	30.30
2.55	6.90	34.10	36.40
2.80	--	--	59.40
3.05	7.40	30.50	64.50
3.30	--	--	49.00
3.55	8.10	31.40	46.70
4.05	8.70	--	42.60
4.60	9.50	--	40.00
5.10	9.80	33.60	37.80
6.35	9.80	--	--
7.60	9.80	29.20	36.50

AXISYMMETRIC SURFACE PRESSURE SURVEY
(Cone-Cylinder-Flare)
Experiment

$M_\infty = 9.31$

$Re_\infty /cm = 5.17 \times 10,^5 \alpha = 40°$

(X-L) cm	P/P∞		(X-L) cm	P/P∞
-11.75	0.64		-1.70	5.80
-11.40	0.76		-1.20	5.80
-11.00	0.99		-0.95	5.44
-10.70	1.49		-0.80	5.47
-10.40	2.55		-0.45	5.72
-10.20	3.05		-0.05	5.90
-9.95	2.80		0.25	6.50
-9.65	4.04		0.25	5.67
-9.45	3.98		0.50	5.67
-9.20	4.37		0.75	5.59
-8.90	4.14	L=69 cm	1.05	5.76
-8.65	4.37	↑	1.25	5.67
- - - - - - - - - - - - -			1.25	5.94
-8.15	4.81	↓	1.55	5.43
-7.95	5.10	L=65 cm	1.80	7.27
-7.72	4.94		2.05	9.10
-7.35	4.77		2.30	7.40
-6.96	5.05		2.30	9.31
-6.55	5.22		2.55	10.55
-6.22	5.10		2.80	13.45
-5.85	4.94		3.05	15.00
-5.45	5.63		3.35	18.66
-5.10	5.47		3.55	19.60
-4.70	5.10		3.80	27.72
-4.35	5.10		4.05	30.70
-3.98	5.47		4.35	33.69
-3.60	5.63		4.55	37.23
-3.20	5.73		4.85	48.64
-2.85	5.57		5.10	76.98
-2.50	5.80		6.35	104.46
-2.10	5.80		7.60	54.31
			7.60	48.50

AXISYMMETRIC SURFACE PRESSURE SURVEY

(Cone-Cylinder-Flare)

Experiment

M_∞ = 8.93

Re_∞/cm = 1.29 x 10^5

α = 30°		α = 35°		α = 40°	
(X-L)cm	P/P_∞	(X-L)cm	P/P_∞	(X-L)cm	P/P_∞
-3.85	0.54	-3.85	0.56	-3.1	1.28
-3.45	0.44	-3.60	0.54	-2.85	1.58
-3.10	0.45	-3.20	0.51	-2.60	1.66
-3.10	0.80	-3.10	0.84	-2.60	1.66
-2.70	0.70	-2.85	0.84	-2.35	1.87
-2.40	0.73	-2.45	0.85	-2.10	2.26
-1.95	0.72	-2.35	0.79	-1.85	2.29
-1.60	0.73	-2.10	0.88	-1.6	3.18
-1.60	0.96	-1.70	0.89	-1.35	3.82
-1.20	1.03	-1.60	1.16	-1.10	3.86
-0.85	1.32	-1.35	1.49	-0.85	4.56
-0.85	1.25	-0.95	1.94	-0.60	5.10
-0.45	1.66	-0.85	1.87	-0.35	5.23
-0.10	2.08	-0.60	2.15	0.25	5.57
0.30	7.03	-0.20	2.71	0.50	8.64
0.50	13.63	0.25	7.06	0.70	13.10
0.75	22.00	0.55	14.54	1.03	18.66
1.00	26.06	0.75	16.08	1.30	22.60
1.30	33.14	1.00	24.55	1.50	33.42
1.55	36.16	1.25	34.93	1.80	46.08
1.80	30.22	1.55	36.38	2.05	59.96
2.05	29.30	1.80	38.90	2.30	59.15
2.30	28.82	2.00	41.83	2.55	63.08
2.55	28.70	2.30	41.58	2.80	62.84
3.05	31.02	2.55	42.96	3.05	56.09
3.55	24.27	2.80	36.29	3.30	42.91
4.05	27.38	3.05	40.56	3.55	46.76
5.10	26.03	3.30	36.73	3.80	46.17
6.35	27.95	3.55	34.27	4.05	48.77
		4.10	34.49	4.30	44.07
				4.55	50.08
				4.80	44.36
				5.10	42.92

Surface Pressure Data - Asymmetric Geometries
Geometry A, $\emptyset$ = 0 deg., α-local = 40 deg.,
M = 9.31, Re∞/cm 5.17 x 10^5.

P/P∞	(X-L)cm	P/P∞	(X-L)cm	P/P∞	(X-L)cm
43.72	8.35	90.05	3.88	5.15	.13
40.91	8.12	88.04	3.86	6.14	-.15
42.77	7.87	92.57	3.61	5.35	-.45
40.63	7.37	68.64	3.39	5.12	-.90
49.78	6.88	87.75	3.37	4.84	-1.20
40.71	6.62	72.82	3.12	4.86	-1.65
41.99	6.39	54.96	3.12	4.78	-2.40
46.19	6.13	72.82	3.12	5.20	-3.15
59.70	5.87	44.02	2.87	4.60	-3.90
45.30	5.61	34.23	2.62	4.52	-4.65
48.02	5.36	27.17	2.38	4.84	-4.95
49.21	5.35	17.73	2.13	3.93	-5.40
45.89	5.12	13.85	1.87	1.82	-5.70
49.36	4.83	12.28	1.63	1.06	-6.15
53.80	4.62	6.88	1.12	.92	-6.90
55.14	4.62	6.06	.87	.98	-7.65
53.68	4.37	6.46	.87	0	0
64.03	4.12	5.19	.63	0	0

Surface Pressure Data – Asymmetric Geometries
Geometry A, $\emptyset$ = 90 deg., α local = 37.5 deg.,
$M\infty$ = 9.31, Re ∞/cm = 5.17 x 10^5

P/P∞	(X-L)cm	P/P∞	(X-L)cm	P/P∞	(X-L)cm
39.76	8.52	80.85	3.77	5.81	-.15
36.46	8.27	60.80	3.53	5.58	-.45
38.36	8.06	60.40	3.52	5.11	-.90
36.48	7.52	53.71	3.28	4.86	-1.20
37.80	6.77	45.35	3.26	4.65	-1.65
40.23	6.51	23.08	2.77	4.73	-2.40
42.66	6.28	30.45	2.52	4.84	-3.15
54.65	6.02	21.34	2.52	4.73	-3.90
33.88	5.80	14.93	2.27	3.17	-4.40
44.02	5.27	12.22	2.02	4.29	-4.65
50.69	5.04	15.67	1.76	2.19	-4.95
62.07	4.78	7.66	1.27	1.87	-5.15
56.16	4.78	7.23	1.02	3.47	-5.40
60.13	4.52	6.14	1.02	1.07	-5.70
69.10	4.52	5.26	0.78	2.37	-6.15
78.22	4.27	4.99	0.53		
57.63	4.02	4.73	0.28		
79.46	4.02	4.80	0.28		
60.13	3.78				
40.02	3.77				

Surface Pressure Data – Asymetric Geometries
$M\infty = 9.31$, $Re\infty/cm = 5.17 \times 10^5$
Geometry A, $\emptyset = 180$ deg., α local $= 35$ deg.

$P/P\infty$	(X–L) cm	$P/P\infty$	(X–L) cm	$P/P\infty$	(X–L) cm
35.92	8.68	46.29	3.67	4.78	−1.65
32.46	8.42	54.16	3.67	4.56	−2.15
33.96	8.18	45.43	3.42	5.58	−2.40
32.88	7.68	29.10	3.17	4.43	−2.90
40.65	7.18	28.65	2.93	4.32	−3.15
33.13	6.92	22.83	2.67	4.27	−3.65
35.86	6.68	13.47	2.43	3.41	−3.90
38.29	6.42	13.02	2.20	2.66	−4.40
39.00	5.93	11.28	1.93	2.59	−4.65
42.04	5.68	7.66	1.46	1.82	−5.15
39.00	5.43	6.90	1.17	1.31	−5.40
58.69	5.17	5.42	.93	1.49	−5.90
47.93	4.93	5.60	.68	.89	−6.65
56.79	4.67	5.07	.21	.91	−6.65
60.16	4.43	5.20	−.15	.97	−7.40
67.20	4.43	4.67	−.65	.93	−7.40
67.93	4.17	5.02	−.90	1.00	−8.15
52.05	3.93	4.48	−1.40	.99	−8.15

Surface Pressure Data – Asymmetric Geometries
$M\infty = 9.31$, $Re\infty/cm = 5.17 \times 10^5$
Geometry B $\emptyset = 0$ deg. α local = 35 deg.

$P/P\infty$	$(X-L)$ cm	$P/P\infty$	$(X-L)$ cm	$P/P\infty$	$(X-L)$ cm
36.57	8.91	45.98	3.17	4.46	-.20
36.71	7.93	46.46	2.93	4.82	-.50
36.52	7.57	56.27	2.69	4.08	-.70
38.29	7.32	50.95	2.32	4.65	-.70
37.93	7.08	42.83	2.07	4.40	-.95
36.90	6.83	31.36	1.83	4.50	-1.25
36.71	6.59	20.79	1.71	3.83	-1.70
37.82	6.35	20.18	1.71	2.72	-2.00
36.03	6.10	17.44	1.38	3.45	-2.20
38.94	5.86	16.39	1.38	2.19	-2.45
36.57	5.61	10.73	1.12	1.84	-2.50
37.01	5.37	11.28	1.10	1.21	-2.75
39.01	5.13	8.31	.85	1.58	-2.95
40.08	4.88	7.53	.85	.91	-3.25
37.93	4.64	7.91	.62	.87	-3.70
38.51	4.39	7.09	.62	.93	-4.00
39.45	4.15	5.73	.38	1.04	-4.75
40.08	3.91	5.73	.38	.87	-5.45
41.53	3.66	5.60	.12	0	0
45.11	3.42	5.19	.12	0	0

Surface Pressure Data – Asymmetric Geometries
$M\infty = 9.31$, $Re\infty$ /cm = 5.17×10^5
Geometry B, $\emptyset$ = 90 deg., α local = 32.5 deg.

$P/P\infty$	(X–L) cm	$P/P\infty$	(X–L) cm	$P/P\infty$	(X–L) cm
32.50	8.78	41.71	2.16	5.03	.28
32.88	8.78	33.42	2.03	5.05	.28
30.81	7.03	19.29	1.79	4.89	.08
34.86	6.53	18.21	1.79	4.96	−.15
33.69	6.28	13.59	1.40	4.54	−.65
30.24	5.54	12.01	1.28	4.26	−.90
32.88	5.03	12.55	1.28	3.91	−1.40
32.39	4.78	12.55	1.28	2.57	−1.65
36.54	4.28	8.31	1.03	1.93	−2.15
38.54	3.53	8.75	1.03	1.11	−2.40
41.00	2.90	7.53	1.03	.92	−2.90
44.71	2.79	8.59	1.03	.89	−3.20
40.76	2.79	8.31	1.03	.89	−3.95
44.62	2.79	5.16	.28	.94	−4.70
37.77	2.54	5.01	.28	0	0
38.86	2.54	5.33	.28	0	0

Surface Pressure Data – Asymmetric Geometries
$M_\infty = 9.31$, $Re_\infty /cm = 5.17 \times 10^5$
Geometry B, $\emptyset = 180$ deg., α local = 30 deg.

P/P_∞	(X-L)cm	P/P_∞	(X-L)cm	P/P_∞	(X-L)cm
29.37	9.18	31.33	4.18	8.70	.95
27.99	8.69	31.33	4.13	6.71	.69
27.01	8.45	33.83	3.94	5.35	.44
28.63	7.82	34.73	3.69	5.05	.24
28.69	7.68	35.87	3.44	5.19	.24
28.07	7.55	33.97	3.19	4.92	.13
28.17	7.19	36.90	2.94	4.70	.13
29.10	6.94	37.82	2.69	5.07	-.20
28.69	6.70	31.25	2.44	3.45	-.95
27.64	6.44	27.17	2.19	1.41	-1.70
29.24	6.19	20.90	1.94	.87	-2.45
29.10	5.95	15.57	1.69	1.20	-2.90
28.71	5.69	15.76	1.69	.91	-3.20
29.84	5.44	12.88	1.44	.87	-3.65
31.33	5.20	12.88	1.44	.89	-3.95
31.33	5.20	13.59	1.44	.92	-4.40
31.17	4.94	9.47	1.19	.89	-4.70
31.33	4.69	8.75	.95	.90	-5.15

Surface Pressure Data - Asymmetric Geometries
$M\infty$ = 9.31, $Re\infty$ /cm = 5.17 x 10^5
Geometry C, $\emptyset$ = 0 deg., α local = 35 deg.

$P/P\infty$	(X-L)cm	$P/P\infty$	(X-L)cm	$P/P\infty$	(X-L)cm
39.84	7.69	38.04	3.54	4.00	-.50
36.95	6.96	41.47	3.30	3.87	-.75
39.84	6.74	44.56	3.05	3.97	-1.00
35.87	6.54	46.66	2.81	3.42	-1.25
37.77	6.25	53.53	2.56	2.99	-1.50
37.93	6.04	52.72	2.20	2.38	-1.75
38.80	5.80	42.17	2.07	1.62	-2.00
37.77	5.49	27.96	1.83	1.06	-2.50
35.62	5.25	18.37	1.50	.91	-2.75
37.93	5.04	9.97	1.05	1.01	-3.25
38.04	4.52	5.95	.40	.86	-3.50
37.47	4.30	4.84	.20	.83	-4.00
37.47	4.03	4.40	-.05	0	0
39.02	3.78	4.07	-.25	0	0

Surface Pressure Data - Asymmetric Geometries
$M\infty = 9.31$, $Re\infty /cm = 5.17 \times 10^5$
Geometry C, $\emptyset = 90$ deg., α local = 35 deg.

FLARE

$P/P\infty$	(X-L) cm	$P/P\infty$	(X-L) cm	$P/P\infty$	(X-L) cm
36.76	7.35	36.04	4.85	36.04	2.32
36.76	7.08	37.07	4.64	28.01	2.10
36.55	6.83	36.27	4.34	19.67	1.83
33.98	6.59	38.46	4.09	13.62	1.59
35.94	6.35	40.67	3.91	13.08	1.35
36.81	6.10	40.26	3.59	9.40	1.10
34.01	5.85	45.05	3.30	6.95	.85
33.72	5.61	53.03	3.05	5.46	.35
34.60	5.37	51.49	2.84	4.69	.13
35.94	5.09	49.17	2.56	0	0

CYLINDER

$P/P\infty$	(X-L) cm	$P/P\infty$	(X-L) cm	$P/P\infty$	(X-L) cm
0.69	-3.45	3.90	-1.95	5.02	-0.70
0.78	-3.25	4.23	-1.75	4.93	-0.45
1.03	-2.95	4.26	-1.45	5.52	-0.25
2.26	-2.70	4.82	-1.20		
2.39	-2.50	5.15	-1.00		
3.30	-2.20				

Surface Pressure Data - Asymmetric Geometries
$M_\infty = 9.31$, $Re_\infty/cm = 5.17 \times 10^5$
Geometry C, $\emptyset$ = 180 deg., α local = 35 deg.

FLARE

P/P_∞	(X-L) cm	P/P_∞	(X-L) cm	P/P_∞	(X-L) cm
33.14	7.15	41.92	4.64	22.98	2.44
37.74	6.70	45.56	4.44	17.50	2.20
36.18	6.40	47.81	4.15	14.14	1.95
37.21	6.14	54.11	3.94	11.71	1.65
36.04	5.94	56.53	3.70	7.57	1.44
36.43	5.64	56.92	3.39	6.16	.95
37.47	5.44	46.67	3.15	6.51	.70
37.71	5.19	37.33	2.93	6.32	.40
43.74	4.89	35.47	2.65	5.71	.15

CYLINDER

P/P_∞	(X-L) cm	P/P_∞	(X-L) cm	P/P_∞	(X-L) cm
1.57	-4.00	4.61	-2.75	5.53	-1.25
1.09	-4.00	4.47	-2.50	5.39	-1.00
1.82	-3.75	4.67	-2.25	5.39/5	-1.00
2.99	-3.50	4.98	-2.00	5.35	-1.00
3.68	-3.25	5.22	-1.75	5.34	-0.75
3.81	-3.25	5.33	-1.75	5.50	-0.50
3.89	-3.00	5.36	-1.50		

Surface Pressure Data – Asymmetric Geometries
$M\infty = 8.93$, $Re\infty/cm = 1.29 \times 10^5$
Geometry A, $\emptyset = 0$ deg., α local $= 40$ deg.

FLARE

$P/P\infty$	(X–L) cm	$P/P\infty$	(X–L) cm	$P/P\infty$	(X–L) cm
47.92	8.37	43.50	4.88	65.26	2.38
47.54	8.13	49.09	4.62	58.74	2.38
36.13	7.87	53.28	4.37	63.02	2.13
47.24	7.62	46.32	4.18	48.95	1.88
47.83	7.37	50.26	3.88	49.58	1.62
43.60	7.18	52.31	3.63		
47.83	6.86	53.09	3.12	12.27	.87
46.17	6.63	49.45	3.12	10.26	.87
43.90	6.39	61.08	2.87	8.77	.63
48.70	6.12	66.50	2.87	6.26	.38
48.70	5.87	54.50	2.87	6.92	.13
45.62	5.61	67.62	2.62	5.24	.13
47.15	5.12	60.48	2.62	0	0

CYLINDER

$P/P\infty$	(X–L) cm	$P/P\infty$	(X–L) cm	$P/P\infty$	(X–L) cm
5.14	−0.15	2.16	−1.65	1.09	−2.75
4.44	−0.35	1.94	−1.85	0.65	−3.15
3.78	−0.50	1.70	−2.00	0.54	−3.35
3.58	−0.90	1.60	−2.40	0.55	−3.50
3.06	−1.10	1.31	−2.60		
2.60	−1.25				

Surface Pressure Data – Asymmetric Geometries
$M_\infty = 8.93$, $Re_\infty/cm = 1.29 \times 10^5$
Geometry A, $\emptyset = \pm 90$ deg., α local = 37.5 deg.

FLARE

P/P_∞	(X–L) cm	P/P_∞	(X–L) cm	P/P_∞	(X–L) cm
40.10	8.27	48.02	3.53	38.96	1.78
39.25	6.77	48.70	3.26	38.05	1.76
42.08	6.28	60.35	3.26	25.41	1.51
41.42	6.02	66.24	2.77	15.20	1.27
43.15	5.77	47.95	2.77	12.96	1.27
43.15	5.54	80.85	2.52	16.75	1.02
40.95	5.27	73.89	2.52	9.13	.78
40.13	5.02	58.74	2.52	7.01	.53
41.59	4.78	49.14	2.27	8.67	.53
44.13	4.28	50.46	2.27	5.84	.28
45.00	4.03	55.13	2.02	5.55	.28
44.43	3.77	52.56	2.02	0	0

CYLINDER

P/P_∞	(X–L) cm	P/P_∞	(X–L) cm
4.08	–0.1	1.49	–1.95
3.66	–0.45	1.05	–2.35
2.61	–0.85	0.95	–2.70
2.52	–1.20	0.50	–3.10
1.63	–1.60	0.50	–3.45

Surface Pressure Data – Asymmetric Geometries
$M_\infty = 8.93$, $Re_\infty/cm = 1.29 \times 10^5$
Geometry A, $\emptyset = 180$ deg., α local = 35 deg.

FLARE

P/P_∞	(X–L) cm	P/P_∞	(X–L) cm	P/P_∞	(X–L) cm
36.23	8.42	39.16	3.93	53.40	2.17
39.97	7.68	40.63	3.67	43.56	2.17
37.75	6.92	40.68	3.42	42.93	1.93
39.36	6.18	40.67	3.17	20.63	1.17
39.47	5.93	41.46	3.17	12.41	.93
40.63	5.68	52.35	2.93	11.41	.67
38.05	5.43	40.73	2.93	7.43	.43
38.43	5.17	67.01	2.67	4.71	.23
38.32	4.93	45.25	2.67	5.24	.12
43.80	4.67	46.02	2.43	0	0
40.63	4.43	45.02	2.43	0	0

CYLINDER

P/P_∞	(X–L) cm	P/P_∞	(X–L) cm
3.16	−0.1	0.99	−2.0
2.67	−0.5	0.94	−2.35
2.13	−0.85	0.76	−2.75
1.67	−1.25	0.58	−3.10
1.23	−1.60		

Surface Pressure Data – Asymmetric Geometries
$M_\infty = 8.93$, $Re_\infty/cm = 1.29 \times 10^5$
Geometry B, $\emptyset = 0$ deg., α local $= 35$ deg.

FLARE

P/P_∞	(X–L)cm	P/P_∞	(X–L)cm	P/P_∞	(X–L)cm
40.62	8.87	39.66	4.13	44.91	2.12
36.72	8.13	39.35	3.88	47.13	1.88
37.50	7.37	39.94	3.63	41.50	1.67
39.66	6.63	40.37	3.63	34.19	1.37
38.57	5.86	41.58	3.37	24.73	1.12
39.55	5.37	39.84	3.12	16.56	.88
39.97	5.13	41.38	2.87	11.49	.62
40.67	4.88	45.82	2.62	11.91	.62
38.57	4.64	43.35	2.38	7.06	.38
42.99	4.38	43.35	2.12	2.82	.12

CYLINDER

P/P_∞	(X–L)cm	P/P_∞	(X–L)cm	P/P_∞	(X–L)cm
2.33	−0.35	1.11	−1.6	0.83	−2.85
1.99	−0.60	0.93	−1.85	0.81	−3.10
1.83	−0.85	0.79	−2.10	0.58	−3.35
1.63	−1.10	0.80	−2.35	0.53	−3.60
1.33	−1.35	0.91	−2.60	0.56	−3.85

Surface Pressure Data – Asymmetric Geometries
$M_\infty = 8.93$, $Re_\infty/cm = 1.29 \times 10^5$
Geometry B, $\emptyset = \pm 90$ deg. α local = 35 deg.

FLARE

P/P_∞	(X-L)cm	P/P_∞	(X-L)cm	P/P_∞	(X-L)cm
32.01	8.03	31.37	5.52	40.07	2.25
32.54	7.78	34.14	5.04	35.22	2.02
31.69	7.78	31.80	4.79	36.13	1.78
32.86	7.28	38.45	4.50	26.64	1.54
28.38	7.28	33.72	4.28	23.31	1.30
32.86	6.99	32.86	4.03	19.98	1.03
32.12	6.99	33.31	3.79	16.96	.85
34.14	6.53	38.20	3.53	11.51	.78
34.25	6.53	35.21	3.28	10.09	.53
33.40	6.28	32.30	3.08	4.34	.28
31.80	6.28	36.17	2.79	2.62	.12
33.18	5.77	35.75	2.54	3.33	.08
32.12	5.77	37.04	2.54	0	0
33.72	5.52	36.43	2.28	0	0

CYLINDER

P/P_∞	(X-L)cm	P/P_∞	(X-L)cm	P/P_∞	(X-L)cm
2.13	-0.3	1.00	-1.45	0.88	-2.80
1.85	-0.55	0.84	-1.80	0.90	-2.95
1.69	-0.70	0.87	-2.05	0.47	-3.30
1.40	-1.05	0.83	-2.20	0.59	-3.55
1.12	-1.30	0.82	-2.55	0.62	-3.70

Surface Pressure Data − Asymmetric Geometries
$M_\infty = 8.93$, $Re_\infty/cm = 1.29 \times 10^5$
Geometry B, $\emptyset = 180$ deg., α local $= 30$ deg.

FLARE

P/P_∞	$(X-L)$ cm	P/P_∞	$(X-L)$ cm	P/P_∞	$(X-L)$ cm
29.81	8.95	25.72	4.96	32.24	2.69
28.14	8.95	29.27	4.94	31.27	2.19
28.24	8.20	30.78	4.73	32.73	2.19
29.22	8.20	30.20	4.44	31.63	2.19
29.27	7.55	28.26	4.44	32.40	2.19
30.29	7.55			31.17	1.96
28.16	6.94	29.51	4.19	30.28	1.94
29.18	6.70	28.66	3.93	26.24	1.69
29.51	6.70	30.78	3.69	22.40	1.44
28.56	6.44	28.97	3.69	23.21	1.44
23.82	6.19	32.44	3.46	18.90	1.19
29.32	5.95	29.77	3.44	10.13	.69
29.32	5.95	26.75	3.23	9.08	.69
28.26	5.95	29.32	2.94	5.94	.45
		30.29	2.94	3.12	.24
30.29	5.20	30.50	2.94	1.75	.13
30.48	5.20	33.31	2.69	0	0

CYLINDER

1.91	−0.25	0.90	−1.4	0.78	−2.75
1.68	−0.50	0.76	−1.75	0.76	−2.90
1.39	−0.65	0.76	−2.00	0.53	−3.25
1.13	−1.00	0.73	−2.15	0.52	−3.50
1.00	−1.25	0.80	−2.50	0.53	−3.65

Surface Pressure Data — Asymmetric Geometries
$M_\infty = 8.93$, Re_∞/cm $= 1.29 \times 10^5$
Geometry C, $\emptyset = 0$ deg., α local $= 35$ deg.

FLARE

P/P_∞	(X-L) cm	P/P_∞	(X-L) cm	P/P_∞	(X-L) cm
33.86	8.24	33.68	5.49	34.37	2.56
31.27	7.99	33.68	5.25	35.48	2.20
30.78	7.49	33.77	5.25	32.66	2.20
29.86	7.30	31.27	5.04	32.66	1.83
30.78	6.96	32.49	4.76	30.09	1.50
30.78	6.74	32.49	4.52	33.17	1.50
35.31	6.74	31.89	4.52	24.06	1.05
29.78	6.54	30.69	4.03	19.66	.79
32.23	6.25	31.29	3.78	7.35	.40
30.61	6.04	32.19	3.54	7.44	.40
30.78	6.04	40.18	3.05	3.42	.20
31.11	5.80	29.20	2.81	0	0

CYLINDER

P/P_∞	(X-L) cm	P/P_∞	(X-L) cm	P/P_∞	(X-L) cm
2.59	−0.15	1.31	−1.15	0.81	−2.15
2.23	−0.40	1.07	−1.40	0.70	−2.4
2.06	−0.65	0.88	−1.65	0.68	−2.65
1.58	−0.90	0.85	−1.90	0.69	−2.90

Surface Pressure Data - Asymmetric Geometries
$M_\infty = 8.93$, $Re_\infty/cm = 1.29 \times 10^5$
Geometry C, $\emptyset = \pm 90$ deg., α local $= 35$ deg.

FLARE

P/P_∞	(X-L) cm	P/P_∞	(X-L) cm	P/P_∞	(X-L) cm
32.23	8.04	32.19	5.37	34.37	2.04
29.41	7.30	33.68	4.85	33.17	1.84
28.04	6.84	34.26	4.64	34.43	1.59
31.89	6.54	30.78	4.30	29.15	1.34
32.23	6.35	34.20	4.15	18.81	1.10
31.27	6.10	33.18	3.91	12.78	.85
32.91	5.80	33.35	3.05	6.41	.35
33.86	5.61	31.38	2.84	3.51	.13

CYLINDER

P/P_∞	(X-L) cm	P/P_∞	(X-L) cm	P/P_∞	(X-L) cm
2.58	-0.2	1.36	-1.25	0.82	-2.2
2.29	-0.5	1.07	-1.45	0.80	-2.2
2.08	-0.7	1.12	-1.45	0.83	-2.45
2.09	-0.7	0.92	-1.70	0.53	-2.95
1.80	-0.95	0.85	-2.00	0.51	-2.95
				0.50	-3.2

Surface Pressure Data – Asymmetric Geometries
$M_\infty = 8.93$, $Re_\infty/cm = 1.29 \times 10^5$
Geometry C, $\emptyset = 180$ deg., α local = 35 deg.

FLARE

P/P_∞	$(X-L)$ cm	P/P_∞	$(X-L)$ cm	P/P_∞	$(X-L)$ cm
31.89	7.64	33.17	4.64	38.22	2.20
27.16	7.15	33.68	4.44	37.96	1.65
35.48	6.90	33.07	4.15	28.90	1.44
32.23	6.69	35.65	3.94	23.02	1.15
30.78	6.14	33.07	3.94	16.33	.95
29.81	6.14	35.31	3.94	18.26	.95
26.33	6.14	35.48	3.70	17.70	.95
30.78	5.94	33.51	3.39	10.17	.70
28.84	5.64	34.37	3.15	6.44	.40
31.75	5.44	34.37	3.15	2.82	.15
30.78	5.44	33.51	3.15	4.06	.15
31.57	4.89	34.20	3.15	4.27	.15
30.78	4.64	35.45	2.44	0	0
32.89	4.64	34.37	2.44	0	0

CYLINDER

P/P_∞	$(X-L)$ cm	P/P_∞	$(X-L)$ cm	P/P_∞	$(X-L)$ cm
3.13	−0.1	1.6	−1.5	0.78	−2.75
2.37	−0.5	1.14	−1.6	0.77	−2.50
2.18	−0.75	1.18	−1.75	0.82	−3.00
2.10	−0.85	0.86	−2.00	0.47	−3.10
1.90	−1.00	0.93	−2.25	0.77	−3.25
1.71	−1.25	0.85	−2.35	0.50	−3.50
				0.51	−3.75
				0.58	−4.00

Heat Transfer Data – Axisymmetric Flow (CCF)
Coleman (1973)
$M_\infty = 9.31$, Me 8.65,
$Re_\infty/cm = 5.17 \times 10^5 \alpha - 30$ degrees

(X-L) cm	$\dot{q}$ (Watts/cm^2)
-3.70	4.00
-2.50	4.03
-1.80	4.17
-1.20	4.00
-0.50	3.45
0.55	34.90
1.15	44.10
1.70	65.80
1.75	73.70
2.15	84.20
2.30	77.80
2.80	76.30
3.20	79.00
3.90	80.00
4.85	79.10
5.10	78.50
5.75	79.40
6.10	73.30
6.80	71.10
7.20	75.90

Heat Transfer Data - Axisymmetric Flow (CCF)
Coleman (1973)
M_∞ = 9.31, M_e = 8.65
Re_∞ /cm = 5.17 x 10^5 α = 35 deg.

(X-L) cm	$\dot{q}$ Watts/cm^2	(X-L) cm	$\dot{q}$ Watts/cm^2
-8.4	3.7	0.65	18.4
-7.15	3.8	1.0	28.7
-6.00	4.2	1.3	30.0
-5.00	3.9	1.5	45.0
-4.4	10.0	1.8	50.0
-4.4	7.4	2.1	54.0
-3.7	9.4	2.3	64.0
-3.7	8.4	2.5	75.0
-3.1	7.7	2.8	86.0
-2.5	6.75	3.0	110.0
-1.8	7.0	3.5	136.0
-1.15	8.0	3.8	151.0
-0.5	9.1	4.2	116.0
		4.35	117.0
		4.5	110.0
		4.85	108.0
		5.1	99.0
		5.4	105.0
		5.6	102.0
		5.9	95.0
		6.5	98.0
		7.15	100.0

Heat Transfer Data – Asymmetric – CCF Experiments
Geometry A, $\emptyset$ = 0 deg., α local = 40 deg.
M_∞= 9.31, M_e = 8.65
Re_∞/cm = 5.17 x 10^5

(X-L) cm	$\dot{q}$ Watts/cm^2	(X-L) cm	$\dot{q}$ Watts/cm^2
-6.3	3.98	0.22	7.93
-5.9	4.05	0.97	6.29
-4.85	8.69	1.00	20.81
-4.8	8.31	1.60	29.73
-4.4	7.68	1.75	26.72
-4.1	7.91	2.35	44.00
-3.7	8.07	2.47	42.32
-3.3	7.39	3.22	81.86
-2.9	7.53	3.25	90.42
-2.65	8.07	3.85	88.50
-1.85	7.66	4.00	75.72
-1.05	7.95	4.60	63.44
		5.47	60.40
		6.25	47.19
		6.85	52.85

Heat Transfer Data – Asymmetric –CCF Experiments
Geometry A, $\emptyset$ = 180 deg. α local = 35 deg.
$M\infty$ = 9.31, Me = 8.65
$Re\infty$/cm = 5.17 x 10^5

(X-L) cm	$\dot{q}$ Watts/cm²	(X-L) cm	$\dot{q}$ Watts/cm²
-6.2	4.22	1.00	15.85
-5.5	4.10	1.60	19.82
-4.7	6.40	2.35	20.43
-4.65	6.64	2.75	50.02
-4.30	7.20	3.25	61.56
-4.00	8.47	3.50	71.62
-4.00	7.25	3.85	61.56
-3.85	7.37	4.00	73.72
-3.30	6.78	4.60	57.30
-3.20	7.44	5.75	58.51
-3.15	7.25	6.25	54.74
-2.80	6.39	6.83	53.79
-2.5	7.12		
-2.45	7.33		
-2.40	7.11		
-2.10	7.06		
-1.65	6.16		
-1.60	5.49		
-1.30	6.57		
-0.85	5.22		
-0.80	6.65		
-0.50	5.71		

Heat Transfer Data – Asymmetric. – CCF Experiments
Geometry B, $\emptyset$ = 0 deg. α local = 35 deg.
M_∞ = 9.31, Me = 8.65
Re_∞/cm = 5.17 x 10^5

(X-L)cm	$\dot{q}$ Watts/cm^2	(X-L)cm	$\dot{q}$ Watts/cm^2
-4.55	3.30	0.25	11.10
-4.30	2.49	0.75	19.82
-4.05	2.37	1.00	15.72
-3.85	3.46	1.50	26.72
-3.60	3.35	1.90	47.57
-3.35	3.35	2.50	75.03
-3.05	6.18	2.65	56.58
-2.40	4.57	3.00	71.18
-2.15	7.05	3.25	60.38
-1.90	8.27	3.75	57.30
-1.55	9.31	4.15	63.48
-1.30	8.23	4.90	51.16
-1.05	8.23	5.50	50.96
-0.75	7.21	6.00	50.96
-0.50	8.32	7.15	47.19
-0.25	9.70		

Heat Transfer Data – Asymmetric –CCF Experiments
Geometry B, $\emptyset$ = 180 deg. αlocal = 30 deg.
$M\infty$ = 9.31, Me = 8.65
$Re\infty$/cm = 5.17 x 10^5

(X-L) cm	$\dot{q}$ Watts/cm^2	(X-L) cm	$\dot{q}$ Watts/cm^2
-4.45	3.30	0.35	12.28
-4.15	2.45	0.60	14.27
-3.95	2.54	1.10	16.97
-3.75	3.45	1.35	15.72
-3.45	3.35	2.00	45.59
-3.25	3.45	2.60	60.15
-2.30	4.38	2.75	47.15
-2.00	4.28	2.85	59.64
-1.80	4.00	3.35	49.51
-1.45	5.20	3.60	50.74
-1.15	6.15	4.25	56.75
-0.95	8.22	5.00	45.84
-0.65	9.15	5.10	57.23
-0.35	8.32	5.85	47.55
-0.15	9.15	7.25	45.30

Heat Transfer Data - Asymmetric - CCF Experiments
Geometry C, $\emptyset$ = 0 deg. α local = 35 deg.
M_∞ = 9.31, Me = 8.65
Re ∞ /cm = 5.17 x 10^5

(X-L)cm	$\dot{q}$ Watts/cm²	(X-L)cm	$\dot{q}$ Watts/cm²
-5.5	4.17	1.00	25.76
-4.4	4.05	1.30	34.68
-4.2	4.4	1.75	34.57
-4.0	3.94	1.95	57.48
-3.3	3.74	2.05	51.86
-2.9	3.41	2.70	55.00
-2.7	3.50	3.25	67.33
-2.5	2.73	3.55	65.41
-2.5	3.28	4.00	57.29
-2.2	2.88	4.20	61.56
-2.0	4.90	4.30	55.25
-1.8	7.49	4.95	51.15
-1.7	8.44	6.25	50.02
-1.4	9.31	6.55	49.07
-1.2	10.13	7.20	47.19
-1.0	8.21		
-0.9	6.96		
-0.6	7.20		
-0.4	8.20		
-0.2	7.45		

Heat Transfer Data – Asymmetric –CCF Experiments
Geometry C, $\emptyset$ = 180 deg. α local = 35 deg.
$M\infty$ = 9.31, Me = 8.65
Re∞/cm = 5.17 x 10^5

(X-L)cm	$\dot{q}$ Watts/cm^2	(X-L)cm	$\dot{q}$ Watts/cm^2
-6.55	4.17	0.15	6.74
-6.20	4.05	0.90	9.42
-5.05	3.33	1.10	15.86
-4.7	2.9	1.1	17.72
-4.35	5.19	1.7	25.77
-4.3	8.10	1.85	18.85
-4.0	5.85	1.85	17.29
-3.55	9.31	2.4	51.94
-3.20	8.63	2.45	28.29
-2.80	6.40	3.15	73.67
-2.75	6.96	3.35	69.26
-2.4	5.96	3.95	76.95
-2.1	6.92	4.1	73.67
-1.3	6.98	4.7	60.37
-0.5	7.70	5.4	56.62
		6.95	52.85